Flexural Response of Corroded Reinforced Concrete Beams at Elevated Temperatures

A thesis submitted to

the Faculty of Graduate Studies and Research

in Partial Fulfillment of the requirements for the degree

Master of Applied Science

By

Gian-Luca Francesco Porcari

Bachelor of Engineering, Carleton University, 2004

Department of Civil and Environmental Engineering

Carleton University

Ottawa-Carleton Institute of Civil and Environmental Engineering

January 2011

Your file Votre référence
ISBN: 978-0-494-79547-7
Our file Notre référence
ISBN: 978-0-494-79547-7

Abstract

This first of its kind study examines the effects of fire on corrosion damaged reinforced concrete beams. Nineteen beams were cast with the same external dimensions and amount of reinforcement. Corrosion was induced in the beams by a constant current source. One group of specimens were tested at constant service load while being exposed to fire conditions until failure. A second group of specimens were exposed to a pre-determined fire exposure while under service load then allowed to cool; subsequently the cooled beams were loaded to failure to study the residual flexural capacity after a fire exposure.

The results indicated that corrosion damaged reinforced concrete beams reached higher deflection values during a fire exposure as the level of corrosion damage increased. Residual test results showed that the ultimate loads of corrosion damaged beams decreased with increasing corrosion level, while deflection at ultimate load increased.

Acknowledgements

I sincerely thank my wife for her tremendous support and continuous encouragement throughout my graduate studies and life. I also thank my family for their patience and continued support throughout my graduate studies.

I am very grateful to both of my supervising Professors, Dr. Burkan Isgor and Dr. Ehab Zalok. They are both very knowledgeable and have provided me with great direction and advice throughout my research. They are also both very caring people and I truly appreciated their dedication to this project and me as their student. I am also thankful to Professor Beatriz Martin-Pérez from the University of Ottawa for her guidance in the early stages of my project.

I also thank all my colleagues for their help and support. In particular I would like to thank Dr. Pouria Ghods, Mr. Osama Salem and Mr. Ashish Sharma for their generous help at various times throughout my work.

This experimental program could not have been run without the expertise and assistance of Mr. Stanley Conley and the Carleton University Civil and Environmental Engineering laboratory staff and also Mr. Ba Lam-Thien and the staff at the Carleton University Fire Research Facility in Almonte, Ontario.

I have received tremendous support and encouragement to pursue my desire for research and higher education from all of these people as well as many other family and friends, and for this I am grateful. Thank you.

Table of Contents

List of Tables

List of Figures

List of Nomenclature

A_{Fe}	The atomic weight of iron.
b	Beam width.
C_c	Magnitude of concrete compression block.
Cl^-	Chloride
CO_2	Carbon dioxide.
CSH	Calcium silicate hydrate.
c	Bottom concrete cover thickness.
c'	Top concrete cover thickness.
c_l	Lateral concrete cover thickness.
c_p	Specific heat.
D	The initial diameter of the reinforcement bar.
DOC	Degree of corrosion.
d_c	Distance to the centroid of the tensile reinforcing from the outermost compression fibre.
dT	The distance from the top of the beam to the line of action of the thrust force.
E	Modulus of elasticity.

E_o	Modulus of elasticity at ambient temperature.
e_c	Distance between the centroid of the compression block and the line of action of the thrust force
F	Faraday's constant.
Fe^{2+}	Ferrous iron.
$Fe(OH)_2$	Ferrous hydroxide.
$Fe_2O_3 \cdot H_2O$	Ferric oxide.
h	Beam depth.
I	The corrosion current.
k	Thermal conductivity.
$k_{c,T}$	Compressive strength as a function of temperature.
$k_{E,T}$	Modulus of elasticity as a function of temperature.
$k_{y,T}$	Yield strength as a function of temperature.
L	Length.
LVDT	Linear variable differential transducer.
M_{Fire}	Ambient moment resistance during fire.
M_{Total}	Total moment resistance.

NaCl	Sodium chloride.
OH^-	Hydroxide.
P-δ	Product of the internal force and the distance between the line of action of the force and the geometrical centroid.
PIT	Maximum rebar pit depth.
pH	Measure of acidity of a solution.
R	The applied loading.
RC	Reinforced concrete.
Rcr	The corrosion rate.
RILEM	Reunion Internationale des Laboratoires D'Essais et de Recherches sur les Materiaux et les Constructions.
RLC	Residual load carrying capacity.
r_o	Initial radius of rebar.
T	Temperature.
TC	Thermocouple.
T_H	Thrust force developed in concrete member.
Ty	Tension force in steel.
t	Time.

w/c	Water to cementitious materials ratio.
Z	The valency of the reacting electrode.
Δ	Deflection.
$\Delta\varepsilon$	Change in strain.
ΔL	Change in length.
$\Delta\omega$	Metal weight lost due to corrosion.
δ	The material loss.
ε	Total strain.
ε_{cc}	Concrete compression fibre strain.
ε_{cr}	Creep strain.
ε_i	Initial strain.
ε_{th}	Thermal strain.
ε_s	Steel strain.
ε_σ	Stress related strain.
γ	The density of the material.
σ_u	Ultimate compressive strength.

CHAPTER 1: Introduction

1.0 General

Reinforced concrete structures are prevalent throughout the world due to the widely available and relatively cheap constitutive materials that are used to produce concrete and the versatile uses of reinforced concrete. The Cement Association of Canada estimates that approximately 28.1 million cubic meters of concrete are used each year in various construction projects throughout Canada (CAC, 2008).

The basic structural engineering premise in reinforced concrete design is the composite interaction that develops between the embedded reinforcing steel and concrete. The composite action is a direct result of the mechanical and chemical bond between the embedded steel and the concrete within the reinforced concrete member. More precisely, the composite action involves the transfer of internal forces between the steel and the concrete so that both materials (the steel and the concrete) can act together in resisting the applied load.

When a reinforced concrete structure experiences some form of deterioration, the fundamental composite action that gives reinforced concrete its inherent strength characteristics can be compromised. There are many mechanisms through which reinforced concrete structures deteriorate; however, it is estimated that nearly eighty percent of the deterioration of reinforced concrete structures worldwide is due to corrosion of the reinforcing steel (El-Reedy, 2008). Corrosion of steel in concrete can be due to exposure to chlorides or as a result of loss of alkalinity of concrete cover

surrounding the reinforcement because of carbonation. Structures in coastal areas and in areas where de-icing salts are widely used are particularly vulnerable to chloride-induced corrosion of the embedded steel. These reinforced concrete structures include parking structures, bridges, tunnels and buildings in coastal areas. Carbonation is a major problem in areas where the relative humidity of the concrete is between 75 and 95% (Tuutti, 1982).

The deterioration of reinforced concrete structures due to steel corrosion is a major concern for infrastructure owners and engineers. Corrosion can lead to loss of design capacity due to reduction of cross sectional area of reinforcement and/or loss of bond between steel and concrete. It can also manifest itself during service through cracking and/or spalling of concrete cover and excessive deformations. Figures 1.1-1.2 show the deterioration of corrosion damaged reinforced concrete structures.

Figure 1-1: A corrosion damaged reinforced parking structure in Ottawa, Ontario. (Isgor, 2010).

Figure 1-2: A severely damaged reinforced concrete parking structure where the concrete cover has completely delaminated and collapsed. (Cryotech, N.D.).

1.1 General objective of this study

Since so many reinforced concrete structures of various ages and construction techniques exist so prevalently in so many parts of the world, it is conceivable that at least a portion of these structures may be vulnerable to fire exposure at some point during their service life. Although the behaviour of reinforced concrete members experiencing steel corrosion has been studied extensively, the understanding of how these deteriorated members behave at elevated temperatures is not well developed. This experimental program examines the coupled structural degrading effects of both fire and corrosion in reinforced concrete flexural members. A list of specific objectives of this study is presented at the end of Chapter 3, following a literature review.

1.2 Organization of this thesis

This thesis is organized so as to provide a logical progression through from the reasoning for this research, the methodology employed and finally the results of the study. More specifically:

Chapter 1 provides the introduction, general research objective and how this thesis is organized.

Chapter 2 presents the background on corrosion damaged reinforced concrete and reinforced concrete behaviour at elevated temperature. The information presented in Chapter 2 provides the theoretical foundation for the work presented in subsequent chapters.

Chapter 3 presents an extensive literature review. Due to the lack of research studies combining both corrosion damaged reinforced concrete and fire exposure, the Chapter is divided into literature reviews of corrosion of reinforcing steel in concrete and behaviour of reinforced concrete beams at fire temperatures. A specific list of research objectives is provided at the end of this chapter.

Chapter 4 outlines the details of the experimental program undertaken as well as the rationale behind the design of this unique experimental program. This chapter covers the specimen geometrical properties, the specimen instrumentation, the accelerated

corrosion technique used, as well as a description of the flexural test assembly in the structural fire test furnace.

Chapter 5 provides the results and discussion. The thermal and structural response of the beams is presented and discussed in this chapter. Furthermore, the results of the residual strength tests are presented and compared to those of Mangat and Elgarf (1999).

Chapter 6 expands upon the detailed results and discussion presented in Chapter 5 and explains the potential practical implications of this study and how the results may affect real-world engineering applications.

Chapter 7 provides the summary and conclusions of the research. Potential areas of future work within this area that may warrant further investigation to be able to fully understand the coupled effects of both corrosion damage and fire as they relate to reinforced concrete are presented.

CHAPTER 2: Background

2.0. General

This chapter presents an overview of the mechanisms of corrosion of reinforcing steel in concrete; more detailed information can be found in Bentur (1997), Bohni (2005), Broomfield (1997), Elgarf (1994) and others. The effects of high temperatures on reinforced concrete and more specifically its components (cement, water, aggregate and reinforcing steel), will also be presented; further details can be found in Buchanan (2002).

2.1. Corrosion of reinforcing steel in concrete

Reinforcing steel bars in concrete are protected from corrosion by a passive oxide film formed on the surface of the steel bar due to the naturally high alkalinity (pH > 12.5) of concrete (Design and Control of Concrete Mixtures, 2002; Ghods *et al.*, 2010). However, the protective passive layer can be destroyed by either carbonation of the concrete or by chloride attack. It is common practice to idealize the problem of reinforcement corrosion in concrete in two successive stages (Tuutti, 1982). The first stage, or the initiation stage, can be simply defined as the period during which corrosive agents, such as chlorides or carbon dioxide, move towards the reinforcement from the surface of concrete, but the steel remains passive. The loss of passivity marks the onset of the second or propagation stage; during which active corrosion of the reinforcement takes place (Broomfield, 1997; Mangat and Elgarf, 1999; Torres-Acosta *et al.*, 2007).

The corrosion of steel reinforcement in concrete typically begins with the formation of pits along the steel bar (Broomfield, 1997; El-Reedy, 2008). Multiple pits along the same bar can merge, forming what is termed 'generalized corrosion' (Broomfield, 1997; El-Reedy, 2008).

The corrosion of the steel reinforcing bars in concrete is an electrochemical process which can only begin and be sustained if the following four conditions are met (Böhni 2005):

- depassivation of the steel must occur, thereby allowing the possibility of an anodic reaction,
- there is sufficient oxygen available at the corrosion interface thereby allowing the possibility of a cathodic reaction,
- there is enough conductivity between the anodic and cathodic reaction sites thereby allowing a flux of ions between the two sites, and
- a flux of electrons is possible due to a metallic connection between the anodic and cathodic sites. Figure 2-1 shows a schematic of the corrosion process.

The anodic reaction is the process of the metal dissolution whereby the loss of metal takes place and is given by the equation (Bohni, 2005; Broomfield, 1997):

$$Fe \rightarrow Fe^{2+} + 2e^{-} \qquad (1.1)$$

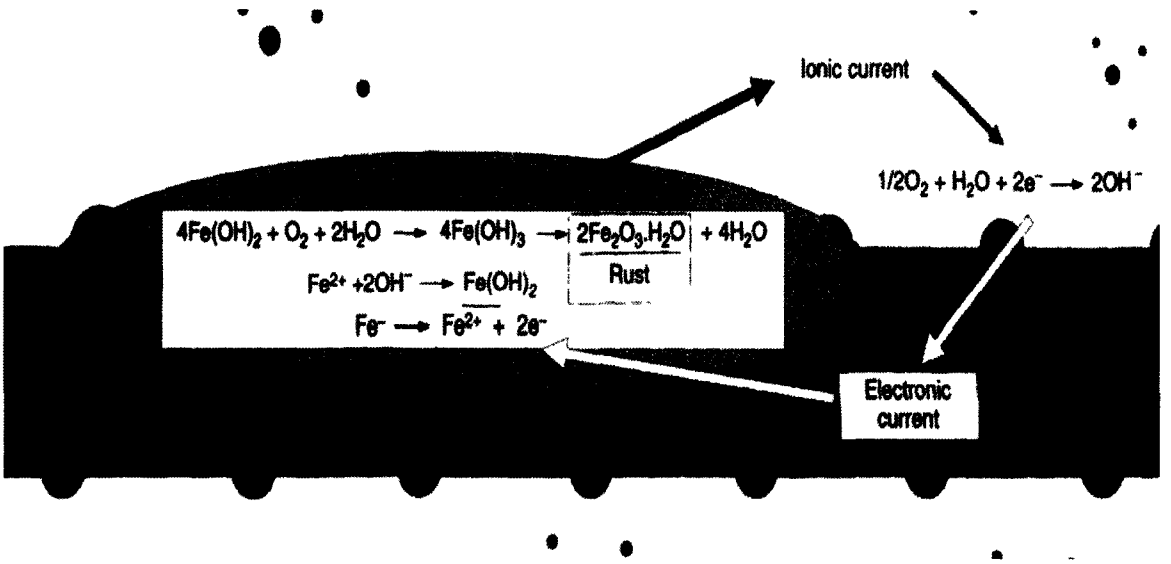

Figure 2-1: Schematic of the corrosion process (taken from Broomfield, 1997).

There is a coupled simultaneous cathodic reaction that occurs within the same steel member but at a different site, which uses the electrons flowing from the anodic reaction site, in conjunction with oxygen and water to produce hydroxide ions (OH^-) and is given by the equation (Bohni, 2005; Broomfield, 1997):

$$\frac{1}{2}O_2 + H_2O + 2e^- \rightarrow 2OH^- \qquad (1.2)$$

The resulting hydroxide ions (OH^-) from anodic and cathodic reactions will then begin breaking down the metal by reacting with the ferrous iron (Fe^{2+}) producing ferrous hydroxide ($Fe(OH)_2$) as shown in the following equation (Bohni, 2005; Broomfield, 1997):

$$Fe^{2+} + 2OH^- \rightarrow Fe(OH)_2 \qquad (1.3)$$

The resulting ferrous hydroxides will react with oxygen and water to produce ferric hydroxides ($Fe(OH)_3$) as well as ferric oxide ($Fe_2O_3 \cdot H_2O$), known commonly as rust. These reactions are given by the following equations (Bohni, 2005; Broomfield, 1997):

$$4Fe(OH_2) + O_2 + 2H_2O \rightarrow 4Fe(OH)_3 \quad (1.4)$$

$$2Fe(OH)_3 \rightarrow Fe_2O_3 \cdot H_2O + 2H_2O \quad (1.5)$$

In order for the corrosion process to continue there must be sufficient water and oxygen available at the cathodic site to allow for the reaction of all of the electrons produced at the anodic site. The flow is from the anode site where they are deposited, creating a higher potential energy, and flow to the lower potential energy cathode site. The corrosion current is described by the flow of electrons from the anodic to cathodic areas (electron current) and the coupled ion flow in the concrete (ionic current). The ionic current is made up of ferrous ions (Fe^{2+}) moving from the anode to the cathode and hydroxide ions (OH^-) moving in the opposite directions. This flow is possible through the concrete due to the fluid within the pores. When the oppositely charged ions meet, the reactions shown in equations 1.3, 1.4 and 1.5 take place; producing corrosion products. The corrosion products produced as a result of the chemical reactions occurring during the corrosion process are deposited at locations along the steel bar (Broomfield, 1997; El-Reedy, 2008). The corrosion products are less dense (hence more voluminous) than the metal (Fe) it came from, and when it accumulates on the steel reinforcement it can increase the original volume of the steel bar as much as 10 times

(Broomfield, 1997; El-Reedy, 2008). This will in turn produce internal expansion stress within the concrete cover around the reinforcing bars. Once the concrete cover can no longer sustain the internal stresses, spalling will occur and the reinforcing bars can be exposed (Broomfield, 1997; El-Reedy, 2008).

2.1.1 Practical considerations

Reinforced concrete structures under typical loading conditions tend to experience some level of cracking (Malumbela *et al.,* 2009). This inherent cracking can be induced by the loading cycles, freezing and thawing or chemical attack. The presence and resulting influences of these cracks on the corrosion process must be considered, more specifically the cracks in the area of the protective concrete cover. The cracks provide for easy pathways for the passage of CO_2 and Cl^- ions, thereby increasing the rate of penetration and consequently decreasing the time to initiation of corrosion (Vidal *et al.,* 2007).

Another important consequence of cracking is the effect it has in reducing confinement pressure and thus the bond strength between the steel bar and the surrounding concrete. This loss of rebar confinement is attributed to the development of longitudinal cracks at the rebar level which can cause a decrease in bond strength (Mangat and Elgarf, 1999). Furthermore, loss of the rib profile of deformed bars due to corrosion can lead to bond failure by loss of mechanical contact between the steel and the concrete (Almusallam *et al.,* 1996).

The problems associated with service load cracking of reinforced concrete are further compounded by the fact that the corrosion products produced and deposited on the reinforcing steel bars during the corrosion process will itself lead to further deterioration of the concrete cover through the development of expansive stresses within the confining concrete directly around the reinforcing bars. This can lead to longitudinal cracking along the steel bars, delamination or spalling of the concrete cover (Bentur *et al.,* 1997; Broomfield, 1997; El-Reedy, 2008). While the effect of the loss of the protective concrete cover on the steel bars is difficult to quantify, it can be expected that corrosion rates can be accelerated by as much as 10 times (Bentur *et al.,* 1997). In addition the spalling effects will expose new previously un-corroded areas of reinforcing steel to the effects of corrosion. Cracking of the concrete cover is also dependant on the design of the member and the properties of the concrete. A less dense concrete will tend to be less effective in resisting the internal stresses caused by the increased volume of the corroding steel bars; therefore, aggregate size, quantity of portland cement, water-cement ratio and construction and compaction techniques are important considerations. Furthermore, the geometry of the cross section of the member is also very important. Namely, the cover thickness, bar diameter and location of the bars all play a role in the development and extent of cracking (Shannag and Al-Ateek, 2006; Torres-Acosta *et al.,* 2007; Vidal *et al.,* 2007). In general a large cover thickness in relation to the reinforcing bar diameter is desirable to delay chloride penetration (Sahmaran and Yaman, 2008).

2.2 Reinforced concrete in fire

Given concrete's non-combustible composition of mainly portland cement, aggregate and water, it is expected that it would generally perform well at elevated temperatures. The cement paste is composed of both free water and chemically bound water (Haddad and Shannis, 2004). At temperatures of approximately 100°C and 300°C respectively, this water is released (Haddad and Shannis, 2004; Morley and Royles, 1979). Additional water is expelled from the pores of the concrete at a temperature of 500°C (Haddad and Shannis, 2004). This dehydration causes the concrete matrix to become more porous and also causes shrinkage in the cement paste (Haddad and Shannis, 2004; Morley and Royles, 1979). Normal weight concrete has a density between 2200 kg/m^3 to 2300 kg/m^3 (Buchanan, 2002).

In general the aggregates are composed of either siliceous materials or carbonic materials which begin to degrade at temperatures of 500 °C and 1200 °C, respectively (Haddad and Shannis, 2004). The net result of these expansion and contraction forces is the introduction of large thermally induced stresses which can cause excessive cracking, increased porosity and spalling of the concrete (Haddad and Shannis, 2004; Morley and Royles, 1979). These physical changes are reflected in reduced mechanical properties and reduced bonding strength between the reinforcing and the main concrete matrix (Haddad and Shannis, 2004). This reduction in bond strength is critical to the concrete's ability to transfer the appropriate loads to the reinforcing and allow the section to withstand the applied loads.

Steel bars used in reinforced concrete structures are typically hot rolled steel, with either a smooth profile or with a deformed surface to promote bonding to the adjacent concrete matrix. The strength of the steel bars depends mostly on the carbon content of the atomic structure (SFPE, 2002). Steel has a high thermal conductivity and consequently heats up quickly during a fire. This is one of the reasons that reinforcing is typically protected with a specific thickness of concrete known as 'cover'. While the apparent yield strength of hot rolled steel tends to increase as its temperature increases up to approximately 250 °C, its actual yield strength will quickly drop off as the temperature continues to increase (Morley and Royles, 1979). At ~600°C hot rolled steel is said to be at 50% of its actual yield strength (Morley and Royles, 1979). The steel density is typically 7850 kg/m^3. Since reinforced concrete (RC) is a composite material, it is important to study both components in terms of their thermo-chemical and thermo-mechanical properties.

2.2.1 Thermo-chemical properties

Concrete and steel have very different thermo-chemical properties, which change as a function of temperature. During heating, two factors affect the density of concrete and they are evaporation of water and degradation of the cement paste and the aggregates at the associated temperatures mentioned above. The steel also experiences little to no density change as a function of increasing temperature (Buchanan, 2002). A short summary of the thermo-chemical properties of each is described below.

2.2.1.1 Concrete

The thermal decomposition of concrete at high temperatures begins with endothermic dehydration of chemically bound water from the calcium silicate hydrate (CSH) at a temperature of approximately 110°C; followed by an exothermic release of gases as the hydrated calcium silicate is dehydrated at approximately 300°C (Arioz, 2007). Another endothermic reaction occurs around 500°C which signifies the dissociation of the calcium silicate hydrate (the main strength constituent in the cement paste) and causes significant shrinkage (Arioz, 2007). At temperatures in excess of approximately 500°C the concrete is said to have suffered irreversible damage; at 800°C the CSH gel (cement paste) has degraded to the point where the concrete has suffered significant cracking and spalling, and at approximately 1150°C the concrete experiences severe microscopic structural changes leading to a complete loss of strength. As a result the dehydration causes a gradual mass loss up to approximately 800°C, with a dramatic increase in mass loss at higher temperatures (Arioz, 2007).

The thermal conductivity of concrete is relatively low, and varies with temperature, and is strongly dependant on the type of aggregate used (Figure 2-2). Amorphous aggregates tend to have a lower thermal conductivity as compared to denser crystalline aggregates (SFPE, 2002). As the temperature increases, the thermal conductivity decreases. Buchanan (2002) reports that, for design purposes the thermal conductivity values are taken as 1.6 W/mK and 1.3W/mK for siliceous and carbonic aggregates respectively.

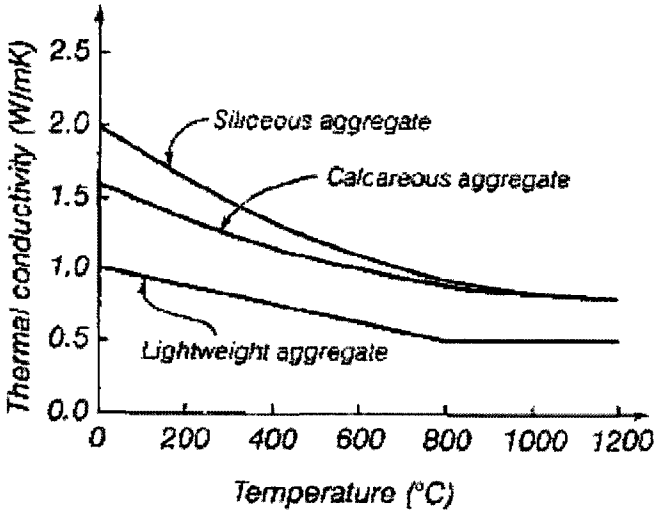

Figure 2-2: Thermal Conductivity of Concrete (taken from Buchanan, 2002).

The values presented by Buchanan (2002) agree well with theoretically derived values shown in SFPE (2002) in Figure 2-3. The lines numbered 1, 2 and 3,4 represents the theoretically calculated limits for various aggregate types (represented by points in the Figure 2-3) of normal weight and light weight concrete respectively (SFPE, 2002). The specific heat c_p of concrete also varies with temperature as shown in Figure 2-4.

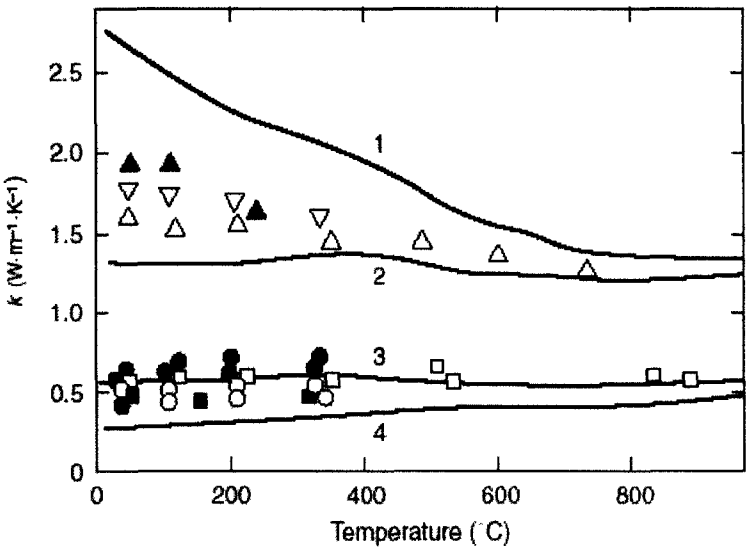

Figure 2-3: Theoretical thermal conductivity for normal and lightweight concrete (taken from SFPE,2002).

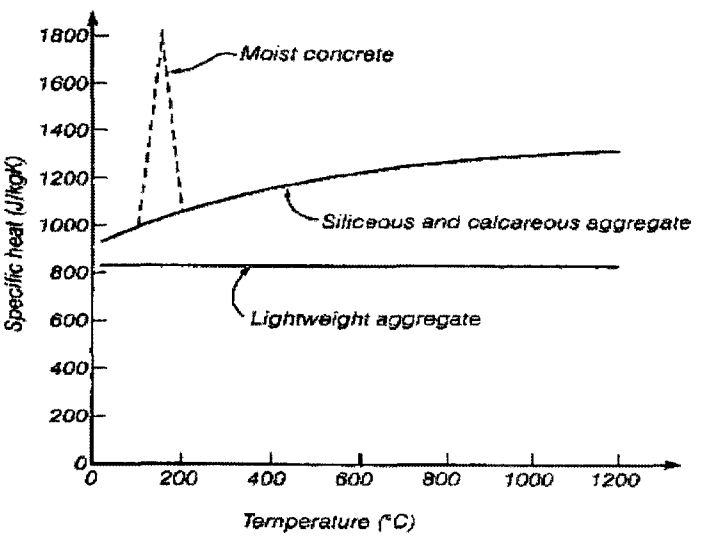

Figure 2-4: Specific heat of concrete (taken from Buchanan, 2002).

It can be seen that for normal weight concrete of either siliceous or carbonic aggregates, the specific heat increase with temperature. The spike in the specific heat

area around 200°C represents the energy required to dehydrate the sample (Buchanan, 2002). Buchanan (2002) reports using a design value 1000 J/kgK for either siliceous or carbonic aggregates.

2.2.1.2 Steel

The thermal conductivity of steel is also temperature dependent and is shown in Figure 2-5.

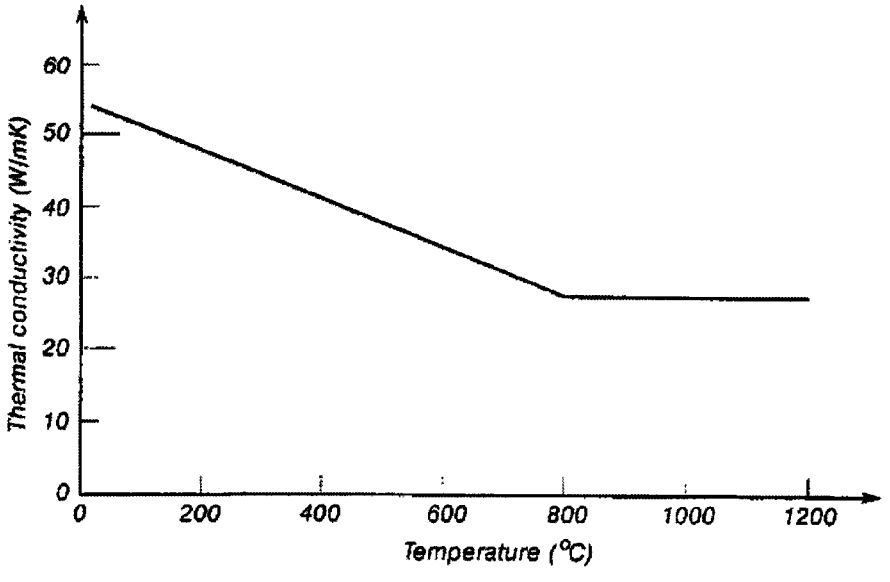

Figure 2-5 Thermal conductivity of steel (taken from Buchanan, 2002).

It can be seen that the thermal conductivity decreases linearly from 54 W/mK to its lowest value, 27.3 w/mK at ± 800°C. More precisely, the thermal conductivity k, of steel is given as (Buchanan, 2002);

$k = 54\text{-}0.0333\ T$ for, $20°C \leq T < 800°C$ (1.6)

$k = 27.3$ for, $800°C \leq T \leq 1200°C$ (1.7)

where;

T is the steel temperature (°C)

The temperature dependant specific heat of steel is shown in Figure 2-6.

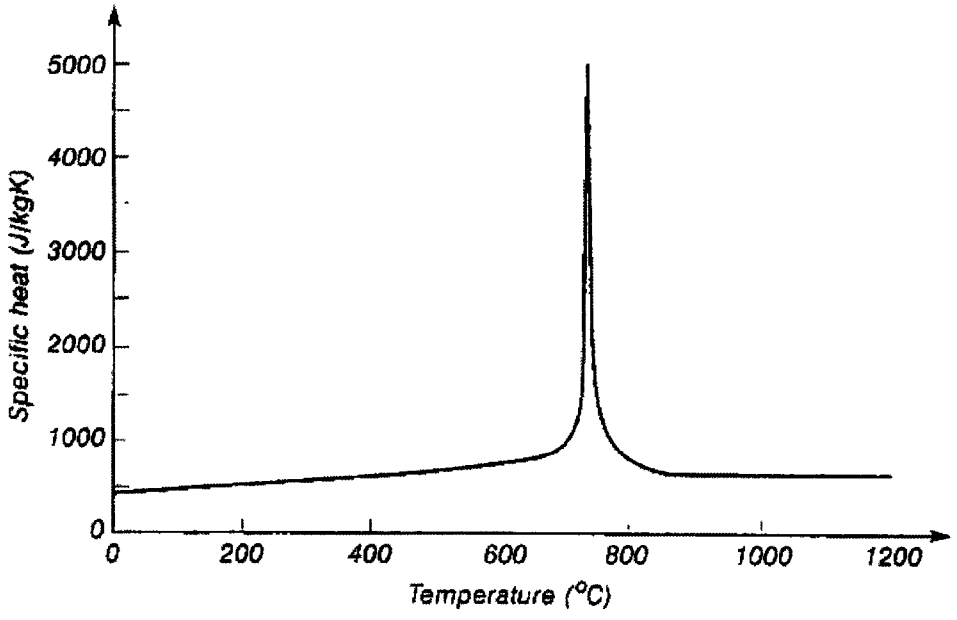

Figure 2-6: Specific heat of steel (taken from Buchanan, 2002).

The large spike in specific heat around 750 °C represents a rearrangement of the metallurgical structure of the steel (Buchanan, 2002). The specific heat c_p, of steel can be represented by the following equations (Buchanan, 2002);

$c_p = 425 + 0.773\,T - 1.69 \times 10^{-3}\,T^2 + 2.22 \times 10^{-6}\,T^3$ for, $20°C \leq T < 600°C$ (1.8)

$$c_p = 666 + \frac{13002}{738 - T} \qquad \text{for, } 600°C \leq T < 735°C \qquad (1.9)$$

$$c_p = 545 + \frac{17820}{T - 731} \qquad \text{for, } 735\ °C \leq T < 900°C \qquad (1.10)$$

$$c_p = 650 \qquad \text{for, } 900°C \leq T \leq 1200°C \qquad (1.11)$$

where;

T is the steel temperature (°C).

2.2.2 Mechanical properties

The mechanical properties of both concrete and steel also vary appreciably with an increase in temperature. The effects of which are described in the following sections.

2.2.2.1 Concrete

The modulus of elasticity $k_{E,T}$ and relative compressive strength $k_{c,T}$ as a function of temperature, as reported by Buchanan (2002) are shown in Figures 2-7 and 2-8 respectively. It can be seen that both the residual concrete compressive strength and modulus of elasticity decrease rather rapidly with increasing temperature. The critical temperature where the modulus of elasticity and compressive strength are no longer the same as ambient is approximately150°C and 350°C respectively, for normal weight concrete. The dotted line shown on the modulus of elasticity versus temperature graph is an increase proposed to increase the temperature where the modulus of elasticity becomes zero, which is between 700°C to 1000°C (Buchanan, 2002). The equations for the

relative modulus of elasticity $k_{E,T}$ and relative compressive strength $k_{c,T}$ are given as follows (Buchanan, 2002) relative to the respective value at ambient temperature;

$$k_{E,T} = 1.0 \qquad \text{for, } T < 150°C \qquad (1.12)$$

$$k_{E,T} = \frac{700 - T}{550} \qquad \text{for, } T > 150°C \qquad (1.13)$$

$$k_{c,T} = 1.0 \qquad \text{for, } T < 350°C \qquad (1.14)$$

$$k_{c,T} = \frac{910 - T}{560} \qquad \text{for, } T > 350°C \qquad (1.15)$$

where;

T is the temperature (°C).

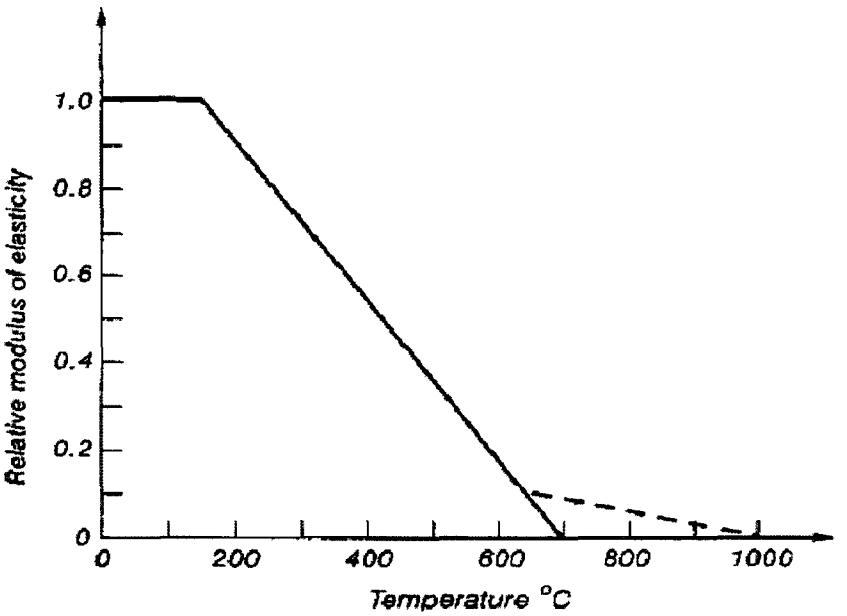

Figure 2-7: Relative modulus of elasticity as a function of temperature (taken from Buchanan, 2002).

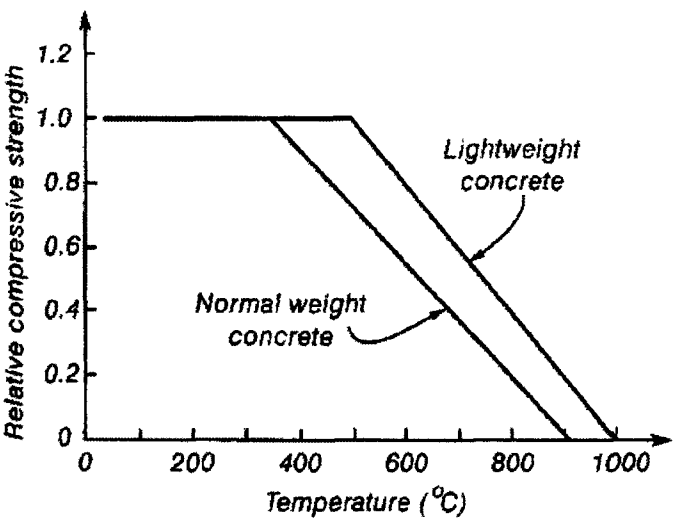

Figure 2-8: Relative compressive strength as a function of temperature (taken from Buchanan, 2002).

The SFPE (2002) gives slightly different correlations for decreasing modulus of elasticity, E and compressive strength σ_u (based on siliceous and carbonate aggregates) as a function of temperature, as is shown in Figures, 2-9 and 2-10 respectively. Figure 2-9 shows the differentiation and relationship between the aggregate type and the modulus of elasticity as a function of increasing temperature. Figure 2-10, is further differentiated into Figure 2-10a and Figure 2-10b, showing the effects of increased temperature on the compressive strength of concrete for siliceous and carbonate aggregates respectively. Further to being dependant on the type and quantity of aggregate used, the compressive strength and modulus of elasticity is strongly dependant on the age of the concrete, the water to cement ratio at the time of mixing as well as the curing condition (SFPE, 2002). In Figures 2-10a and 2-10b, the notation 'un-stressed' refers to specimens heated and tested without any applied load; 'stressed' refers to specimens tested and heated under load (40% of the ultimate load); finally, 'unstressed residual' refers to samples that were heated without load, then cooled and tested at ambient conditions (SFPE, 2002). In general the effects of elevated temperature on the relative strength of concrete are more pronounced on mixes which contained siliceous aggregates, when discussing the unstressed residual capacity (Arioz, 2007).

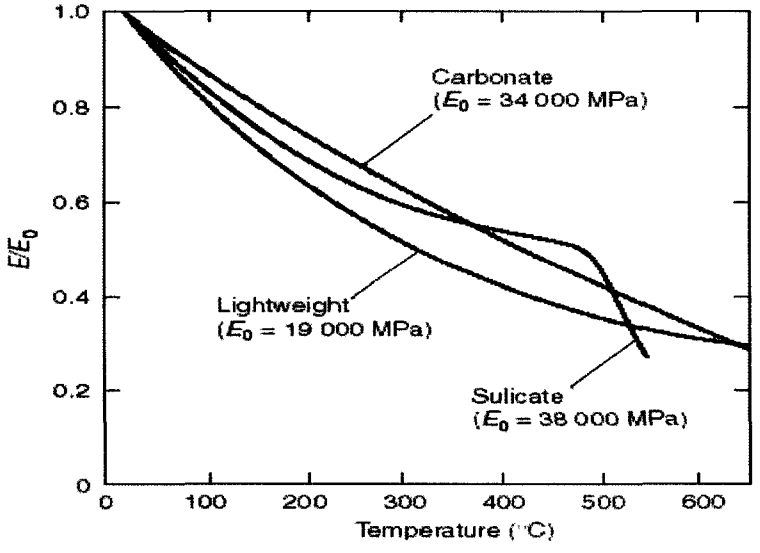

Figure 2-9: Effects of temperature on the modulus of elasticity, E. The value E_o represents the modulus of elasticity at ambient conditions (taken from SFPE, 2002).

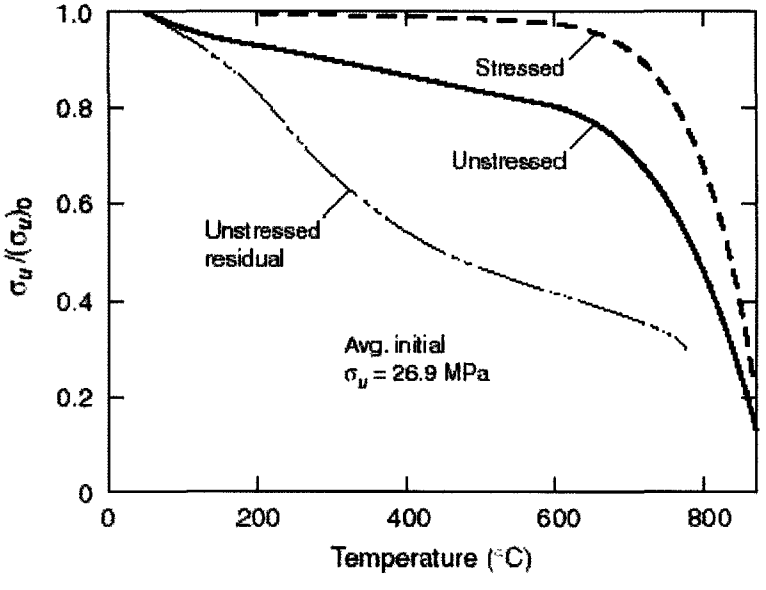

Figure 2-10a: Compressive strength ratio as a function of increasing temperature for normal weight concrete with siliceous aggregates (taken from SFPE, 2002).

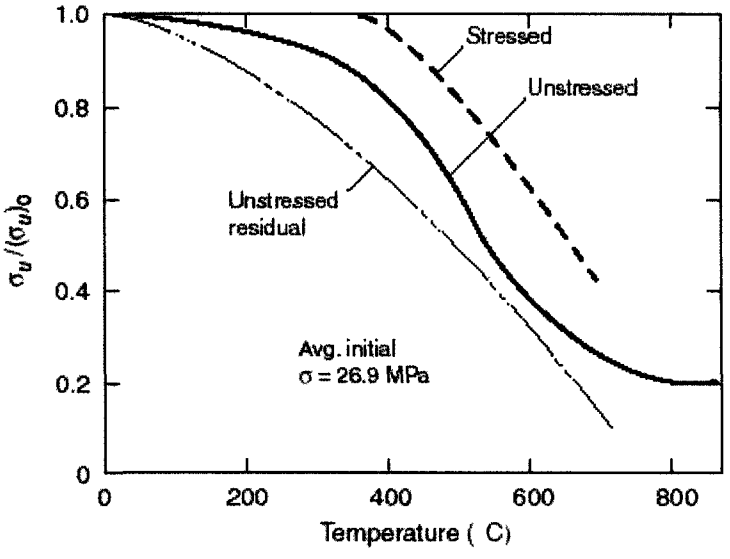

Figure 2-10b: Compressive strength ratio as a function of increasing temperature for normal weight concrete with carbonate aggregates (taken from SFPE, 2002).

2.2.2.2 Steel

While steel is a more homogenous material than concrete its properties still vary with increasing temperature. Furthermore, the chemical composition of the steel can have an appreciable effect on the mechanical properties at elevated temperatures (Cooke, 1988). The effect of increasing temperature on modulus of elasticity *E*, as presented in SFPE (2002) are shown in Figure 2-11. Also, the reduction in yield strength with increasing temperature is presented in Figure 2-12 (SFPE, 2002). The modulus of elasticity and yield strength decreases with increasing temperature.

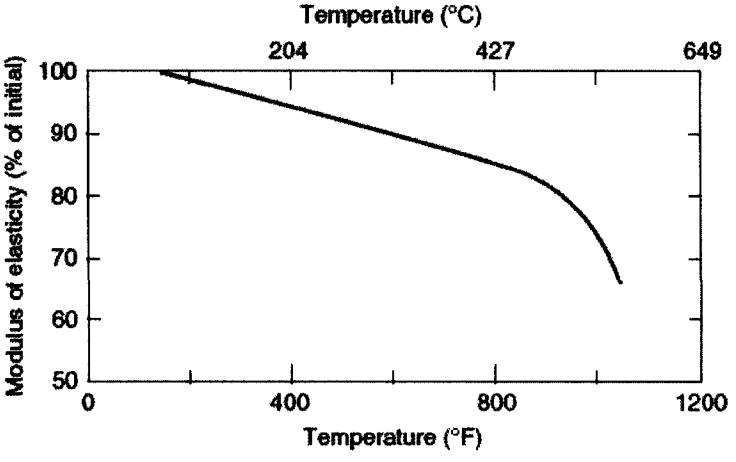

Figure 2-11: Effects of temperature on modulus of elasticity (taken from SFPE, 2002).

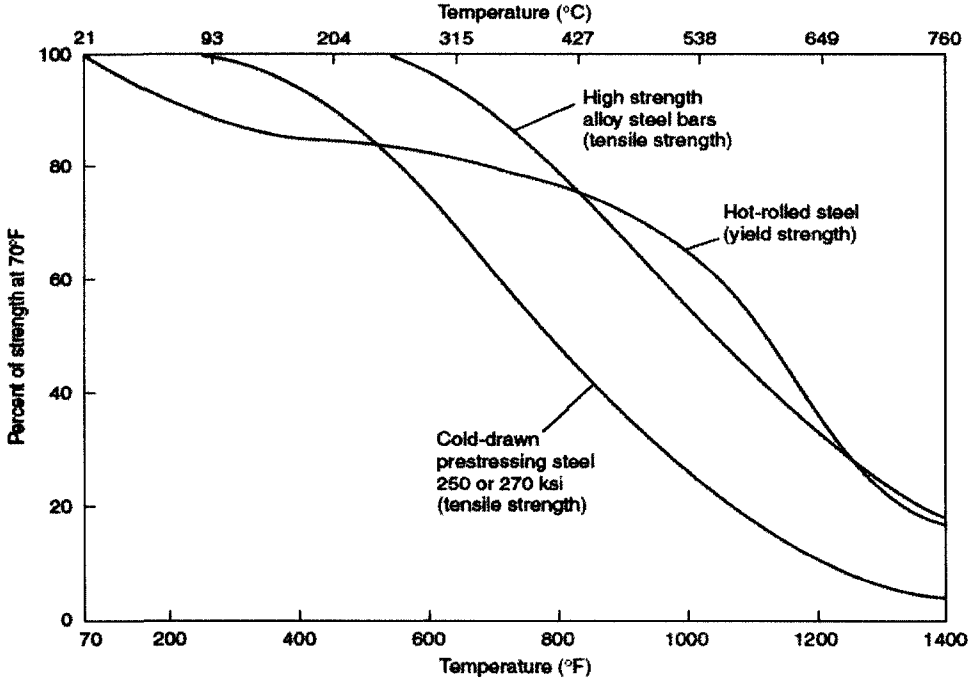

Figure 2-12: Effects of temperature yield strength (taken from SFPE, 2002).

To further quantify the reduced strength parameters, Buchanan (2002) presents empirical relations (from EC3, 1995) for reduction in yield strength $k_{y,T}$ and reduction in modulus of elasticity $k_{E,T}$.

$$k_{y,T} = [0.9674x(1+e^{\frac{T-482}{39.19}})]^{\frac{-1}{3.833}} \tag{1.16}$$

$$k_{E,T} = 1.0 + \frac{T}{2000 \ln \frac{T}{1100}} \qquad \text{for, } 0°C < T \leq 600°C \tag{1.17}$$

$$k_{E,T} = 690\frac{(\frac{1-T}{1000})}{T-53.5} \qquad \text{for, } 600°C < T \leq 1000°C \tag{1.18}$$

Strain in steel member is characterized as an elongation or shortening of the steel. The strain experienced by hot rolled steel members is described as a change in strain $\Delta\varepsilon$, which is described as follows (Buchanan, 2002);

$$\Delta\varepsilon = \varepsilon - \varepsilon_i = \varepsilon_{th}(T) + \varepsilon_{\sigma}(\sigma,T) + \varepsilon_{cr}(\sigma,T,t) \tag{1.19}$$

where, ε is the total strain at time t; ε_i is the initial strain; $\varepsilon_{th}(T)$ is the thermal strain and is solely dependent on the temperature.

An empirical relationship is presented in Buchanan (2002) for the elongation of steel due to thermal forces as;

$$\frac{\Delta L}{L} = 14x10^{-6}(T-20) \tag{1.20}$$

where,

L is the length of the specimen; and T is the temperature.

In Equation (1.19.), $\varepsilon_\sigma(\sigma,T)$ is the stress related strain, which is dependent on the applied stress as well as the temperature. Figure 2-13, shows that as the temperature increases the yield strength and modulus of elasticity decrease, however the ultimate strength appears to increase up to temperatures around 320°C before decreasing (Buchanan, 2002).

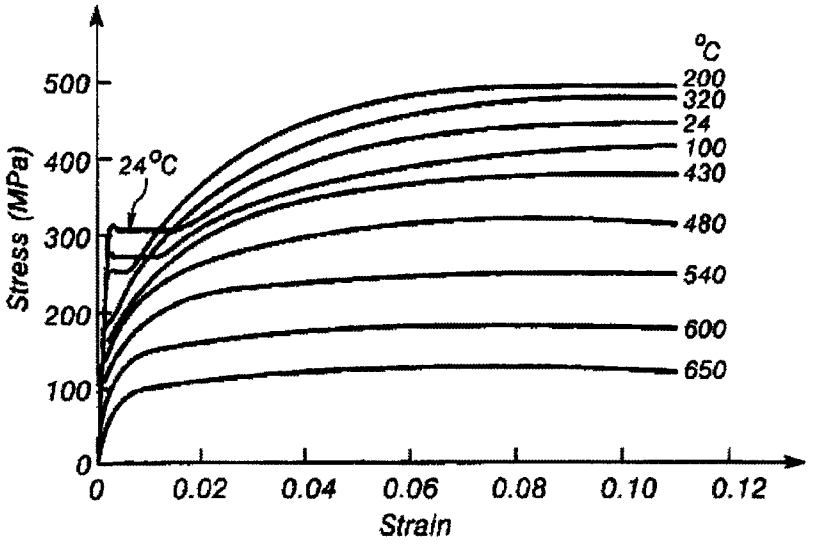

Figure 2-13: Stress-strain relationship for hot rolled steel at different temperatures (taken from Buchanan, 2002).

In Equation (1.19.), $\varepsilon_{cr}(\sigma,T,t)$ is the creep strain experienced in steel which is a transient term affected by stress, and temperature over time. Figure 2-14 shows that

while creep strain in steel at temperatures below ± 300°C is rather insignificant; the effects of creep strain at higher temperatures are quite pronounced (Buchanan, 2002).

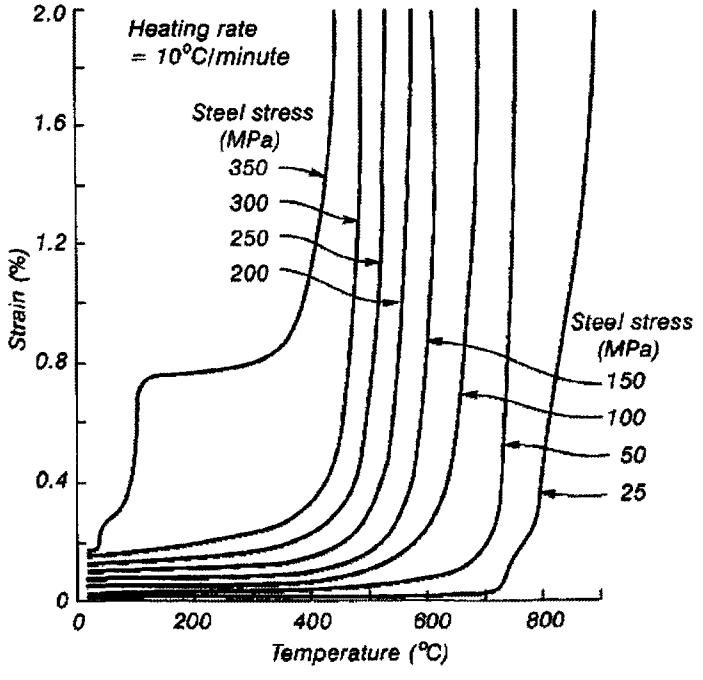

Figure 2-14: Effects of creep strain of steel tested in tension at different temperatures (taken from Buchanan, 2002).

2.2.3 Practical considerations of RC at elevated temperatures

When considering the actual structural application of steel embedded into concrete, the importance of the bond interaction becomes clear. The frictional and mechanical interlocking forces that transfers the tensile loads from the concrete to the steel (particularly in flexural members) is critical, and can be affected by high temperatures (Morley and Royles, 1979; Bingöl, 2009). This bond is affected mainly by changes in the confining concrete as it is heated due to cracks that will develop. These

cracks develop because the circumferential stresses that develop at the steel-concrete interface due to thermal expansion can no longer be sustained by the tensile resistance of the surrounding concrete, induced by the difference in thermal expansion between steel and concrete (Xiao and König, 2004). Figure 2-15, shows the thermal expansion of concrete and steel at elevated temperatures.

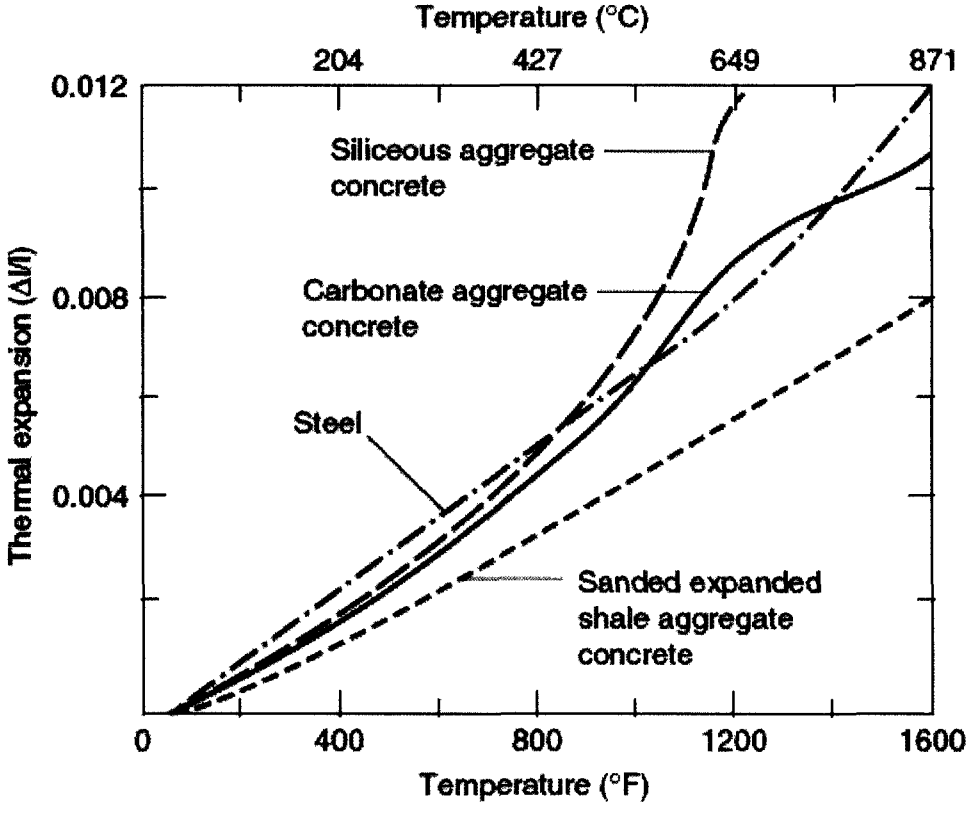

Figure 2-15: Thermal expansion of concrete and steel at elevated temperatures (taken from SFPE, 2002).

As the temperatures increase, the crack widths and number of cracks in the cover will increase leading to exposed section of reinforcing steel thereby facilitating a more

rapid temperature increase in the steel bar, nearing the steel critical failure temperature (Shi *et al.,* 2004). Cracks can start to be visible around 600°C and will be significant by 800°C with further propagation until spalling occurs around 1200°C (Arioz, 2007). Furthermore, excessive unreleased pore pressure (particularly in denser high strength concrete) can lead to spalling. In addition to exposing the highly thermally conductive steel bar directly to fire gases, the loss of concrete confinement and subsequent bond degradation can lead to loss of ductility and structural failure.

2.2.4 Axial restraint in concrete beams

Internal axial forces develop within a reinforced concrete member (particularly beams) when it is subjected to heat at one point along the member while cooler parts of the same member prevent thermal expansion of the heated element. This is known as axial thrust force and it can have a beneficial effect on the fire performance of reinforced concrete beams (Buchanan, 2002).

Figure 2-16 (reproduced from Buchanan, 2002) shows the axial force developed within a reinforced concrete beam where the ends of the beam are not free to expand. The thrust force developed, T_H, multiplied by the distance between the centroid of the compression stress block and the line of action of the thrust force (e_c) serves to provide a total moment resistance during a fire of; (Buchanan, 2002)

$$M_{Total} = M_{Fire} + T_H e_c \qquad (1.21)$$

where,

M_{Fire} is the moment resistance at ambient conditions without the influence of the fire, R is the applied loading and reaction forces, C_c represents the magnitude of the concrete compression block, Ty represents the tension force in the steel, d_c represents the distance to the centroid of the steel reinforcing from the outermost compression fibre and dT represents the distance from the top of the beam to the line of action of the thrust force.

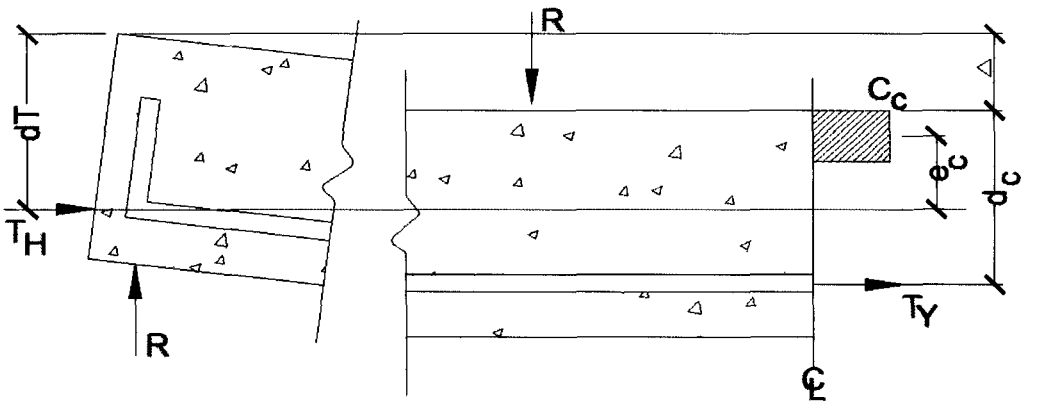

Figure 2-16: Diagrammatic representation of a beam where axial thrust forces are developed during a fire exposure (reproduced from Buchanan, 2002).

The axial thrust force developed is based on the temperature gradient developed to cause the thermal expansion force, and also the stiffness of the member resisting the expansion force. Furthermore, as can be seen from equation (1.21) and Figure 2-16, the benefits of the thermally induced axial thrust restraint moment is dependent on the variable 'e_c'. Once the internal concrete compressive block is at the same level as the

axial thrust force line of action, then the 'e_c' value becomes negative and the axial thrust moment becomes detrimental to the overall performance of the beam (Buchanan, 2002).

Figure 2-17, shows another component of axial restraint force that must be considered, the P-δ effect. This effect is based on the line of action of the thrust force and the geometrical centroid of the beam cross-section. This effect is most beneficial at the early stages of a fire and quickly decreases as the fire exposure progresses (Dwaikat and Kodur, 2008).

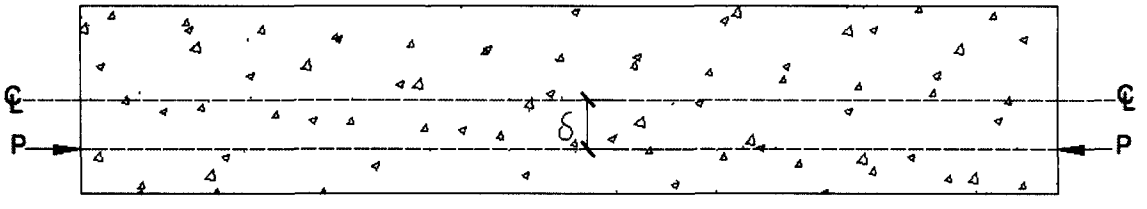

Figure 2-17: Diagrammatic representation of the P-δ Effect (Reproduced from Dwaikat and Kodur, 2008).

The development of the axial restraint forces and subsequent moment redistribution is expected to have a positive effect on a reinforced concrete beams' fire resistance due to the low thermal conductivity of the concrete naturally creating a rotational restraint force because the supports sections will be at a lower temperature than the main fire-exposed flexural zone (Dwaikat and Kodur, 2008).

Although there are increased strength and stiffness associated with the development of the thermally induced axial restraint force, it must be considered that the

'arch' action created due to the axial restraint may lead to increased spalling which will actually hinder the fire performance of the RC beam (Dwaikat and Kodur, 2008).

CHAPTER 3: Literature Review

3.0 General

Although the research in the areas of steel corrosion and fire response of reinforced concrete members is extensive, at the time of this study, to the best of author's knowledge, there is no published work on how structural flexural members behave when exposed to both phenomena. This review is provided to give a background on related literature to establish a base to the present study. The first part of the review consists of an overview of pertinent publications that studied the effects of steel corrosion in reinforced concrete elements, particularly beams loaded in flexure, at ambient temperature. The second portion of the chapter consists of a review of published studies in which the effects of fire and elevated temperature were applied to un-corroded steel reinforced concrete members, in particular flexural elements. Based on this literature review, the final section of this chapter presents the specific research objectives of this study.

3.1 Corrosion of reinforcing steel in concrete

As described in Chapter 2, the corrosion of concrete is a complicated but well-studied process. The objective of this section is not to provide a comprehensive review of all works in this area but to present the pertinent work related to the present study. This review has been carried out in parts, the first group of three studies deal with the overall picture of a corroded reinforced concrete flexural member's response to loading. A study by Vidal *et al* (2007) presents the results of a realistic long-term experiment which

attempts to simulate actual conditions. This study is followed by the works of Shannag and Al-Ateek (2006) and Torres-Acosta *et al.* (2006) which present the results of flexural testing on concrete beams that have undergone accelerated corrosion process by the application of a direct current.

The second group deal with the study of the interfacial bond between the steel and the confining concrete, and the effect of corrosion in reducing the critical cross-sectional area of the steel reinforcement. Castel *et al.* (2000) discussed the individual and combined effects of both bond strength and steel cross sectional area loss while Fang *et al.* (2004) investigated the bond effects and differences between deformed and smooth bars, with and without stirrups. Almusallam *et al.* (1995), pointed out the weakness of the concentric pull-out test (used by Fang *et al.*, 2004) and then used a modified version of this test to study the bond strength degradation as a function of degree of corrosion, and then related this to structural elements through practical terms such as crack widths. Mangart and Elgarf (1998) presented a detailed explanation of the theory behind Faraday's law for determining corrosion as a function of current intensity, duration and mass loss. Mangat and Elgarf (1998) also completed an experimental program which used a very complex flexural loading system to accurately simulate bond failure due to flexural loading. Since many different current densities and exposure durations were used for each experiment, resulting in varying degrees of corrosion, a review of El Maaddawy and Soudki (2003) was carried out to demonstrate the effects of varying the current densities and durations, and how close theoretical mass loss predictions based on Faraday's law were to actual measured degrees of corrosion. Finally, a comprehensive

study by Mangart and Elgarf (1999), which ties the above-mentioned works, is presented to close the review.

3.1.1 Flexural members with corrosion damaged reinforcement

The study conducted by Vidal *et al.* (2007), dealt with the long term (17 years) exposure to a salt fog spray applied to a set of reinforced concrete beams. At various ages certain beams were removed and tested to collect data on the corrosion cracking patterns, the chloride content at the level of the reinforcement, the corrosion distribution along the bar and the mechanical properties of the beams at different ages. The researchers also assessed the Degree of Corrosion (DOC) in the members.

A total of 36 beams measuring 150 mm wide x 280 mm deep x 3000 mm long, and with a 28-day compressive strength of 45 MPa, were subjected to a long-term program of salt fog spray (35g/l of NaCl) in a confined room to simulate exposure to a high chloride environment. The exposure regime was as follows; for the first 6 years the beams were subjected to continuous salt fog spray in laboratory conditions. From the 6^{th} year to the 9^{th} year the beams were subjected to wetting and drying cycles of 1 week of spray and one week of drying time, once again under laboratory conditions. After 9 years the entire confined room with the specimens were moved to the outdoors where they experienced temperature gradients ranging from -5°C to 35°C under the same wetting and drying cycles. The authors stated in their study that while this is still an accelerated corrosion technique, the actual results of corrosion distribution and corrosion products more closely resemble actual in-service conditions as compared to the commonly used

impressed current technique. The beams were divided into two groups of A and B, based on the depths of cover of 40 mm and 10 mm, respectively. Group A beams had two deformed 16 mm diameter tension bars and two deformed 8 mm compression bars. Group B had two 12 mm deformed bars for tensile reinforcement and two deformed 6 mm bars for compression reinforcement. To simulate real-life loading, the beams were placed under constant three point flexural loading. Several un-corroded control beams were stored in a climate controlled environment at 50% relative humidity and 20°C. Beams were then tested at 6, 14 and 17 years after casting.

Cracking maps were produced at each stage of testing as well as at the initial onset of flexural loading at 28 days after pouring for beams in Group B. At the onset of loading transverse flexural cracks appear on the tension face of the specimens and were concentrated at mid span. The maximum crack width was no larger than 0.25 mm. At the 6 year mark, the first longitudinal and parallel corrosion cracks to the steel were mapped. The longitudinal corrosion cracks appeared on the side of the beam. After 14 years the tensile zone cracking had increased to a maximum width of 1.1 mm. At 17 years the tensile cracking had propagated immensely; cracks increased largely in length and width with a maximum measured width on the tensile face of 2.4 mm. The actual chloride content at the depth of the steel reinforcing bars was measured by core drilling 10 mm diameter samples from the concrete to the depth of the reinforcing steel; the resulting cement powder was analyzed for chloride content. Vidal *et al.* (2007) cautioned that the values obtained for the chloride content using this test method may be underestimated since the core drill size was not bigger than the maximum aggregate size,

and consequently, if drilling was done on an aggregate then the sample would not be representative of the cement paste. Nevertheless the data provided gives insight into the evolution of the chloride through the concrete. They noted that after approximately 5 years the chloride content was approximately 0.8% and 0.5% by weight of cement for the tensile and compressive zones, respectively. The graph of total chloride (as a percentage of the weight of cement) versus time showed that the chloride content in the tensile section increased at a faster rate than the compression zone. This was attributed to the tensile cracking, which allowed chloride and oxygen to penetrate more easily. The chloride content in both the tensile and compressive zone seemed to reach a maximum saturated value after approximately 14 years and remained fairly constant up to 17 years.

The mechanical behaviour of a corroded beam showed an increase in deflection of 20% at 14 years and 70% at 17 years versus testing against an un-corroded member. The loss in stiffness was attributed to the excessive cracking and the subsequent loss of bond strength and confinement pressure.

Vidal *et al.* (2007) stated that the presence or width of flexural cracks (less than 0.3 mm wide) did not play a significant role on the overall corrosion process. They justified this statement, by pointing out that: despite the presence of flexural cracks after 6 years, there was no sign of corrosion on the tensile face. After 14 years of exposure, corrosion cracking on the tensile face was present but not concentrated in the area of the flexural cracks. While the level of corrosion cracking increased between 14 and 17 years, the corresponding chloride concentration had already reached its threshold value. Vidal

et al. (2007) attributed this partially to work of other researchers that showed that the corrosion products can actually be beneficial in filling up the early developed small flexural cracking thereby slowing down chloride penetration and subsequently corrosion. The chloride content and subsequent corrosion formation along the steel bars was heterogeneous. Interestingly, the first corrosion cracking was visible after 6 years and only on the compression face, where the earlier testing showed that the chloride concentration was lower in the compression zone. The authors stated that quality and strength of the original steel-concrete bond was critical in delaying the onset of corrosion, by eliminating voids where chloride and oxygen can accumulate.

After 6 years one of the group B beams experienced only localized corrosion in the compressive zone in the form of six pits randomly distributed along the length of the bar, with an average cross-sectional loss of steel of approximately 4 mm^2. No corrosion cracking, and consequently no corrosion, was observed for the tensile zone; hence any corrosion that had taken place at this stage was not voluminous enough to induce longitudinal cracking. Vidal *et al.* (2007) attribute the early onset of cracking in the corrosion zone to a phenomena called `"the top-bar effect," in which steel cast in the upper level of the concrete (compression reinforcing in the case of simply supported beam) is more prone to the creation of voids beneath the horizontal bars, resulting in an increased presence of chloride and oxygen therefore facilitating corrosion. For the same beam after 14 years, two new pits formed on the steel surface in the compression zone, with the width and cross-sectional steel loss increasing substantially in the existing pits, to a maximum value of approximately 24 mm^2. At this point corrosion cracking was

evident in the tensile zone as well and was rather localized with a concentration at mid span, giving an average steel cross-sectional area loss of approximately 8 mm^2 at that location. There was also some highly localized intense pitting at one end of the beam giving rise to a maximum cross-sectional steel loss of approximately 24 mm^2. At the 17 year stage, no new corrosion cracking occurred in the compression zone; however the intensity of the existing pits increased to produce a maximum steel cross-sectional loss of approximately 29 mm^2. In general the increase in cross-sectional steel loss in the tensile reinforcement between 14 and 17 years was substantial, indicating intense corrosion propagation. The maximum value in steel cross-sectional area loss was at the mid span and near a support; the values were approximately 43 mm^2 and approximately 46 mm^2, respectively.

The authors plotted the average tensile and compression zone steel mass loss versus time. The resulting figure indicated that once corrosion began, after approximately 4 years and approximately 5 years for the compression and tension zones respectively, the rate of increase of percent corrosion increased linearly and relatively gradually up to 14 years, after which both lines followed the same trend of a sharp increase up to the 17 year mark. This was attributed to the extensive corrosion cracks present at this stage. The lines being similarly parallel indicated that both zones increase DOC at similar rates. It was noted that the percent corrosion of the compressive bar was higher because the original diameter of the compression reinforcing bar in this sample was 6 mm in diameter; therefore the reduction in cross-sectional area was more pronounced than the thicker tensile zone bars.

Up to 14 years of age, there was little reduction in the bending stiffness of the member tested. However, between 14 and 17 years the tested bending stiffness dropped considerably (approximately 30%). Compression zone corrosion cracking had little effect on the bending stiffness, which is evident by the fact that during the first 14 years when corrosion was dominant in the compression zone, the specimen had very negligible bending stiffness reduction. Conversely once corrosion of the tension zone steel propagated rapidly (between 14 – 17 years) the bending stiffness dropped approximately 25%. This drop in bending stiffness in the tension zone at advanced levels of corrosion was attributed to lost steel cross-sectional area as well as deteriorating steel to concrete bond and loss of confining pressure. Therefore, the first significant detrimental structural effects evident in this study occurred at ~ 14 years and ~ 4% average corrosion of the tension zone steel.

Shannag and Al-Ateek (2006) tested a series of under-reinforced concrete beams with different levels of steel corrosion and the effects that different types of fibre reinforced cover can have on the ultimate flexural capacity and the failure mode. The different types of fibres used in the cover matrix were hooked steel fibres, brass-coated steel fibres, glass-fibre, and a 50/50 blend of hooked steel fibres and brass coated steel fibres. Particularly important to this work were the results obtained from samples of standard portland cement concrete cover.

The test specimens were divided into two groups. The first group of specimens consisted of one sample of each type of mix described above, without any corrosion. The

second group of samples, consisted of two samples of each type of mix with steel bars that were corroded to degrees of 2% and 5.5% of the original rebar diameter. The 100 mm wide by 150 mm deep and 1000 mm long beams were cast in two separate stages in order to test the different effects of the different cover matrices. The overall thickness of the cover layer was 40 mm, which gave the 2-10 mm diameter reinforcing steel bars a depth of cover of 25 mm measured from the bottom of the section to the steel centroid. All mixes were designed to meet the American Concrete Institute's guidelines for concrete mixtures to achieve a cylindrical compressive strength of 20 MPa and 72 MPa for the main concrete and the cover concrete, respectively, while maintaining acceptable workability.

The beams were cast in two layers, with the cover-zone layer being poured first, with two reinforcing bars being embedded in this layer. A vibrating table assembly was used to ensure good compaction and a low void ratio. After the initial setting time, at the onset of the solidification phase (90 minutes after pouring), the interface between the two pours was roughened and then the remaining concrete mix was poured. The beam specimens were then cured for 28 days in water. After the 28 day curing, the beams were transferred to ambient environmental conditions, and then the beams that were to be subjected to corrosion were transferred to the accelerated corrosion, electrolytic cell.

The accelerated corrosion process was carried out by submerging the beam in a tank containing a solution of 5% sodium chloride (NaCl) in distilled water. A 3 mA/cm^2

current intensity was applied with the positive terminal connected to the steel bars extending from the concrete specimens acting as the anode, and the negative terminal was connected to a stainless steel plate that served as the cathode. Care was taken to prevent corrosion at the ends of the concrete specimens, where the steel bars protruded, by applying a rubber coating to the exposed bar and the adjacent concrete surface. Based on the current intensity the duration required to achieve 2% and 5.5% corrosion of the steel bars was 25 hours and 70 hours, respectively. This was calculated based on a derivation given in Mangat and Elgarf (1998), which considers the degree of corrosion as percent reduction in reinforcing bar diameter.

The beams were tested in flexural loading by a four point bending apparatus which applied two loads through the use of hydraulic jacks at one third span increments, at a displacement controlled rate of 0.001 mm/s which loaded the beams to failure. A linear variable differential transducer (LVDT) was used to record the mid-span deflections. To ensure flexural failure of the specimens occurred as opposed to shear failure, the shear zones at the supports were externally reinforced with steel collars.

Test results showed that in general the beams that had cover which was reinforced with one of the fibrous admixtures described above generally had a higher flexural capacity at corrosion rates ranging from 0-5% than the non-fibre reinforced portland cement cover specimens. The portland cement cover specimens' load deflection curves for all three corrosion rates showed the same general trend with decreasing slope as the corrosion rate increased, which represents a loss in beam stiffness. For example, at

approximately 5 mm of deflection the load was 45 kN, 43 kN and 40 kN for 0%, 2% and 5.5% corrosion, respectively.

The failure modes due to corrosion were similar for all of the specimens regardless of the mix. The factors affecting the performance included the initial strength of the concrete mix as well as the concrete's ability to resist cracking and the subsequent de-bonding that occurred between the reinforcing steel bars and the confining concrete. The cracking and de-bonding was the result of internal expansive stresses that developed along the length of the bar as the products of corrosion were deposited along the bar. The formation of these cracks led to increased corrosion rates and the possibility of spalling. The positive effects of the fibres included in the cover mix were attributed to the fibre's ability to strengthen the concrete matrix and limit any cracks that did form, to very small widths, thereby maintaining the integrity of the concrete cover. These experiments all showed that the mid span deflections decreased with an increasing level of corrosion which indicates that these beams experienced a more drastic and brittle failure mode. This can be detrimental to the life safety of an occupied structure since little or no warning will be given of imminent structural failure. The reduction in ductility was more evident in the mixes which achieved a higher ultimate load capacity, namely the blended mix and the glass fibre mixture.

While the results of these experiments provide useful data on the effects of different reinforcing fibres used in the concrete mix, the methodology of the specimen preparation was not truly indicative of real-life scenarios. The concept of creating two

layers within the same specimen, one reinforced with fibres and one un-reinforced raises some questions as to the interaction of the interface between the two layers and how this affects the flexural performance. Furthermore, since these two layers were not poured monolithically as in real applications, the transfer of the internal shear forces induced by the loading conditions at the layer interface needs to be considered. Shannag and Al-Ateek (2006) addressed this by roughening the interface layer to increase bonding and using a vibrating table to produce a dense concrete. They pointed out in their report that they achieved good bond interaction between the layers, and that this was evident in their results since they reported no layer serration at the time and location of specimen failure.

Torres-Acosta *et al.* (2007) conducted experiments to investigate the residual flexural capacity of steel reinforced concrete beams with a reduced steel cross-sectional area due to corrosion. From their experimental results in conjunction with data generated and published by other researchers, they derived empirical relationships between the average corrosion penetration, the initial radius of the rebar and the maximum concrete surface crack width. They also derived empirical relationships between the average corrosion penetration and the maximum rebar pit depth.

They completed this work based on the principles of defining the service life of a reinforced concrete structure exposed to a corrosive environment. They defined the life of such a structure based on three stages; the first one being the corrosion initiation stage which begins at construction and carries on until corrosion begins. This stage has a more or less constant ultimate load capacity of the concrete member. The second stage is

marked by the onset of corrosion of the reinforcing steel and continues until a critical level of corrosion occurs and the load capacity drops considerably; this unacceptable level of corrosion was defined by the authors as the time when concrete begins to undergo visual degradation and the first crack of <0.1mm in width is visible on the concrete surface. The end of the second stage marks the end of the service life of the structure. The last phase represents a drastic drop in the load carrying capacity over time and ends with structural failure. To validate the model described above, the authors collected data from other previously published works on reinforced concrete beams, columns and slabs, and normalized it to be independent from the type of loading (tension, compression, bending). They did this by plotting the corrosion induced rebar loss, which was defined as the ratio of average corrosion penetration and initial radius of the rebar versus the load capacity ratio. The load capacity ratio was defined as the ratio of the load capacity of the corroded reinforced concrete elements divided by the load capacity of the same non-corroded element.

Twelve reinforced concrete beams with dimensions of 100 mm wide by 150 mm deep and 1500 mm long with 1-10 mm diameter rebar were cast. Chlorides in the form of 3% NaCl by weight of cement were added to the concrete mix over the entire length of the beam. The presence of chloride in the mix at the time of casting eliminates the need for wetting and drying cycles and reduces the time required for ion penetration. The concrete specimens were all cast from the same Type I portland cement mix, designed for a 28 day compressive strength of 27 MPa. Four of the beams were used as un-corroded control samples; the remaining eight were subjected to accelerated corrosion

by applying a 80 $\mu A/cm^2$ anodic current density to the rebar, for periods of ~40, ~80, and ~200 days to achieve levels of 5, 10 and 15% rebar radius loss respectively. A 30 mm wide by 1200 mm long steel plate was fixed to the side of the concrete specimen and acted as the cathode. Wet sponges were placed on top of the beams and kept moist throughout the accelerated corrosion process. After the corrosion process was stopped, the beams were carefully inspected for cracks, and all crack widths were recorded. The beams were then loaded to failure by a three point loading system that applied simply supported conditions at the ends and a uniformly distributed load over the beam at a loading rate of 1 mm/min. After structural failure, the rebar were retrieved and a gravimetric mass loss analysis was performed. From the mass loss data, the value of average corrosion penetration was obtained. Further analysis of the rebar was also performed to identify and measure the depth of any pits that formed on the reinforcing bar. All beams which were corroded developed one crack in the concrete cover running parallel with the reinforcing bar.

The load versus displacement data were presented for all of the specimens, with nine showing the same trend of a linear increase in the graph up to the ductile limit, after which plasticity was observed. Three of these beams, however, did not follow the same trend since they were fractured. Subsequent investigation of the rebar revealed that significant localized pitting corrosion had occurred on the bars reducing the cross-sectional area of the steel at the failure plane by more than half of the initial radius of the rebar.

Since crack width measurement is an easy and practical method for estimating degree of degradation in reinforced concrete, the authors derived an empirical relationship between the maximum concrete surface crack width and the associated average corrosion penetration / initial radius of the rebar ratio. They showed that based on small sample testing (max span of 2 m or less) of their specimens, that there in fact exists a strong trend which shows that the maximum concrete surface crack width is proportional to 6.4 times the ratio of the average corrosion penetration to the initial radius of the rebar.

Further empirical correlation was made between average corrosion penetration and the maximum rebar pit depth which further addressed the simplifying assumption that the entire rebar experiences uniform corrosion, when in fact in real life scenarios the corrosion degree is dependent on the local conditions at the anodic site (i.e. pore structure, chloride concentration, available oxygen concentration) and consequently deeper pits may form. The data produced by Torres-Acosta *et al.* (2007) was plotted and it was shown that the maximum rebar pit depth can be approximated to be 7 times average corrosion penetration.

Finally, the residual load capacity ratio of the corroded beams was obtained by dividing the individual maximum load sustained by each corroded beam by the average load sustained by the control samples without corrosion. A plot of residual load capacity ratio of the corroded beams versus the ratio of the maximum rebar pit depth divided by the initial radius of the rebar showed:

$$RLC = -0.7918 (PIT / r_o) + 0.9279 \quad (3.1)$$

where 'RLC' is the residual load carrying capacity of the corroded beam, 'PIT' is the maximum rebar pit depth and r_o is the initial radius of the rebar. This well-defined trend combined with the other empirical relations described can be useful for estimating residual load carrying capacity based on measurable characteristics. The authors noted the following important findings in their conclusion:

- The residual flexural load capacity depended strongly on the formation of corrosion pits on the steel bar surface. Pits as deep as 73% of the diameter were observed in some specimens, resulting in a residual load carrying capacity as low as 0.4 at average corrosion penetration / initial radius of rebar equals 0.1.

- The formation of the pits was accelerated by the wet environment provided during the corrosion process. The dryer concrete during the accelerated corrosion process exhibited larger maximum concrete surface crack width values than wet concrete under similar conditions. The authors attributed this phenomenon to the ease of transport of the corrosion products within the pore structure of a wet concrete as compared to a dry concrete, in which the corrosion products would quickly build up in one spot and impart large internal expansive stresses at the location of the deposit.

From this study, we understand that careful analysis of the rebar after failure is critical to understanding the effects of the accelerated corrosion process and also in assessing whether or not the accelerated corrosion process achieved its goals.

3.1.2 Bond interface of corroded steel in concrete

To further understand the mechanisms of failure of a corroded reinforced concrete beam in flexure, it is critical to study the interfacial bond between the steel and the confining concrete and the corrosion's effect of reducing the critical cross-sectional area of the steel reinforcement.

The study conducted by Castel *et al.* (2000) focused on investigating the individual influences of steel-concrete bond degradation and steel cross-sectional area loss, as well as their combined effect on a reinforced concrete beam. The four beam specimens used in this experiment were part of a larger long-term research project, in which 36 reinforced concrete beams were cast with two different cover conditions and had been subjected to 17 years of accelerated corrosion through the application of a salt fog spraying system, which included periods of wetting and drying cycles in an effort to emulate as closely as possible actual in-situ conditions. For more complete details on the specimen preparation refer to the literature review of Vidal *et al.* (2007).

For this particular set of experiments three corrosion affected beams and one control sample were subjected to three point constant rate service loads, and a series of three separate simulations were conducted to investigate the results on bond strength and steel cross-section loss, individually and in combination, as a result of a simulated pitting corrosion attack. The simulations measured the overall vertical displacement of the beams at mid span; while 10 sets of strain gauges mounted in vertical groups, spaced horizontally along the length of the beam measured the localized concrete strains. To

simulate the loss of bond strength, segments of the concrete cover were artificially removed, without altering the steel cross-sectional area. To simulate the reduction in steel cross section induced by a pitting attack, a notch was ground into the surface of the steel bar. In the first simulation the steel cross-section was reduced in the central part of the beam, with a notch depth of ~ 3mm corresponding to an approximate 22% loss of total steel cross-section. The effect of steel cross-sectional loss was measured; then the concrete cover in the vicinity of the steel reduction was also removed in two separate stages; representing a partial and then total loss of bond strength respectively. This simulation allowed Castel *et al.* (2000) to study the effects cross-sectional area loss and loss of bond strength together. The second simulation followed a similar procedure, albeit in a somewhat reversed order so that the loss of bond strength could first be studied independently, and then coupled with steel cross sectional loss. The concrete cover was systematically removed in a sequence to simulate actual concrete spalling and bar exposure. Once the bond degradation measurements were completed, a ~2.5 mm notch was made in the steel corresponding to about an 18% average total cross-sectional loss of steel. The third simulation further investigated the tensile properties of three 12 mm diameter, 550 MPa bars, with local steel cross-section reductions of 6%, 11% and 20%.

The measured strains were converted into the representative curvature at a given cross section of the beam where the strain gauges were located. Plotting these curvature values over the length of the beam showed that there was a significant strain increase in the areas of increased corrosion, near mid span of the beam specimen. Castel *et al.* (2000) cautioned that while the results showed a comparable difference between the

control sample and the test specimen, the actual values may have been under estimated due to the fact that the strains were measured on the surface of the concrete and not at the reinforcing steel itself. This increase in curvature value was a result of the coupled action of bond strength reduction and steel cross section loss, which was further investigated by Castel *et al.* (2000), by attempting to isolate the effects of each failure mechanism through the use of the specially designed pitting attack simulations.

The results of the first pitting attack simulation showed that the local reduction in steel cross section as applied during this simulation, had no effect on the behaviour of the beam. With the removal of the bond strength along one of the reinforcing bars, there was also no measurable effect on the beam performance, other than an increase in the tensile steel strain. With total bond loss, the mid-span deflection increased by approximately 35% and the concrete compressive strain increased by about 60% of the maximum value. The second pitting type simulation showed that as the cover was removed, there was an increase in the curvature values, but only at the localized area of reduced confinement pressure. This removal of cover in the tensile zone also increased the concrete compressive zone strains. Moreover it was shown that a 40% increase in the curvature (due to increased strains) caused a 20% increase in mid-span deflection. The third simulation, investigating the mechanical properties of the bar itself, revealed a ductility loss of 50% and 70% for a 6% and 11% steel cross-section reduction.

Castel *et al.* (2000) noted the following important conclusions as part of their study:

- With a relatively small localized reduction in steel cross-section, there weren't any noted effects on the overall beam performance; however, when coupled with a bond strength degradation, an increase in the mid-span deflection and strains were recorded. The fact that a localized cross section reduction of the steel alone had not resulted in a reduction in the beams overall performance was attributed to the contribution of the concrete in tension between the flexural cracks at carrying some of the tensile stress. However, once the bond strength was disrupted then the steel tensile stresses increase to a level where their effects were evident in increased strains and deflections.
- The ductility lost as a function of steel bar cross-section loss decreases exponentially until a value of approximately 25% of the initial ductility was reached. The presence of the notch in the steel bar led to a localized increase in the steel cross section yielding at the point of the increased stress (reduced cross-section) prior to the entire bar reaching the elastic limit, which explains the reduction in bending stiffness and then subsequent premature rupture because the yield reserve had been already used up at the location of the notch. The authors (Castel *et al.*, 2000) also pointed out that the load required to rupture the bar at this notched section may not necessarily be the weakest point of the bar, and so an apparent increase in ultimate load is noticed.

Fang *et al.* (2004) conducted a study to investigate different degrees of reinforcement corrosion and how it affects the concrete-steel bond. The experiments

were designed to evaluate ultimate bond strength and free-end slip by subjecting the specimens to a concentric pull-out test.

Forty, 140 mm x 140 mm x 180 mm plain concrete specimens were cast into moulds with one 20 mm diameter, either smooth or deformed bar having yield strengths of 289.6 and 350.9 N/mm^2 respectively. Variations of specimens were also created for each of the smooth and deformed bars with the addition of 6 mm diameter stirrups. The concrete had an average 28 day compressive strength 52.1 MPa. The bars were thoroughly cleaned and de-scaled prior to embedding them into the concrete. After 28 days of curing, the specimens were subjected to accelerated corrosion.

The accelerated corrosion process used consisted of applying a direct electric current to the steel bar. The specimens were immersed into plastic containers containing a 5% NaCl solution for three days prior to the electric current being applied. The current direction was set-up so that the positive terminal was directly connected by a wire to the end of the steel bar, thereby allowing the steel to act as the anode, while a stainless steel plate immersed into the same plastic tank was connected to the negative terminal and acted as the cathode. The DOC was determined based on Faraday's law which relates the amount of corrosion as a function of time, current and potential.

The concentric pull-out test was used with a loading speed of 0.004 mm/s for slip $\leq$ 2 mm and of 0.02 mm/s for slip > 2 mm. A crack opening displacement gauge measured the slip at values $\leq$ 2 mm and an LVDT measured the displacement values

throughout slip range. The strain monitoring of the steel bars ensured that the steel bars did not yield during these tests.

After the pull-out tests were completed the calculated DOC was compared with the measured DOC by removing the bars from the specimen, cleaning them and weighing them. It was stated that in general, calculated corrosion level values were lower than the measured ones. This was attributed to the permeability of the concrete playing a major role in the facilitation of the corrosion process; this property of the concrete was not accounted for in the design DOC calculations (Fang *et al.* 2004). Furthermore, due to the porosity and other factors related to the randomness of the aggregates dispersed in the concrete mix, generally the longer that the specimen was submerged in NaCl, the closer the theoretical and measured values should have been due to a more even and complete diffusion of the chloride to the bar surface. During the early stages of corrosion the electrical resistivity increased (first quickly then slowly) to a maximum value after which fine surface cracks began to appear and then the electrical resistivity dropped drastically to a minimum constant value. The initial increase might be partially attributed the crack filling effect of the corrosion products at the stage when the concrete could still withstand the internal expansive stresses without bursting or cracking.

For deformed bars without stirrups considerable degradation in free-end slip behaviour was noted as the DOC increased, resulting in a substantial decrease in bond strength. At a 9% level of corrosion the bond strength had reduced to approximately 33% of the control sample result. It was noted that, also as seen by others, when the corrosion

level was low enough for the concrete to sustain the internal expansive stresses imposed on it by the products of corrosion, the bond strength increased. This was most likely due to the increased confinement pressure. For specimens tested with stirrups, the results indicated that the DOC had little effect on the bond strength. The authors noted only a 12% decrease in bond strength at a corrosion level of 6%. This was attributed to the stirrup effect of providing sufficient confinement to the main reinforcing bars thereby maintaining relatively higher levels of bond strength.

The effect of corrosion on smooth bars showed an expected increase in bond strength up to 2.5 times the bond strength of non-corroded control samples, at levels of corrosion between 2 to 4%. Conversely, after a critical value of DOC was exceeded the smooth bar specimens cast without stirrups lost bond strength rapidly. The initial increase in bond at low DOC levels was due to the increased confinement pressure of the corrosion products as described earlier, but also to the increased roughness of the bar surface area and hence increased frictional resistance at the steel-concrete interface. As expected, the addition of stirrups led to an increase in the bond strength as the corrosion level increases.

In general longitudinal cracking was noted on the samples with much smaller cracks appearing on specimens with stirrups as compared to specimens without stirrups. Generally, deformed bars experienced ultimate bond strengths of 3.5-6.9 time that of smooth bars.

It is important to note that while the concentric pull-out test provides a reasonable indication of the bond characteristics, it does not accurately replicate actual bond failure mechanisms such as cracking, slitting of the concrete and bar slip (Almusallam *et al.* 1996). This is due to a few reasons which are intrinsic to the testing apparatus and procedure (Almusallam *et al.* 1996), namely:

- In actual flexural conditions when the steel-concrete bond is being stressed, the surrounding concrete is in tension, whereas during the concentric pull-out test, the confining concrete is in compression; which can eliminate the presence of tensile cracking and consequently appear to increase the bond strength by slowing down the loss of confinement due to tensile cracking.

- This type of test also forces the peak bond stress value to move along the bar ahead of the slip front, which is not characteristic of actual conditions.

- Furthermore, it is suggested that this type of test does not account for the added benefit of the bond strength combined with the added benefit of the strength of the surrounding concrete itself.

It was noted by Almusallam *et al.* (1996) as described above that while the concentric pull-put test is rather simple, quick and inexpensive; its simplified mechanics may not produce bond strength characteristic results which would truly quantitatively represent what could be expected in a real structural beam experiencing actual shear and bending forces.

Almusallam *et al.* (1996) conducted research to consider the effects of differing degrees of corrosion on bond failure between the steel bar and confining concrete interface, while applying the results to the flexural performance of beams and slabs. Firstly, Almusallam *et al.* (1996) defined three stages of concrete cover deterioration based on maximum crack width: pre-cracking (0-4% DOC), cracking (4-6% DOC) and post-cracking (>6% DOC).

152 mm wide x 254 mm deep x 279 mm long specimens were designed and constructed with standard portland cement concrete with a 28 day compressive strength of 30 MPa. The bond was tested on a 12 mm diameter deformed bar, with an embedment length of 102 mm chosen to avoid yielding. To further ensure bond failure, the concrete beam was designed and constructed with both compression reinforcing and stirrups to resist compression and shear failure respectively without influencing the pull-out loads.

The overall structural test procedure used was the cantilevered bond test, under monotonic static loading. Bar slip was measured using an LVDT on each end. Based on Almussallam *et al.*'s review of different bond test methods they chose the cantilevered bond test for the following reasons (Almusallam *et al.* 1996):

- This test method subjects the bar and the concrete to a more realistic bond stress scenario.

- This test method allows both the concrete and the steel bar to experience similar tensile strains; which follow actual strain distributions reasonably accurately.

- External shear and bending moments are induced onto the specimen in this test method as in actual structures.

- It is relatively easy to change the failure mode, by altering the test mechanics and geometry, thereby changing the relationships between bending, shear and bond forces.

- The specimens are generally smaller and more cost effective than full size beam specimens.

- There is flexibility in the number of bars cast into the specimen.

- The undesired effects (for testing purposes) of external reinforcing at the supports interrupting the natural bond stress development and distribution; is avoided.

To induce and promote accelerated corrosion, a constant current of 0.4 A was applied to the steel bar, with the entire specimen being partially submerged in water. A stainless steel plate in the glass fibre tank acted as the cathode. Calibration curves were plotted to determine the relationship between the DOC and duration of accelerated corrosion. The DOC was measured based on the gravimetric weight loss of the steel bars. Neither the calibration curves nor the mathematical relationship was provided as part of the article. Since the mass loss of the bars would not be known until the specimens were destroyed during testing and then cleaned, the DOC in each specimen was not known prior to the structural testing.

The results indicated that the ultimate bond strength increased by ~ 17% and slip decreased up to 4% DOC (pre-cracking). Almusallam *et al.* (1996) attributed this to increased bar volume and roughness thereby increasing the confinement pressure without yet inducing cracking. This trend was also observed in other studies (Mangat and Elgarf, 1998), but the DOC level at which this increases stops and a decrease in bond strength begins, are different. At the onset of the cracking phase the bond strength decreased gradually up to ~ 5% DOC, after which the bond strength decreased quickly. Specifically, at ~ 7% DOC the residual bond strength was at 35% of the 0% DOC value.

Immediately after the onset of corrosion cracking bond strengths of 103% were attainable because of the mechanical interlocking forces generated on the concrete by the rib on the rebar, which hadn't yet degraded sufficiently to allow large slipping. At the DOC of ~ 12% the failure mode changed from brittle failure of the concrete surrounding the bar, to a more constant continuous slip. This marked the DOC at which significant degradation of the ribs on the steel bars had occurred thereby eliminating any positive interlocking effects. At this DOC, significant cracking had occurred and so the confinement pressure was substantially reduced, thereby lowering the bond strength. Gravimetric analysis of the rebar showed that at 7% and 12% DOC, the loss of the rib profile was ~ 45% and ~70% respectively.

At a critical crack width of 0.3 mm, the loss in rib profile was ~ 25%, which corresponded to a DOC of ~ 4%. From this it was stated that once substantial cracking

has occurred, very little additional corrosion is required to greatly reduce the bond strength.

3.1.3 Induced corrosion method

The work presented by Mangat and Elgarf (1998) focused on the failure of corrosion reinforced concrete members due to the loss of critical bond strength at the interface between the embedded reinforcing steel and the confining concrete. This loss was primarily caused by a loss of confining pressure on the steel bars due to concrete cracking.

The most common test method used to evaluate the bond strength is the pull-out test. This test method applies a large concentrated unidirectional in-plane load on a bar embedded in a concrete sample and measures the force required to be overcome to pull-out the bar (bond strength). Mangat and Elgarf (1998) point out two limitations with this test procedure. Firstly, they state that the stress distribution along the bar length is not uniform due to the concentration of stresses at the point of load application. Secondly, in practical applications, the load is carried by the reinforced concrete which transfers the internal forces to the reinforcing steel via the bond interaction at the interface, where as in the pull-out test where the direction of load transfer is reversed, from steel to concrete (Mangat and Elgarf, 1998). A more accurate, yet significantly more complex way of evaluating bond strength is by use of a two part hinged concrete beam specimen, which is a RILEM (Reunion Internationale des Laboratoires D'Essais et de Recherches sur les Materiaux et les Constructions) method for creating the beam

specimen and testing. For further information on this method and the exact specimen construction details, the reader is directed to Mangat and Elgarf (1998). For practical testing purposes, it is important to realize that this method allows the beam bond to fail in more realistic conditions by bending under flexural loading, with an even stress distribution.

Mangat and Elgarf used a slightly modified version of the RILEM test procedure for their work, with the overall beam geometries being 100 mm wide by 150 mm deep with and overall length of 910 mm. Two 10 mm diameter bottom bars with yield strength of 520 MPa were used. The high yield strength bars coupled with the minimum embedment length required to generate full bond strength, helped to ensure that the failure was in the steel-concrete bond. The concrete mix was ordinary portland cement and aggregates to give a 28 day compressive strength of 45 MPa, and the water to cementing ratio was 0.5. Sodium chloride was added to improve conductivity. The moulds were removed twenty four hours after pouring, and the specimens were allowed to cure for 14-18 days at 20°C and 90% relative humidity, after which the specimens were transferred to the accelerated galvanic corrosion apparatus for time spans ranging from 1 – 7 days based on the level corrosion desired, followed by reinsertion into the initial curing environment for the period of time remaining. All samples were tested 28 days after casting. The accelerated corrosion apparatus consisted of a direct current power supply with the positive terminal being connected to the reinforcing bars acting as the anodes and the steel tray containing the 3.5% NaCl solution acting as the cathode.

The accelerated corrosion procedure described by Mangat and Elgarf (1998) is referenced by many researchers in other accelerated corrosion test programs, and so the derivation and theory based on Faraday's law, as derived by Mangat and Elgarf (1998) will be presented as follows:

$$\Delta\omega = \frac{A_{Fe} I t}{ZF} \tag{3.2}$$

where

$\Delta\omega$ is the metal weight lost due to corrosion

A_{Fe} is the atomic weight of iron (56 g)

I is the corrosion current (amps)

t is the elapsed time (sec)

Z is the valency of the reacting electrode, in this case 2 for iron

F represents Faraday's constant (96,500 amp·sec)

Alternatively, the metal weight loss can also be expressed as;

where $\Delta\omega = a\delta\gamma$ (3.3)

a is the rebar surface area before corrosion (cm^2)

δ is the material loss (cm)

γ is the density of the material (g/cm^3), note: for iron $\gamma = 7.86\ g/cm^3$

The corrosion current, I, can be expressed as;

$$I = i\,a \tag{3.4}$$

where

i is the corrosion current density (amp/cm^2)

substituting equations (3.3) and (3.4) in equation (3.2) yields

$$\delta = \frac{A_{Fe}\,it}{\gamma ZF} \tag{3.5}$$

substituting the known values of γ, A, Z and F into equation (3.5) and defining a new variable R such that;

$$Rcr = \frac{\delta}{t} \tag{3.6}$$

setting t equal to 1 year (31,536,000 sec) gives;

$$Rcr = 1156\ i \text{ (cm/year)} \tag{3.7}$$

Therefore, for an applied current density of 1 mA/cm^2 a given bar would corrode at a rate of 11.56 mm/year. We can then apply this corrosion rate to the following formula which gives the degree of corrosion after a given time, t, as follows;

$$DOC = \frac{2(Rcr)t}{D} x100 \tag{3.8}$$

where

DOC is the degree of corrosion (%) (expressed as a percent reduction in bar diameter)

Rcr is the corrosion rate (mm/year)

t is the time since initiation of corrosion (years)

D is the initial diameter of the reinforcement bar (mm)

Mangat and Elgarf (1998) tested two bars at each of 0%, 0.3%, 0.4%, 0.5%, 1.0%, 2.0% and 5.0% degree of corrosion.

The flexural-bond testing was done under four-point loading and the resulting load-slip curves were plotted. Similar to other works, in order to eliminate the possibility of any shear failure, the shear zones were externally reinforced with steel collars. A loading rate increasing by 5 kN every 30 seconds was applied, with the load being held constant between increments. The resulting bar slip was measured by LVDT's at the beginning and the end of each increment. The specimens were loaded until bond failure occurred.

Measurements of the corrosion induced cracking showed that up to a 0.4% DOC the maximum crack width did not exceed 0.05 mm; however there was a drastic increase in the maximum crack width from 0.4 to 0.5% DOC, indicating that a threshold stage had been passed.

The load versus free end slip curves showed that at DOC's from 0% up to and including 0.4%, no free-end slip was observed prior to the complete bond failure. Hence the steel to concrete bond was unaffected by DOC $\leq$ 0.4%. Conversely, above 0.4% DOC there were large free-end slips which commence at the onset of loading and the rate of slip increases with increasing DOC. Mangat and Elgarf (1998) described the process of bond breakdown as a three step process:

- There was a loss of mechanical interlocking due to the corrosion of the steel ribs on a typical deformed steel bar. This resulted in the initiation of free-end slip at relatively low loads.

- There was a loss in frictional resistance between the steel and concrete interface due to the flaky and weak layered type structure of the corrosion products. This was shown in the testing to be represented by the linear increase of free-end slip with increasing load.

- The opening of cracks and subsequent loss of confinement pressure resulted in large free-end slip values for relatively constant load. This was seen on the load versus free-end slip graphs as a nearly constant line of free-end slip at the maximum load. It was also somewhat apparent in this last phase that as the DOC is larger, the load values seemed to decrease with increasing free-end slip.

The maximum load was defined as the point at which the free-end slip increased sharply without significant increase in the applied load. Based on the assumption that the bond stress is uniform over the entire bond length then the bond strength was calculated.

The resulting bond strength values were plotted against the DOC, and the results show that for DOC < 0.4% that there was actually an increase in bond strength (~ 25%) due to the expansive forces developed because of the products of corrosion. At DOC's >0.4% the bond strength decreased with increasing DOC. While other tests show similar increases in bond strength at low DOC values, there is some discrepancy as to what extent the increase in strength will be and what influence the corrosion rate has on this behaviour. The tensile stress in the steel bar was also calculated. The calculation verified that in fact the maximum tensile stress was less than the maximum yield stress of the bars; this verified that the bars were able to develop full bond strength without tensile failure. Similarly, for beams with a DOC $\leq$ 0.4%, no free-end slip was recorded until total bond failure, suggesting a brittle type of failure. For higher DOC the free-end slip increased with the DOC.

The results and theory described in this report, in particular the accelerated corrosion theory, has been used and referenced in many experiments using accelerated corrosion techniques to test reinforced concrete beams in flexural loading. The effect of beginning accelerated corrosion prior to the 28 day curing mark, raises questions as to what influence the sudden introduction of corrosion products to relatively fresh concrete is, particularly in terms of the interface bond. Furthermore, the specimen construction

and test procedure is difficult and highly specialized, making replication somewhat difficult.

El Maaddawy and Soudki (2003) conducted experiments to assess the effectiveness of the commonly used impressed current technique for accelerating corrosion in steel reinforcement. More specifically, they investigated the effect of varying current densities with respect to strains induced in the concrete by corrosion products, crack width due to corrosion and the actual degree of mass loss of steel cross section as compared to the commonly used theoretical values calculated based on Faraday's law.

Four groups of three specimens each of normal strength 150 mm x 250 mm x 300 mm reinforced concrete prisms were subjected to accelerated corrosion at impressed current densities of 100, 200, 350 and 500 $\mu A/cm^2$ and corresponding times of corrosion exposure of 815, 766, 380 and 306 hours, respectively. Each specimen contained two 11.3 mm diameter deformed, 410 MPa (yield stress) bars with 25 mm of cover. The specimens were cast with 5% NaCl by weight of cement mixed into the matrix. The reinforced concrete specimens were cured for one week in 100% relative humidity and then for an additional week in atmospheric conditions. This curing process was followed to control moisture loss and consequently prevent premature shrinkage and cracking. After the second week of curing, the accelerated corrosion procedure was initiated.

The corrosion current was impressed by a direct current power source which self adjusted to provide a constant current. Each group of three specimens was connected

in series so that the reinforcing steel was connected to the positive terminal and 6 mm stainless steel bars cast into the concrete as well were connected to the negative terminal to serve as the cathode. The specimens were kept moist throughout the corrosion process by means of a wetted burlap cover placed over each sample. Strain was measured on the surface of the concrete prisms and the rebar weights were calculated before and after the experiments (after proper cleaning procedure following ASTM G1-90) once the theoretical time to reach the designed DOC was reached.

Maaddawy and Soudki (2003) produced the following conclusions from their work:

- Actual steel mass loss based on gravimetric analysis showed very good agreement to the theoretical calculated values based on Faraday's law, for current densities ranging from 100 to 500 $\mu A/cm^2$ and within the tested steel mass loss range of 4 to 7.27%.

- At low mass loss values of up to 0.8% the effect of current density was negligible. However as the level of corrosion increased, then current densities greater than 200 $\mu A/cm^2$ produced significant concrete strain. This was attributed to a larger current density applying a more concentrated deposit of corrosion products around the bars over a shorter period of time thereby not allowing for any diffusion of the corrosion products through the pore structure.

- For specimens exposed to the same final DOC, the higher the current density the more significant the crack width became. This was again attributed to the concentration of corrosion products experienced during high level of current density, as described above. All corrosion cracking that appeared was parallel to the steel reinforcing bars, and the current intensity did not have any influence on the cracking pattern.

Finally, Maaddawy and Soudki (2003), suggested not to vary the current density over one set of experiments to achieve different DOC, but rather adjust the exposure time accordingly. They also suggested that further work was needed at higher DOC (above 7.27 % mass loss of steel), because they suspect that the increased presence of the corrosion products at higher corrosion levels may hinder the diffusion process and hence affect the accuracy of Faraday's law in predicting the theoretical corrosion values.

3.1.4 Flexural response of beams with corroded reinforcement

Mangat and Elgarf (1999) investigated the flexural behaviour of 111 reinforced concrete beams. The beams were exposed to accelerated corrosion damage and tested under flexure. The specimens were all 100 mm wide by 150 mm deep and 910 mm long. The majority of the specimens were reinforced with 2-10 mm diameter bars placed in the tensile zone of the beam specimen. The bars were 1100 mm long and were bent at the ends to provide an anchorage 'hook end' in the concrete. 25 mm of cover was provided, measured from the bottom of the beam to the centroid of the steel bar cross-section. A few of the specimens were constructed with stirrups; however the majority of the

specimens were externally reinforced with shear collars. External reinforcing was chosen as opposed to stirrups, because the presence of the stirrups interfered with the accelerated corrosion process and made controlling the applied DOC nearly impossible (Mangat and Elgarf, 1999).

The specimens were cast using ordinary portland cement and had a 28 day compressive strength of 40 MPa. The yield strength of the reinforcing bars was 520 MPa. In order to more readily facilitate the corrosion process, 1% by weight of cement sodium chloride was added to the concrete mix. The specimens were cast and covered with a polyethylene sheet for 24 hours. After demoulding the specimen groups were cured in water for durations ranging from 10 days to 1 year. After the initial curing time, the beams were subjected to differing DOC for the associated time period (12 to 384 hours) as described by Faraday's Law and shown in Mangat and Elgarf (1998). After the induced corrosion phase, the specimens where returned to ensure they all cured for at least a minimum of 28 days before flexural testing. The accelerated galvanic corrosion process was induced by immersing the specimens in a plastic tank filled with a 3.5% NaCl solution which acted as the electrolyte. The positive terminal of a power supply was connected to each of the two rebar and the negative terminals were connected to an external cathode within the same solution. Through different reinforcing configurations, DOC's investigated were, 1.25%, 2.5%, 3.75%, 5.0%, 7.5% and 10% (reduction in bar diameter). Within these DOC's investigated, the effects of applying different corrosion rates of 1, 2, 3 and 4 mA/cm^2 were also investigated. More details for the testing matrix can be found in Mangat and Elgarf (1999).

The flexural tests were conducted in four point bending with external shear reinforcement in the form of steel sleeves provided at the shear zones; thereby ensuring a bending failure around mid span. The load was applied at rate of 5 kN/min, and the deflections were recorded with a linear variable displacement transducer.

The load versus deflection results indicated that as the DOC increased the strength of the beams decreased. When comparing the different corrosion rates to achieve the same DOC, there was little change in the load-deflection curves for differing corrosion rates, up to 2.5% DOC. When considering flexural capacity, the corrosion rate did not appear to have a significant influence on the residual capacity up to approximately 5% DOC; however at higher DOC's the flexural capacity dropped with increasing corrosion rates, implying that for an accurate simulation it is best to use the lowest practical corrosion rate to achieve the desired DOC.

As described by Mangat and Elgarf (1999), the corroded beams failed by bond failure at the steel to concrete interface. At load levels between 60% and 70% of the ultimate load, horizontal cracking began to occur along the tensile reinforcement, and at approximately 90% of the ultimate load large tension cracks appeared in the pure bending zone, followed by immanent failure. The bond failure was further explained by the authors such that as the loading increased and the bond began to fail, the load transfer capability from the concrete to the steel became concentrated at the hooked ends of the tensile bars. This increased until the anchorage at the ends could no longer be maintained, which was evident in the form of concrete damage at the anchorage points

right before failure. It is important to note that the hooked portions of the bar were not corroded because they extended out of the corrosion tank apparatus. It was also noted that the presence of shear reinforcement can provide a beneficial effect in that its presence can help maintain confinement provided by the stirrups. They also further concluded that the primary reason for a reduction in the flexural capacity of the beams in this study was due to the bond strength reduction and not the loss in steel cross sectional diameter due to corrosion causing yielding. Based on another group of specimens pre-cured for differing periods ranging from 15 days to 1 year before inducing corrosion, there was no appreciable effect on the flexural capacity. This led to the conclusion that the age of a reinforced concrete structure before corrosion begins may not necessarily have a significant impact on the flexural capacity, once a substantial degree of corrosion has taken place.

The accelerated corrosion technique while effective at accurately being able to provide rapid corrosion of embedded steel members does have an inherent flaw when compared to real situations and can affect the residual flexural strength of a member. In fact the corrosion would progress gradually over an extensive period of time, thereby allowing the for the gradual dissipation of some of the corrosion products in to the surrounding pore structure of the concrete. This would reduce the rapid build-up of the radial stresses at the bond interface and slow down crack formation, propagation and de-bonding. The longitudinal cracks that formed on the bottom and side surfaces of the beam were evidence of the radial expansive forces created by the products of corrosion.

The maximum crack widths were 0.1 mm, 0.2 mm, 0.3 mm and 0.4 mm at DOC's of 2.5%, 3.75%, 5% and 7.5% respectively. It was also found that the widths of the cracks were dependant on the corrosion rate; as expected due to the increased rate at which the products of corrosion are deposited on the steel bars and expansive radial stresses are developed within the confinement zone (Mangat and Elgarf, 1999). Interestingly, at low DOC of <0.5%, the increased expansive radial stresses can lead to a slight increase in the flexural resistance of the member (Mangat and Elgarf, 1999).

Mangat and Elgarf (1999) concluded generally, that; at DOC's exceeding 2%, the bond strength decreases to about 60% of the uncorroded control sample values. At DOC's of 10% the residual strength reduced to 25% of the uncorroded control sample values.

3.2 Behaviour of RC beams at fire temperatures

The behaviour of steel reinforced concrete beams at elevated temperatures is a complex phenomenon that includes many different parameters. Some of these confounding parameters include the uniformity of the temperature distribution within the specimen and its effects on component expansion, deflection, cracking, and when considering flexural members, the steel to concrete bond interface. As the concrete is heated it undergoes dehydration and thermal expansion. These two processes along with the application of service loads lead to the development and propagation of cracking of the concrete. As the temperature penetrates the concrete to the level of the steel the mechanical properties of the steel reinforcing bars also begin to degrade rather rapidly

with an increase in temperature, thereby reducing the strength and stiffness of the steel. Furthermore, the thermal expansion of the steel coupled with the confining concrete degradation will lead to loss of the interfacial bond between the steel reinforcing bars and the concrete. In flexural members when the tensile steel reaches its yield strength or the steel to concrete bond degrades significantly, failure can occur.

To better understand the overall effects of high temperatures on steel bar reinforced concrete beams, a number of published experimental studies were reviewed. Firstly, El-Hawary *et al.* (1995) and Ellingwood and Lin (1991) provided comprehensive test results on the overall effects of fire on the flexural behaviour of reinforced concrete beams. Since the concrete cover protects the reinforcing bars from exposure to fire conditions, the effects of varying the thickness of the concrete cover are further examined by Shi *et al.* (2004). In order to understand the combined effects of the steel and concrete together, it becomes necessary to understand the effects of high temperature on the interfacial bond between the steel and the concrete. Morley and Royles (1979) compare the works of various authors with respect to bond performance at elevated temperatures for both plain and deformed bars. A study that is touched on in Morley and Royles (1979) is further examined in greater detail which is the work on bond strength at high temperatures conducted by Diederichs and Schneider (1981). The majority of the tests for bond strength are done using the 'direct pull-out test'. However, El-Hawary and Hamoush (1996) point out that this test may not accurately describe the interaction between the steel and the concrete, and instead propose studying the bond shear modulus. Post-fire exposure residual strength is investigated by Khan and Royles (1986) and also

Bingöl and Gül (2009); the latter of which examines the effects of differing cooling regimes. Lastly, the review of Dwaikat and Kodur, (2008) which presented and summarized the effects of thermally induced axial restraint forces in reinforced concrete beams during a fire exposure.

3.2.1 Effect of elevated temperature on RC beams

The study conducted by El-Hawary *et al.* (1996) was an experimental investigation of the mechanical behaviour of reinforced concrete beams after exposure to fire after 0, 30, 60 and 120 minutes of exposure. Four 120 mm wide x 200 mm deep x 1800 mm long, portland cement reinforced concrete (25 MPa) beams were tested. The beams were reinforced with 2-10 mm diameter main longitudinal reinforcements, 2-10 mm diameter compression reinforcement, as well as 8 mm diameter stirrups spaced at 80 mm apart. The beams all had 20 mm of cover thickness. The beams were cured in the laboratory for 28 days under wet conditions.

The fire chamber was a custom built furnace designed to specially fit the beam specimens. Forty days after curing the specimens were placed in the furnace. The specimens were not loaded during the fire testing, and the temperature was controlled to follow a non-standard fire curve. The time-temperature curve is presented in El-Hawary *et al.* (1996), and it shows a temperature increase of up to 600°C in approximately 5 minutes and then a constant temperature of ~ 650°C for the remainder of the test. Immediately after the furnace exposure, the beams were sprayed with water and cooled. Once cooled, the beams were subjected to four-point loading in equal increasing 0.5 ton

(453 kg) increments until failure. The deformations, mid-span deflections and cracking patterns were recorded at each load increment.

As expected, the results showed that as the fire exposure time increased the strength of the beams in flexure decreased and the mid span deflections increased. In particular random flexural cracks were observed in all of the specimens after the first 10 minutes of exposure corresponding to a fire temperature of ~ 500°C according to the time-temperature curve. It was noted by El-Hawary *et al.* (1996) that after the beams were sprayed with water the cracking increased; perhaps perpetuated by a rapid change it temperature, a thermal shock, causing excessive contraction forces within the cement paste. The ultimate loads for the beams exposed to 30, 60 and 120 minutes of fire exposure were 11.8%, 19.3% and 38.7% less than the unexposed reference sample, respectively. The mid-span deflection for the exposed beams increased between 1.9 to 3.4 times the deflection for the unexposed control sample at approximately 61% of the ultimate load. El-Hawary *et al.* (1996) also stated that 'the effect of fire on concrete is greater than its effect on the reinforcing bars.' They made this statement based on the measured compressive and tensile strains in the concrete and the steel bars respectively. At approximately 61% of the ultimate load, the concrete compressive strains measured between 2.6 and 9.5 times that of the unexposed reference sample, while the measured tensile strains were only between 1.3 to 1.6 times that of the reference sample at the same load. The estimated compressive strength also decreased as a function of increasing fire exposure, to 42% to 73% of the reference beam value.

When considering the results obtained in this experiment it is important to be conscious of the experimental parameters and the consequent application of these results to real structural fire scenarios. Firstly, when a reinforced concrete structure is subjected to a real fire, there are some loads (while less than ambient design loads) that will still be acting on the structure. The fact that these samples were not loaded while exposed to the fire, may give slightly un-conservative results. Bond was not discussed in this report; however, it was acknowledged that significant bond strength degradation can occur at increased temperatures. The cooling method used in this experimental procedure was realistic and applicable to a real structure fire scenario, as the hot members could be exposed to rapid water cooling during fire extinguishment. Therefore, the effects caused by this rapid temperature gradient, such as increased cracking, were taken into consideration. The effects of different cooling regimes are further examined in Bingöl and Gül (2009).

Ellingwood *et al.* (1991) conducted a study to investigate the flexural and shear behaviour of a reinforced concrete beam during a fire. Part of the theory behind their investigation was that stresses and strains caused by thermal conditions may cause a concrete member to crack and spall, therefore leaving less cross sectional concrete area to provide resistance. This may cause a reinforced concrete beam to fail in shear (Ellingwood *et al.*, 1991).

Six reinforced concrete specimens were cast using normal portland cement concrete and deformed reinforcing bars were used. All of the specimens consisted of a

6.1 m span and a 1.8 m cantilevered section. Beams 1, 2, 3, 5 and 6 had cross-sectional measurements of 228.6 mm (9 in.) by 533.4 mm (21 in.). Beam 4 had a cross section of 254 mm (10 in.) by 609.6 mm (24 in.). Beams 1, 2, 4 and 5 had cover thicknesses of 38 mm; while beams 3 and 6 had covers of 57 mm. Beams 1-4 (inclusive) were exposed to the standard ASTM E119 (2009) time-temperature curve, while beams 5 and 6 were exposed to a short duration high intensity fire which is characterised by a rapid temperature increase up to approximately 1016°C in approximately 45 minutes, followed by a decay period, which cooled to 316°C at 100 minutes from initiation (see Figure 3-1). Using the geometry of the loading, Ellingwood *et al.* (1991) simulated a span of a continuous beam. They did this based on theory described by Lin *et al.* (1987). The application of a load on the cantilevered section allowed the simply supported section to undergo moment redistribution, which is a beneficial mechanism (Ellingwood *et al.* 1991) that typically happens in realistic multi-span structures. A constant load was applied to the simply supported span throughout the duration of the fire exposures. The specimens were instrumented with approximately 75 thermocouples to measure the temperatures of the concrete and the steel during the exposure.

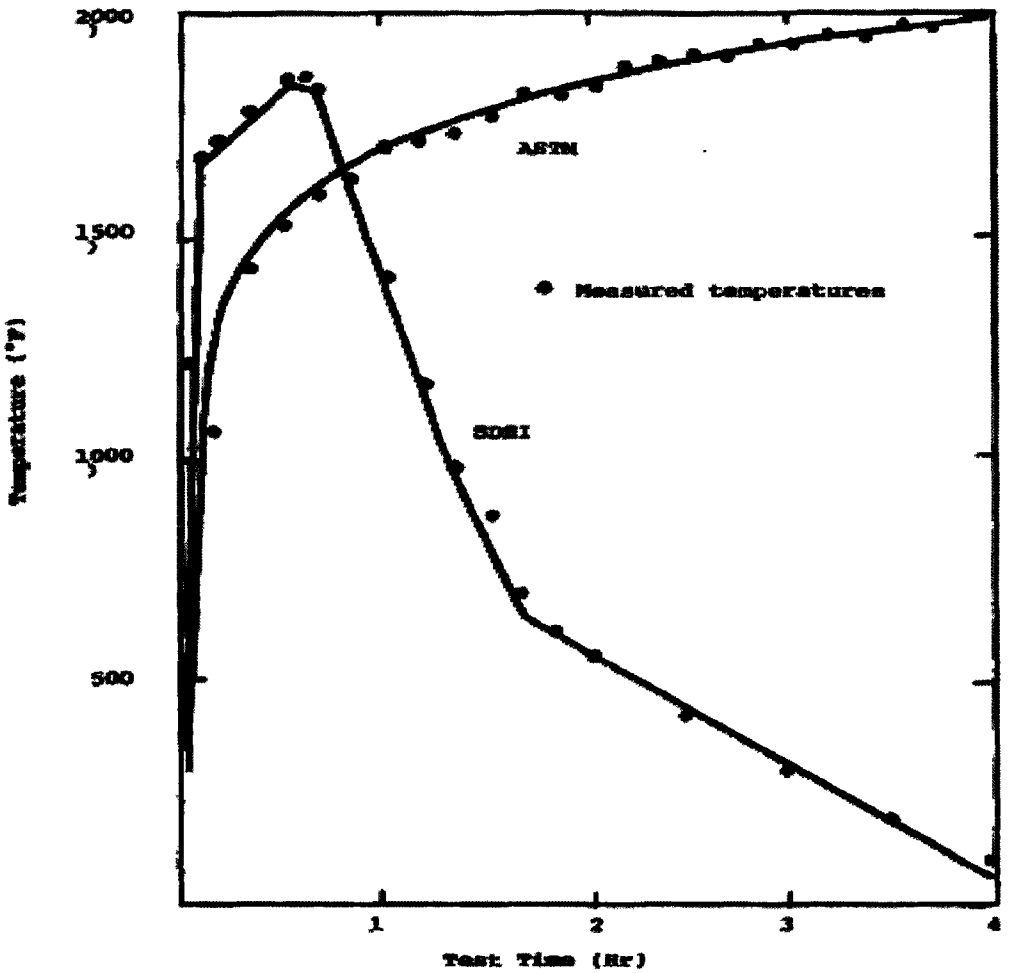

Figure 3-1: Time-temperature curves for the ASTM E119 and the Short Duration High Intensity Fires used in Ellingwood *et al.* (1991). (Taken from Ellingwood *et. al.*, 1991).

The concrete's temperature contours at the cross-section shows that for the ASTM E119 (2009) fire and the short duration high intensity fire after 3 hours that the temperatures contours of the ASTM E119 (2009) fire were significantly higher and the contours took on an open loop shape as opposed to the short duration high intensity contours which were a closed loop. This closed loop contour of the short duration high

intensity fire is because after 3 hours the temperature had decreased to approximately 200°C. Ellingwood *et al.* (1991) also noted that the internal concrete temperatures during the short duration high intensity exposure scenario continued to rise even after the fire began to decay and the exterior surface had cooled. In general the temperature within the steel reinforcing bars followed the same general temperature gradients with both temperatures increasing at a similar rate for both types of exposures. The tests were terminated when the deflection rate became 2.5mm/min; as this was said to indicate imminent collapse. The deflection results indicated that concrete cover had little effect on the deflection of the reinforced concrete beam specimens during the first 3 hours of exposure, regardless of the time-temperature exposure. However, the maximum deflections of the beams exposed to the short duration high intensity fire were 51-76 mm while the ASTM E119 (2009) exposed beams deflected to a maximum of 152 mm. The results of extensive modelling and thermal analysis of the beams in these experiments revealed that none of the beams exposed to the short duration high intensity fire came close to failure during the testing. This was found to be attributed to the fact that although there was a greater amount of thermal strain in the specimen at the beginning of the short duration high intensity exposure, the long decay phase allowed for a more uniform and less intense strain distribution during the cooling phase allowing the effects of heat to stabilize; conversely the ASTM E119 (2009) exposed beams continued to experience increased degradation in their mechanical properties simply due to the unrelenting profile of the time-temperature curve (Ellingwood et al. 1991). Shear cracks were observed in all the specimens as early as 90 minutes into the fire. Flexural cracking

in the beams was observed at approximately 110 minutes into the fire, and progressed. All of the beams failed in flexure and so it was determined that based on the specimen and reinforcing properties and geometries used in this experiment, shear failure of reinforced concrete beams did not appear to be of concern.

The results of this study seemed to suggest as expected that a more realistic fire scenario which includes a decay phase will be beneficial to the concrete member and provide more realistic values when assessing the safety and reusability of a fire damaged reinforced concrete structure. Design fires would provide more useful engineering data when it comes to the real-life situations as opposed the current standard time-temperature curve; however the standardized nature of the time-temperature curves allows for easy comparison between multiple data sets by employing a common fire exposure program.

The experimental program conducted by Shi *et al.* (2004) focused on determining the influence of the concrete cover thickness of a reinforced concrete flexural member. To study this effect, six, 1300 mm long single span, reinforced concrete specimens were cast and tested under various conditions and geometric configurations to study the concrete cover parameter. The geometric combinations of dimensions and cover thicknesses are shown in Table 3-1.

Table 3-1: Specimen geometries for the experimental program by Shi *et al.* (2004).

(Taken from Shi *et al.*, 2004).

Specimen number	Section width b (mm)	Section depth h (mm)	Top concrete cover thickness c' (mm)	Bottom concrete cover thickness c (mm)	Lateral concrete cover thickness c_1 (mm)
TSB2-0	100	180	10	10	10
TSB2-1	100	180	10	10	10
TSB2-2	100	180	10	10	10
TSB2-3	100	180	10	10	20
TSB2-4	100	190	10	20	20
TSB2-5	100	200	10	30	20

Specimen number 0 was tested at ambient temperature to obtain the ultimate moment capacity as a control sample. Specimen number 1 was heated without load to determine the cross-sectional temperature distributions and specimen numbers 2 through 5 were subjected to 50% of the ultimate moment capacity at ambient and were heated on three sides until failure. The specimens were cast with normal portland cement and had an average 28 day compressive strength of 38.95 MPa. The tensile reinforcement consisted of 10 mm diameter plain steel bars with 3.5 mm diameter stirrups.

The beams were loaded in four-point bending in a hydraulic testing machine equipped with an electric furnace. The time-temperature curve applied by the electric furnace differs from the standard time-temperature curve to which it is compared in Shi *et al.* (2004). The main difference between the test curve and the ISO 834 (2002) curve is that the test curve heats up at a significantly slower rate than the ISO 834 (2002). For example at 20 minutes the ISO 834 (2002) curve reached a temperature of 800°C the test

curve was only at ~ 300°C (see Figure 3-2). The internal temperature distribution was recorded using cast in thermocouples.

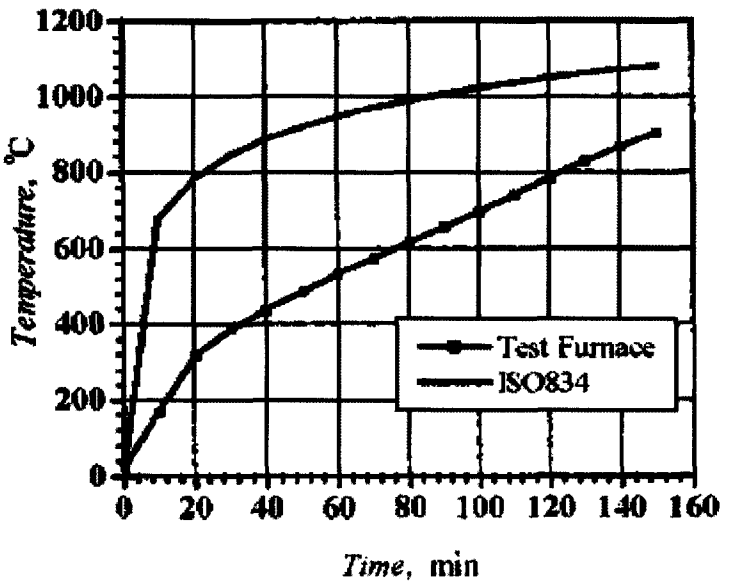

Figure 3-2: A comparison of the time – temperature curve used by Shi *et al.* (2004). (Taken from Shi *et al.*, 2004).

Their test results showed that, at temperatures < 300°C the compressive strength of the concrete itself did not vary appreciably from ambient conditions. However, when temperatures exceeded 300°C, then the concrete compressive strength dropped rapidly with an increase in temperature to a value of ~ 10% residual compressive strength at 900°C.

Similar analysis of the steel rebar showed that at temperatures ≤ 300°C, the yield strength did not decrease rapidly; however at temperatures >300°C the yield strength dropped drastically to a residual value of 5% at a temperature of 800°C .

Temperature readings along the specimen showed that the cross sectional temperature distributions were non-uniform and tended to be symmetrical about the midsection of the beam width. The temperature gradients nearest the top of the specimen were smaller because the transfer of heat to this upper level away from the heat source is governed by conduction. Shi *et al.* (2004) also deduced that concrete cover has little effect on the member deflection at relatively low temperatures, but as the temperature gets higher the beneficial effects on deflection are evident. They also stated that excessively increasing the bottom or lateral cover thickness did not necessarily improve the fire resistance of the member. They also showed that the critical value for loss of steel strength occurs at 527°C regardless of cover thickness. The presence of cracks had a great influence on the temperature distribution within the cross section and consequently as the cracks progress, the cover effectiveness was reduced.

3.2.2 Effect of elevated temperature on bond

Morley and Royles (1979) made a comparison of several other authors' works on the subject of fire exposed reinforced concrete. The authors cited in this review are taken directly from Morley and Royles (1979) publication.

Work conducted in Japan by Harada *et al.*(1971) investigated the residual bond strength after exposure to 20°C, 100°C, 300°C and 450°C on 100 mm diameter, 200 mm long concrete cylinders with an unspecified reinforcing bar diameter. The 26 month old specimens were heated up to the target temperature and held there for 72 hours, after which they were allowed to cool in ambient conditions for 48 hours after which the bond

strength was tested, using the pull-out test. A relatively slow heating rate of 0.5°C/min was used. The results showed that as the temperature was increased the bond decreased to 50% and 10% of the ambient bond strength for temperatures of 100°C and 450°C respectively. The compressive strength of the concrete also decreased to 75% and 60% of the ambient values at temperatures of 100°C and 450°C respectively. This indicated that the bond strength was a more critical parameter than the compressive strength when considering the residual effects of elevated temperature.

Work done by Reichel (1978) to study bond strength using 14 mm diameter bars embedded 300 mm in a 150 mm x 150 mm x 450 mm long concrete prism showed a decrease in bond strength with an increase in temperature. The test specimens were exposed to the ISO 834 (2002) time-temperature curve after 26 weeks of curing. Once the target temperatures were reached the specimens were allowed to cool for 24 hours. The results showed a residual bond strength for deformed bars of 75% and 50% of the ambient strength at temperatures of 500°C and 600°C, respectively. For plain bars at the same temperatures the residual bond strength decreased to 40% and 25% of the ambient value. A main difference between this study and the study by Harada *et al.* (1971) is that the prisms in this study were reinforced with additional steel to prevent premature deterioration of the confining concrete.

Based on their review Morley and Royles (1979) made the following conclusions:

- The rate of temperature rise plays a role in the experimental results in that a fast temperature rise can cause large temperature gradients throughout the specimen

and hence adversely affect its performance through large differential thermal expansion stresses developing. However it is can be argued that a fast temperature rise is more indicative of a real fire, over the long duration of a real fire, the temperature profile at the cross section will approach steady state conditions.

- Many of the researchers' compressive strength values at elevated temperatures also varied widely, and Morley and Royles (1979) attributed this partially to differing concrete mixes and aggregates used. Hence, the concrete mix proportions are important in being able to predict the residual compressive strength of the concrete.
- Morley and Royles (1979) also noted that all of the bond tests performed were some variation of the simple pull-out test, and this may not accurately represent the actual bond failure conditions that may take place in a beam.
- There is also significant scatter in the residual bond strength results obtained by different researchers and Morley and Royles (1979) attribute this to the differences in experimental procedure, the concrete strength, the bar type and diameter, the shape of the samples and the rate of heating.

The objective of Diederichs and Schneider (1981) was to examine the bond strength and bar slip as a function of increasing temperature. 80 mm diameter by 300 mm long cylindrical concrete samples were cast with both deformed (ribbed) and plain reinforcing bars. The cylindrical shape was chosen to promote uniform heating of the

samples. The test specimens were specifically designed to ensure that bond failure happened before yielding of the steel bars by reducing the embedment length by inserting plastic isolation sleeves at pre-determined lengths in the specimens. The specially designed testing apparatus consisted of a pull-out type testing equipment within the confines of a small furnace chamber. The tests were divided into two separate groups: the first group of tests measured the force-slip relationship at constant high temperature and the second group of experiments measured the force-slip data at varying temperatures. In the first group, the specimens were brought up to the desired temperature and held there for 3 hours then tested while at elevated temperature; with the application of a load rate of 1 kN/s. In the second group of experiments, a bond stress was applied at the test onset (20°C), after which the temperature was systematically increased until bond failure occurs. The temperature corresponding to this bond strength loss was defined as the critical bond temperature by Diederichs and Schneider (1981).

For the first test group (with constant high temperature), the results were used to generate force-slip diagrams. For ribbed bars the bond strength deceased slightly for temperatures up to 300°C, however significant loss of bond strength was observed at temperatures >300°C. At a temperature of 800°C the deformed bars showed very little bond strength. The results for the plain (smooth) reinforcing bars showed that the initial surface condition played an important role in the bond performance at elevated temperatures. At temperatures up to 200°C there was little deviation in bond strength from ambient conditions of a severely rusted plain bar. However at 600°C the bond strength was nearly zero. For lightly rusted plain bars the effects of temperature were

much more serious in that by 300°C the bond stress in about 50% of the ambient value and again by 600°C the bond strength was nearly zero. Further conclusions from this group of tests were that for both deformed and plain bars, the affects of high temperature were more evident in the bars as opposed to the concrete strength itself. Furthermore, Diederichs and Schneider (1981) discerned that the bar diameter had no significant effect on the bond performance at high temperatures.

In the second group of specimens (with variable high temperatures) the data obtained were used to generate temperature versus slip graphs for differing degrees of utilization. The degree of utilization indicated what percentage of the bond strength was being used when compared to a sample at ambient conditions (20°C). Importantly, Diederichs and Schneider (1981) pointed out that the apparent slip recorded at temperatures around 400°C in the unloaded (degree of utilization is 0%) condition were a result of the thermal stresses induced between the differing thermal expansion rates of the steel and the concrete. At a degree of utilization of 30%, deformed bars reached a critical bond temperature at failure of 500°C and the plain bars reached a critical bond temperature of 350°C. Diedrichs and Schneider (1981) also stated that the bond temperature was a more crucial parameter since the critical bond temperature can be less than the critical concrete strength loss temperature. In general, as expected the plain bars behaved less desirably then the deformed bars.

El-Hawary and Hamoush (1996) focused on defining a parameter known as the bond shear modulus. The proposed bond shear modulus explicitly accounts for the

interfacial slippage between the concrete and steel, which is not accounted for in the standard pullout test (El-Hawary and Hamoush, 1996).

The experimental program consisted of a series of 100 mm diameter 200 mm long concrete cylinder, with a steel bar inserted into each end of the specimen to an embedment length of 50 mm. The embedment length was determined to be less than what is required to fully develop the bond strength to ensure bond failure as opposed to yielding of the steel bars. The 100 mm long bar diameters tested were, 6 mm, 8 mm and 10 mm in diameter. The specimens were water cured for a period of 28 days, after which they were placed in an oven and heated to pre-determined temperatures of 100°C, 300°C and 500°C. Once steady state temperatures were achieved in the oven, the specimens were held at constant temperature for three different time durations of 2, 4 and 8 hours. After heating, the specimens were cooled, some by gradual atmospheric cooling and some by rapid water cooling. The specimens were then tested by pulling the bars and measuring the load versus elongation for each sample. Three control samples which were not exposed to heating were also tested.

The ultimate load and total elongation at the ultimate load were then used in an analytical model that was developed to calculate the parameter, bond shear modulus. The model considered that the total elongation of the system was represented by the summation of the displacement due to the embedded portion of the bar, the displacement due to the concrete deformation, the displacement due to the interfacial slip of the bar and the displacement due to the stresses in the un-embedded part of the bar (El-Hawary and

Hamoush, 1996). Convergence of the system of equations represented the value of the bond shear modulus.

The combined results of the experimental and analytical studies showed that the bond shear modulus in specimens heated up to 100°C for short durations and then allowed to gradually cool in air displayed a slightly increased bond shear modulus as compared to the control samples. This can be related to the increase in bond strength shown by other researchers in the similar temperature range. This increase was most likely due to an increase in concrete compressive strength within this temperature range (Bingöl and Gül, 2009). Similarly for higher temperatures, the bond shear modulus decreased. El-Hawary and Hamoush (1996) also noted that the reduction in bond shear modulus increased with higher temperature and exposure durations. Finally, the effect of the cooling regime was evident in that similarly to the bond strength tests conducted by Bingöl and Gül, (2009) the bond shear modulus also was considerably lower for specimens subjected to rapid water cooling. The bond shear modulus was found to be independent of the reinforcing bar diameter (El-Hawary and Hamoush, 1996).

3.2.3 Post-fire behaviour of reinforced concrete beams

The research conducted by Khan and Royles (1986) investigated the bond and general behaviour of reinforced concrete beams after a sustained heat exposure. Specifically, they examined the thermal response of the sections, the load-deflection behaviour, the crack development, the bond-slip behaviour and then used the data gathered to calculate the residual flexural strength.

Two groups of specimens were designed; the first group having a cross section of 66 mm wide by 140 mm deep and the second group having cross sectional dimensions of 107 mm wide by 140 mm deep. All specimens were 960 mm long and a clear cover of 25 mm was provided to all of the samples. Within the groups the reinforcing was also varied. Combinations of plain bars and high-yield strength deformed bars were combined to further examine the effect of both types of bars. The diameter of the main bottom steel bars was always 16 mm while variations with 8 mm top bars were also considered. The specimens were designed to ensure tensile yielding of the steel bars and so 6 mm diameter shear reinforcement (stirrups) were also provided. The concrete mix was made of normal portland cement and 19 mm aggregates. Thermocouples were also provided at the cross-section of the specimens as well as at the steel bar to concrete interface. The specimens were cured under a polyethylene sheet for approximately 90 days at room temperature and 60% relative humidity.

The heating was applied by an electric furnace at a rate of 2°C/min. Different specimens were heated to temperatures of up to 800°C. The specimens were held at the desired temperature for one hour to achieve steady state, and then were cooled naturally in ambient conditions for 24 hours. Once cooled, the specimens were tested in four-point loading. Deflection measurements were taken at the two load application points and also at the mid-span using dial gauges. Bar slip measurements were also taken using dial gauges. The specimens were loaded till failure.

The thermal response of the specimen to the heating conditions revealed that as expected, the furnace temperature was always greater than the temperature inside the specimen. Furthermore, the rate of temperature rise within the specimen decreased with increasing depth into the cross-section; which was attributed to the presence of moisture within the concrete.

The deflections recorded showed that as the temperature increased the ratio of load to mid-span deflection decreased. Khan and Royles (1986) noted that the deformed bars were stronger and stiffer as compared to the plain bars. At temperatures up to 200°C the flexural capacity was not decreased, but at 600°C the flexural capacity was reported to be at 50% of the ambient value. The rapid decrease in residual flexural strength at temperatures between 300°C and 500°C was said to follow the same general trends for strength loss of concrete compressive strength, as reported by others, indicating that the deterioration of the confining concrete coupled with cracking and the effects of bond degradation will lead to a rapid decrease in mechanical behaviour in this temperature range.

Visual observation of the test specimens revealed that thermal honeycomb style cracking occurred rather uniformly on all faces of the beam. The cracking appeared to begin at the top and bottom of the specimen and migrated towards the mid-depth of the specimen. Generally, the amount of cracking increased with an increase in temperature. The cracking pattern was consistent with the effects of differential shrinkage caused by the outer layers releasing moisture at a faster rate than the interior of the specimen.

Deflection cracking was present in the shear zones as well as the tensile zone of the specimens. Cracking due to the applied loads began to appear when the loading was at 30% to 50% of the ultimate load. The deflection cracking appeared to follow some of the thermal cracks.

The authors pointed out that the results obtained for the bond-slip behaviour were consistent with pull-out tests that had been done by others. Generally bond strength appeared to increase up to temperatures of approximately 200°C and then decreases with further increase in temperature. At temperatures of approximately 775°C the bond stress appeared to be at 50% of the ambient values.

The following conclusions were drawn from this work (Khan and Royles, 1986):

- At temperatures below 600°C bond-shear was the failure mode, while at temperatures >600°C flexural strength became the failure mode.
- The data showed that bond-slip behaviours in flexural conditions followed the same general behaviours as direct pull-out tests done by others. With the exception that the residual bond strength under flexural conditions was better than the purely tensile conditions of the direct pull-out test. This can be attributed to the concretes beneficial action of providing better confinement pressure in the flexural configuration.
- The overall performance of deformed bars was better than the plain (smooth) bars.

The work undertaken by Bingöl and Gül (2009) focused on the post fire residual bond strength between steel reinforcing bars and concrete. This study was unique in that

it further investigated the effects of natural cooling versus rapid water cooling. The effect of this 'thermal shock' on the bond strength and other residual mechanical properties was investigated.

The specimens were cast with normal portland cement. Two different groups of 20 MPa and 35 MPa compressive strengths were cast. The steel bars were 8 mm diameter ribbed steel bars, installed at different embedment lengths of 6, 10 and 16 cm. With the specimens broken down into two groups by compressive strength and then further broken down into two differing specimen diameter groups and embedment lengths. Three of these samples for each group and sub-group were cooled in air after heating and three were cooled rapidly in water. The test specimens were cured in water, and after 28 days were dried in the laboratory air then heated to the target temperatures. 24 hours after the specimens were cooled by their specific cooling regime, they were tested using the standard pull-out test. Besides control samples tested at ambient conditions, the heated specimens were heated to temperatures of 50, 100, 150, 200, 250, 300, 350, 400, 450, 500, 600 and 700 °C at a heating rate of 12-20°C per minutes and held constant at the target temperature for a period of 3 hours.

Bingöl and Gül (2009) presented the following results of their investigation. Firstly in general as the temperature increased above 150°C the residual bond strength decreased for all embedment lengths. At temperatures between 50°C and 150°C an increase in residual bond strength was observed in the order of 14% and 12% for 20 MPa and 35 MPa concrete respectively; for the 6 cm embedment length under water cooling

condition. The increase in bond strength was attributed to an increase in concrete compressive strength within the same temperature range. At temperatures of 700°C the specimens had lost 89% and 76% of their initial bond strength for the 20 MPa and 35 MPa samples respectively, at an embedment length of 6 cm. The authors noted that due to the short embedment length and significant bond strength loss, the effects of the cooling regimes were negligible.

The 10 cm 20 MPa samples showed increased residual bond strength values only at temperatures of 50°C and 100°C, with a reduction in residual bond strength for all higher temperatures. The 35 MPa samples showed decreasing bond strength for all temperatures except 100°C (Bingöl and Gül, 2009). At 700°C under air cooled conditions the residual bond strength loss values were 72% and 55% for 20 MPa and 35 MPa respectively. For water cooled specimens at 700°C the residual bond strength loss was reported as 74% and 60% for 20 MPa and 35 MPa respectively.

For the 16 cm embedment length, an increase in residual bond strength was observed up to 150°C for the 20 MPa samples and 100°C for the 35 MPa samples; with a reduction in residual bond strength at all higher temperatures. At 700°C under air cooled conditions the residual bond strength loss values were 45% and 44% for 20 MPa and 35 MPa respectively; and similar but slightly higher bond strength loss values at the same temperature under water cooled conditions.

The increase in residual bond strength was related to an increase in the concrete compressive strength at the same temperature range. In general, at temperatures

above 150°C there was a loss of residual bond strength as the temperature increased, with the effects being more pronounced at shorter embedment lengths. The results did show that at the longer embedment lengths (10 cm and 16 cm) tested, the effects of the cooling regime were more evident. Generally, the specimens exposed to rapid water cooling experienced a greater loss in residual bond strength with increasing temperature. This was attributed to the damage caused to the concrete matrix by the rapid thermal contraction of its components when subjected to rapid water cooling, leading to increased damage perhaps in the form of cracking of the concrete and delamination at the steel concrete bond interface.

3.2.4 Thermally induced axial force

Dwaikat and Kodur (2008) used a numerical model to investigate the effects of fire induced restraint effects on reinforced concrete beams. Dwaikat and Kodur, (2008) explained that because, generally, the line of action of the axial restraint force is below the neutral axis of the beam due to higher temperature rise in the bottom of the beam, an 'arch action' is developed which increases the strength and stiffness during fire conditions. In their experimental program their goal was to quantify the influence of the fire induced restraint forces and moments on the fire response of reinforced concrete beams.

The details of the numerical study are presented in Dwaikat and Kodur (2008), however the basic principle is a model which uses moment-curvature relationships to simulate the structural response of the beam from initial loading to structural failure. The

significance of this model is that it is able to consider the influence of the axial restraint forces. The beams used to validate this model had dimensions of 300mm x 500mm and a span of 6m. Within the numerical model, each segment is analyzed for its temperature and strength capacities while being exposed to the ASTM E119 (2009) standard fire; and failure has been defined by Dwaikat and Kodur (2008) as follows:

- The temperature in the tensile steel exceeds 593°C.
- The beam is unable to resist the applied load.
- The maximum deflection of the beam exceeds 1/20 of the beam length.
- The rate of deflection exceeds a preset limit.

They found that during the early stages of a fire exposure counteracting moments developed and reduced the deflection of the beam. The development of the counteracting moment was dependent on the distance between the line of action of the thrust force and the neutral axis. Early into a fire exposure the thrust line of action was significantly below the neutral axis, which created a larger counteracting moment. The immediate reduction in deflection at the early stages of a fire actually reduced the development of the axial thrust force for a period of time. However as the fire progressed, increased thermal expansion led to an increase in axial restraint force developed. At later stages into a fire exposure the thermally induced axial restraint forces became less effective at reducing deflection because as the neutral axis of the beam moved downward (because of

an increase in axial restraint force requires an increase in the concrete compression zone depth); the distance required to produce the resisting moment couple was reduced.

Dwaikat and Kodur (2008) also stated that there is a contribution from a P-δ effect which created additional moments that increased deflections. This is based on the line of action of the axial restraint force and the geometrical centroid of the beam. Highest eccentricity is experienced at the beginning of the fire exposure then decreased rapidly with increasing fire exposure time; this was due to the large thermal gradients present at the beginning of the fire exposure between the center and the ends which decreased with fire exposure time. They also showed that as the amount of axial restraint provided was increased, the beams experienced a lower rate of reduction in moment capacity and deflection; due to the development of the axial thrust force.

3.3 Brief summary of the literature review

Reduction in reinforced concrete beams structural capabilities due to corrosion damage is clearly illustrated in the first part of this literature review. More specifically, many researchers have identified the reduction in interfacial bond strength between the steel rebar and the concrete as the leading cause for deteriorating structural performance of corrosion damaged reinforced concrete beams.

Clearly, the common method for inducing corrosion within a reasonable time frame is the method of applied current. The corrosion values obtained using this method with low current densities have been shown to correlate well with predicted values based on scientific principles.

Reinforced concrete beams exposed to fire structurally degrade as the fire duration and intensity increases. Similarly to corrosion damaged beams, much of the reliance on the performance of the reinforced concrete beam during a fire is on the concrete to steel bond interface. Many authors provide differing critical bond temperatures and parameters however the general consensus is that once the heat front penetrates the cover to the level of the steel then significant structural deterioration can occur. Even if the reinforced concrete beam survives the actual fire scenario, the residual strength available is reduced. While conducting the literature review it was evident that a study of corrosion damaged reinforced concrete beams focusing on the combined effects of corrosion damage and fire had not been previously studied.

3.4 Specific objectives of this study

Based on the background described in Chapter 2 and the literature review above, the specific objectives of this study are to develop understanding about:

1. How various degrees of corrosion damage and cracking affect the temperature distribution of the embedded reinforcing steel during a fire exposure.

2. How reinforced concrete beams with various degrees of corrosion will behave when exposed to fire conditions;

3. The lasting residual effects of a corrosion damaged reinforced concrete beam after a fire exposure.

4. How temperature differential created within the beam specimen will affect the structural performance during fire exposure.

5. Identify potential areas of further research in the field of corrosion damaged reinforced concrete structures exposed to fire scenarios.

For this experimental program the focus is on the flexural performance of corrosion damaged reinforced concrete beams. This is a hybrid of both flexural testing of corrosion damaged beams subjected to a fire exposure, and so elements and experimental techniques were chosen from both areas of research to achieve our goals.

CHAPTER 4: Experimental Program

4.0 General

This chapter presents the experimental program used in this research. First the general experimental methodology will be discussed followed by details of the specimen design, construction and curing. Descriptions will be given about the individual experimental components, specifically, the corrosion induction apparatus, the loading frame and the furnace, as well as the instrumentation necessary to capture the data. The ancillary tests necessary for validation of some of the experimental variables will also be described.

4.1 Experimental methodology and parameters

The general objective of this experiment program is to capture data indicating the coupled effects of reinforced concrete beams which have corroded steel reinforcement and which are exposed to fire conditions. In an effort to keep the generated data as useful as possible, the program has been designed such that the testing procedure is built upon existing knowledge and data available concerning the individual effects of corrosion and fire on reinforced concrete beams.

The experiment is unique in that the procedure to be employed is a hybrid version of two different testing methodologies which have to be merged into one experiment. Firstly, the reinforced concrete beams were designed, poured and cured based on current standards and best practices techniques and CSA A23.3-04 (2004). A total of 19 beams

were tested all having the same external dimensions and reinforcement. The beams are categorized based on the DOC, cover thicknesses and testing regimes. The DOC of the beam specimen is denoted as D*X* in the beam designation; where *X* represents the DOC level. The beam specimens are then further divided into two groups based on the thickness of the concrete cover, denoted in the beam designation as C*X*; where *X* represents the cover thickness (See Table 4-1).

The corrosion was induced using an accelerated procedure, in which an external current was applied, after a minimum 28 days of curing. Once the desired DOC was achieved based on theoretical calculations, the samples were then exposed to the CAN/ULC-S101 (2004) standard time-temperature curve. The testing regime, denoted as sub-group 'F' (Fire resistance) specimens were held at a constant service load while being exposed to the fire and the time to structural failure was recorded. The beam was considered to have survived the fire exposure after 55 minutes. The 'R' (Residual) group testing regime consisted of exposing the sample to the fire while under the same constant load as the 'F' group specimens. The 'R' group specimens were exposed to a predetermined fire duration exposure based on the results of the 'F' group tests. Once the preset fire duration was reached, the furnace was turned-off and the specimens were allowed to cool back to ambient conditions. Following this cooling down period the specimens were loaded until failure at a constant loading rate. The 'F' group specimens and experiments are designed to give an indication of the specimen behaviour during fire conditions, while the 'R' group specimens give an indication of the loss in residual strength of the specimens. Table 4-1 shows the experimental grid and specimen

designations. In all tests, the beams were tested under four-point loading, with adequate external shear reinforcement to ensure flexural failure; with the exception being the last sub-series of tests that investigated the effects of the external shear reinforcement. The 'NS' (No Shear clamps) group of specimens were tested last because the un-insulated steel shear clamps would be severely damaged by the direct fire exposure. Lastly, the 'C' group control specimens were tested without any fire exposure.

Table 4-1: Experimental grid used in the current testing program.

	Beam Designation	DOC (%)	Cover (mm)	Group	Sample No.	Remarks
Fire Behaviour	D0-C20-F-I	0.00	20	F	I	Fire behaviour test
	D0-C20-F-II	0.00	20	F	II	Fire behaviour test
	D0-C20-F-III	0.00	20	F	III	Fire behaviour test
	D125-C20-F-I	1.25	20	F	I	Fire behaviour test
	D125-C20-F-II	1.25	20	F	II	Fire behaviour test
	D375-C20-F-I	3.75	20	F	I	Fire behaviour test
Residual Behaviour	D0-C20-R-I	0.00	20	R	I	Residual behaviour test
	D125-C20-R-I	1.25	20	R	I	Residual behaviour test
	D375-C20-R-I	3.75	20	R	I	Residual behaviour test
	D525-C20-R-I	5.25	20	R	I	Residual behaviour test
	D750-C20-R-I	7.50	20	R	I	Residual behaviour test
	D525-C30-R-I	5.25	30	R	I	Residual behaviour test
Control Beams	D0-C20-C-I	0.00	20	C	I	U.K.[1] calibration sample
	D0-C30-C-I	0.00	30	C	I	Control beam
	D375-C30-C-I	3.75	30	C	I	Used to verify DOC
No Shear Clamps	D0-C30-NS-I	0.00	30	NS	I	Effect of shear clamps
	D0-C30-NS-II	0.00	30	NS	II	Effect of shear clamps
	D375-C30-NS-I	3.75	30	NS	I	Effect of shear clamps
	D525-C30-NS-I	5.25	30	NS	I	Effect of shear clamps

[1] *U.K. refers to the study which was used to compare residual strength values of non-fire exposed corrosion damaged reinforced concrete beams (Mangat and Elgarf, 1999).*

For beam D375-C30-C-I, the reinforcing steel bars were removed from the specimen and a mass loss gravimetric analysis (ASTM G 1 – 03, 2003) was performed to verify the actual degree of corrosion that took place. Also, concrete cylinder compression tests were performed on samples taken at the time of pouring.

4.2 Specimen design for flexural testing

The specimen design was based on the work by Mangat and Elgarf (1999), who investigated the flexural strength of concrete beams with corroding reinforcement. With this approach, the results obtained in this study with the coupled effects of fire and corrosion would be comparable to the results obtained by Mangat and Elgarf (1999), who only studied the effect of corrosion on flexural behaviour of reinforced concrete beams. Given these parallel data sets, it would be possible to further explain the effects of elevated temperatures with corroded steel reinforcement.

4.2.1 Geometrical design

The beam specimens were rectangular cross sections of 100 mm wide by 150 mm deep and 910 mm long. The specimens contained two 10M reinforcing bars with a diameter of 11.3 mm and a yield strength of 400 MPa. The steel bars were 1100 mm long and were bent at the ends to ensure proper anchorage, similar to the procedure used by Mangat and Elgarf (1999). One end of the steel bars protruded 15 mm out of the top of the beam specimen to facilitate the installation of the induced corrosion wiring. A cross-sectional and longitudinal view of the test specimens is shown in Figure 4-1. Stirrups were not provided in the beam specimens to eliminate difficulty in accurately

predicting and controlling the degree of induced corrosion as the applied current would also corrode the stirrups (if they are in contact with the longitudinal reinforcement).

The concrete cover thickness at all sides was 20 mm of clear concrete cover for the C20 group, and 30mm of clear cover for the C30 group (see Figure 4-1). Shi *et al.* (2004) investigated the influence of concrete cover on the fire resistance of reinforced concrete flexural members, and they determined that while increasing the concrete cover will increase the fire resistance of the member, this beneficial effect is limited. The specimen geometries used by Shi *et al.* (2004) had very similar dimensions to the Mangat and Elgarf (1999) study, and they (Shi *et al.*, 2004) tested both 20 and 30mm cover thicknesses; therefore, the results of our testing will show whether or not similar trends exist between increasing cover and improved fire performance, when corrosion of the bars exists.

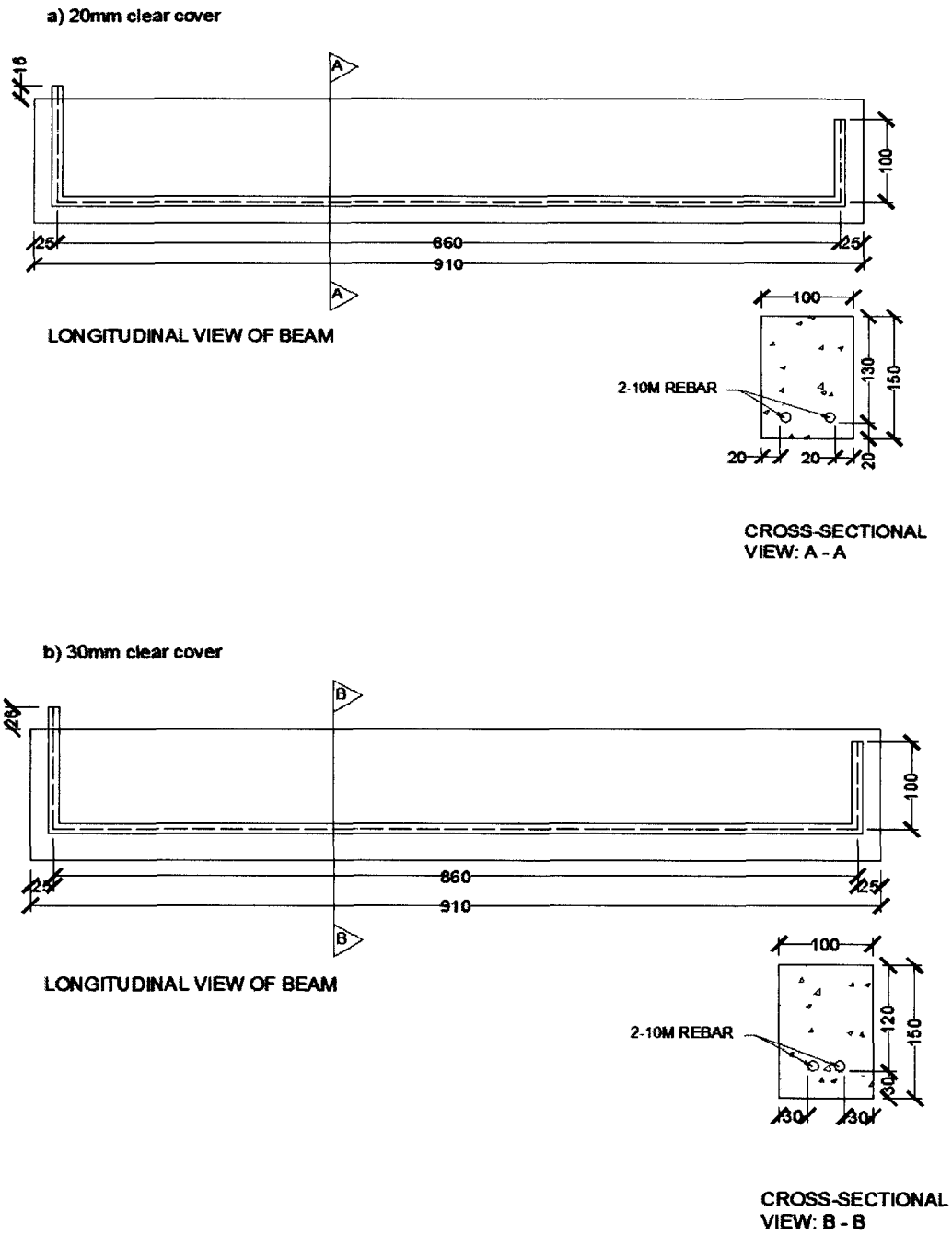

Figure 4-1: The cross-sectional and longitudinal drawings of the test specimens. Drawing a) shows the dimensions for the specimens with 20mm clear cover and b) shows the specimen dimensions for 30mm of clear cover.

4.2.1.1 Theoretical flexural strength analysis

The theoretical flexural strength analysis of the reinforced concrete beams was completed. The calculations were based on ambient temperature conditions and did not consider the effects of rebar corrosion. The bi-linear idealized moment-curvature relationship is shown for both beam geometries in Figure 4-2. The analysis shows that the beams are under-reinforced, and at steel yielding ($\varepsilon_s = 0.002$), the maximum concrete compression strain is significantly lower than the CSA A23.4 limit of $\varepsilon_{cc} = 0.0035$. The ultimate moment capacities for 20 mm cover and 30 mm cover sections are 10.21 kN-m and 9.13 kN-m, respectively, at $\varepsilon_{cc} = 0.0035$.

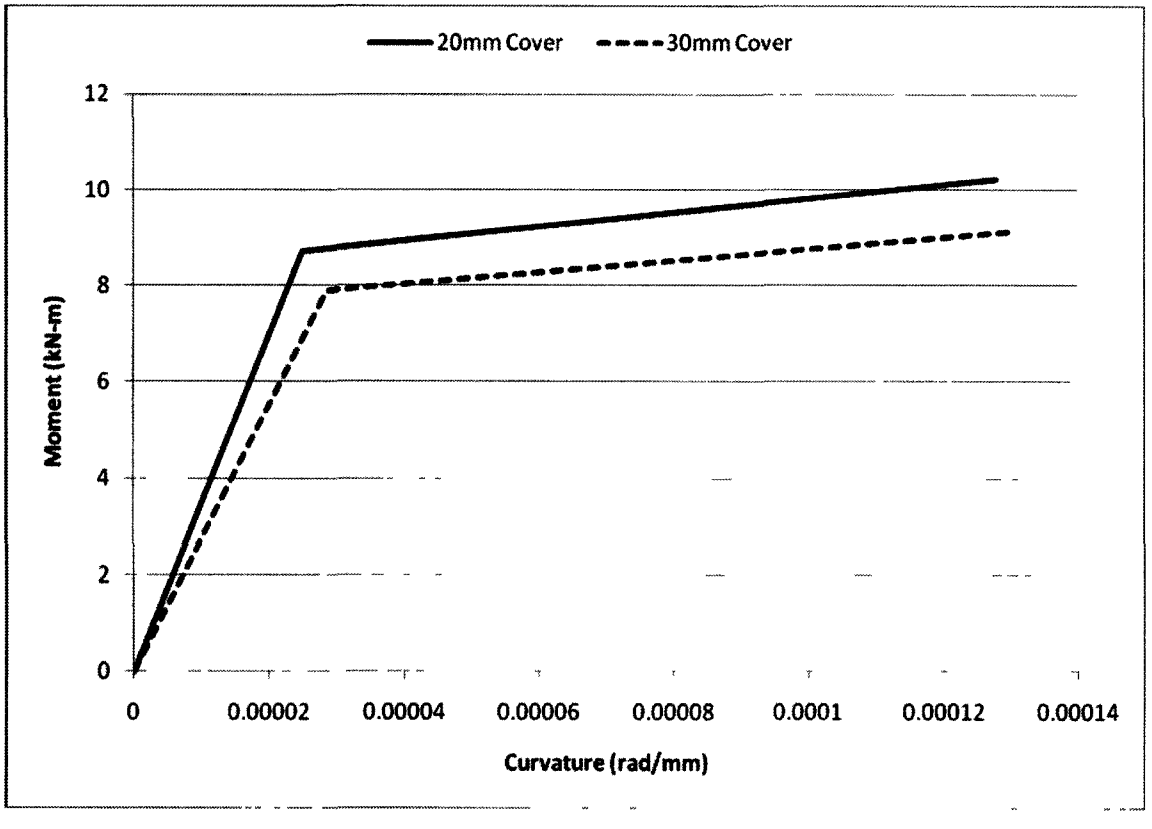

Figure 4-2: The theoretical moment-curvature relationship for both specimen geometries.

4.2.2 Concrete mix

The concrete mix was pre-ordered from a ready-mix concrete company (Lafarge North America) to meet the following specifications: Normal Type 10 Portland cement was used with a maximum rounded gravel aggregate size not exceeding 10 mm and natural sand fine aggregate. The average 28 day compressive strength was to be 40 MPa, with a water-to-cementitious material (w/c) ratio of 0.45, for non-air entrained concrete. The concrete from the ready mix truck had an initial slump of 80 mm. The cement content of the mix was 380 kg/m^3. In order to facilitate the induced corrosion process within the specimens, 1% (by mass of cement) of NaCl (sodium chloride) was added to the concrete mixture. The NaCl was dissolved in water and was combined with the plain concrete in a mobile cement mixer and mixed together for 30 seconds. After the addition of the NaCl solution, the water to cementitious material ratio was 0.48 and the concrete had a slump of 100 mm. 1% NaCl was chosen in order to ensure adequate chloride was present at the initiation of corrosion, since ~ 0.15% of water soluble chloride (by mass of cement) content can begin to depassivate reinforcing steel (Design and Control of Concrete Mixtures, 2002). Furthermore, the sodium chloride also increases the thermal conductivity of the concrete (Mangat and Elgarf, 1999).

4.3 Casting and curing of beam specimens

Wooden forms were constructed to meet the finished beams size specifications, and the forms were two-coated with a releasing agent, to ensure ease of de-moulding. The 10 mm diameter, 1100 mm long reinforcing steel was bent at each end as shown in

the specimen design. The bars were then cleaned of any loose rust and dirt, before they were placed on plastic bar seats in the forms at the correct depth to achieve the desired cover and bar spacing. The necessary embedded instrumentation was completed and then the pre-mixed concrete was placed into each of the forms. Six cylinder samples of the plain (no NaCl) concrete were taken; thirteen cylinders of the mixed (with 1% NaCl solution) concrete were also cast. To ensure good consolidation and uniform concrete distribution within the forms and particularly, around the reinforcing bars, a vibrating table was used during pouring.

Immediately after pouring the specimens, the filled moulds were covered with a polyethylene sheet. Twenty-four hours after casting, the moulds were removed and the specimens were all placed in a dedicated sealed concrete curing room. The curing room has a large tub of water with a submersible heater that allows the relative humidity in the room to be maintained at ~90% and ~ 30°C for a minimum period of 28 days. After this curing period the specimens were removed and the external applied current corrosion technique was then applied, for the duration specified in section 4.5 to achieve the theoretical DOC. After the curing period and the induced corrosion period, the specimens were prepared to be tested in flexure in the furnace as described in section 4.6.

4.4 Instrumentation of flexural test specimens

The challenge in instrumenting a specimen for testing in high temperature environments is that some of the most common instrumentation in structural tests, particularly strain gauges, will not survive the high temperature environment.

The burn chamber is equipped with six thermocouples to monitor the internal temperature within the furnace during the test. In order to capture the temperature of the steel reinforcement, two thermocouples were installed at mid span and at 1/3 points, as shown in Figure 4-3. Thermocouples were installed on opposing sides of the steel rebar to capture an average temperature reading across the bar from both the internal and external exposures. In order to prevent any damage from occurring to the thermocouple wire during the accelerated corrosion process, the thermocouples were set into a localized, thin bed of epoxy in order to insulate the thermocouple from the corrosion current. Furthermore, the applied load data were recorded by the load cell, and mid span deflections were measured using an LVDT Displacement Transducer. The LVDT set-up is shown in Figure 4-4; it consisted of a ceramic rod which is not susceptible to expansion or deformation during the fire exposure, which extended down through the loading frame and was connected to an LVDT which was connected to a fixed point.

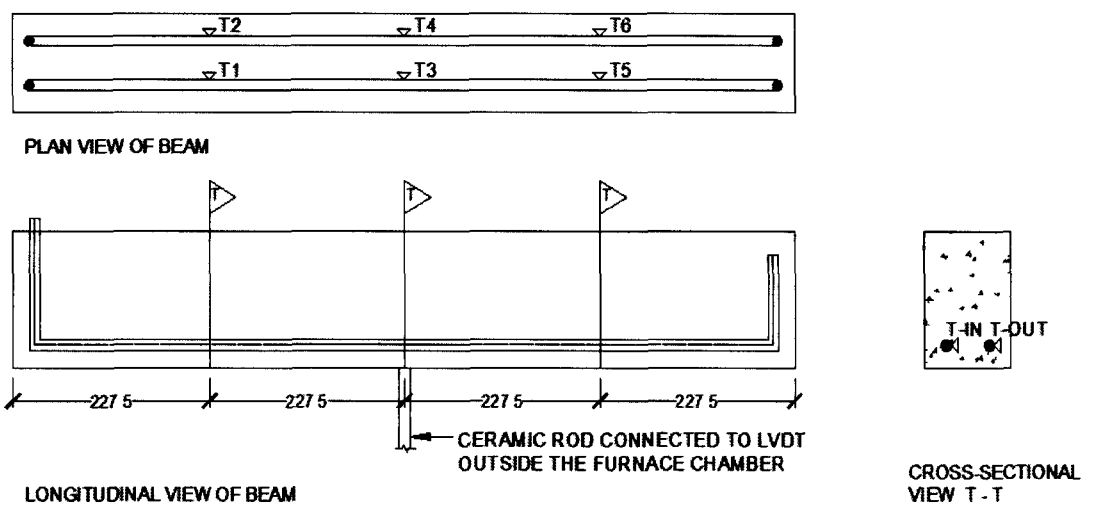

Figure 4-3: The location of the thermocouples at mid-span and the 1/3 spans.

Figure 4-4: The LVDT set-up outside of the burn chamber.

4.5 Accelerated corrosion setup

The accelerated corrosion process used in this study is a common and practical way of inducing corrosion in steel reinforcement over a relatively short duration. The basic principle of the corrosion induction process is to introduce an electro-chemical potential through the reinforcing steel (anode) and a sacrificial cathode; which forces the corrosion process to take place on the steel bar within the concrete (El Maaddawy; Soudki, 2003).

4.5.1 Theoretical considerations

The natural corrosion process of reinforcing steel bars within concrete generally occurs at current densities ranging from 0.1 $\mu A/cm^2$ to 1 $\mu A/cm^2$ (Broomfield, 1997). Long-term experimental studies have shown that exposure of a steel reinforced concrete beam to a corrosive environment showed no measurable corrosion up to the completion of the initiation phase at approximately 5 years (for tensile reinforcement), after which

the propagation phase progressed slowly to a corrosion percentage of approximately 4% after 14 years (Vidal *et al.*, 2007). In order to accelerate the corrosion process a constant current density is applied to the reinforcing bar. The accelerated corrosion process can cause a more rapid build-up of corrosion products at the steel to concrete interface, thereby leading to more severe cracking as compared to natural corrosion. In order to be able to complete structural testing projects of corrosion damaged reinforced concrete beams within a reasonable time frame, the induced corrosion method was used. In order to keep the corrosion rate as realistic as possible, the lowest practical impressed current was used. It is acknowledged that using large current densities may result in conditions that are different from those typically observed in naturally corroding systems. In particular, the rate of formation of corrosion products and the types of corrosion products could be different. However, it should be acknowledged that this study is a comparative study in which all beams (19 in the current program and 111 by other researchers) be corroded under similar conditions; using a large corrosion rate to accelerate the process can be justified, particularly as a first study of its type. As it will be listed in the proposed future work, a long term-study, which the corrosion rates are more realistic, should be carried out later.

4.5.1.1 Applied current density

The main parameter in inducing a realistic and predictable degree of corrosion is the applied current density. Mangat and Elgarf (1999) investigated the flexural response of corroded beams which were induced with different degrees of constant corrosion current densities ranging from 1 to 4 mA/cm^2. They found that up to degrees of

corrosion of 3.75%, the effect of different constant corrosion current densities had little effect on the residual flexural capacity results. For the purposes of comparing the results published by Mangat and Elgarf (1999) to the results obtained in our study a constant current density of 1mA/cm^2 was selected for this study.

4.5.1.2 Predicted degree of corrosion

The predicted DOC is based on Faraday's Law and is presented in Mangat and Elgarf (1998; 1999) and also described in detail in section 3.1.2. Studies have shown that using Faraday's law to predict the DOC correlate well with the actual measured mass loss as tested up to 7.27% (El Maaddawy and Soudki, 2003). Based on this theory, the time required to achieve the predicted DOC for each specimen based on the applied current density is presented in Table 4-2.

Table 4-2: The predicted DOC and associated induced corrosion duration.

Beam Designation	DOC (%)	Corrosion Current Density (mA/cm^2)	Calculated Corrosion Duration (hrs.)
D125-C20-F-I	1.25	1	54
D125-C20-F-II	1.25	1	54
D375-C20-F-I	3.75	1	161
D125-C20-R-I	1.25	1	54
D375-C20-R-I	3.75	1	161
D525-C20-R-I	5.25	1	225
D750-C20-R-I	7.50	1	321
D525-C30-R-I	5.25	1	225
D375-C30-C-I	3.75	1	161
D375-C30-NS-I	3.75	1	161
D525-C30-NS-I	5.25	1	225

4.5.2 Corrosion process

The specimens were placed in the electrolytic solution (3.5% NaCl) within a plastic tank and submerged to a level just above the level of the tensile reinforcement within the specimen. The circuit was set-up as shown in Figure 4-5; with the positive terminal being connected to the protruding rebar, while the negative terminal was connected to a stainless steel plate cathode within the same plastic tank. The constant current was applied using a power supply, which automatically adjusted the voltage parameter to ensure constant current. The level of the solution was adjusted to ensure that the rebars were below the solution level. Figure 4-6 shows the power supply and the connections to the beam. Care was taken to prevent corrosion at the ends of the concrete specimens where the steel bars protruded, by applying an epoxy coating to the exposed bar and the perpendicular concrete surface. Software connected to the power supply allowed continuous control and monitoring of the power supply.

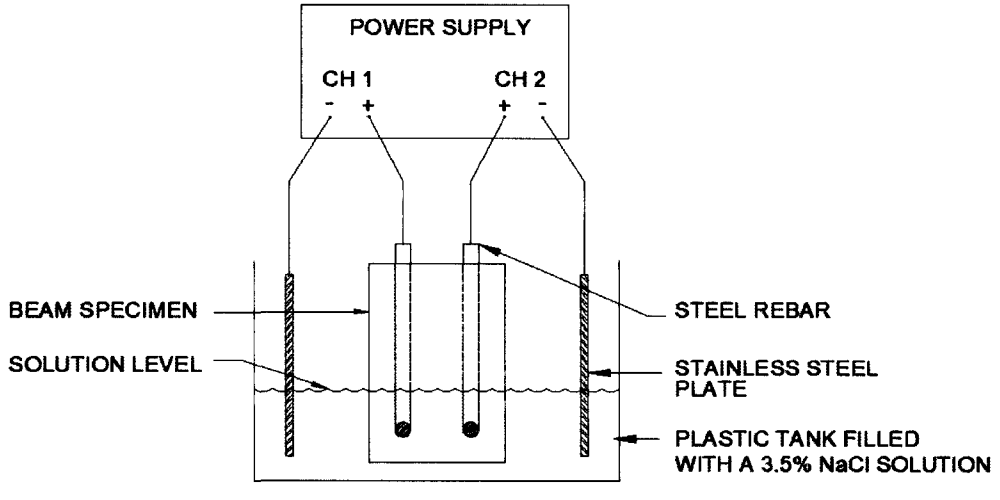

Figure 4-5: The schematic of the accelerated corrosion set-up.

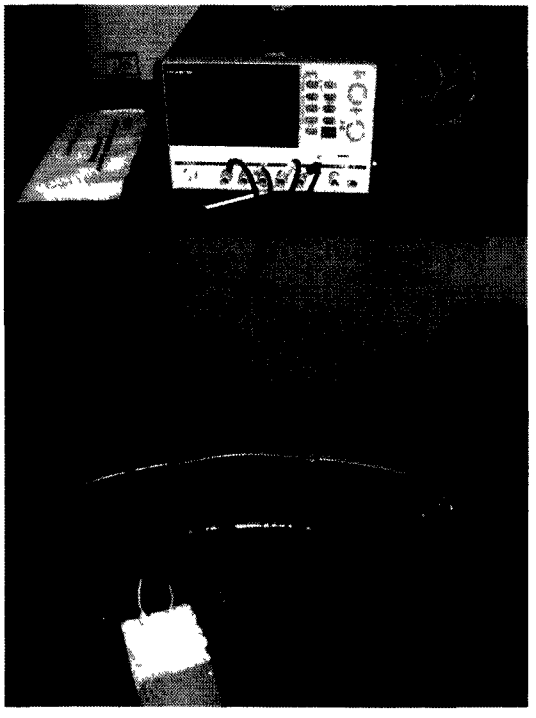

Figure 4-6: The power supply and beam corrosion set-up.

4.6 Test apparatus for flexural testing

This section provides details on the combined loading and fire testing apparatus. The apparatus consists of a hydraulic loading frame and a propane fired furnace. This testing apparatus is at Carleton University's Fire Research Facility located in Almonte, Ontario, Canada. After the specimens were corroded to the desired calculated levels, they were transferred to the testing furnace, where they were concurrently heated and loaded. Figures 4-7 and 4-8 show drawings of the test furnace and loading apparatus. Figure 4-9 shows a picture of the outside of the chamber.

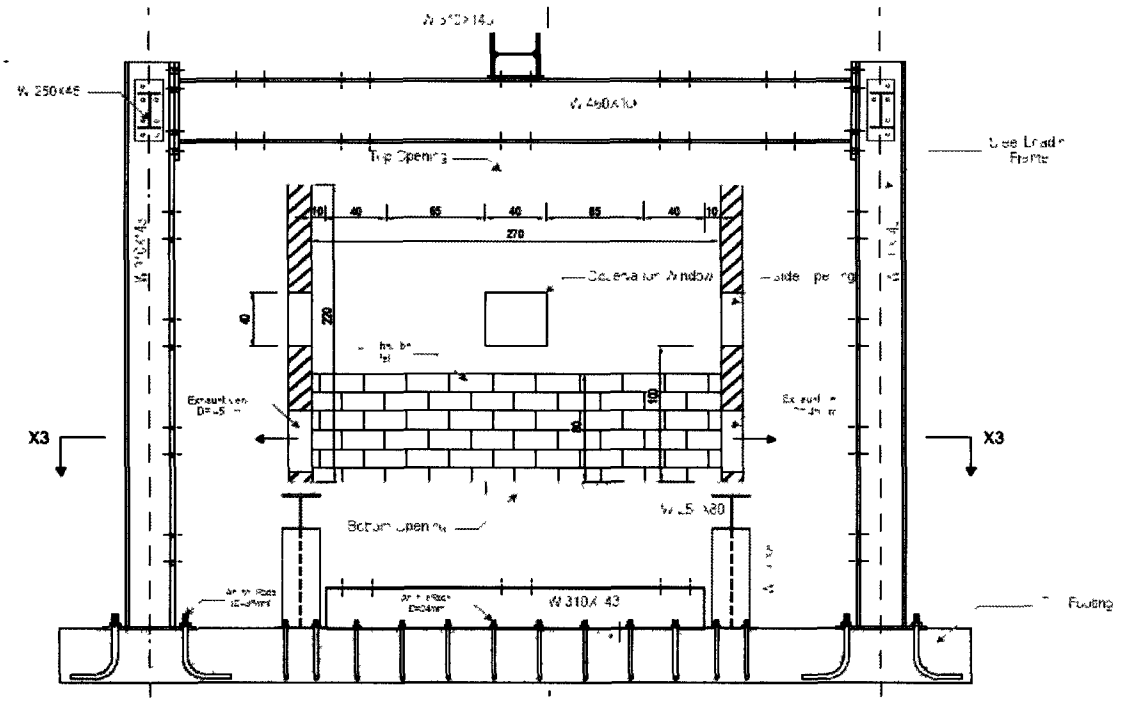

Figure 4-7: An elevation view of the testing apparatus (Reproduced with permission from Osama Salem, 2009).

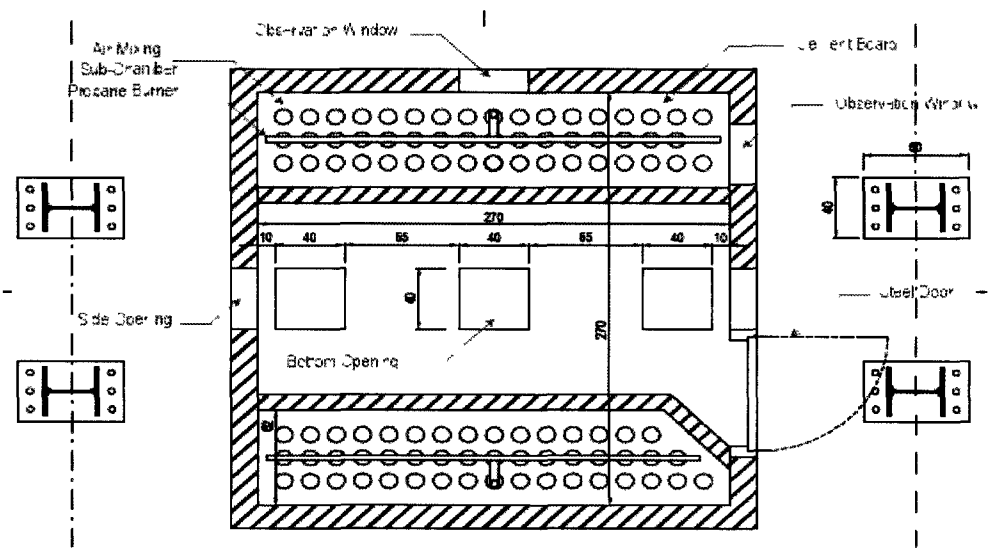

Figure 4-8: Plan view of the testing apparatus (Reproduced with permission from Osama Salem, 2009).

Figure 4-9: The outside view of the testing apparatus, including the burn chamber and the external loading frame.

4.6.1 Furnace parameters

The furnace was designed, built and calibrated by the faculty, graduate students and technicians of Carleton University. The furnace is 3 m x 3 m in plan and 2.2 m high inside the burn chamber. The burning fuel is propane. Through control of the burners in the furnace, the specimens were exposed to the CAN/ULC-S101 (2004) standard time-temperature curve. See Appendix 'C' for the Time-Temperature curves for the fire tests. A picture of the inside of the furnace is shown in Figure 4-10. The furnace is lined with a refractory ceramic fibre high temperature insulation known as 'Fiberfrax'. Six thermocouples capture the temperature data in the furnace chamber.

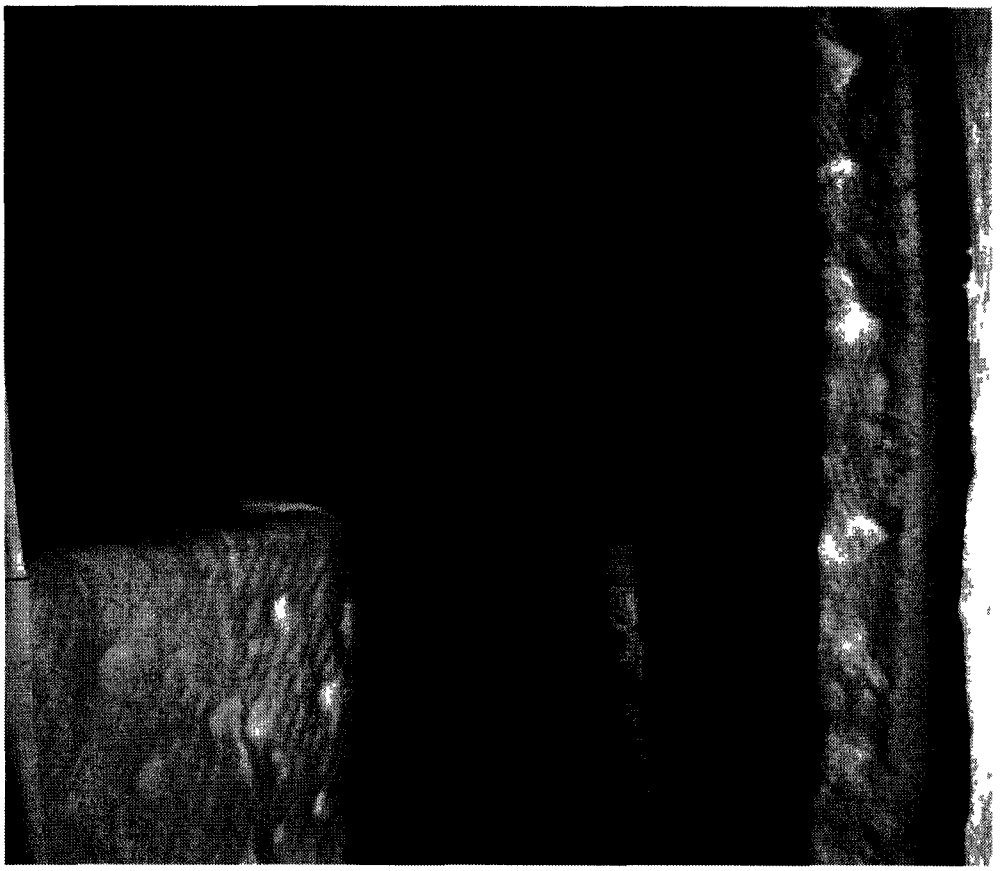

Figure 4-10: The inside view of the burn chamber.

4.6.2 Loading and support conditions

In order to support the specimen within the existing openings in the burn chamber floor, a specimen support frame was constructed as shown in Figure 4-11. In order to ensure that flexural failure occurred, external shear reinforcement was provided at both shear zones for most samples. The specimens were reinforced by using a series of intermittent steel clamps, theoretically acting similarly to conventional stirrups in reinforced concrete beams (see Figure 4-12). The external shear clamps protruded 100 mm past the side faces of the beam so that when wrapped with the necessary insulation,

hot fire gases could still pass behind the shear clamp insulation and contact the side faces of the beam as well as the soffit, allowing the beam to be heated on 3 sides. The top of the beam was insulated to simulate a beam in service being exposed to fire from below. The beam specimen itself rested on the two partial height support columns. The Steel support structure within the furnace area including the support rigs and the external shear reinforcement were wrapped with refractory ceramic fibre high temperature insulation so that the steel support sections and shear reinforcement could be re-used for each test. The beam loading geometry is shown in Figure 4-13.

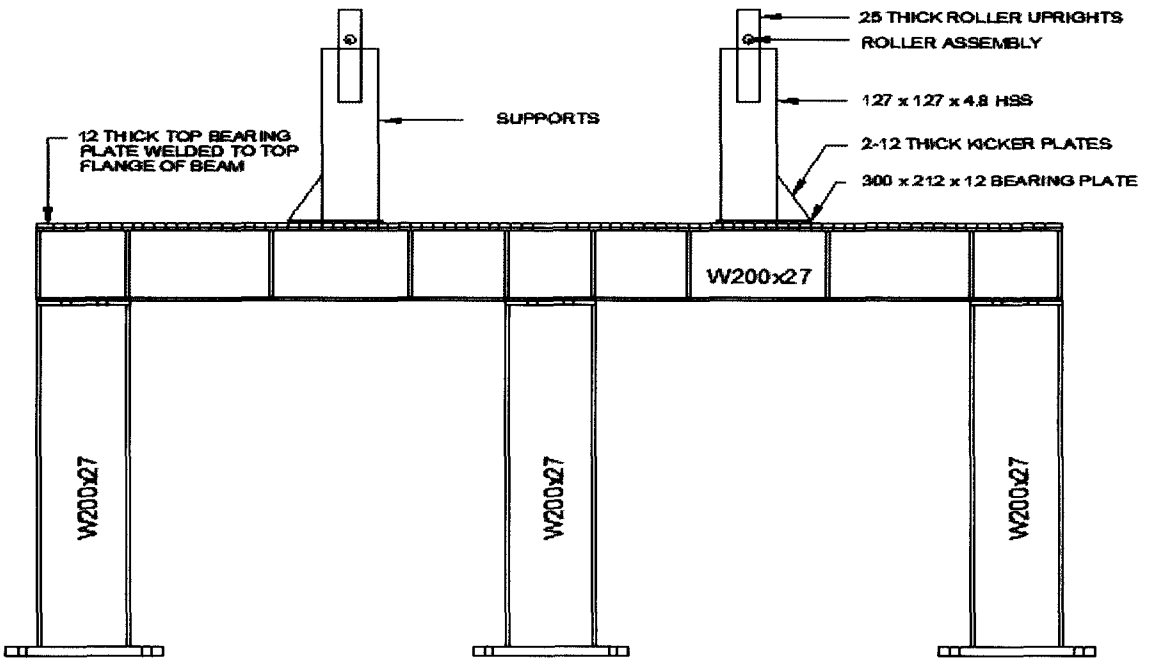

Figure 4-11: Schematic of the loading frame.

Figure 4-12: A typical beam installation on the loading frame within the furnace. Note the external shear clamps which have been wrapped with 'Fibrefrax' Insulation in (a) and a picture of a typical shear clamp without insulation as shown in (b). The shear clamps are 100 mm away from the concrete beam sides to allow hot gas flow along the face.

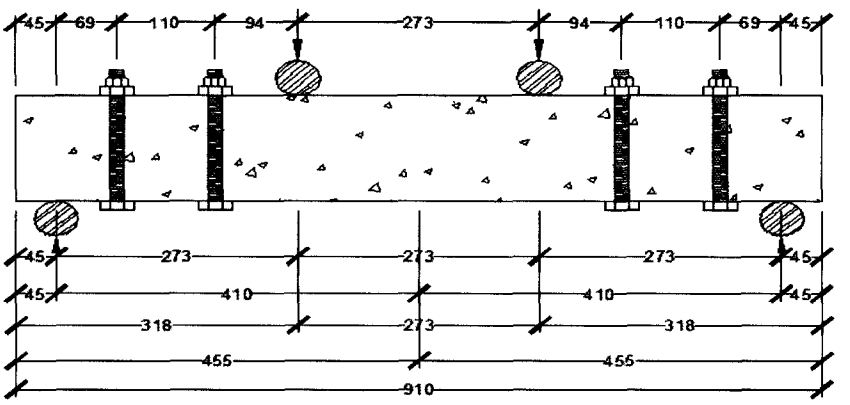

Figure 4-13: The beam loading geometry as well as the location of the shear clamps.

The load was applied to the specimen via a hydraulic jack fixed to the upper portion of the loading frame. The hydraulic jack was connected to a load cell which penetrates through an opening in the ceiling of the burn chamber. The force being applied by the hydraulic jack was controlled by a manual hydraulic pump.

Based on Moment-Curvature relationships calculated at ambient conditions, the moment required to cause yielding as well as the ultimate moment capacity for the 20 mm cover and 30 mm cover beams are shown in Table 4-3. Table 4-3 also shows M_{Fire} which represents the moment that was to be sustained by the beam during the fire resistance test. M_{Fire} was taken as $0.51M_u$, which translated to $0.60M_y$ based on the steel being at 60% of its yield stress while at service load. Based on the geometrical loading scheme the total applied jack load to achieve M_{Fire} is the product of the applied point load and the distance between that load and the support.

Table 4-3: The loading values for both beam geometries.

Beam Cover (mm)	**Calc. M_y (kN-m)**	**Calc. M_u (kN-m)**	**Calc. M_{Fire} (kN-m)**	**Calc. Point Load, P_{Fire} (kN)**	**Calc. Total Applied Jack Load (kN)**
20	8.7	10.21	5.22	19.12	38.24
30	7.9	9.13	4.67	17.09	34.18

The Fire Behaviour ('F') group of tests were based on a standard fire resistance test. The samples in this group were pre-loaded to M_{Fire} at a rate of 5 kN/min. Once M_{Fire} was reached, the load was held constant for a period of 30 minutes without any fire

exposure. After the pre-loading period the fire exposure began. The specimens were exposed to the standard CAN/ULC S101 (2004) Time-Temperature curve, while maintaining constant load, M_{Fire}. This continued until the specimen failed to carry the applied load or the beam had survived 'burnout'.

The residual behaviour group of strength tests were based on the fire behaviour observed in the F group tests. The samples in this group were pre-loaded to M_{Fire} at a rate of 5 kN/min. Once M_{Fire} was reached the load was held constant for a period of 30 minutes without any fire exposure. After the pre-loading period the fire exposure began and continued under constant load, until the time predetermined from the 'F' Group series of tests. The specimens were exposed to the standard CAN/ULC S101 (2004) Time-Temperature curve. Once the pre-determined fire exposure time was reached, the furnace was turned off and the specimen was allowed to cool back down to ambient temperature, while maintaining M_{Fire}. Once cooled, the specimen was loaded to failure at a rate of 5 kN/min.

The 'NS' group beams were tested using the same methodology as the 'F' group beams. Since the 'C' group control beams were not exposed to fire, they were loaded from zero to failure at a rate of 5 kN/min.

4.7 Ancillary tests

Two ancillary tests were performed to verify the actual 28 day compressive strength of the concrete and also to compare the calculated versus the predicted steel mass loss due to the accelerated corrosion process.

4.7.1 Concrete cylinder compressive test

At the time of pouring the beam specimens, six cylinder samples (152 mm diameter x 305 mm length) of the concrete before the addition of the NaCl and 13 cylinders of the concrete with the NaCl were also poured. Six specimens were then tested after 28 days, and the average compressive strength of the concrete was determined. The remaining specimens were tested at the end of the experimental program at 143 days post-pour. The results are summarized in Table 4-4, which shows that there was only a very marginal difference of 1 Mpa between the plain (no NaCl) cylinders and the cylinders which contained NaCl and this difference was maintained all the way through the 143 days of curing, indicating that the NaCl mixed into the concrete did not affect the compressive strength up to 143 days after pouring. The failure pattern was typical for all cylinder tests and could be described as `well-formed cone on one end, vertical cracks running through caps, no well defined cone on other end.`

Table 4-4: The average results of the concrete cylinder compression tests.

	Average Strength	
Curing Period (Days)	**Plain Cylinders (MPa)**	**NaCl Cylinders (MPa)**
28	40	41
143	47	48

4.7.2 Gravimetric analysis (ASTM G 1 – 03, 2003)

In order to verify that the corrosion set-up was functioning properly and that the predicted DOC corresponded well with the actual DOC, a beam was corroded, then

verified using ASTM G 1 -03 (2003). A mid-range DOC of 3.75% was chosen for the corrosion test beam. The beam, designated, D375-C30-C-I was corroded using the accelerated corrosion technique described in section 4.5.2 at 1 mA/cm^2 for the duration prescribed in Table 4-2. Once complete, the cracking patterns were mapped, and the cover was carefully removed (mechanically) without disturbing the steel re-bar. Once the cover was removed the corroded bars were then removed and carefully cut into pre-determined equal lengths and labelled. Figures 4-14 to 4-16 illustrate this process.

Figure 4-14: The cover being removed from beam D375-C30-C-I.

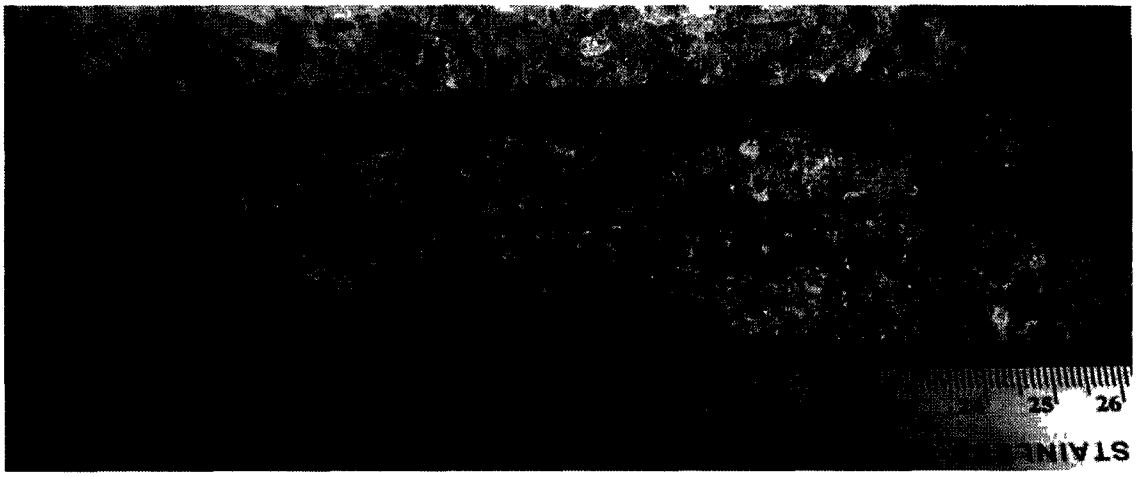

Figure 4-15: A close-up of the bars in place in beam D375-C30-C-I.

Figure 4-16: The bars from beam D375-C30-C-I cut into 3 equal parts and placed in a sealed bag along with moisture removing minerals.

Once the bar samples were adequately dry, then ASTM G 1 – 03 (2003) 'Standard Practice for Preparing, Cleaning and Evaluating Corrosion Test Specimens' was

performed. The test involves repeatedly cleaning the bar samples in a solution of hydrochloric acid, antimony trioxide and stannous chloride; then weighing them until there is no further change in mass loss. This cleaning process is designed to remove the corrosion products while not damaging the steel. The stabilized weights are then compared to un-corroded samples to determine how much mass was lost as a result of the corrosion process. Figure 4-17 shows the bar segments after cleaning. The overall results of the mass loss test are presented in Table 4-5, and show that the measured DOC was ~10% lower than calculated. Certain types of corrosion products may not have been completely removed by the chemical solution method used and perhaps a more aggressive method corresponding to ASTM G 1 – 03 (2003) would further remove additional corrosion products. Another reason for the difference could be attributed to stray currents passing through the concrete instead of the steel bars thereby making the externally applied current less than 100% efficient at inducing corrosion.

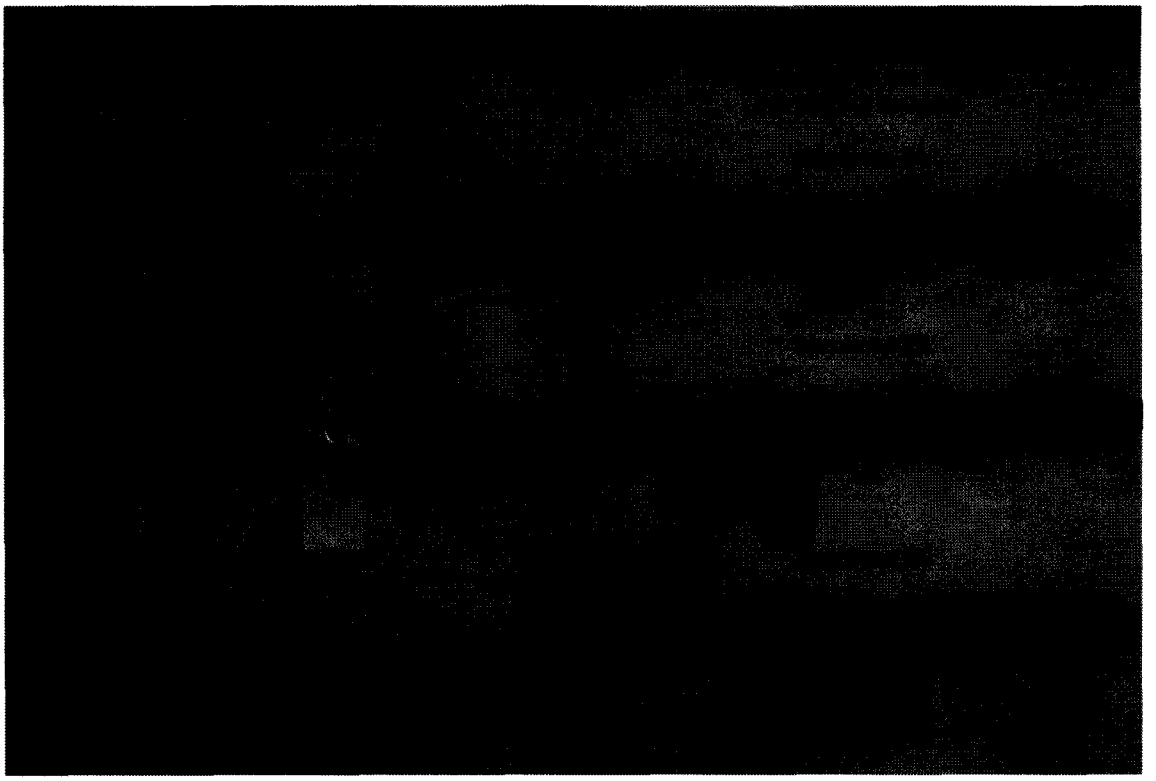

Figure 4-17: The re-bar segments from beam D375-C30-C-I after cleaning.

Table 4-5: The results of the ASTM G 1 – 03 mass loss test.

Sample	Mass Loss, ΔW (g)	% Mass Loss	Diameter Loss, ΔD (mm)	% Diameter Loss (DOC)	% Difference
1A	8.01	5.09	0.28	2.51	-33.06
1B	13.25	8.50	0.47	4.19	11.85
1C	11.65	7.48	0.41	3.68	-1.64
2A	11.64	7.45	0.41	3.67	-1.98
2B	9.75	6.26	0.34	3.08	-17.67
2C	9.02	5.87	0.32	2.89	-22.69
			Average	3.34	-10.86

4.8 Beam corrosion application

In applying the induced corrosion technique it was important that the power supply maintained the desired current so that the calculated corrosion duration was accurate. For safety purposes the power supply used for this project had a voltage output limit of 30 volts. At the very start of the corrosion period some beams provided a high enough resistance which pushed the power supply to its safe voltage limit; thereby not being able to achieve the desired current. This issue was carefully monitored and the corrosion duration for each bar was adjusted as required. As shown in Figures 4-18 and 4-19, this only occurred for a short duration in the very beginning of the corrosion process when the resistance was highest. Figures 4-18 and 4-19 show the current and voltage curves for the corrosion control beam only; all other current and voltage curves for all other beams can be found in Appendix 'A'.

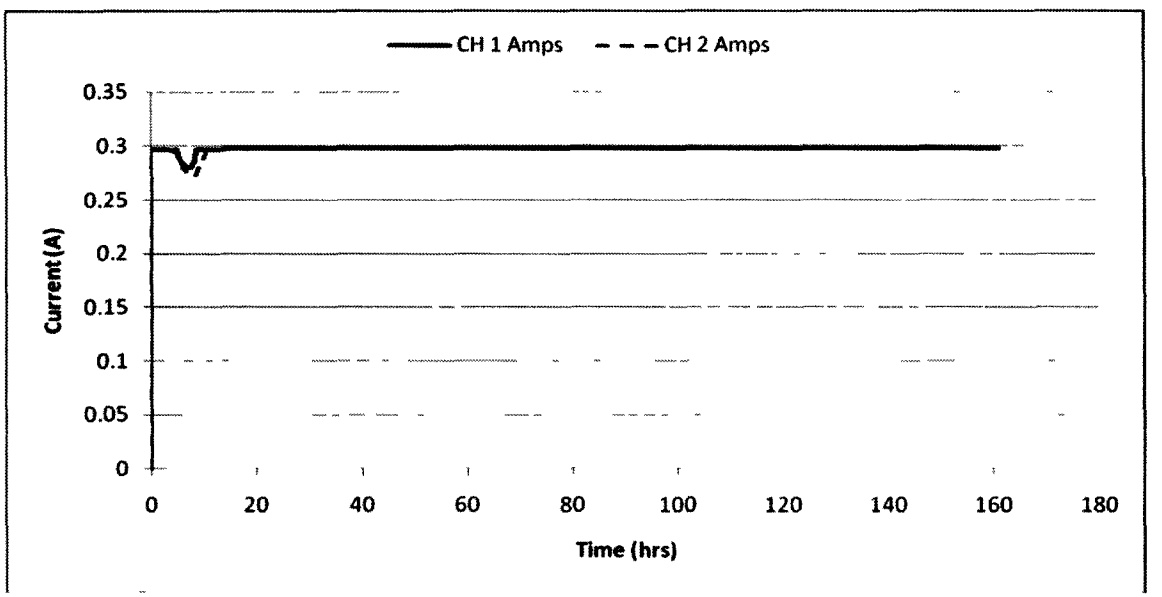

Figure 4-18: The current versus time graph for beam D375-C30-C-I.

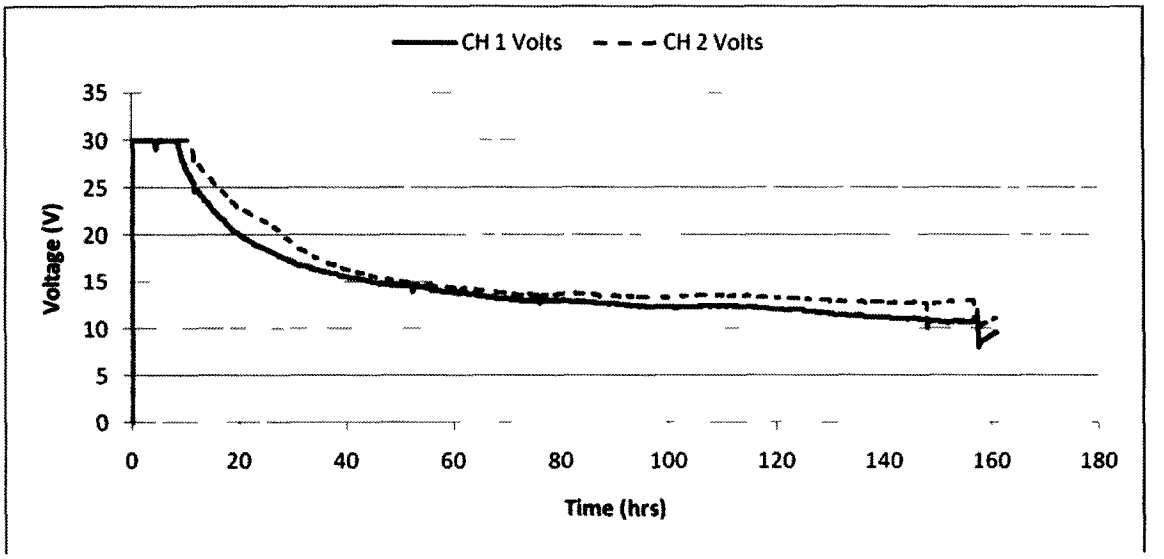

Figure 4-19: The voltage versus time graph for beam D375-C30-C-I.

4.9 Crack mapping of corrosion damage

As a result of corrosion, cracks formed within the cover of the beams. After the corrosion process, the crack widths and locations were carefully measured using a concrete crack microscope and recorded. Figure 4-20 shows the scanned image of the crack mapping for beam D375-C30-C-I. All other beam crack maps can be found in Appendix 'B'. Figure 4-21 shows a typical side of the beam once the corrosion process was complete. The results of the crack mapping for all beams are summarized in Table 4-6, which shows that as the DOC increases the average overall crack width increases. Interestingly, the 30 mm cover beams seemed to have a higher average crack width as a function of DOC than the 20 mm cover, however it is important to note that for the 30mm cover beams there were less crack locations but more severe crack widths.

Table 4-6: A summary of the crack mapping as a result of the corrosion process. Note the highlighted rows which are the 30 mm cover beams.

	Average Measured Crack Width							
Beam Designation	**Top (mm)**	**Face A (mm)**	**Face B (mm)**	**Side A (mm)**	**Side B (mm)**	**Bottom (mm)**	**Average (mm)**	**Average *f*(DOC) (mm)**
D125-C20-F-I	0.00	0.00	0.00	0.11	0.08	0.08	0.05	0.08
D125-C20-F-II	0.00	0.00	0.10	0.20	0.00	0.15	0.08	
D125-C20-R-I	0.00	0.00	0.08	0.16	0.24	0.16	0.11	
D375-C20-F-I	0.00	0.00	0.02	0.21	0.15	0.21	0.10	0.09
D375-C20-R-I	0.00	0.06	0.04	0.10	0.00	0.28[1]	0.08	
D525-C20-R-I	0.10	0.10	0.10	0.28	0.00	0.54	0.19	0.19
D750-C20-R-I	0.10	0.15	0.10	0.05	0.23	0.73	0.23	0.23
D375-C30-C-I	0.10	0.00	0.25	0.34	0.21	0.28	0.20	0.25
D375-C30-NS-I	0.04	0.20	0.20	0.60	0.00	0.70	0.29	
D525-C30-R-I	0.00	0.20	0.22	0.45	0.10	0.55	0.25	0.32
D525-C30-NS-I	0.40	0.00[2]	0.40	0.13	0.60	0.80	0.39	

[1] *a large concentrated 'bulge' occurred within the concrete cover*

[2] *complete break-off of concrete cover at the top corner of one of the bars. This was repaired before the beam was exposed to the fire exposure*

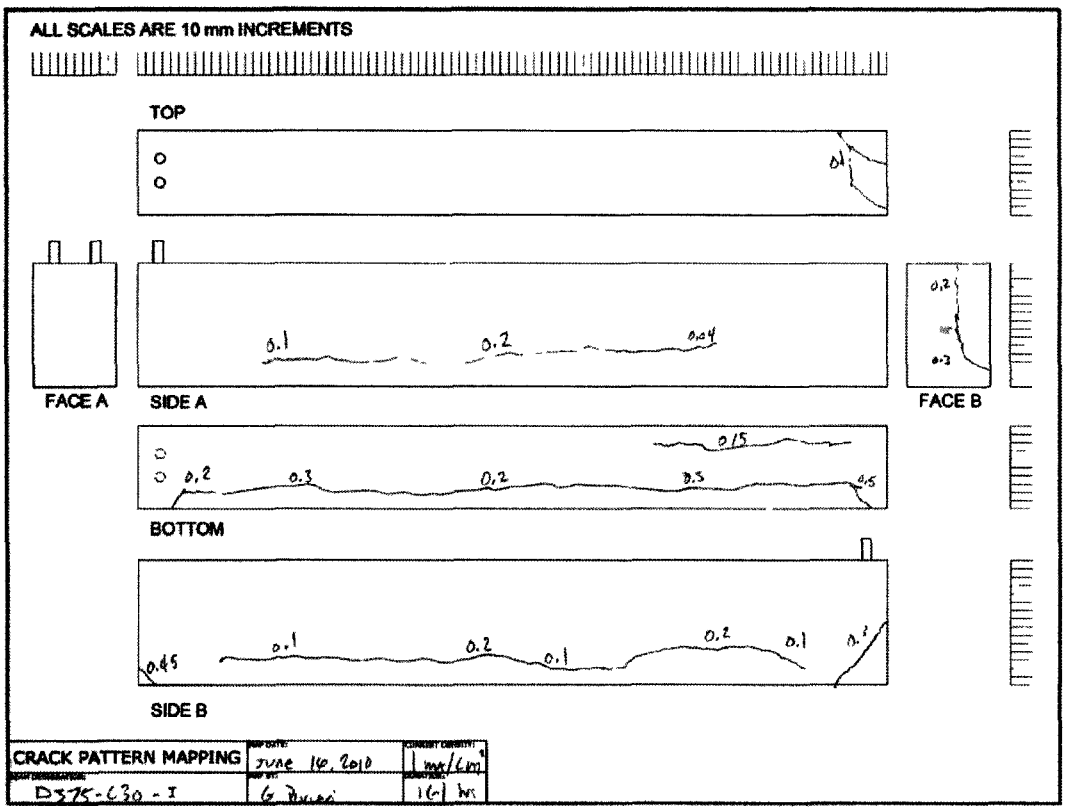

Figure 4-20: The crack mapping for beam D375-C30-C-I.

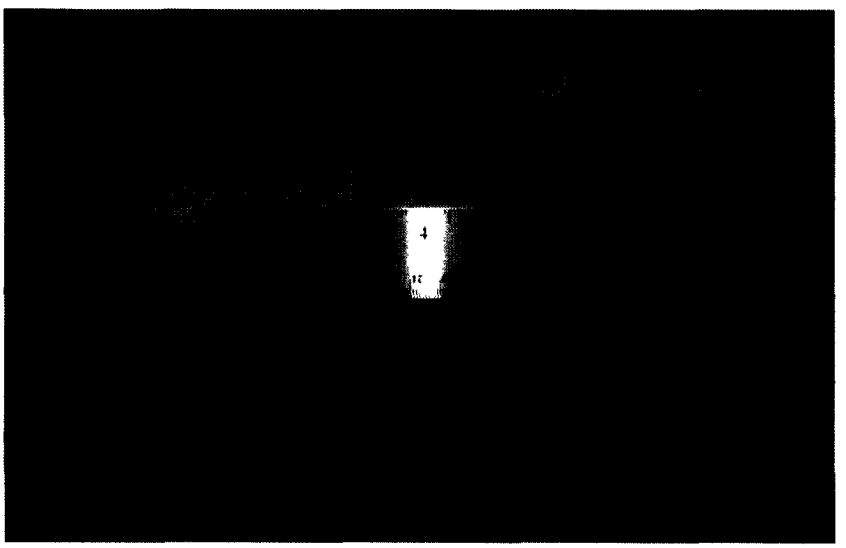

Figure 4-21: A typical side view of a beam after corrosion.

CHAPTER 5: Results and Discussion

5.0 General

The results of the experiments described in Chapter 4 are multi-dimensional. The time to failure by deflection or critical temperature rise are a function of the amount of deflection at service load, the rate of temperature increase through the cover to the steel, as well as the development and subsequent loss of the thermally induced axial thrust force. The figures presented in this chapter attempt to combine and show the interrelation of all of these concurrent factors affecting the flexural behaviour of corrosion damaged reinforced concrete beams exposed to high temperatures.

5.1 Thermal response of beams

The thermal response of the beams is affected by the location of the thermally insulated external shear reinforcement (same for all tests) and the DOC through corrosion-induced cracking and corrosion products being present within the pores of the concrete matrix.

It was observed that as the DOC increased some of the thermocouples embedded within the concrete beams failed to function. The more severe the cracking, the more probable that the thermocouples were damaged. Up to 5.25% DOC, thermocouples 1, 3 and 5 consistently continued to function for the first group of tests, giving an accurate temperature profile along at least one of the two bars.

Generally it was observed that as the DOC increased (up to 5.25%) the temperature rise within the beams was slower and more uniform over the bar length than in the un-corroded beams. Consequently for the same fire duration time, lower temperatures were observed in the specimens with increasing corrosion (see Figure 5-1). It can be noted at after 40 minutes of exposure the temperatures for 3.75% and 5.25% DOC were similar. The temperature was higher at the center of the beam as expected due to the presence of flexural cracking, which increased over time as deflection increased. In Figures 5-2 to 5-5 the maximum temperature difference between DOC's was greater for the center thermocouples; with thermocouples 3 and 4 being in the centre of the beam on the bar face closest to the center and closest to the beam surface (laterally), respectively. Thermocouples 1, 2, 5 and 6 were in two groups at a distance 227 mm away from the centre of the beam in both directions, with the odd numbered thermocouples being on the bar face closest to the center of the beam (inside) and the even numbered thermocouples being on the bar face closest to the surface (laterally, outside) (see Figure 4-3). This was again attributed to the presence of flexural cracks allowing the center thermocouples to experience more heating. The temperature plateau at ~100°C seen in Figures 5-2 to 5-5 was most likely due to the evaporation of water from the pores. Figures 5-2 to 5-5 clearly show lower overall thermocouple temperatures for increasing DOC. This can be explained by the concrete pores being more filled with corrosion products as the level of corrosion increased.

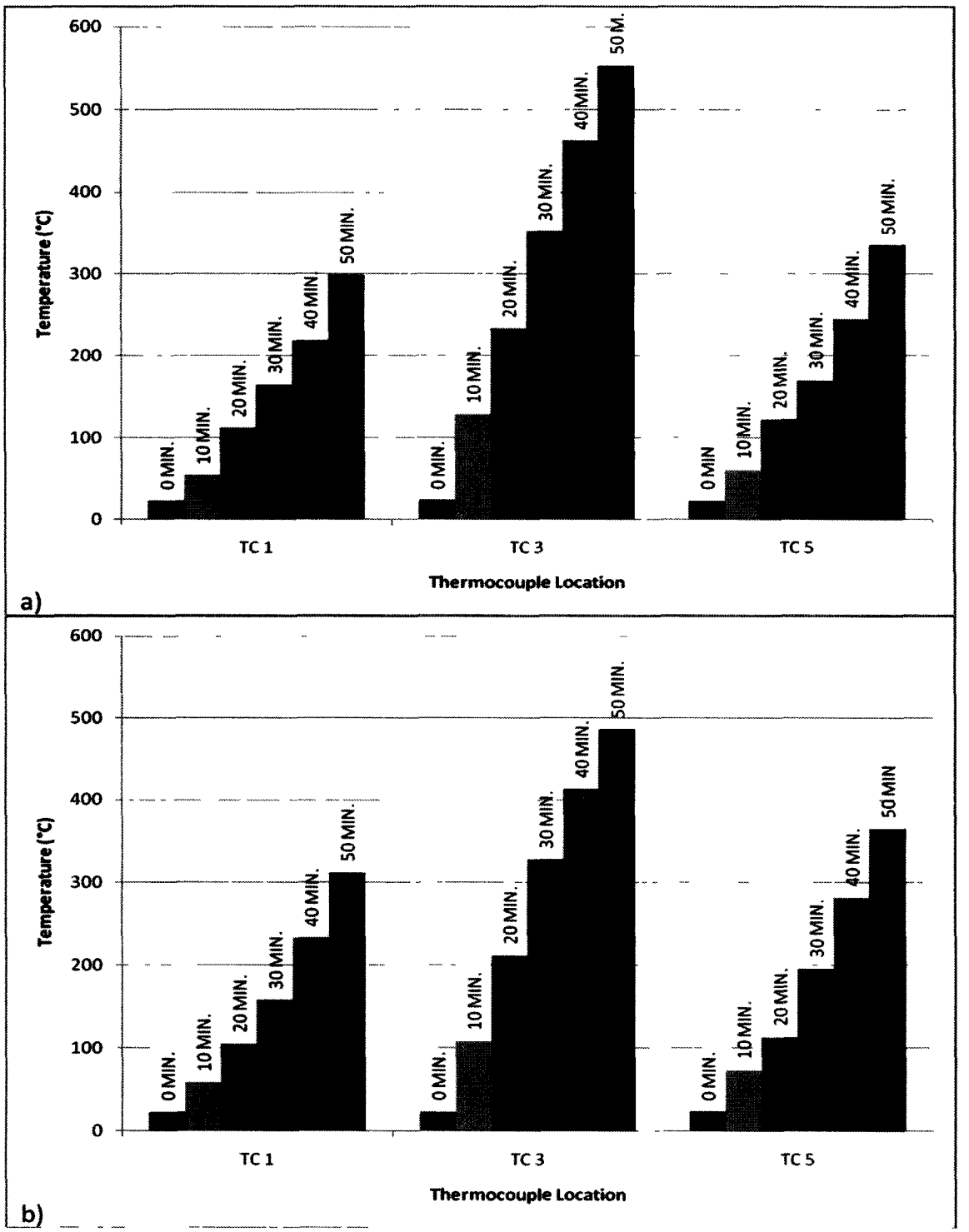
600
500
400
300
200
100
0
Temperature (°C)
0 MIN.
10 MIN.
20 MIN.
30 MIN.
40 MIN.
50 MIN.
TC 1
TC 3
TC 5
Thermocouple Location
a)
b)

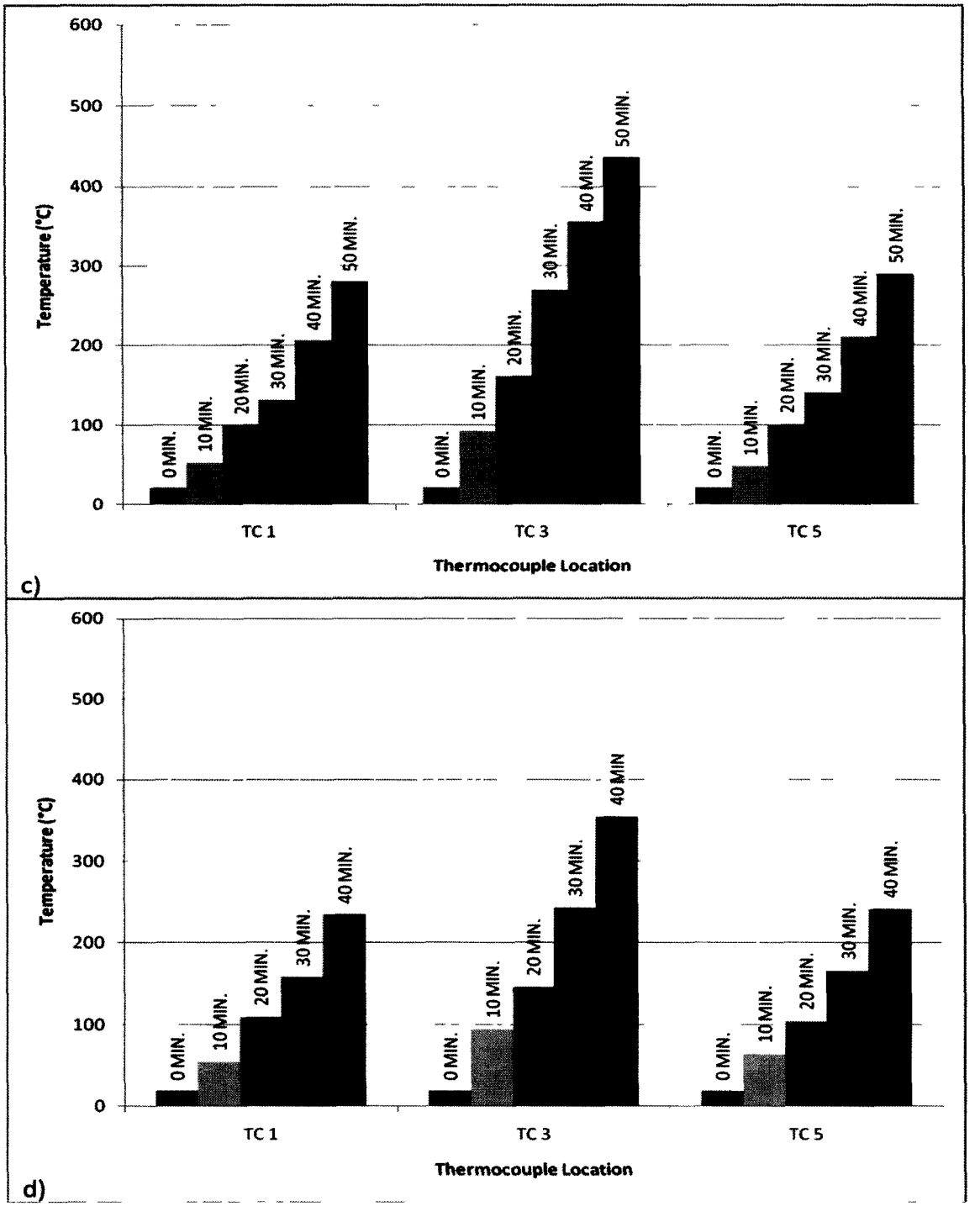

Figure 5-1: The temperature profile for each DOC at 10 minutes time intervals: a) 0% DOC, b) 1.25% DOC, c) 3.75% DOC, d) 5.25% DOC.

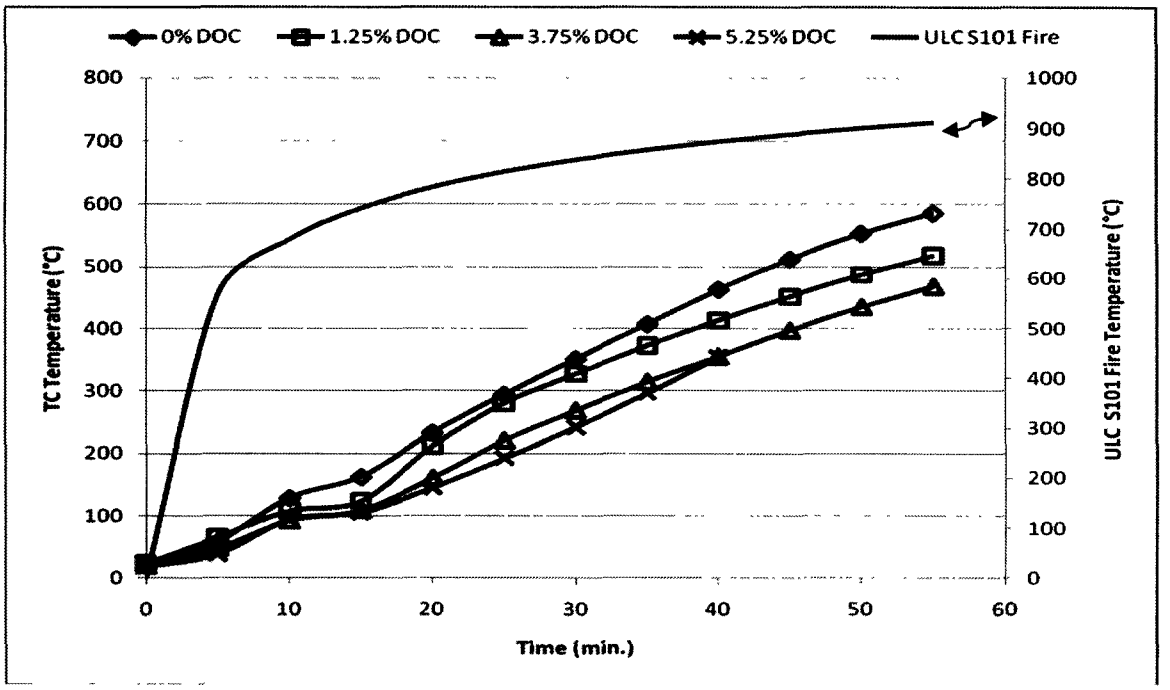

Figure 5-2: The temperature increase over time at the thermocouple location 3 (inside).

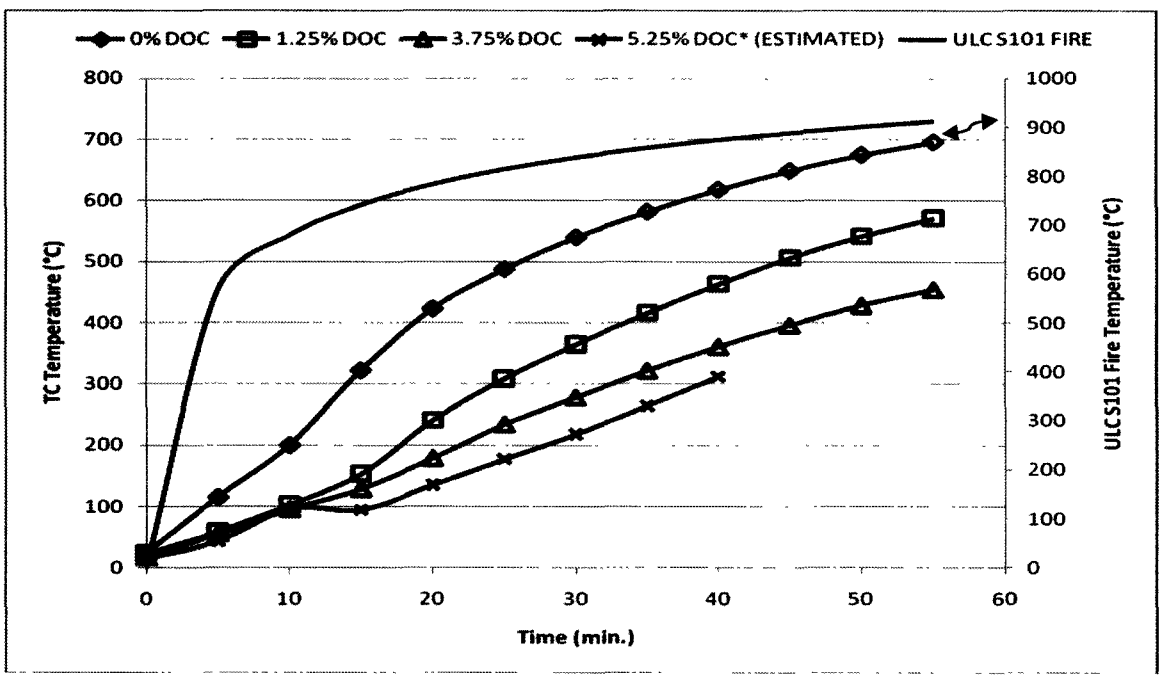

Figure 5-3: The temperature increase over time at the thermocouple location 4 (outside).

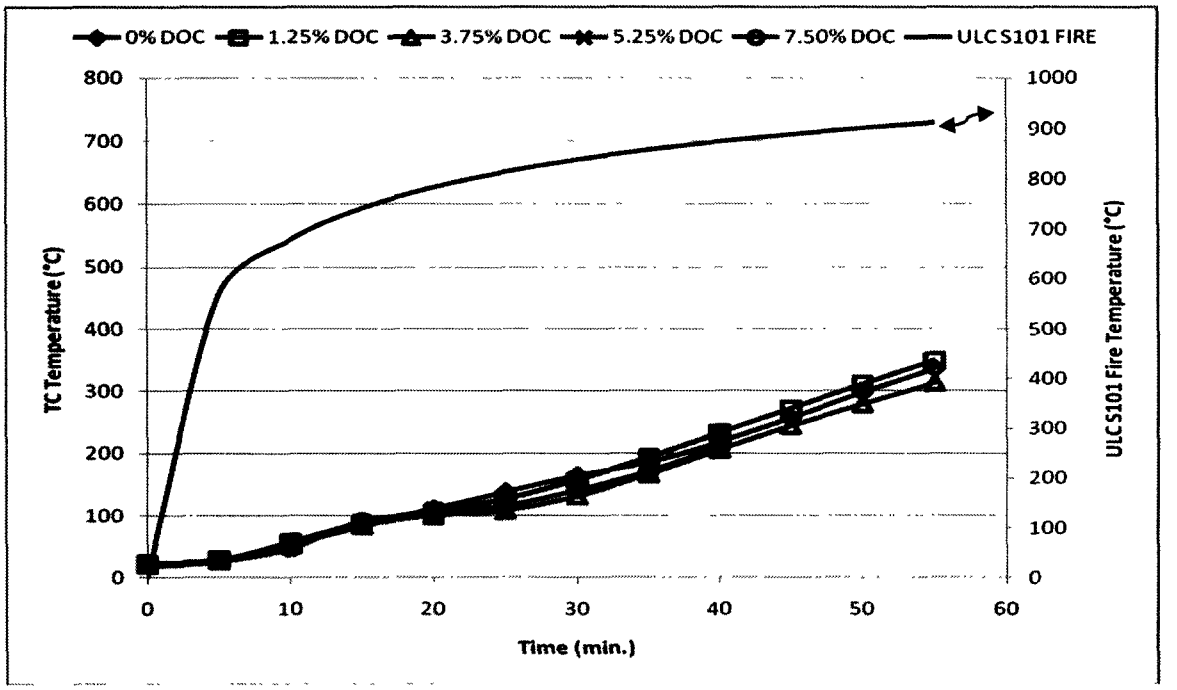

Figure 5-4: The temperature increase over time at the thermocouple location 1 (outside).

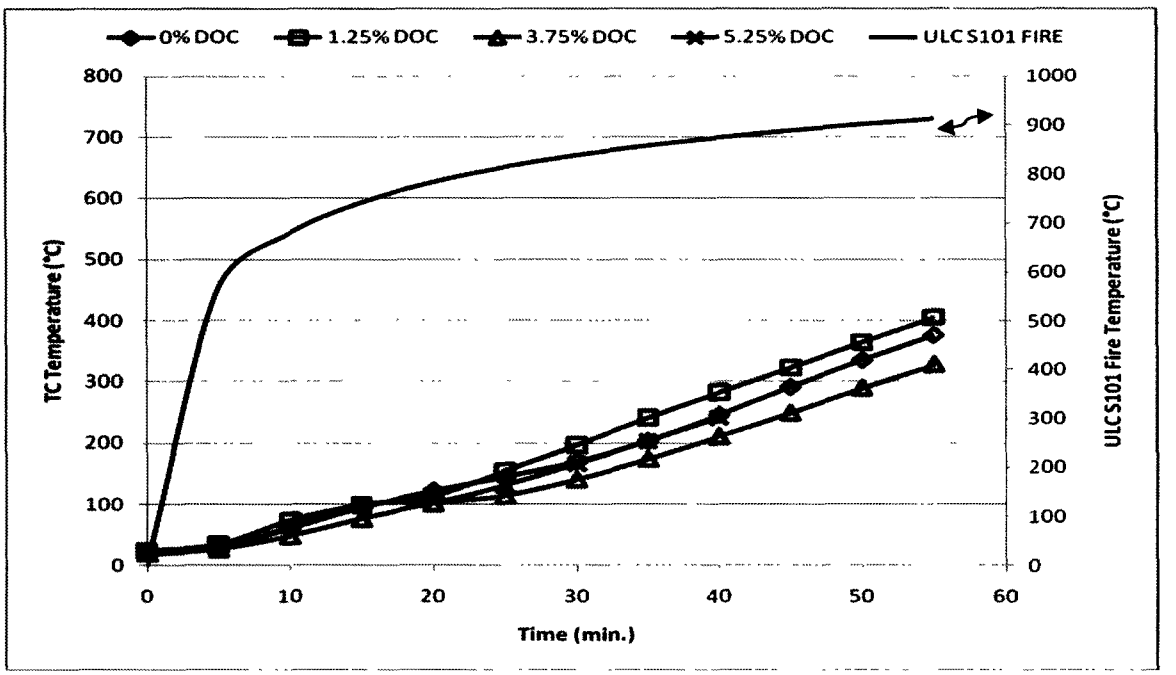

Figure 5-5: The temperature increase over time at the thermocouple location 5 (outside).

As the DOC increased the difference in temperature between the center of the beam (flexural region) and a point 227.5 mm away decreased resulting in a more uniform heating pattern for the flexural portion of the beam at the tensile steel level. Figures 5-6 to 5-9 show the temperature distribution for each corrosion level at different time intervals. The temperature difference between the centre and the ends was markedly lower for the corroded beams, as shown in Figure 5-10. The 'dip' shown in all the temperature graphs at ~100°C was most likely due to the evaporation of the pore water at this temperature.

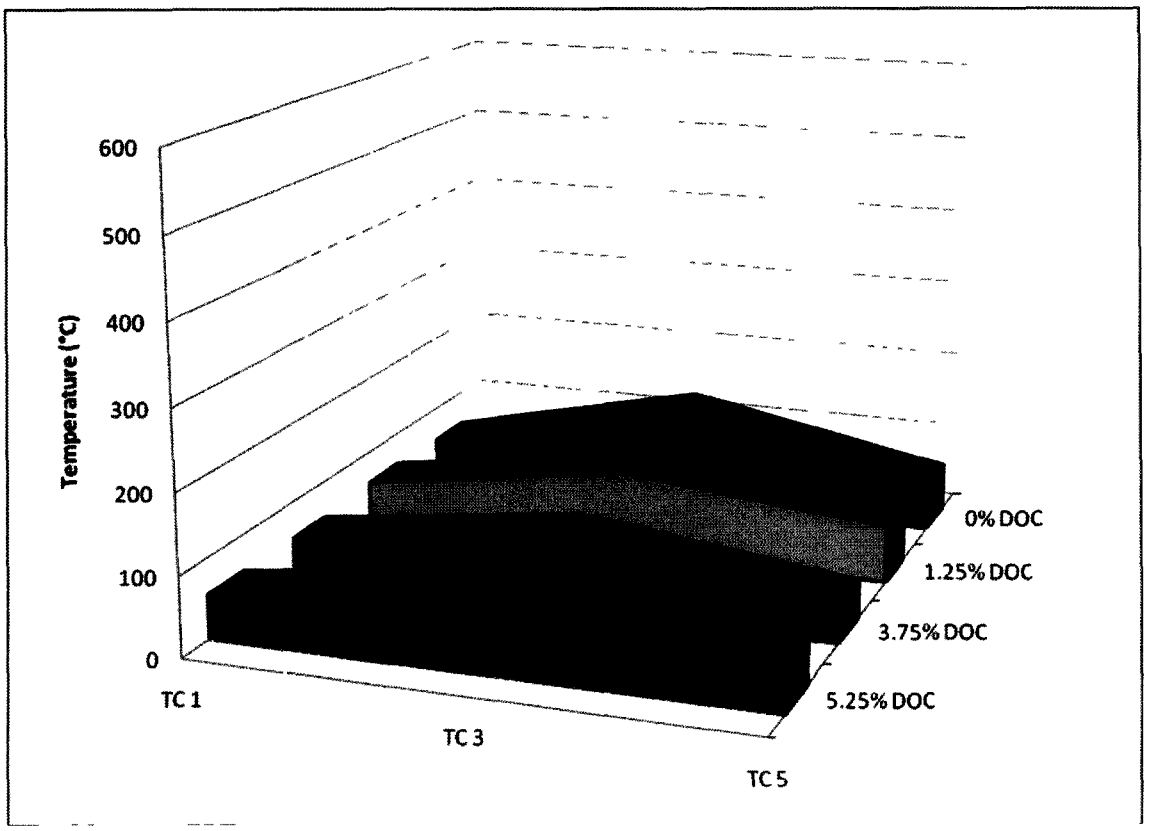

Figure 5-6: The temperature distribution along the beams after 10 minutes.

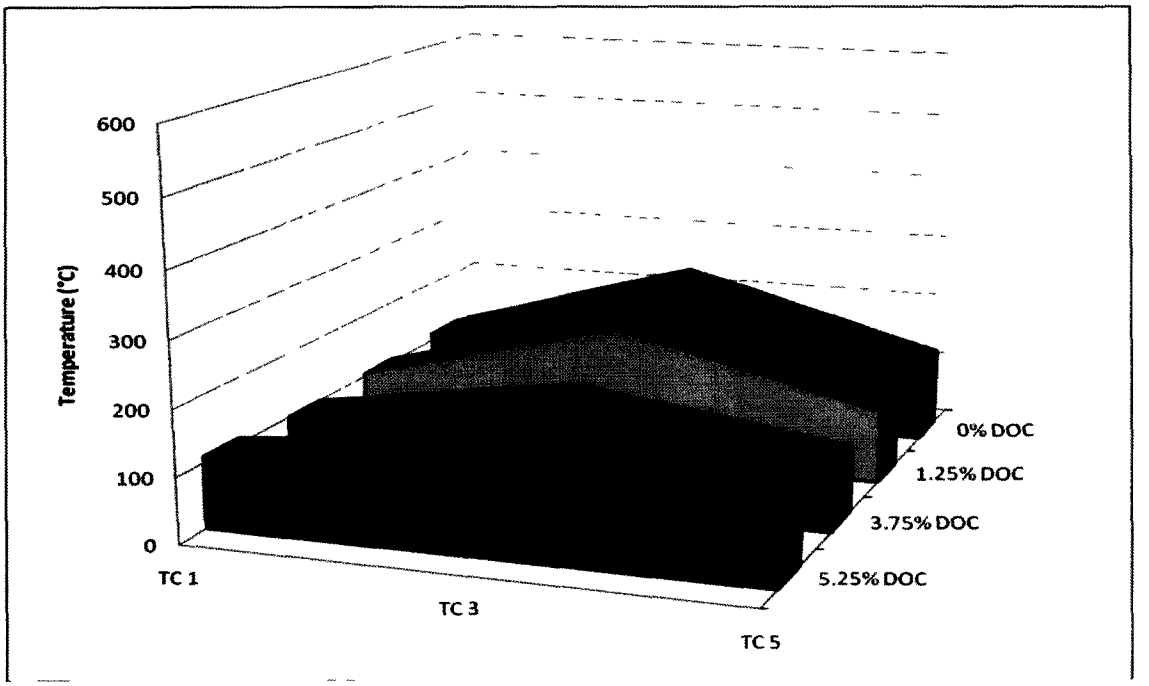

Figure 5-7: Shows the temperature distribution along the beams after 20 minutes.

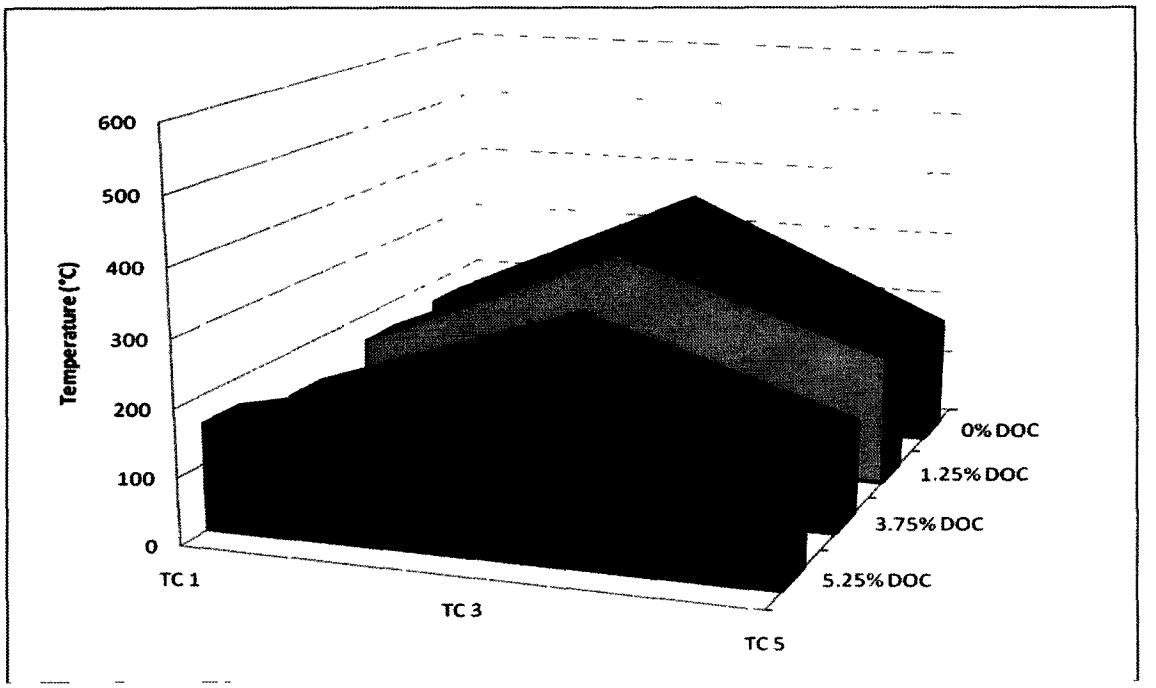

Figure 5-8: The temperature distribution along the beams after 30 minutes.

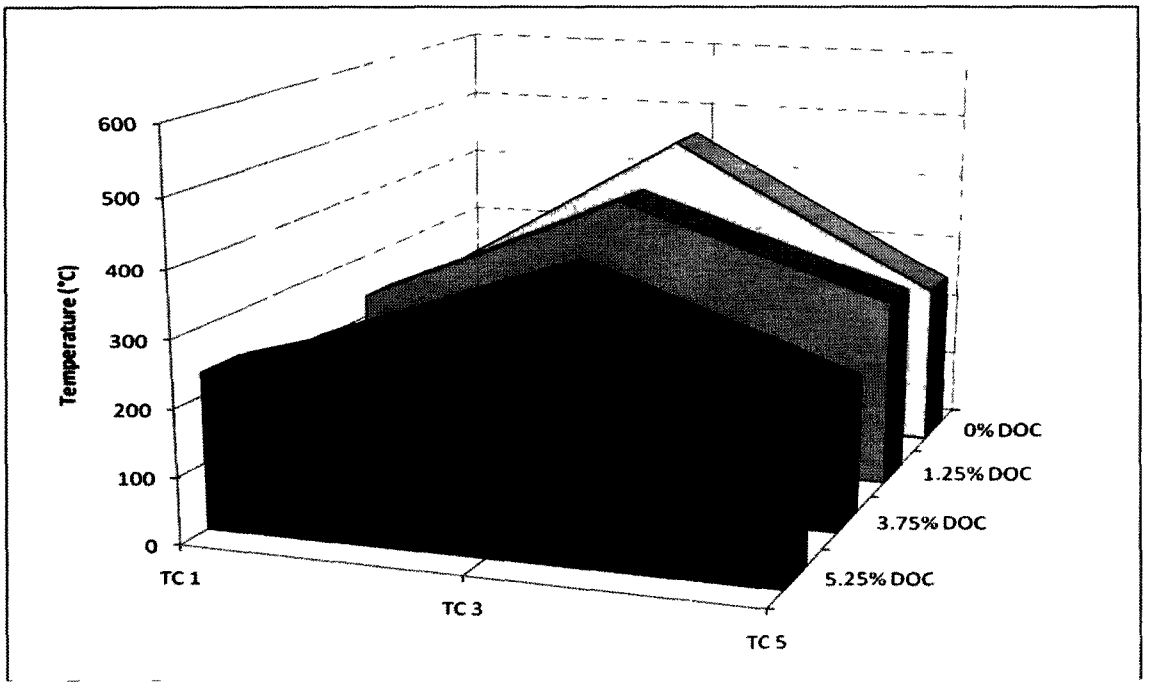

Figure 5-9: The temperature distribution along the beams after 40 minutes.

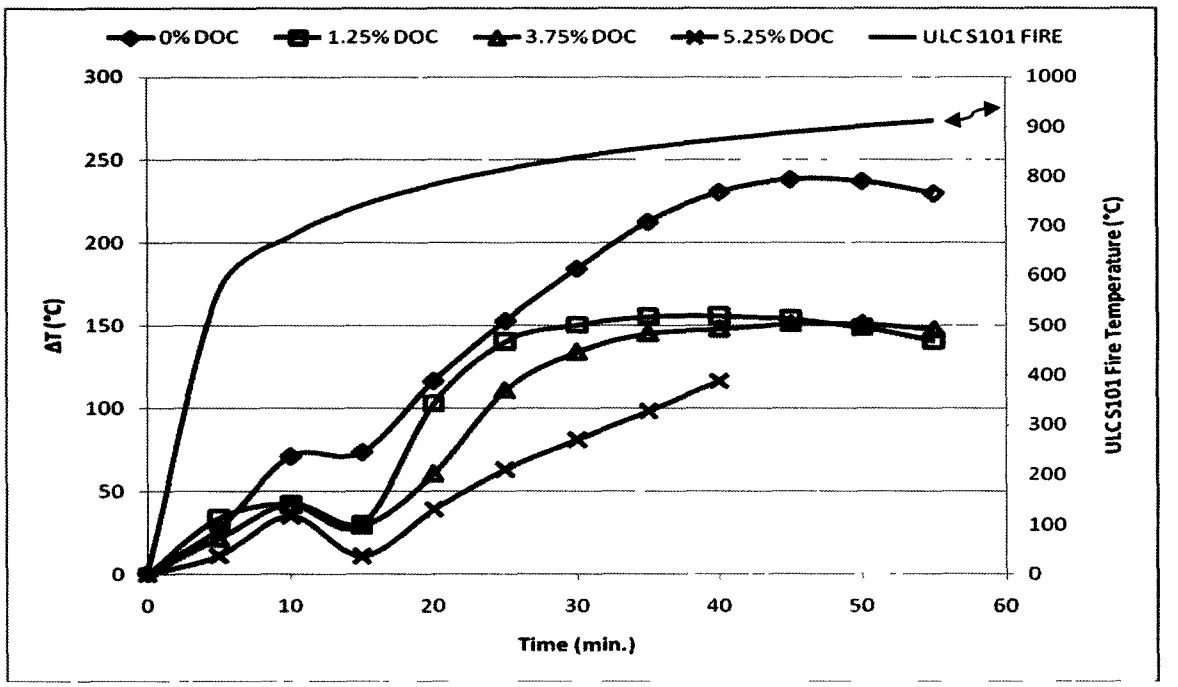

Figure 5-10: The temperature difference between the center and ends of the beams.

5.2 Structural response at elevated temperatures

This section describes the structural response of the corrosion damaged reinforced concrete beams in terms of the DOC, deflection, time, temperature and the thermal response parameters described in the previous section, 5.1.

5.2.1 Thermally induced axial restraint secondary moment

As described in section 2.3, when a reinforced concrete beam is subjected to high temperature an internal horizontal thrust force develops and assists the beam in resisting the applied load. This is termed the thermally induced axial restraint secondary moment (also referred to as secondary moment). The thermally induced axial restraint secondary moment was beneficial in terms of time in resisting the deflection of the beams. This force was reflected in the data as an 'increase in load' values. Since deflection and axial restraint secondary moment are directly related, the following Figures 5-11 to 5-19 show on the positive vertical axis as 'increase in load' (due to thermal response) while the negative vertical axis represents beam deflection.

5.2.2 Deflection and thermally induced axial restraint secondary moment

Figure 5-11 shows the mid-span deflection response of the beams versus time. It can be seen that the rate of deflection for all corrosion levels was similar. However the actual deflection value reached for any given time was significantly larger as the amount of corrosion damage increased. The difference in the deflection value between corrosion levels is mainly attributed to damage caused by corrosion while at the service loads.

The development and magnitude of the thermally induced axial restraint was similar for all corrosion levels with respect to time with the exception that there was a slight increase in the time required for the release of the axial restraint secondary moment for the corroded samples. This can be attributed to the fact that the steel in the corroded beams did not achieve as high a temperature for the same fire duration as shown in Figures 5-6 to 5-9. The only exception to this is the 7.50% DOC beam which began to plateau at a slightly lower increase in load and then began to deflect at a higher rate. This corresponded to the time at which a significant piece of concrete cover on one of the bars was observed falling off during the fire test (~ 24 minutes) thereby exposing one bar directly to the fire temperature. The other bar which still had intact cover continued to provide a beneficial thrust but only for a limited time (the plateau) before failure. A slight increase in the rate of deflection was observed after the release of the thermally induced axial secondary moment. This happened much sooner for the 7.50% DOC beam.

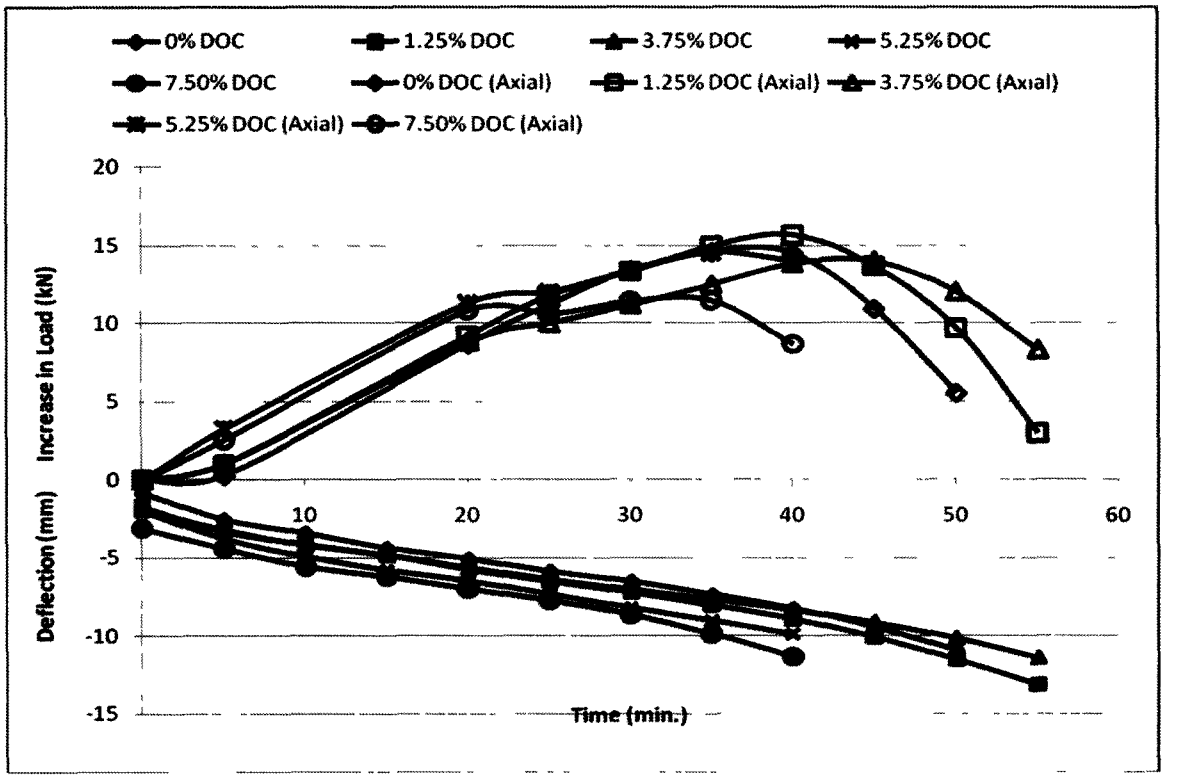

Figure 5-11: The deflection and thermally induced axial restraint as a function of time.

The area under the temperature distribution graphs (Figures 5-6 to 5-9) for all corrosion levels (up to 3.75% DOC) at the time when the increase in load is maximum is similar as shown in Table 5-1. When divided by the length of the direct heating zone (50% of total bar length – see Figure 5-12), the critical temperature at which the secondary moment begins to release is ~ 320-335°C, which corresponds to the temperature at which reinforcing steel begins to decrease in yield strength and modulus of elasticity and is also the critical bond temperature associated with degradation in bond strength.

Table 5-1: The critical flexural zone temperature at release of secondary moment.

DOC	Max Secondary Moment (min.)	Area under the Temperature Distribution Graph at given Time (mm-°C)	Critical Flexural Zone Bond Temperature (°C)
0 %	37.6	147,647	325
1.25 %	40	152,425	335
3.75 %	44.7	145,373	320

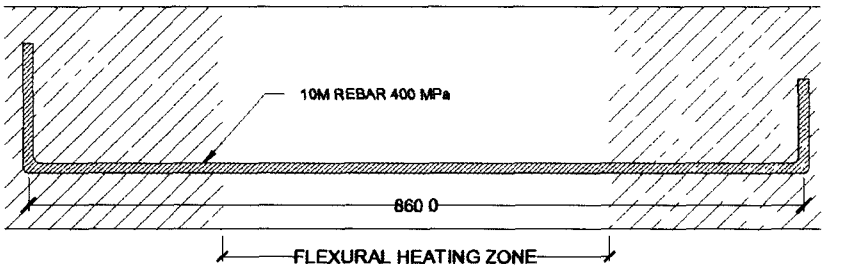

Figure 5-12: The flexural zone of the steel bar most susceptible to heating during the fire.

A similar increase in rate of deflection with the release of the secondary moment at the corresponding critical flexural zone bond temperatures can be seen in Figure 5-13. The reason that this increase in rate of deflection was small is because the rate of release of the secondary moment was similar to the rate of increase regardless of the corrosion level.

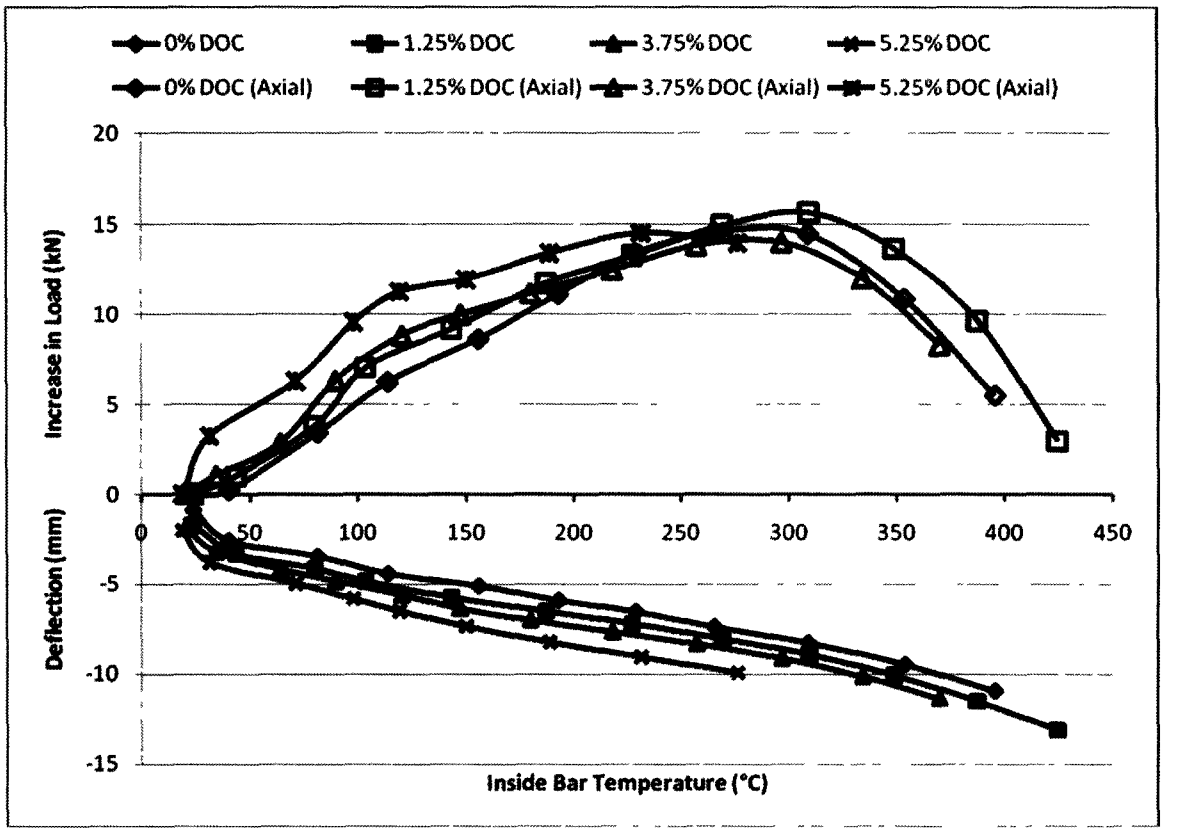

Figure 5-13: The effects of the average bar temperature in the flexural zone on the axial thrust force and consequently the rate of deflection.

Figure 5-14 shows that for increasing DOC the temperature gradient at which the thermally induced secondary moment began to degrade (without any further increase in temperature gradient) was lower for increasing DOC. However due to the insulating effect of the corrosion products in the pores, it still took slightly longer for the corroded specimens to reach the critical flexural zone bond temperature as shown in Table 5-1 and Figure 5-11.

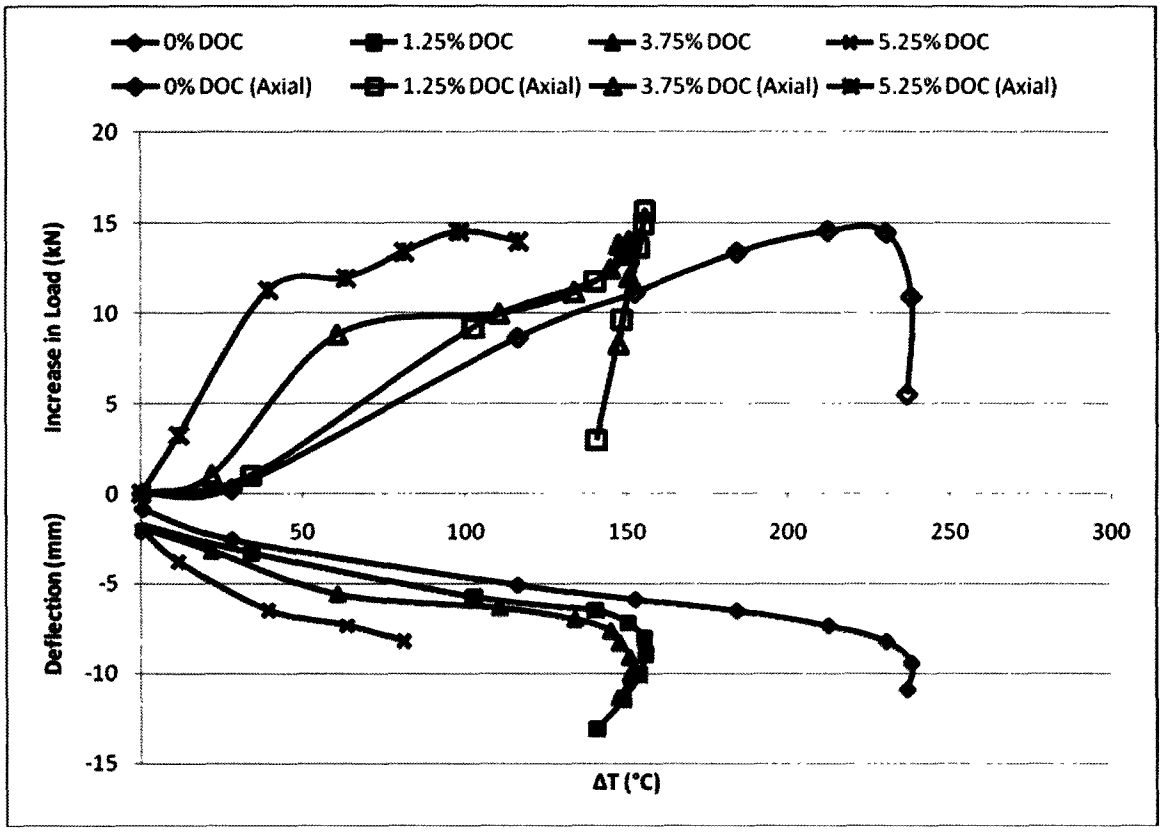

Figure 5-14: The effects of the temperature difference in the flexural zone on the axial thrust force and consequently the rate of deflection.

The thermally induced axial resistant force began to degrade at a much lower temperature difference for the corroded samples. This indicates that although the heating is slower due to a slower heat front penetration due to the thermal effect of the pores being blocked, the cracking in the corroded samples allowed for a more uniform temperature build-up along the bar. Since there was more uniform heating of the corroded samples, the maximum temperature at the centre (which some would consider being the critical temperature for failure) was actually lower for higher DOC as shown in Figure 5-15. Post-release of the secondary moment it can be seen that the deflection rate

began to increase, indicating that structural failure was imminent. Figure 5-15 shows that the corroded beams deflected further before the release of the secondary moment, due to degradation in bond strength as the DOC increased.

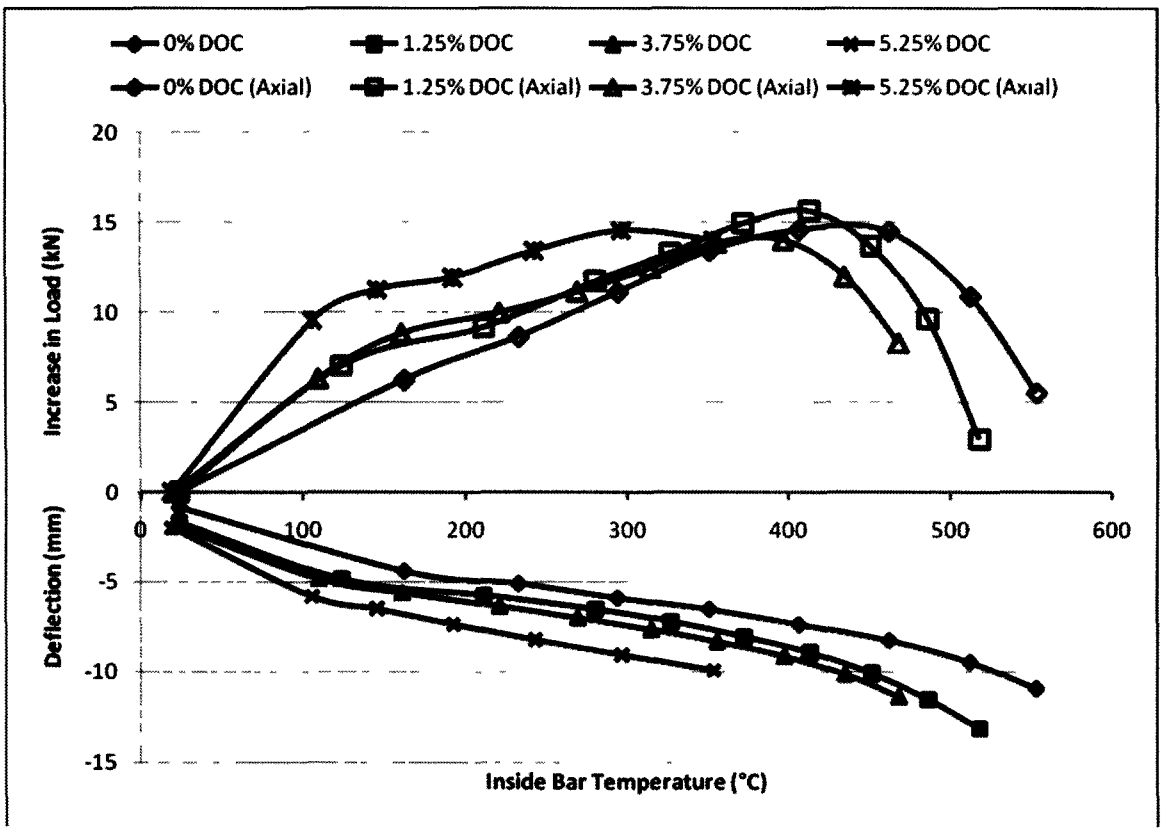

Figure 5-15: The effects of the temperature at mid-span on the axial thrust force and consequently the rate of deflection.

The effects of the cover delaminating during a fire exposure are shown in Figure 5-16; for the same beam we see a drop in the secondary moment developed and consequently an increase in deflection corresponding with the loss of the concrete cover during the fire exposure.

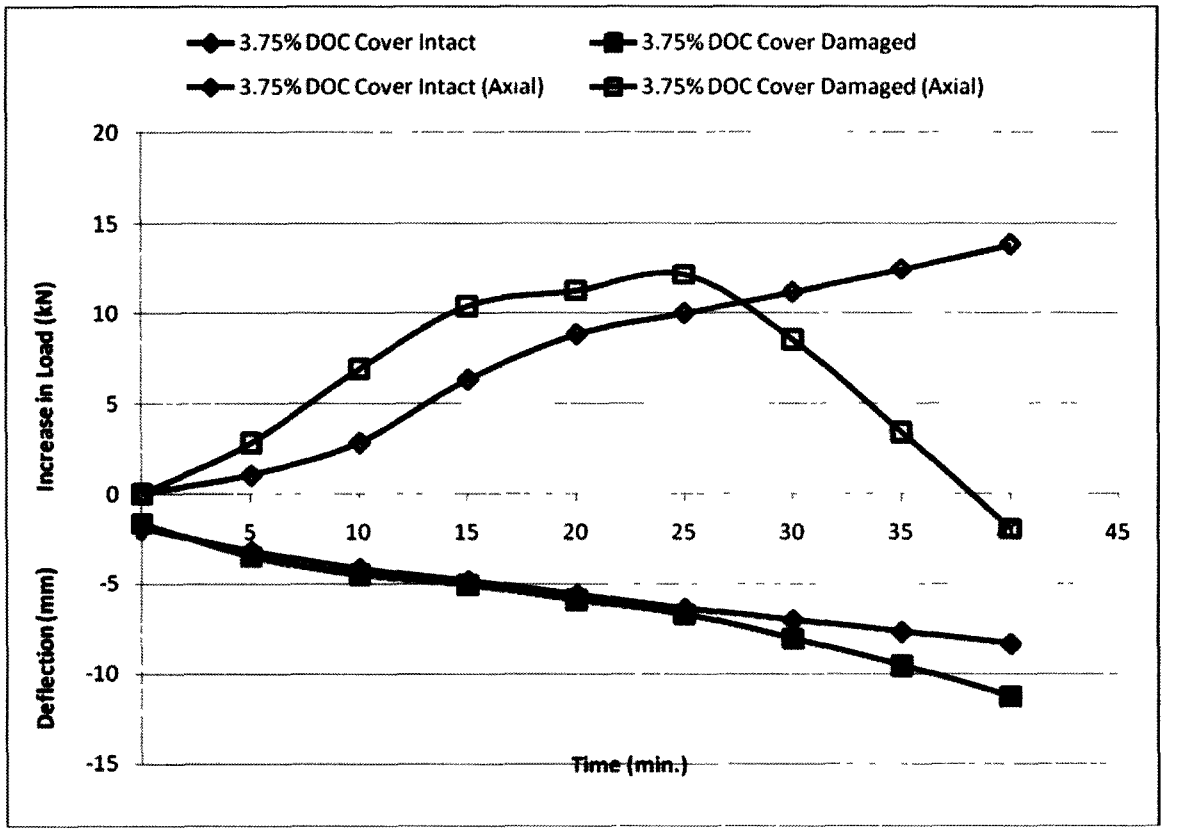

Figure 5-16: The effects of the cover spalling off during a fire exposure.

5.2.3 Effects of external shear clamps and insulation

This section presents the effects of the externally applied shear clamps and particularly the effects of the insulation that was used to protect the steel shear clamps during the fire exposure.

Figure 5-17 shows the effects of the external shear clamps and their associated insulation on the structural response of the beams with respect to time and fire exposure. It can be seen that without the beneficial effects of the external shear reinforcement, the beams designated as '30 mm No Shear Clamps' failed less than ten minutes into the

exposure while the beams with the shear clamps and insulation sustained a forty minute exposure; consequently the beams without shear clamps were affected by a much lower room fire temperature.

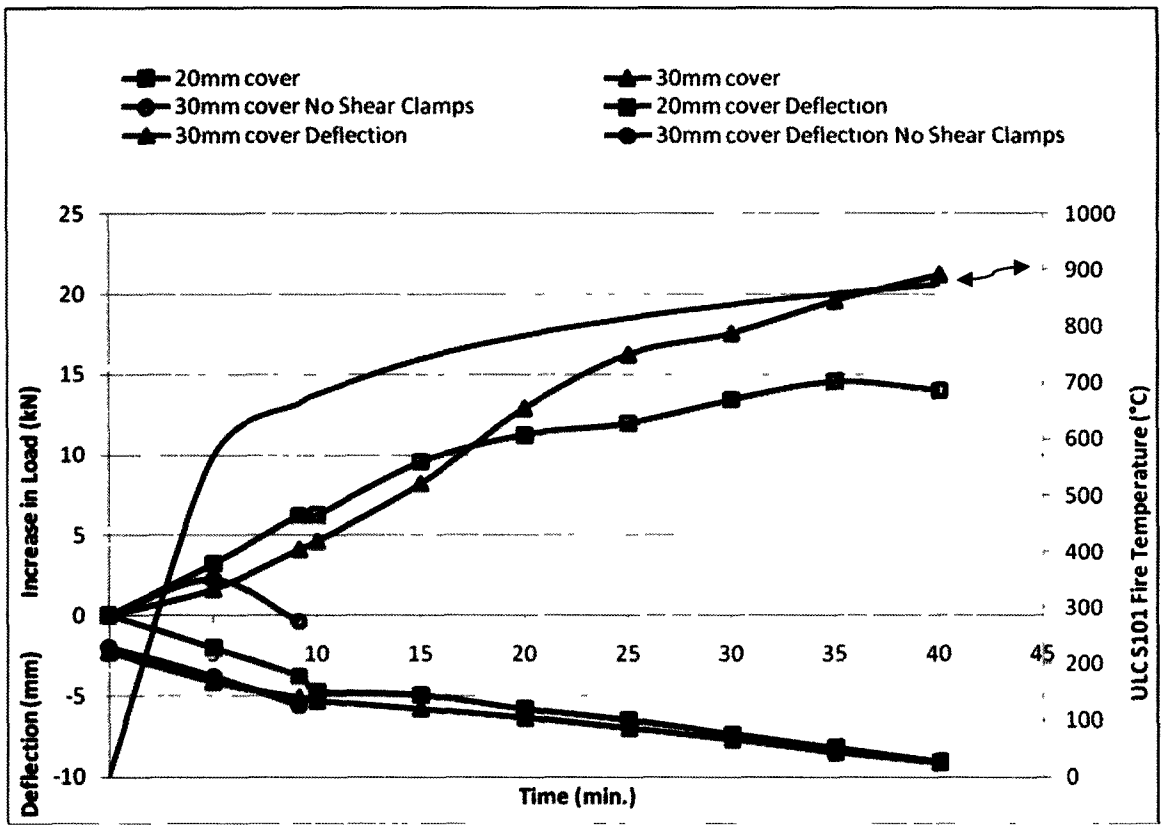

Figure 5-17: The effects of the external shear clamps and the associated insulation, at a constant level of 5.25% DOC.

Figure 5-17 also shows that for the same DOC of 5.25%, the beams with shear clamps exhibited a similar deflection response for both the 20 mm and the 30 mm cover samples. The only difference was that as the fire exposure progressed the load increase

was slightly higher for the 30 mm cover sample, likely due to the slower heat front penetration for the thicker cover.

The temperature gradients developed in two specimens of similar corrosion level showed that the shear clamps with their associated insulating coverings allowed for the development of an internal temperature difference between the center and the ends of the beam, as compared to a beam without external shear clamps for the same time duration, as shown in Figure 5-18.

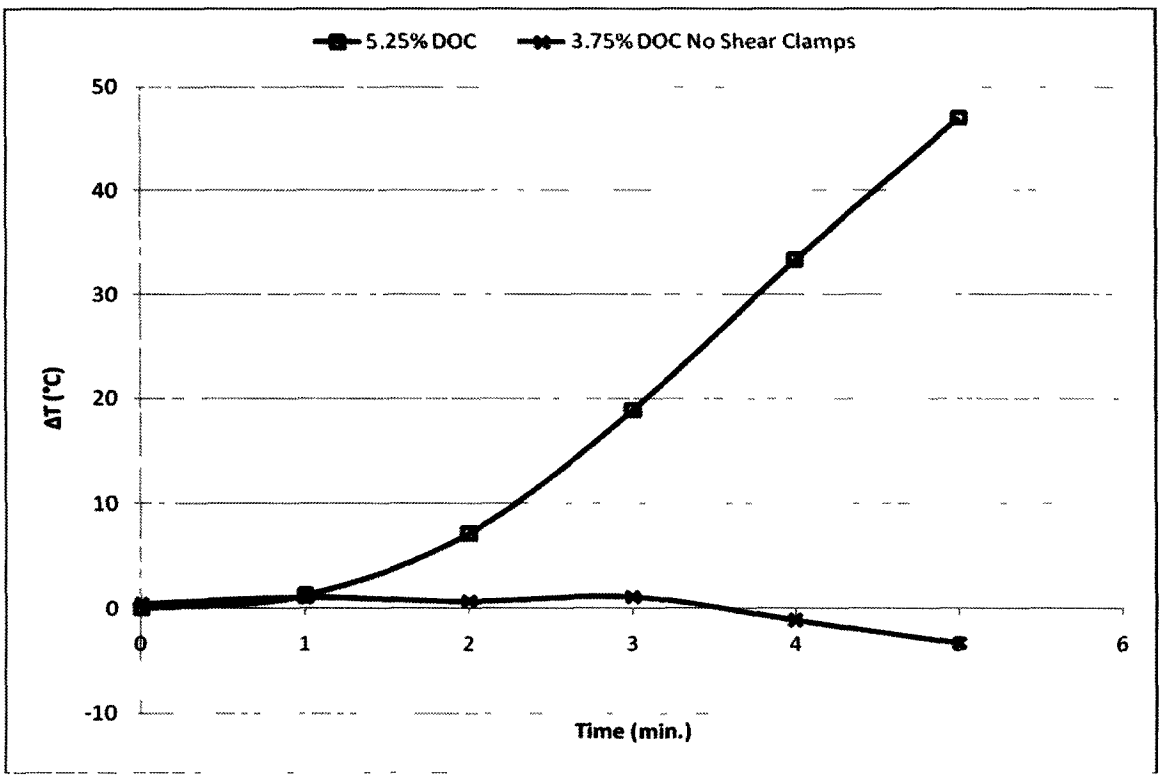

Figure 5-18: The temperature gradient developed between the center and the ends for the first 5 minutes of exposure for a 5.25% DOC beam with shear clamps and a 3.75% DOC beam without shear clamps.

For the same two beams shown in Figure 5-18, Figure 5-19 represents how the temperature gradient affected the increase in load. It can be seen that for the same time duration, the beam with the shear clamps developed (and continued to increase with fire exposure) a temperature gradient between the center and the ends, thereby also allowing the load to be sustained (and increased over time); while the beam without the shear clamps and insulation did not develop a temperature gradient and consequently did not develop or maintain any noticeable increase in load. The 5.25% DOC beam with shear clamps and insulation shown in Figure 5-19 sustained a 40 minute fire (burn-out) while the 3.75% DOC beam without shear clamps and insulation failed within the first five minutes of exposure corresponding to the negative temperature difference shown in Figure 5-19.

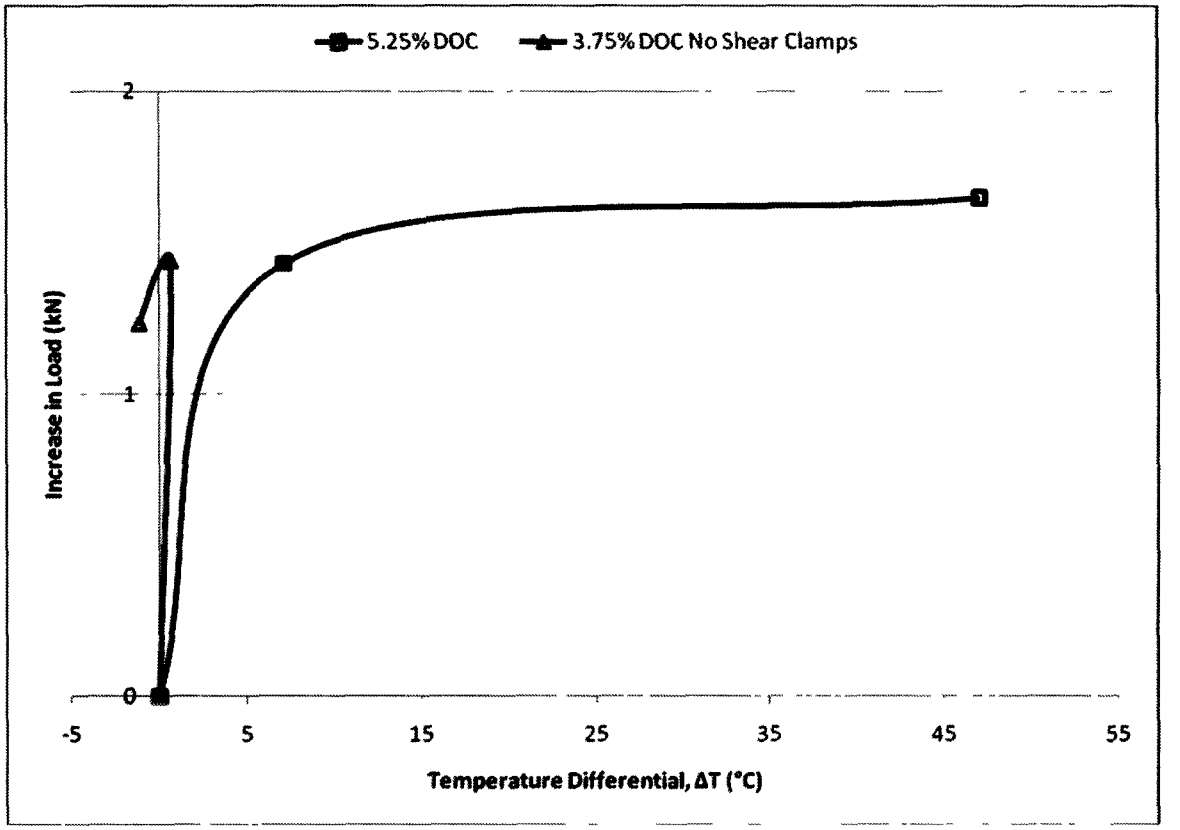

Figure 5-19: The effect of temperature gradient on the development of the secondary moment for the first 5 minutes of exposure for a 5.25% DOC beam with shear clamps and a 3.75% DOC beam without shear clamps.

Figure 5-20 shows the deflection as a function of time for three corrosion levels for beams tested without shear clamps. The time to failure of the beams tested without external shear reinforcement increased as the DOC increased, up to 5.25%. This can be attributed to the insulating effects of the corrosion products within the pores, slowing the critical heat front penetration through the cover to the steel level; and enhanced anchorage due to a build up of corrosion products at the bar ends could delay the failure of corrosion damaged beams (Cairns *et al.*, 2008).

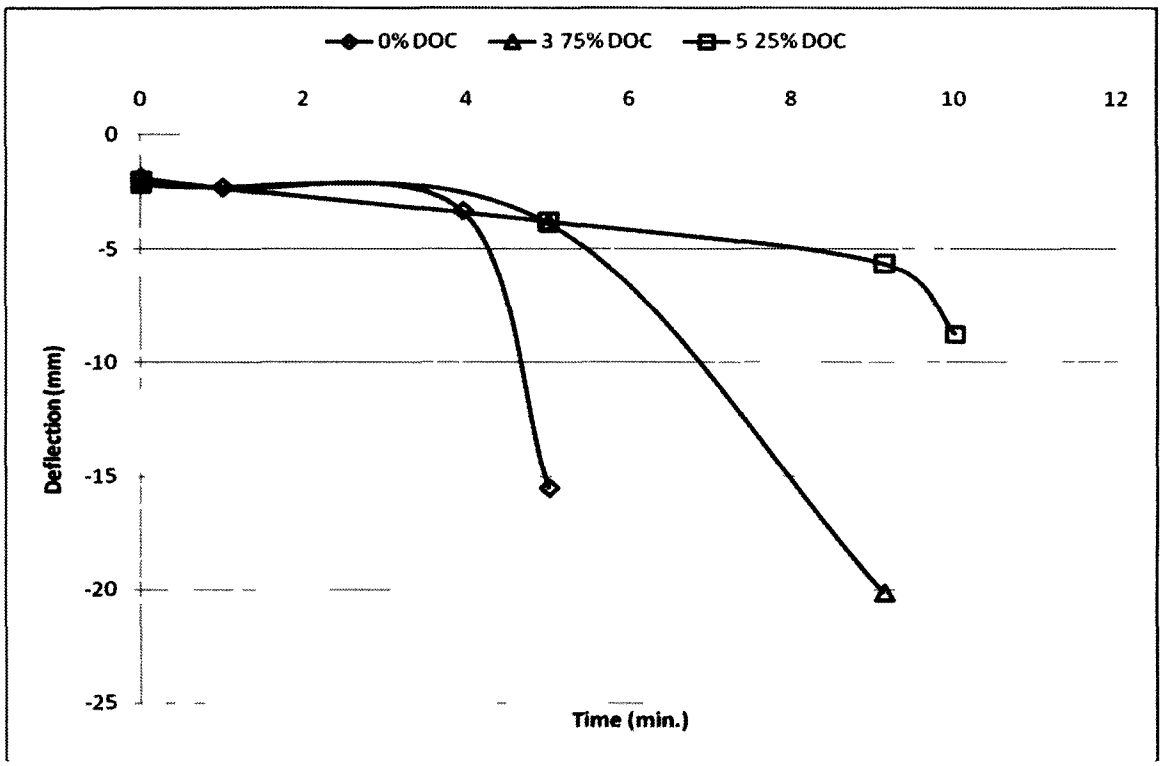

Figure 5-20: The deflection as a function of time for three corrosion levels for beams tested without shear clamps.

Figures 5-21 and 5-22 show the failure patterns of the beams without shear clamps. The pre-dominant failure mode in these beams without any internal or external shear reinforcement was a typical shear failure as shown in Figure 5-21 for the beam with 0% DOC, with 45 degree cracks through the shear zone. For the corrosion damaged beams the failure mode was a mixture of bond failure with a large vertical crack closer to the shear region of the beam, as seen in Figure 5-22. While residual tests on corrosion damaged beams exhibited a similar failure to that of Figure 5-22, with the difference being that the single vertical crack was clearly in the flexural zone of the beam very close to mid-span.

Figure 5-21: Typical shear failure of the beam with 0% DOC and no shear reinforcement.

Figure 5-22: Typical bond failure of the beam with 3.75% & 5.25% DOC and no shear reinforcement.

5.3 Post-fire Exposure Residual Response

As shown in Figure 5-23 and described above, the critical temperature at the steel concrete interface was ~ 325°C. This corresponded to an average fire exposure temperature of 850°C (for 20 mm cover) and a corresponding fire exposure time of 40 minutes. Following this exposure and the specimen cooling naturally while under sustained service load, the results of residual tests are presented as follows in this section.

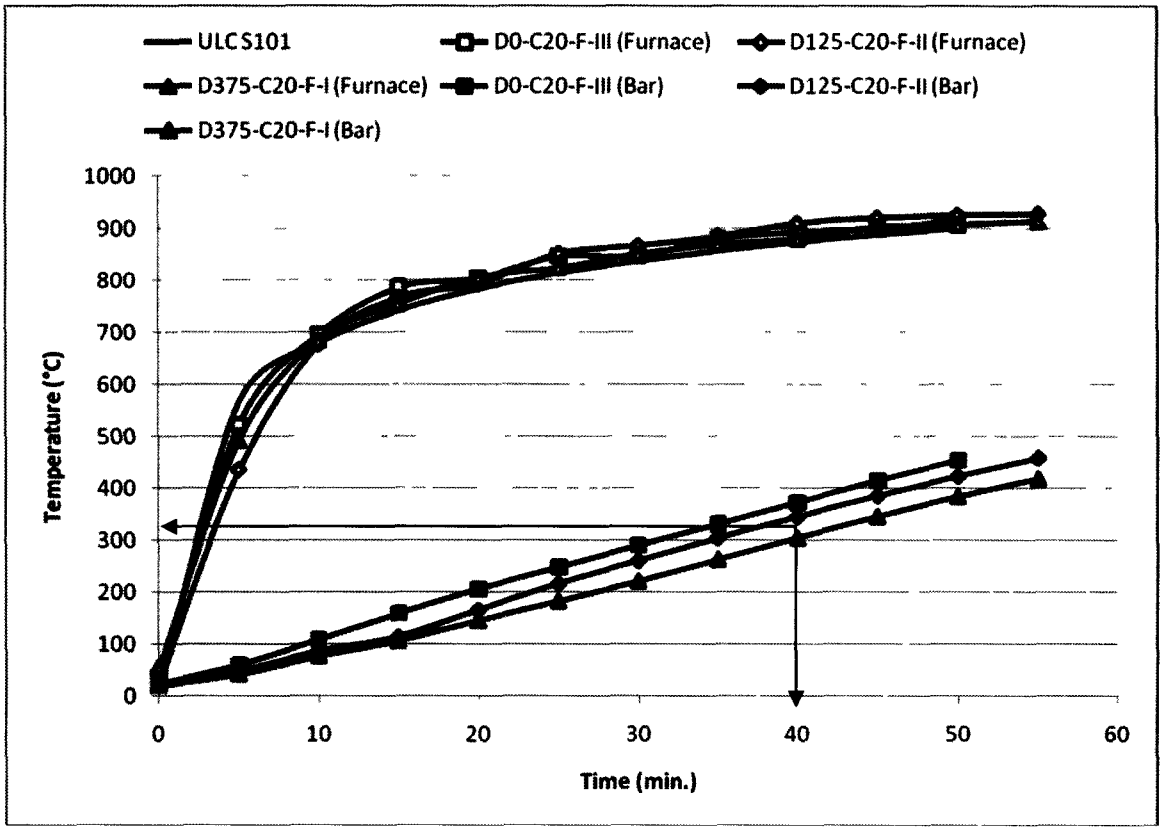

Figure 5-23: The relationship between time and temperature used to determine the fire exposure time for the residual strength tests.

5.3.1 Residual load and deflection

This section presents the results of flexural testing of the beams to failure after cooling back to ambient conditions following a 40 minute exposure to the standard fire.

The residual load versus deflection curves for varying DOC's are shown in Figure 5-24. The load values commence at the service load level with the deflection corresponding to the value obtained as a result of the fire exposure and subsequent cooling. This figure also shows the results of a control beam test that was tested without

any fire exposure or corrosion damage, so that the results could be normalized and compared to Mangat and Elgarf (1999).

It can be seen that the residual deflections obtained during the fire exposure were significant. The residual deflection obtained for the 0% DOC beam occurred at more than two times the load level for the 0% DOC control beam. Also it can be noted that once the yield plateau level was reached, there was significantly less ductility before failure for all of the combined corrosion / fire damaged beams. It is noted that the 3.75% DOC result is slightly skewed because the cover partially spalled off ~20 minutes into the fire exposure, thereby directly exposing a portion of the steel and the interior concrete to the high temperatures thereby causing further degradation and deflection during the fire exposure; resulting in reduced residual strength performance.

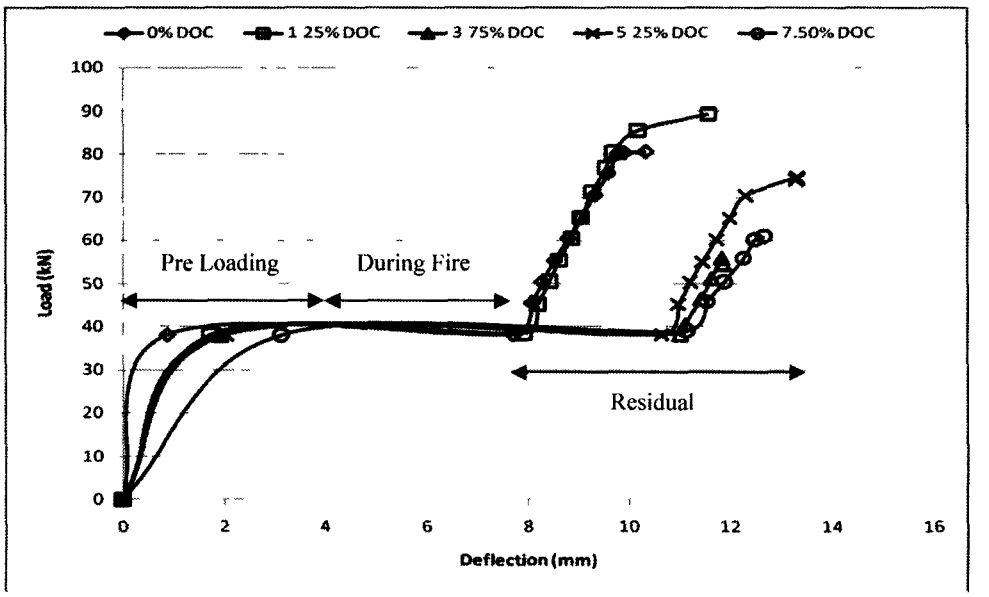

Figure 5-24: The residual strength and deflection relationships for all tested DOC. Note the pre-loading phase ends once the service load level is reached.

In order to compare the data gathered during this research project to research published by Mangat and Elgarf (1999), a portion of their results are presented in Figure 5-25. The beams of Mangat and Elgarf (1999) are built with the same specifications as the beams used in this research project. The corrosion was applied using the same technique and the flexural test set-up was also the same. The only difference being that the Mangat and Elgarf (1999) beams were not exposed to fire conditions.

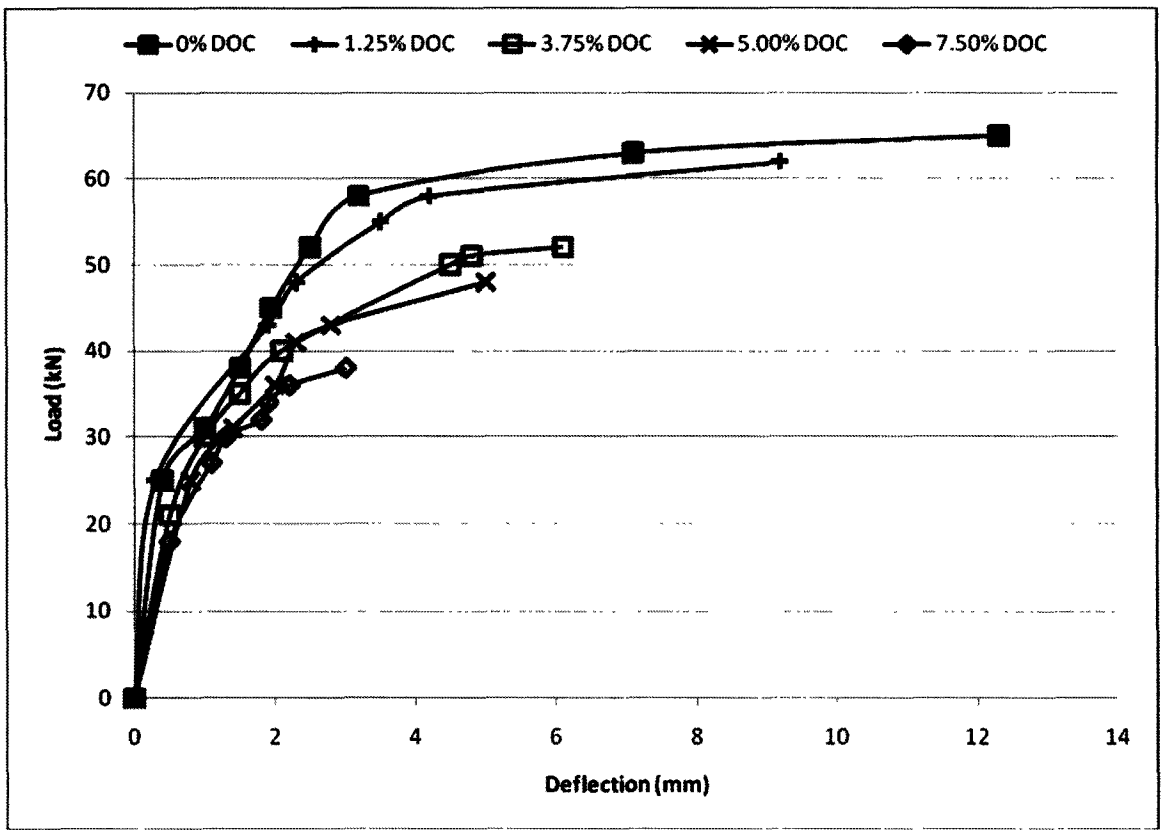

Figure 5-25: The residual strength and deflection relationships for varying corrosion levels as published by Mangat and Elgarf (1999).

A comparison of Mangat and Elgarf (1999) at 0% DOC and our control beam (0 % DOC) shows that although the specifications were followed as closely as possible, some variation in both ultimate strength and deflection existed as seen in Figure 5-26. In order to be able to compare the ultimate load and deflection values, the Mangat and Elgarf (1999) ultimate values published by Mangat and Elgarf (1999) were adjusted by 46% and 18% for the ultimate load and ultimate deflection, respectively. Normalizing the ultimate state values for these two similar beams facilitates a comparison at ultimate load and deflections for both studies.

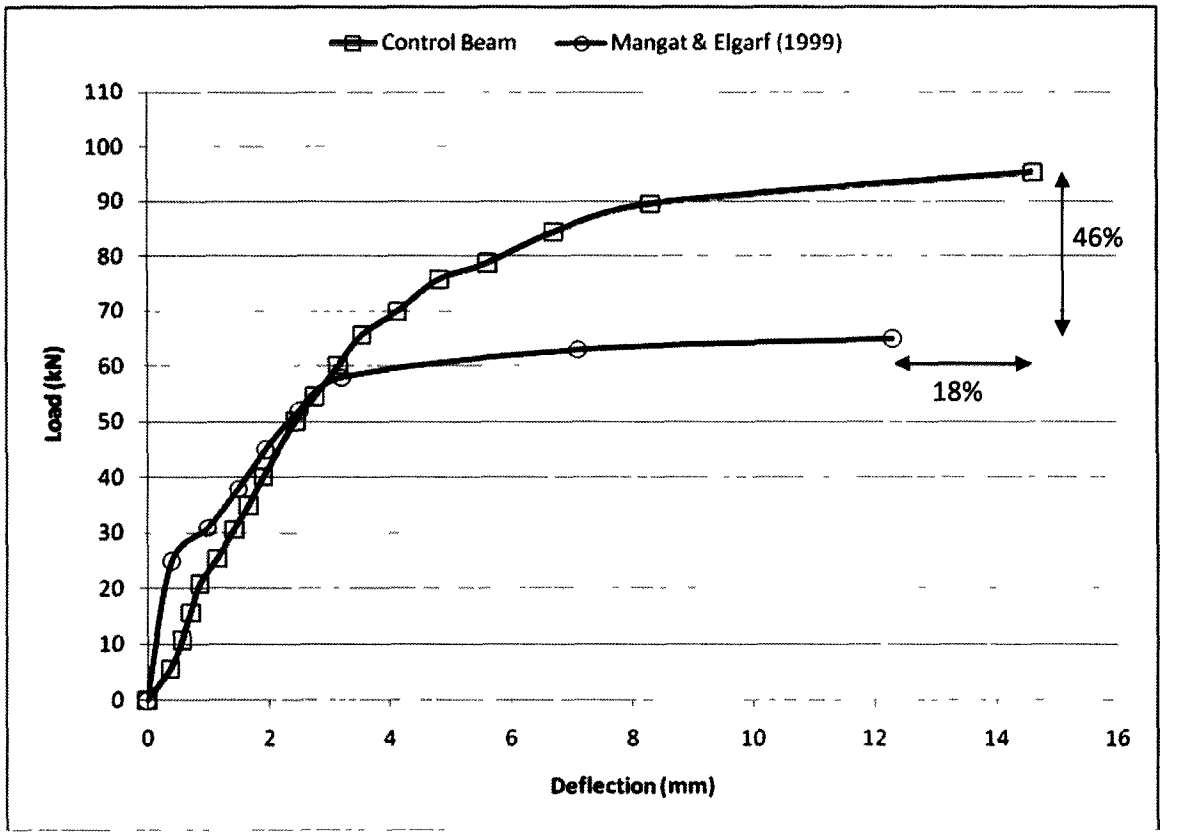

Figure 5-26: The normalization comparison between the results of this research project and the work by Mangat and Elgarf (1999).

A comparison of the ultimate strength attained for both this project and the non-fire exposed Mangat and Elgarf (1999) beams shows that as the corrosion level increased, the residual strength values decreased (see Figure 5-27). The corroded beams from this study are within 10% of the adjusted Mangat and Elgarf (1999) ultimate load values. The near linear relationship shown in Figure 5-27 represents the decrease in load with increasing DOC. The data points associated with this research are labelled GL (2010).

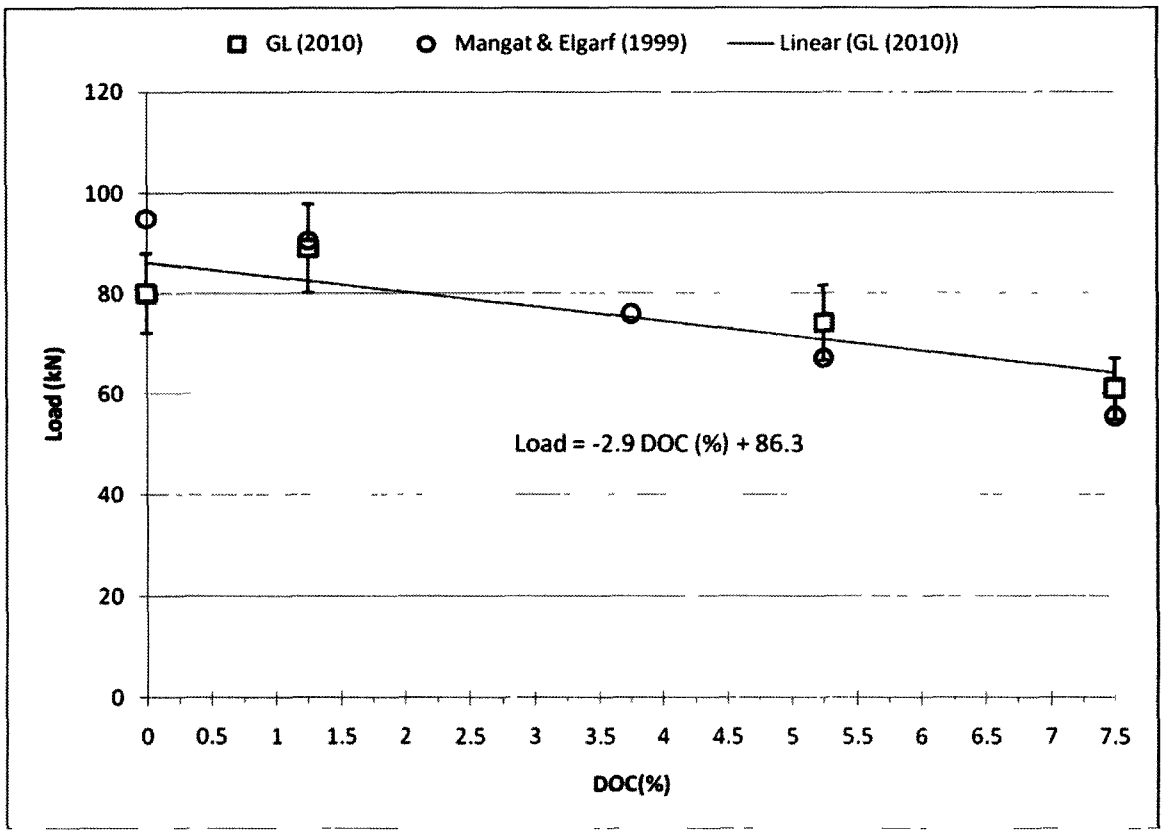

Figure 5-27: The strength at maximum deflection values for this study and Mangat and Elgarf (1999).

The percentage residual strength at failure as a function of the residual strength at 0% DOC was consistently higher for the fire exposed beams as compared to the non-fire exposed beams, as seen in Figure 5-28. The corrosion damaged beams exposed to fire generally had a ~20% higher residual load capacity (for all tested corrosion levels) then the unexposed beams while at maximum deflection. The linear correlation shown on Figure 5-28 represents the loss in residual strength as a function of DOC, for the fire exposed beams tested in this study.

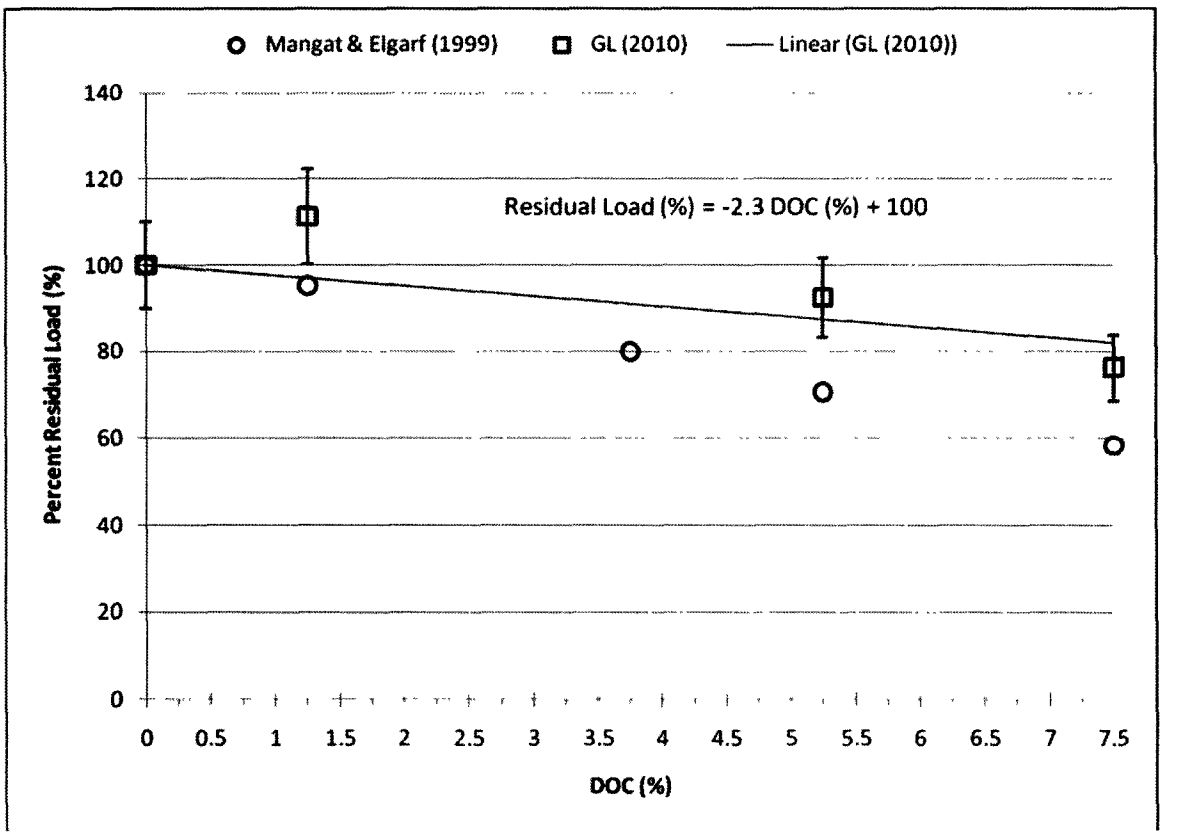

Figure 5-28: The percent residual strength at maximum deflection for all corrosions levels at failure for this study and Mangat and Elgarf (1999).

While the residual strength at failure was ~20% higher for the fire exposed beam as previously discussed and shown in Figure 5-28, it must be considered that the deflection was significantly higher at ultimate loads for the fire exposed beams as compared to the non-exposed beams, as shown in Figure 5-29. While the ultimate deflection values decreased with increasing DOC for the non-fire exposed beams; conversely the fire exposed beams experienced an increase in ultimate deflection with increasing DOC as seen in Figure 5-29. As the corrosion level increased the difference between the fire exposed and non-exposed beams increased to a maximum of ~400% more deflection at failure at 7.5% DOC.

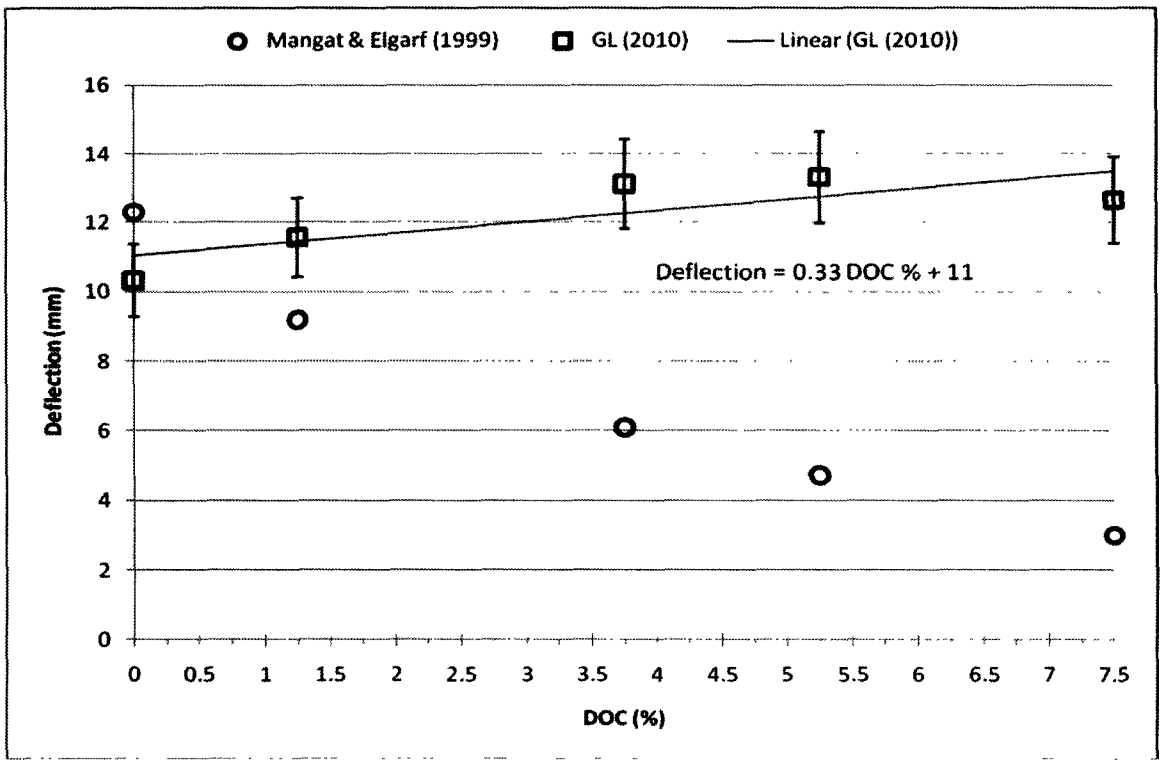

Figure 5-29: The maximum deflection at failure for all corrosions levels for this study and Mangat and Elgarf (1999).

In terms of percentage of deflection increase relative to 0% DOC, the trend line of increasing deflection value at failure as a function of DOC in shown in Figure 5-30. Clearly there is a strong divergence of the deflection values at failure as the DOC increased; between the fire and non-fire exposed beam.

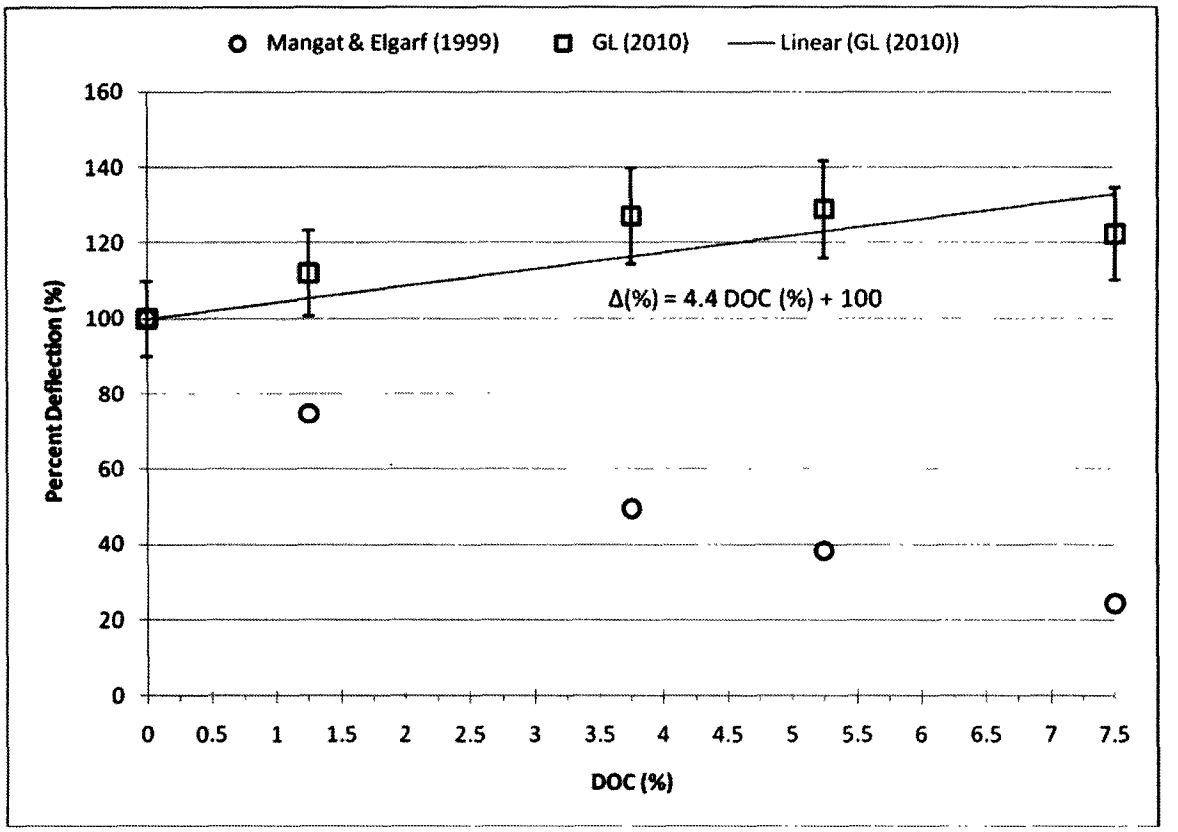

Figure 5-30: The maximum percent deflection at failure for all corrosion levels as a function of 0% DOC for this study and Mangat and Elgarf (1999).

Comparing the deflections at service load levels (see Figure 5-31) shows an average of 8 times increase in deflection values after the fire exposure. As expected, the deflections at service load increased with increasing DOC at similar rates for the pre and

post fire cases. Since considerable deflection had occurred due to the fire exposure, there was little residual deflection available.

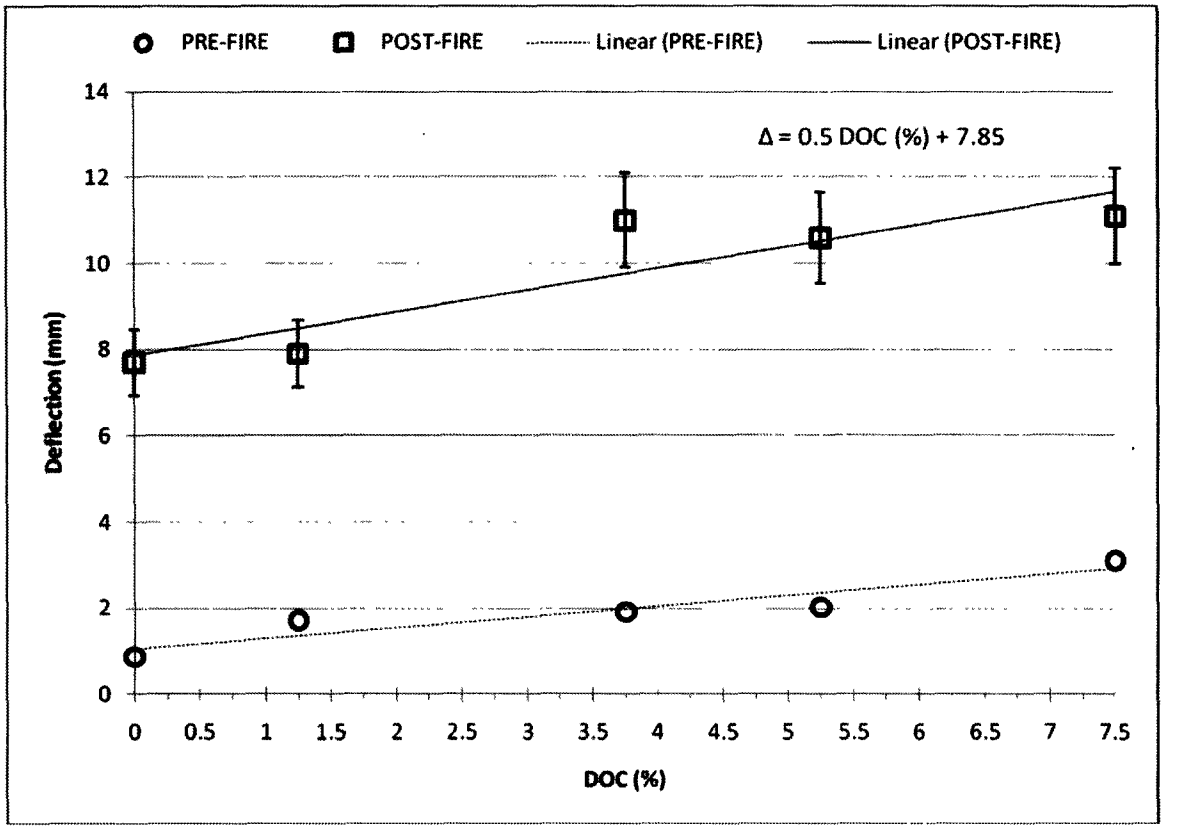

Figure 5-31: A comparison of pre-fire and post fire deflections for all corrosion levels at service load.

In terms of fire exposure and corrosion damaged beams it is necessary to consider both the load and corresponding deflection when discussing maximum residual load at failure. Figure 5-32 summarizes the residual strength and deflection interactions for both fire exposed and non-exposed beams. Clearly, for the fire exposed beams, as the

maximum load decreased with increasing DOC, the amount of deflection attained at these maximum loads increased with the same increasing DOC.

Conversely, as the residual load decreased for the non-fire exposed beams, the maximum deflection value attained at the failure load also decreased sharply with increasing DOC. This means that for the same DOC, the fire exposed beams had more ductility before failure. The only exception is that for beams without any corrosion damage (0% DOC), the residual strength was ~20% lower for the fire-exposed exposed beam. Furthermore the fire exposed beams exhibit ~40% less deflection at 0% DOC as compared to the same non-fire exposed beam. Figure 5-32 also shows plotted data points of the non-normalized load and deflection values published by Mangat and Elgarf (1999) which demonstrate the same trends as the normalized values.

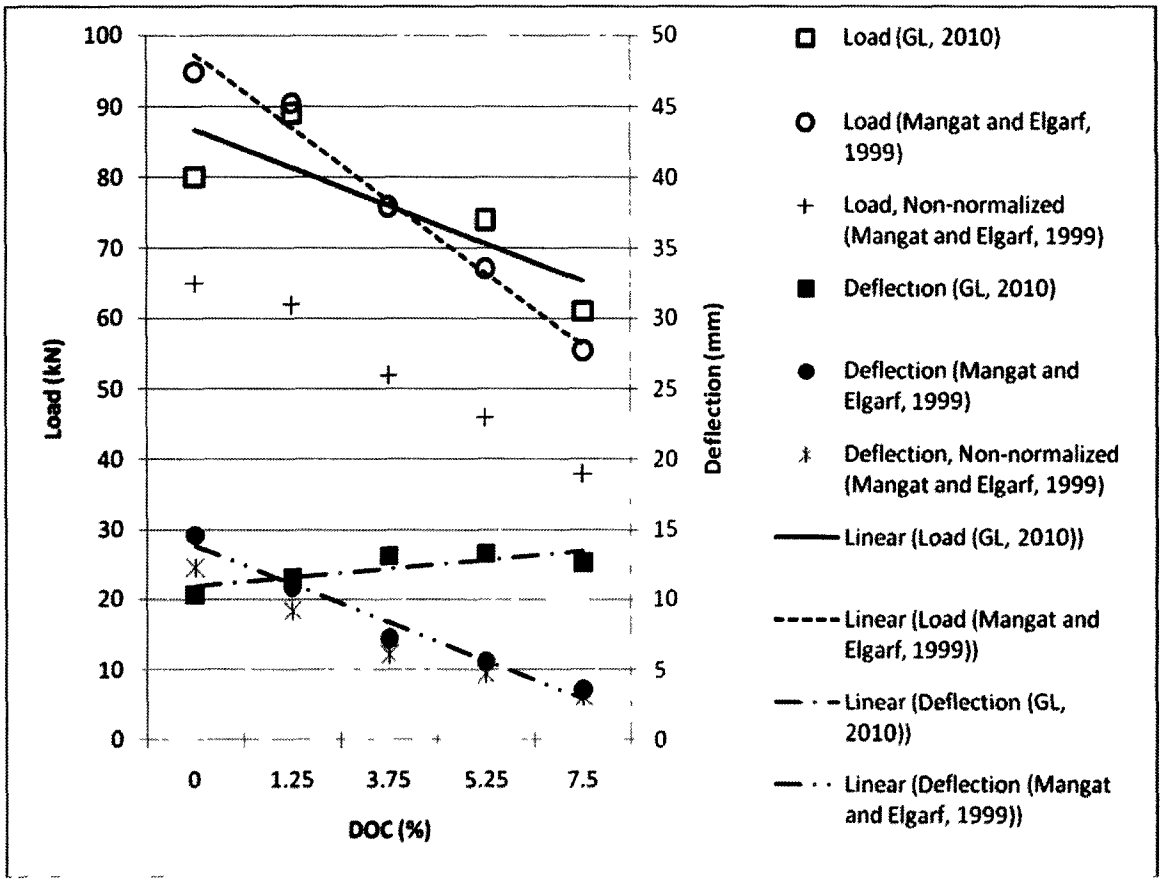

Figure 5-32: The summary of the residual strength and deflection values for all corrosion levels, for both fire exposed and non-exposed beams.

5.3.2 Effect of cover thickness

A comparison of 20 mm and 30 mm cover thickness at 5.25% DOC as shown in Figure 5-33, showed that the 30 mm cover beam had an additional ~7.5% residual strength capacity. The ultimate deflections at failure were similar.

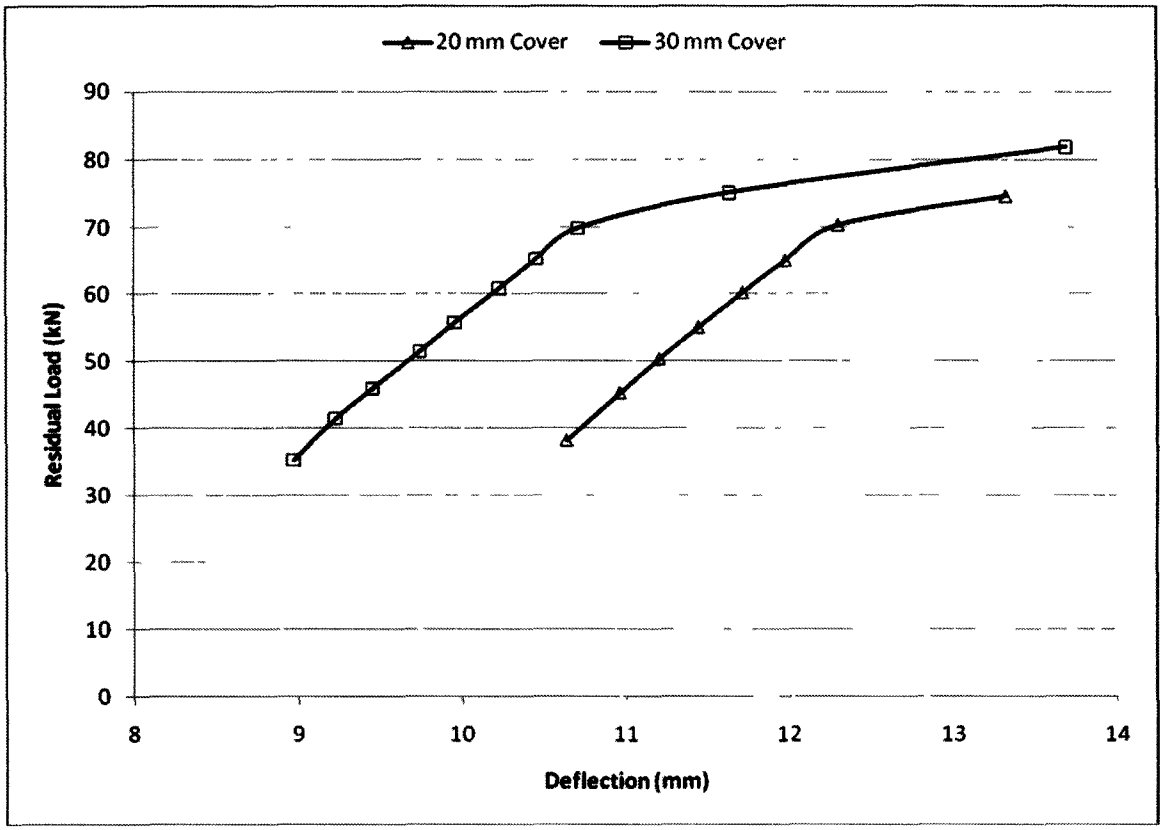

Figure 5-33: The effect of increasing the cover thickness on residual load and deflection for 5.25% DOC.

CHAPTER 6: Practical Implications

6.0 General

This chapter further expands on the results and discussion presented in Chapter 5 and interprets the significance and practicality of these results as they apply to engineering applications.

6.1 Thermal response

For the same fire duration time, lower temperatures were observed in the specimens with increasing DOC. As the DOC increased the corrosion products provided thermal resistance within the concrete pores. The build-up of corrosion products in the concrete pores is a phenomena reported by corrosion researchers in helping to stop or slow down the ingress of chloride necessary for the corrosion reactions (Vidal *et al.*, 2007); a similar phenomenon occurred with the delayed heat front penetration into the concrete. This phenomenon can be labelled the 'insulating effect', because of its heat flow resistant behaviour. The insulating effect seemed to reach a plateau at approximately 3.75%-5.25% DOC. A plateau in the insulating properties would be expected, because once the pores are blocked then the thermal conductivity of the surrounding concrete would govern the heat front penetration. Furthermore, as the amount and size of cracking increased with increasing DOC then the there must exist an equilibrium point where the corrosion products produced cannot possibly fill the large gaps created by higher levels of corrosion. This insulating effect can be beneficial during a fire scenario in delaying the heat front penetration.

The temperature difference that developed in the beams was the result of flexural cracking at the center due to deflections (worsened by DOC) and also the necessary insulation used on the external shear clamps (common in corrosion testing). This insulation reduced the heat exposure to the soffit and sides of the beam at the ends where the shear clamps were located. The temperature gradient between the center and the ends, as well as the temperature at the center of the beam after 40 minutes of fire exposure is shown in Table 6-1. As the degree of corrosion increased, the difference in temperature between the center of the beam (flexural region) and a point 227.5 mm away decreased resulting in a more uniform heating pattern for the flexural portion of the beam at the tensile steel level. This more uniform distribution is likely due to two factors. Firstly, for the corroded specimens longitudinal cracks were present at the steel level all the way through the concrete cover on the soffit and the sides for the entire length of the bars. This allowed more efficient heating of the corroded samples (steel) through the longitudinal cracks that were present allowing hot gases to have a more direct route of entry to the steel level while bypassing the blocked pores caused by the insulating effect. Secondly, for the same time duration less heat was able to be conducted through the concrete pores for the corroded samples than the un-corroded so the there was less of a drastic increase in the center bar temperature allowing more efficient heating by convection gases passing through the cracks along the entire length of the beam. However, even with the cracking present, the shear clamp insulation did have some effect on the temperature rise which is why there was still a slight temperature difference between the center and the ends even for the highly corroded samples. This is an

important consideration when determining how long after a fire exposure begins until the critical bond temperature is reached. As shown in this study and by others (Diedrichs and Schneider, 1981) at temperatures >300°C in the flexural zone, the bond strength begins to degrade appreciably; resulting in loss of axial restraint secondary moment and consequently increased rate of deflection.

Table 6-1: The decrease in temperature gradient and center bar temperature attained for increasing DOC's after 40 minutes of fire exposure.

DOC (%)	ΔT (°C)	T Center (°C)
0.00	230	470
1.25	155	415
3.75	145	350
5.25	115	340

6.2 Structural response at elevated temperatures

The deflection value reached for any given time during a fire exposure were significantly larger as the amount of corrosion damage increased; resulting in a lower safe egress time for occupants or fire fighting personnel in a structure with corrosion damage reinforced concrete beams. If we choose any limiting deflection value, the time to reach this limiting deflection would decrease with increasing corrosion. As shown in Table 6-2, at 5.25% DOC the time to reach the limiting deflection is approximately half of the time required to reach the same deflection for the 0% DOC beam. The percent

reduction in safe egress time as a function of the un-corroded beam predicted time to reach the limiting deflection is shown in Figure 6-1.

Table 6-2: The reduction in safe egress time for increasing DOC's.

DOC (%)	Time to reach limiting deflection L/180
0.00	20 Minutes
1.25	15 Minutes
3.75	15 Minutes
5.25	10 Minutes
7.50	7 Minutes

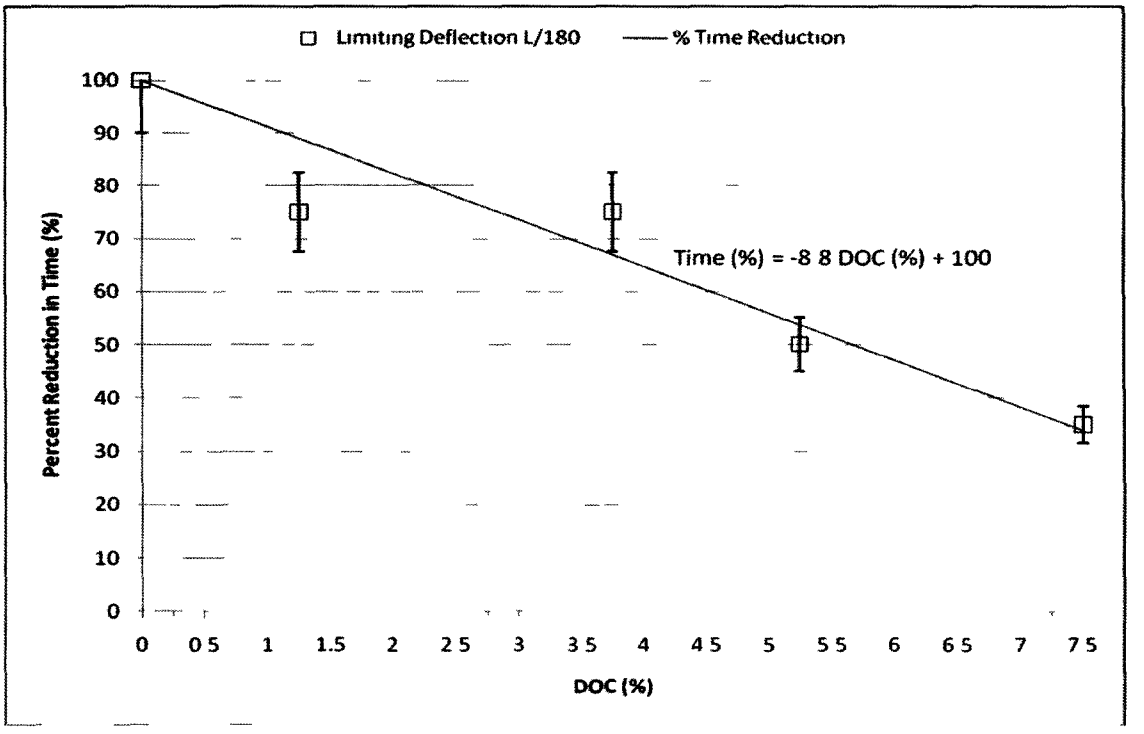

Figure 6-1: The percent reduction in safe egress time for increasing DOC's based on the predicted time to reach the limiting deflection value of an un-corroded beam.

Since there was more uniform heating of the corroded samples (as shown in Table 6-1), the maximum temperature at the centre (which some would consider being the critical temperature for failure of a beam) was lower at failure for higher degrees of corrosion. This implies the maximum steel temperature of 593°C failure criterion used in typical concrete beam analysis may not be conservative, since corrosion damaged beams can fail at much lower maximum temperatures as shown in Table 6-1.

Corrosion damaged beams will fail sooner due to increased deflections at service loads as well as lower temperature differentials due to more uniform heating of the re-bar. The uniform heating does not allow for re-distribution of stresses in the steel to cooler/stronger/stiffer sections, since more of the bar is experiencing a reduction in strength and stiffness due to the uniform heating scenario; as compared to a localized heat source which allows for redistribution of stresses to cooler elements, as seen in the 0% DOC samples.

The magnitude of the thermally induced axial restraint secondary moment developed did not seem to be directly affected by the DOC. The duration of the thermally induced axial restraint secondary moment developed was however shortened by increasing DOC because of the increased deflection and reduced temperature gradients associated with higher DOC. However, since the DOC had no significant impact on the magnitude of the axial thrust force developed, it is beneficial that the rate of release of the secondary moment is similar to that of the rate of development, thereby ensuring a ductile failure of the beam even at high DOC. The decrease in secondary

moment was due to the softening of the concrete and steel at the higher temperatures and consequently the beam had a reduced ability to resist the axial force and produce the axial thrust moment (Dwaikat and Kodur, 2008). Furthermore, as the axial restraint force increased, the neutral axis of the beam was moving lower in order to maintain internal equilibrium. Once the critical value of the eccentricity between the concrete stress block and the line of action of the force was reduced, then the axial restraint secondary moment was no longer beneficial at resisting deflection.

A major factor on the performance of corrosion damaged beams during a fire exposure is the ability of the concrete cover to remain in place. As the level of corrosion increased, the cover was more prone to spall-off completely due to cracking and advanced delamination at the steel concrete interface. Loss of concrete cover is a critical parameter which will cause imminent and rapid failure of a beam, and corrosion damaged beams are more prone to this. Even though cover may be damaged, as long as it remains in place it is beneficial to the structural performance during fire conditions.

Figures 5-17 to 5-19 clearly showed the relationship of shear clamps and the associated insulation in terms of temperature differences developed. This means that there definitely is a correlation between the development of the secondary moment and the temperature difference in the beam. This suggests that for a long RC beam experiencing an isolated fire near mid-span, the temperature gradient developed between the center and the cooler ends would help the beam resist excessive deflection and delay failure.

Furthermore, should the same beam described above have internal corrosion damage (up to 5.25% DOC), then the beam can provide increased structural resistance due to the insulating effect; thermal resistance provided by the corrosion products as shown in Figure 5-20. The above statements are contingent on the cover remaining in place throughout the fire exposure.

Also the corroded beams tend to delay the effects of shear failure when tested without shear reinforcement from ~4 minutes at 0% DOC to ~8.5 minutes at 5.25% DOC, as summarized in Figure 5-20. This can be attributed to the fact that for the 0% DOC beams, there is less ductility and more rigidity resulting in the concrete experiencing larger internal stresses in the shear zone. For higher DOC's there was significant damage at the steel/concrete interface which led to a higher probability of bond failure occurring before shear failure during fire conditions because of increased ductility while at elevated temperatures.

6.3 Post-fire Exposure Residual Response

The difference in the residual deflections at service load was due to the deflection accumulated during the 40 minute fire exposure for each beam. At 1.25% DOC there was a slight increase in ultimate load as compared to 0% DOC (as shown in Figure 5-24) most likely due to the confining effect of the corrosion products at the steel/concrete interface at low corrosion levels before significant cracking damage; this phenomenon was consistent with other authors and was within the large variance of DOC's were this apparent increase was noted. A possible explanation for the large reported range of

DOC's where an apparent increase in residual strength occurs can be the magnitude of the current used to induce corrosion. The larger the applied corrosion current the more cracking at lower DOC's, therefore less apparent increase in residual strength. At higher DOC's the ultimate load was less than that for 0% DOC. All the specimens experienced approximately an additional 2 mm of deflection (from the initial 38 kN state) before concrete crushing in the compression zone caused a failure consistent with a bond failure for the corroded specimens and a pure flexural failure for the un-corroded beam as shown in Figures 6-2 & 6-3.

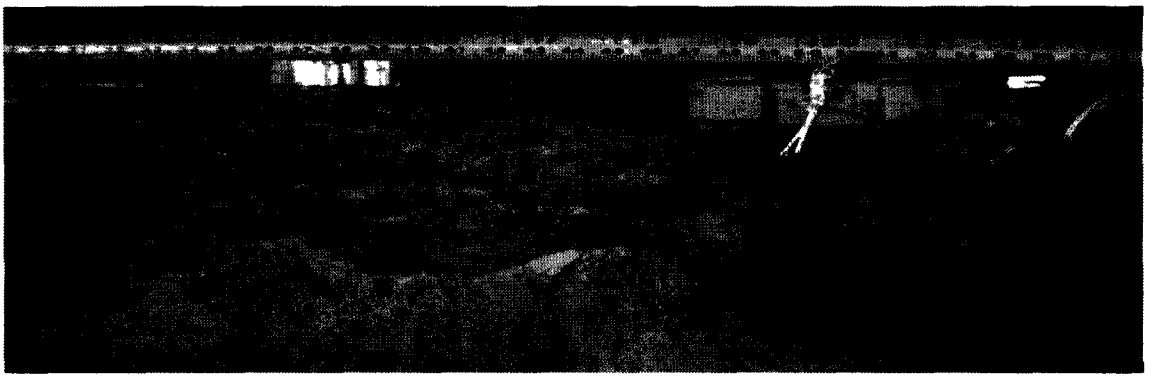

Figure 6-2: The typical flexural failure pattern for un-corroded beams, where multiple cracks extend from the bottom of the beam up to the compression zone throughout the flexural region.

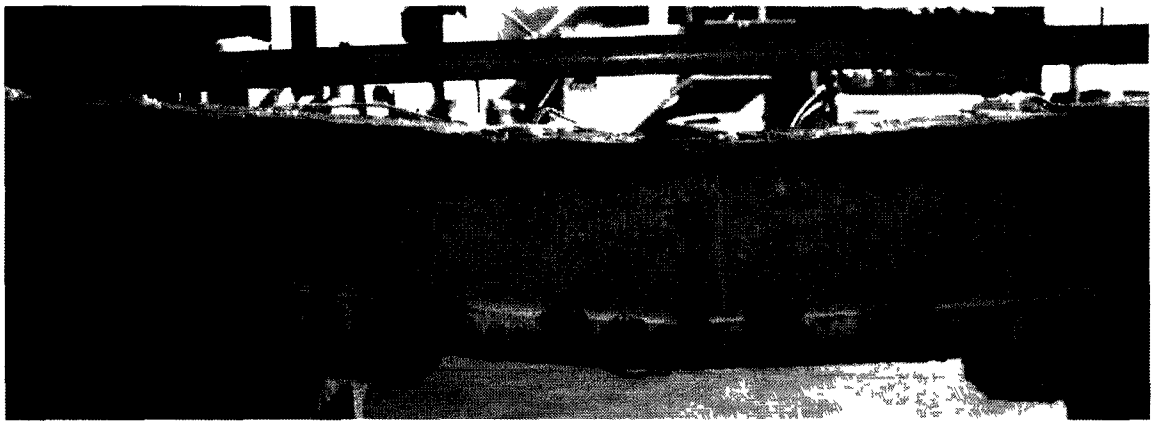

Figure 6-3: The typical flexural failure pattern for corroded beams, where a single predominant crack extends from the line of cracking at the rebar level up to the crushed concrete in the compression zone. Smaller cracks appeared in the cover at the edges of the flexural region.

Table 6-3 summarizes that the beams which were not loaded during a fire condition experienced a decline in ultimate deflection values with increasing corrosion level (Mangat and Elgarf, 1999); while the beams which were exposed to fire experienced an increase in deflection (with respect to ultimate load) with increasing DOC (see Figure 5-32). This can be attributed to the corrosion damage causing a decrease in bond strength as well as a dehydration of the cement paste in the immediate cover zone, as witnessed by increasing brittleness of the cover zone as the DOC increased in the residual beam tests; as visible in Figures 6-4 and 6-5 (the concrete pieces which were completely delaminated which happened upon cooling). This dehydration in the immediate cover zone caused damage at the ribs where the steel to concrete bond is normally developed (see Figures 6-6 and 6-7). This concrete bond zone damage coupled

with elongation of the steel bar caused by excessive deflections during the fire explains the reason for an increase in deflections for the corrosion damaged fire-exposed beams as compared to the non-fire exposed beams. This is consistent with Shi *et al.* (2004), who reported concrete degradation at the bond interface at temperatures >300°C.

The high deflections at higher DOC's for the fire-exposed samples also explains the reason for the higher residual load values obtained for higher DOC's as compared to the stiffer non-fire exposed beams by Mangat and Elgarf (1999). Conversely, for beams without any corrosion damage the residual load was lower for the fire-exposed beams as compared to the non-fire exposed beams; as expected due to dehydration and degradation of the concrete and the steel due to elevated temperatures. The loss in stiffness is attributed to the excessive cracking and the subsequent loss of bond strength and confinement pressure, as noted in Vidal *et al.* (2007). In practice it is a benefit to be able to visually see significant deflections that may be present after a fire, but still be able to realize that the corrosion damaged RC beam still has some considerable residual capacity (depending on the DOC and the fire exposure).

Table 6-3: The comparison between the residual behaviour of fire exposed and non-fire exposed beams for increasing DOC's.

DOC (%)	Mangat & Elgarf (1999)		GL (2010)	
	Residual Strength (kN)	Deflection (mm)	Residual Strength (kN)	Deflection (mm)
0	94.9	14.6001	80	10.32
1.25	90.52	10.9204	89	11.56
3.75	75.92	7.2407	55.96	13.12
5.25	67.16	5.60264	74	13.31
7.5	55.48	3.561	61	12.64

Figure 6-4: Delaminated pieces of concrete cover typical of the corrosion damaged beams.

Close inspection of the beams (see Figure 6-4 and 6-5) shows that the concrete in the cover region is 'whiter' than the typical concrete cross section and the cover is extremely brittle, which is indicative of concrete dehydration caused by heat exposure.

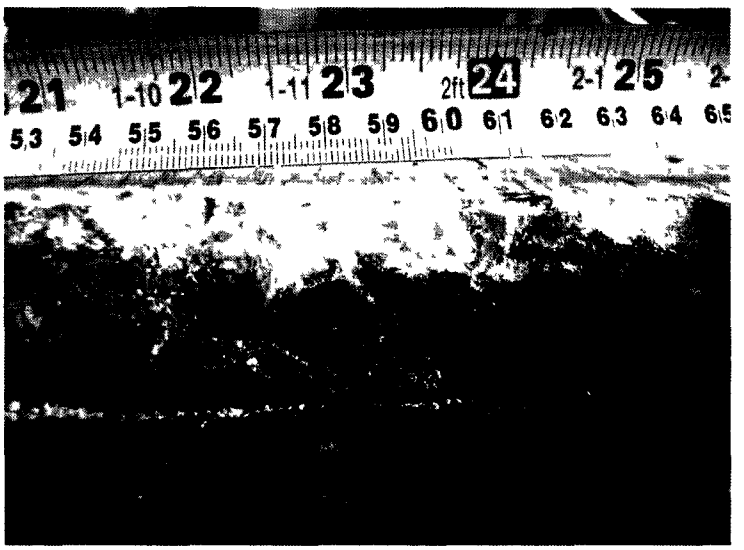

Figure 6-5: A horizontal view of one of the bars in the bottom of the beam (5.25% DOC).

Close inspection (see Figure 6-5) shows evidence of concrete dehydration at the cover depth, as well as deep pits in the rebar and visual evidence of damages to the rebar's rib profile and loss of mechanical bond at the steel-concrete interface due to brittle concrete at this interface causing slip.

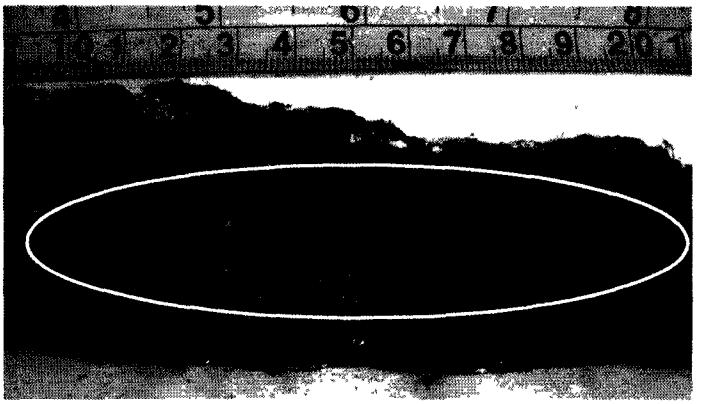

Figure 6-6: A close-up view of one of the pieces of cover (5.25% DOC).

Figure 6-6 shows heavy corrosion staining as well; very faint outline of where the re-bar ribs were within the concrete before it was damaged. Figure 6-7 shows a rebar with severe corrosion damage; also the concrete around the re-bar which is normally enveloping the bar, has actually been so badly damaged that it appears as though the concrete which normally encases the bar has been 'smoothened' thereby greatly reducing the mechanical bond capabilities and increasing the potential bar slip.

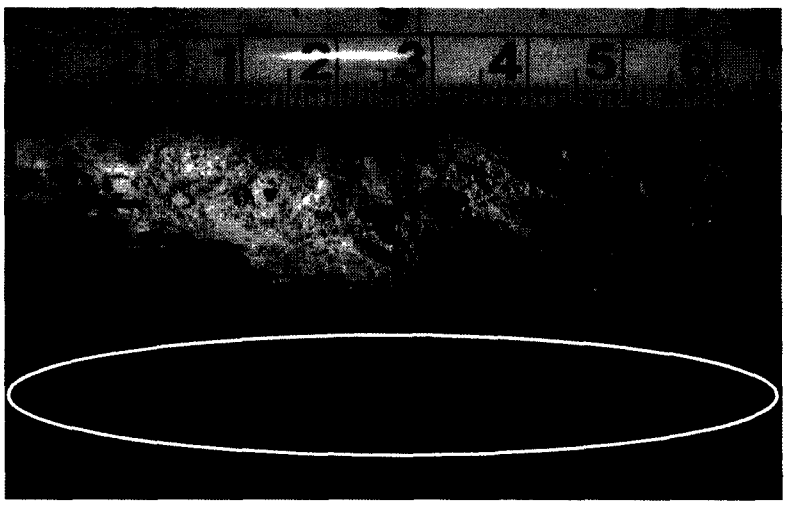

Figure 6-7: The rebar with severe corrosion damage (7.5% DOC).

6.4 Temperature differential

The beneficial effects of creating an internal temperature differential to resist excessive deflections as discussed in section 6.2, is also beneficial in delaying the onset of shear failure when coupled with corrosion damaged beams as shown in section 5.2.3, and summarized in Table 6-4 for beams tested without shear reinforcement. This can be attributed to the insulating effects of the corrosion products within the pores, slowing the critical heat front penetration through the cover to the steel level, and also the increased ductility of corrosion damaged beams during a fire exposure.

Table 6-4: The time to failure and predominant failure mode for beams exposed to fire conditions without any shear reinforcement for increasing DOC's.

DOC (%)	Time to failure	Failure Mode
0.00	~4 Minutes	Pure Shear
3.75	~5 Minutes	Bond/Shear
5.25	~9.5 Minutes	Bond/Flexure

6.5 Effect of cover thickness

The benefits of increased cover thickness are well established in terms of improving the fire resistance during an exposure as well as providing increased travel distance for a corrosion front to penetrate the cover and cause corrosion damage. Furthermore, the beams corroded with 30 mm cover experienced less surface cracking and consequently less probability of the cover delaminating or delaminating during or after the fire exposure as compared to the 20 mm cover samples. Due to the extra

protection provided by the 30 mm cover, the residual strength was approximately ~7.5% higher than the same beam (5.25% DOC) tested with 20 mm cover; as shown Figure 5-33. A small increase in residual capacity by increasing the cover by 10mm for corroded beams is similar to Shi *et al.* (2004) who reported similarly marginal improvements for beams without corrosion damage, therefore it appears that the corrosion damage is not affecting the covers ability to protect the steel, provided that it remains relatively intact and in place throughout the fire exposure

.

CHAPTER 7: Summary, Conclusions and Future Work

7.0 General

This chapter summarizes and presents the key findings of this research project. The information below is a synopsis of the data obtained during the experimental program as well as relevant observations.

7.1 Summary and Conclusions

1. Generally it was observed that as the DOC increased (up to 5.25%) the temperature rise within the beams was slower and more uniform over the bar length as opposed to the un-corroded beams. As the corrosion level increased the corrosion products provided additional thermal resistance (insulating effect) within the concrete pores; thereby allowing beams with higher DOC's to have lower temperatures for the same fire duration.

2. As the DOC increased, the difference in temperature between the center of the beam (flexural region) and a point 227.5mm away decreased resulting in a more uniform heating pattern for the flexural portion of the beam at the tensile steel level.

3. The deflection value reached for any given time during a fire exposure is larger as the amount of corrosion damage increases.

4. Corrosion damaged beams will fail sooner due to increased deflections at service loads as well as lower temperature differentials due to more uniform heating of the re-bar.

5. The time to reach a limiting deflection of L/180 is reduced by ~65% for 7.50% DOC as compared to un-corroded beams.

6. The magnitude of the secondary force developed does not seem to be affected by the DOC.

7. A major factor on the performance of corrosion damaged beams during a fire exposure is the ability of the concrete cover to remain in place. As the DOC increases, the cover is more prone to spall-off completely due to cracking and advanced delamination at the steel concrete interface.

8. Temperature differential developed at the steel level will help to delay failure of a reinforced concrete beam by the development of the axial thrust force. However, increasing DOC reduces the temperature gradient by ~50% at 5.25% DOC as compared to un-corroded beams.

9. Corrosion damaged beams can delay the time to failure during a fire exposure by a factor of two, at 5.25% DOC as compared to un-corroded beams when tested without shear reinforcement.

10. The residual strength of the fire-exposed corrosion damaged beams was ~10% higher than the non-fire exposed beams; however this additional strength came at

severely increased deflections; up to 4 times the deflection value for fire exposed 7.5% DOC as compared to the same DOC non-fire exposed beam.

11. The residual strength of the beam with 30mm cover was approximately ~7.5% higher than the same beam (5.25% DOC) tested with 20mm cover.

7.2 Closure

This hybrid experimental program has provided great exploratory research into the combined effects of corrosion damage and fire-exposure simultaneously attacking a reinforced concrete structure. This work provided valuable information to the users of reinforced concrete structures, particularly during critical times when our structures are tested such as during fire-scenarios. While the occurrence may be rare, this experiment has shown that corrosion damaged concrete structures can be more adversely affected by fire than non-corrosion damaged structures.

The results presented are a valuable piece of the engineering framework from which we can learn and improve our construction technologies, techniques and designs to be able to better use passive fire protection systems. If the benefits of increased cover thickness on fire performance and corrosion protection can be combined with the benefits of creating a temperature differential between the center and the ends, to be able to allow for the development of the beneficial secondary axial thrust force, combined with the insulating effects of corrosion damaged RC beams; improved performance can be achieved. A technique of tapering the flexural reinforcement upwards in the shear zone of reinforced concrete beams is used in certain parts of the world and its use can be

further investigated in North America. This technique allows for increased cover thickness near the ends of the beam which would naturally provide the benefits of increased cover thickness as well as acting as a greater thermal barrier at the ends thereby passively creating a natural temperature gradient, should the beam be exposed to a fire near mid span.

7.3 Future work

Many lessons were learned in preparing this unique experimental testing regime. While much effort, care and research was put into trying to devise a perfect experimental program some challenges were faced, particularly with instrumentation. With the steps outlined in Chapter 4, taken to protect the thermocouple wires from damage during the corrosion process, some damage still did occur. As the DOC increased more of the cast in place thermocouples failed. Further work should be done to devise an improved method for installing cast-in place thermocouples for this type of testing application so that they can be more reliable and resist corrosion damage.

With regards to the specimens themselves; the beams in this study were identical beams cast by Mangat and Elgarf (1999) and did not contain any internal shear reinforcement, since they had reported that the presence of stirrups did not allow good control of the DOC through the accelerated corrosion technique. If a reliable method of isolating the stirrups from the flexural steel can be devised, then beams could be tested without any external shear reinforcement and consequently no external insulation, more closely emulating actual conditions. It would also be beneficial to study the size effects

of varying the length and cross sectional dimensions of the members; as well using a more realistic corrosion rate as part of a long term study. It would be beneficial to study the coupled effects of corrosion damage and fire exposure on post-tensioned reinforced concrete structures, since many multi-storey parking structures utilize this type of construction.

A specific, experimental program directly focused on studying the steel to concrete bond interaction for combined corrosion damaged and fire-exposed specimens would be beneficial to better understand the mechanics at the concrete to steel interface of a corrosion damaged structural element exposed to fire.

Lastly, as mentioned in the conclusion, perhaps it would be beneficial to devise an experimental program to try and capture all the benefits of increased cover thickness at the ends resulting in a temperature gradient, by employing a technique of tapered flexural bottom steel, as is used in other parts of the world.

This experimental program allows us to begin to have a better understanding of the behaviour of corrosion damaged reinforced concrete beams exposed to fire conditions and future work would serve to increase the breadth of this subject area.

References

Almusallam AA, Al-Gahtani AS, Aziz AR, and Rasheeduzzafar (1996). Effect of reinforcement corrosion on bond strength. *Construction and Building Materials*; **2**:123-129.

Arioz O. (2007) Effects of elevated temperatures on properties of concrete. *Fire Safety Journal*; **42**:516-522.

ASTM E119 – 09c (2009). Standard test methods for fire tests of building construction and materials. West Conshohocken, Pennsylvania, U.S.A.: ASTM International.

ASTM G 1 – 03 (2003). Standard practice for preparing, cleaning and evaluating corrosion test specimens. West Conshohocken, Pennsylvania, U.S.A.: ASTM International.

Bentur, A., Diamond, S., and Berke, N.S. (1997). Steel corrosion in concrete. New York, New York, U.S.A.: Chapman & Hall.

Bingöl AF, and Rüstem G. (2009). Residual bond between steel bars and concrete after elevated temperatures. *Fire Safety Journal*; **6**:854-859.

Bohni, H. (2005). Corrosion in reinforced concrete structures. Florida, U.S.A.: CRC Press.

Broomfield JP. (1997). Corrosion of steel in concrete: understanding, investigation and repair. London, U.K.: CRC Press.

Buchanan AH. (2002). Structural design for fire safety. London, U.K.: John Wiley & Sons Ltd.

CAC (2008). 2008 Facts and figures on the Canadian cement and concrete industries. Cement Association of Canada. Web: http://www.cement.ca/en/economic-contribution.html.

CAN/ULC-S101-04 (2004). Standard methods of fire endurance tests of building construction and materials. Toronto, Ontario, Canada: Underwriters Laboratories of Canada.

Cairns J, Du Y, and Law DW. (2008). Structural performance of concrete beams affected by reinforcement corrosion. *Magazine of Concrete Research*; **5**:359-370.

Castel A, François R, and Arliguie G. (2000). Mechanical behaviour of corroded reinforced concrete beams – part 2: bond and notch effects. *Materials and Structures*; **33**:545-551.

Cooke GME. (1988). An introduction to the mechanical properties of structural steel at elevated temperatures. *Fire Safety Journal*; **13**:45-54.

Cryotech (N.D.). Parking structure cover failure. Online image: http://www.cryotech.com/products/CMA/parking.php. December 2010.

CSA A23.3-04 (2004). Design of Concrete Structures. Ottawa, Ontario, Canada: Cement Association of Canada.

Design and Control of Concrete Mixtures (2002). EB101, 7th Edition, Ottawa, Ontario, Canada: Cement Association of Canada.

Diederichs U, and Schneider U. (1981). Bond strength at high temperatures. *Magazine of Concrete Research*; **115**:75-84.

Dwaikat MB, and Kodur VKR. (2008). A numerical approach for modeling the fire induced restraint effects in reinforced concrete beams. *Fire Safety Journal*; **43**:291-307.

Dwaikat MB, and Kodur VKR. (2009). Response of restrained concrete beams under design fire exposure. *Journal of Structural Engineering*; **11**:1408-1417.

EC 3 (1995). Eurocode 3: Design of steel structures. Brussels, Belgium: European Committee for Standardization.

Elgarf MSA. (1994). The effect of reinforcement corrosion on the structural performance of concrete flexural members. Ph.D. Thesis. Aberdeen, United Kingdom: Kings College University of Aberdeen.

El-Hawary MM, Ragab AM, El-Azim AA, and Elibiari S. (1996). Effect of fire on flexural behaviour of RC beams. *Construction and Building Materials*; **2**:147-150.

El-Hawary MM, and Hamoush SA. (1996). Bond shear modulus of reinforced concrete at high temperatures. *Engineering Fracture Mechanics*; **6**:991-999.

El-Maaddawy TA, and Soudki KA. (2003). Effectiveness of impressed current technique to simulate corrosion of steel reinforcement in concrete. *Journal of Materials in Civil Engineering*; **1**:41-47.

El-Reedy, MA (2008). Steel reinforced concrete structures. Florida, U.S.A.: CRC Press.

Ellingwood B, and Lin TD. (1991). Flexure and shear behaviour of concrete beams during fires. *Journal of Structural Engineering* ; **2**:440-458.

Fang C, Lundgren K, Chen L, and Zhu C. (2004). Corrosion influence on bond in reinforced concrete. *Concrete and Cement Research*; **34**:2159-2167.

Ghahramani A and Sabzevari A. (1969). Studies on reduction of bond in reinforced concrete due to heat cycle. *International Conference on Shear, Torsion and Bond in Reinforced and Prestressed Concrete;* Session 3, Paper 2: Coimbatore, India.

Ghods P, Isgor OB, McRae GA and Gu GP. (2010). Electrochemical investigation of chloride-induced depassivation of black steel rebar under simulated service conditions. *Corrosion Science;* **52**:1649-1659.

Haddad RH and Shannis LG. (2004). Post-fire behavior of bond between high strength pozzolanic concrete and reinforcing steel. *Construction and Building Materials;* **18**:425-435.

Harada T, Takeda J, Yamane S and Furumura F. (1971). Strength, elasticity, and thermal properties of concrete subjected to elevated temperatures. *ACI SP: Temperature and Concrete;* **25**:377-406..

ISO 834 (2002). Fire resistance tests – Elements of building construction. Geneva, Switzerland: International Organization for Standardization.

Isgor OB (2010). Ottawa area parking structure. Personal photograph.

Kemp EL. (1986). Bond in reinforced concrete: behaviour and design criteria. *ACI Journal*; **34:**50-57.

Khan MR, and Royles R. (1986). Post heat exposure behaviour of reinforced concrete beams. *Magazine of Concrete Research*; **135**:59-66.

Malumbela G, Moyo P, and Alexander M. (2009) Behaviour of RC beams corroded under sustained service loads. *Construction and Building Materials*; **23**:3346-3351.

Mangat PS, and Elgarf MS. (1998). Bond characteristics of corroding reinforcement in concrete beams. *Materials and Structures*; **32**:89-97.

Mangat PS, and Elgarf MS. (1999). Flexural strength of concrete beams with corroding reinforcement. *ACI Structural Journal*; **96**:149-158.

Morley PD, and Royles R. (1979). The influence of high temperature on the bond in reinforced concrete. *Fire Safety Journal*; **2**:243-255.

Reichel V. (1978). How fire affects steel to concrete bond. *Building Research and Practice;* **6**:176-186.

Schneider U. (1988). Concrete at high temperatures – a general review. *Fire Safety Journal*; **13**:55-68.

SFPE (2002). Handbook of Fire Protection Engineering. Bethesda, Maryland, U.S.A.: Qunicy Mass.: National Fire Protection Association: Society of Fire Protection Engineers.

Sahmaran M, and Yaman IO. (2008). Influence of transverse crack width on reinforcement corrosion initiation and propagation in mortar beams. *Canadian Journal of Civil Engineering;* **35**:236-246.

Shannag MJ, and Al-Ateek SA. (2006). Flexural behaviour of strengthened concrete beams with corroding reinforcement. *Construction and Building Materials*; **20**:834-840.

Shi X, Tan TH, Tan KH, and Guo Z. (2004). Influence of concrete cover on fire resistance of reinforced concrete flexural members. *Journal of Structural Engineering*; **8**:1225-1232.

Torres-Acosta AA, Navarro-Gutierrez S, and Terán-Guillén J. (2007). Residual flexure capacity of corroded reinforced concrete beams. *Engineering Structures*; **29**:1145-1152.

Tuutti K. (1982). Corrosion of steel in concrete, 1st ed. Stockholm, Sweden: Swedish Cement and Concrete Research Institute.

Vidal T, Castel A, and François R. (2007). Corrosion process and structural performance of a 17 year old reinforced concrete beam stored in chloride environment. *Cement and Concrete Research*; **37**:1551-1561.

Xiao J, and König G. (2004). Study on concrete at high temperature in China – an overview. *Fire Safety Journal*; **39**:89-103

Appendices

Appendix A contains the current and voltage versus time graphs for each corroded beam.

Appendix B contains the crack mapping diagrams for each corroded beam.

Appendix C shows a graph of all of the Time-Temperature curves for each fire test.

Appendix A: Current and Voltage versus Time Graphs

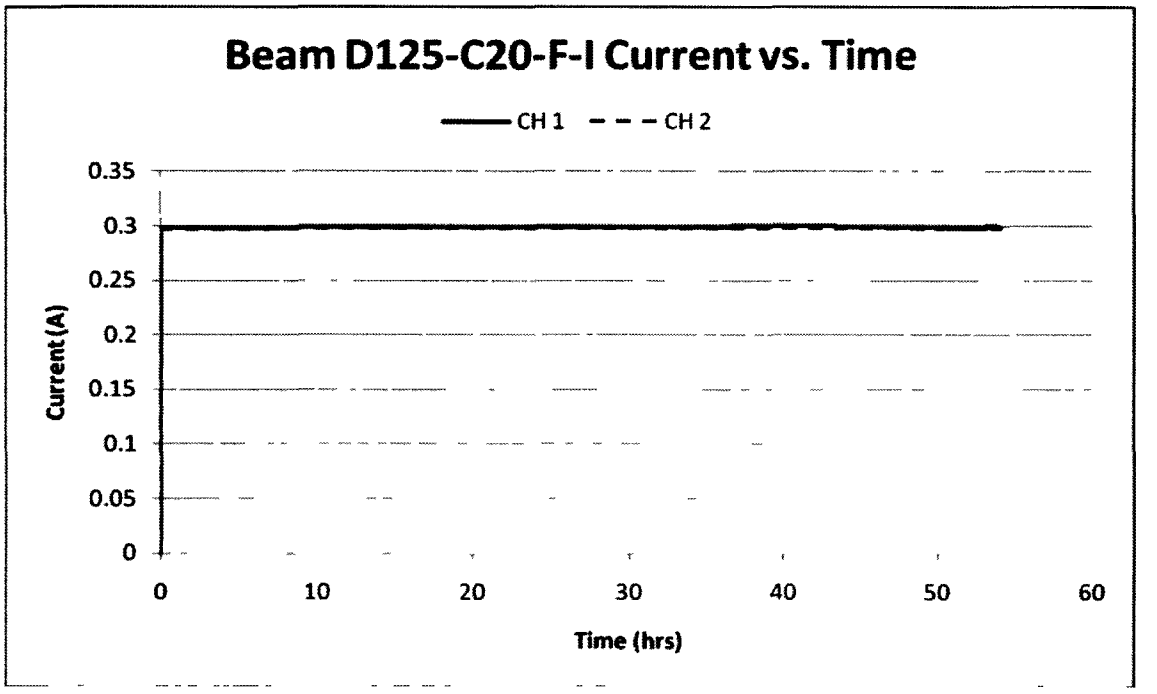

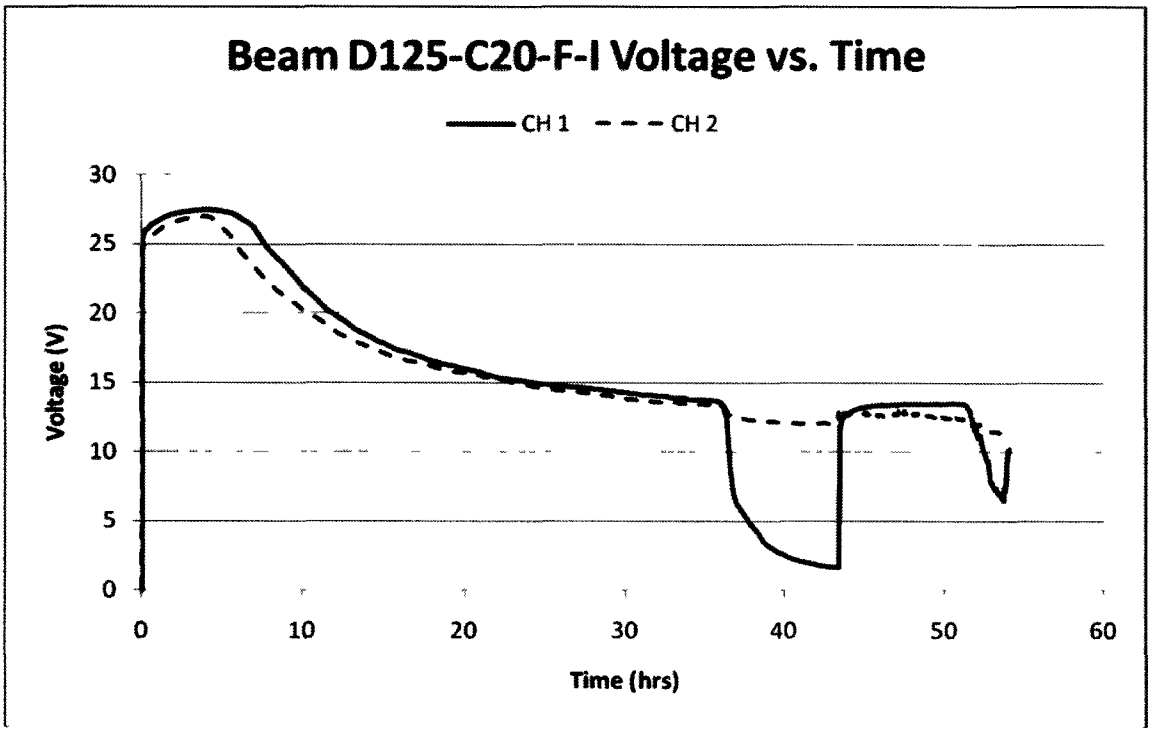

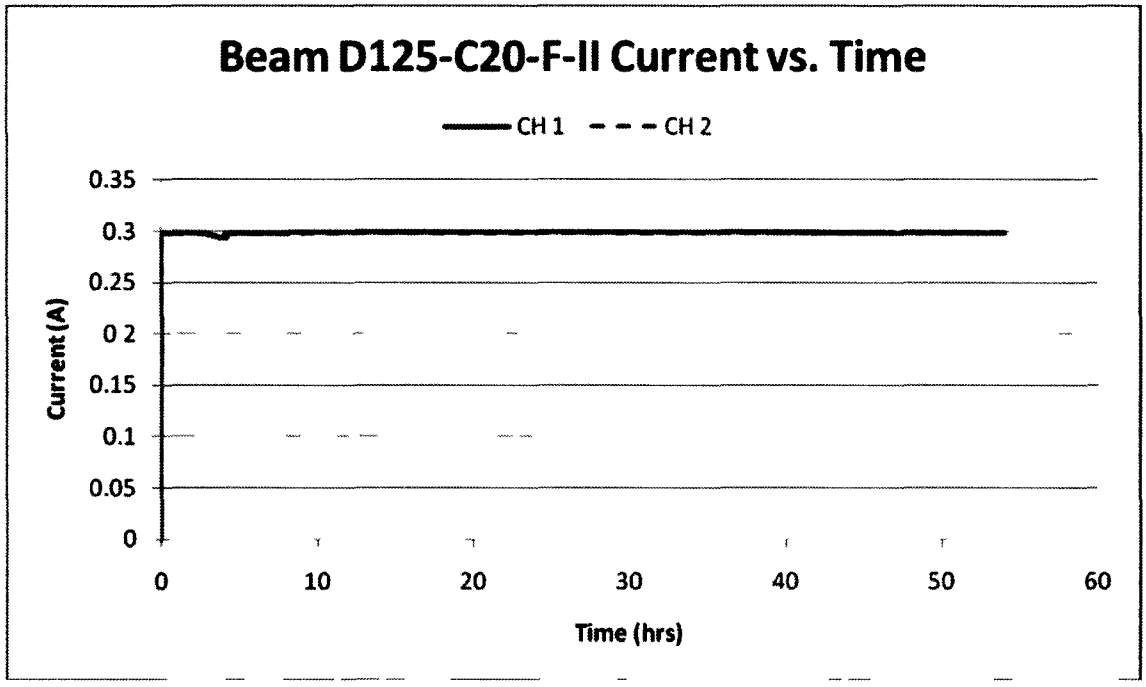
Beam D125-C20-F-II Current vs. Time
CH 1
CH 2
Current (A)
0.35
0.3
0.25
0.2
0.15
0.1
0.05
0
0
10
20
30
40
50
60
Time (hrs)

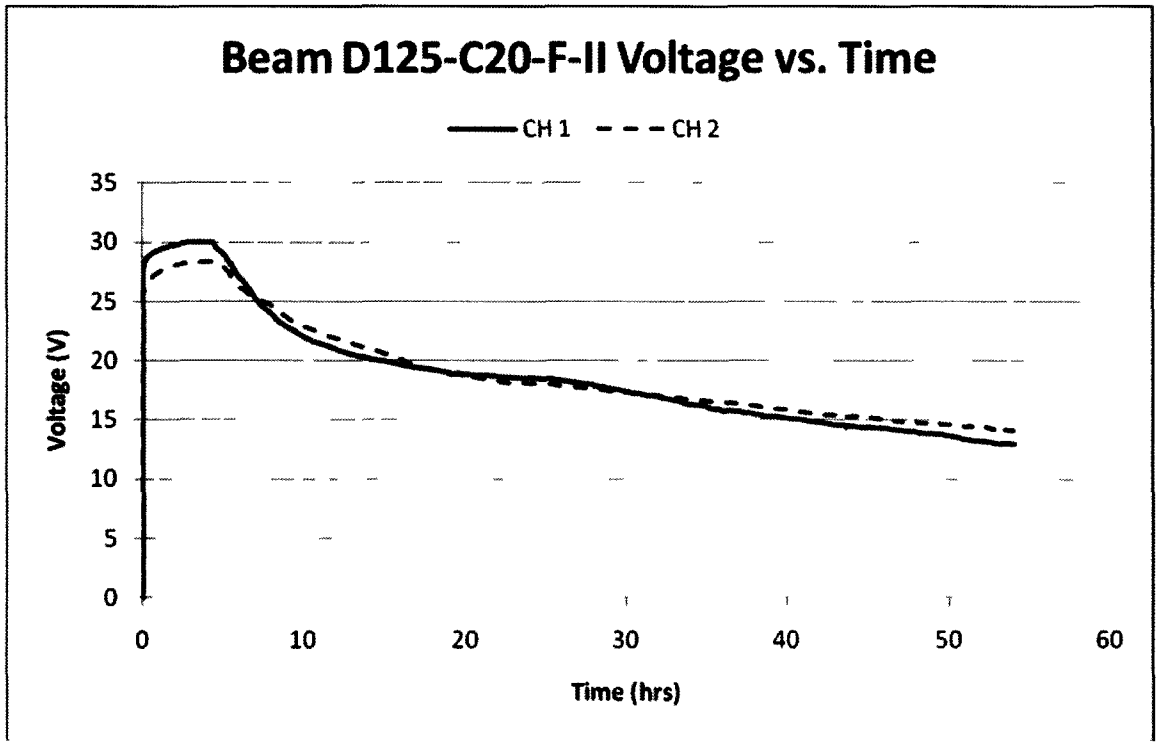
Beam D125-C20-F-II Voltage vs. Time
CH 1
CH 2
Voltage (V)
35
30
25
20
15
10
5
0
0
10
20
30
40
50
60
Time (hrs)

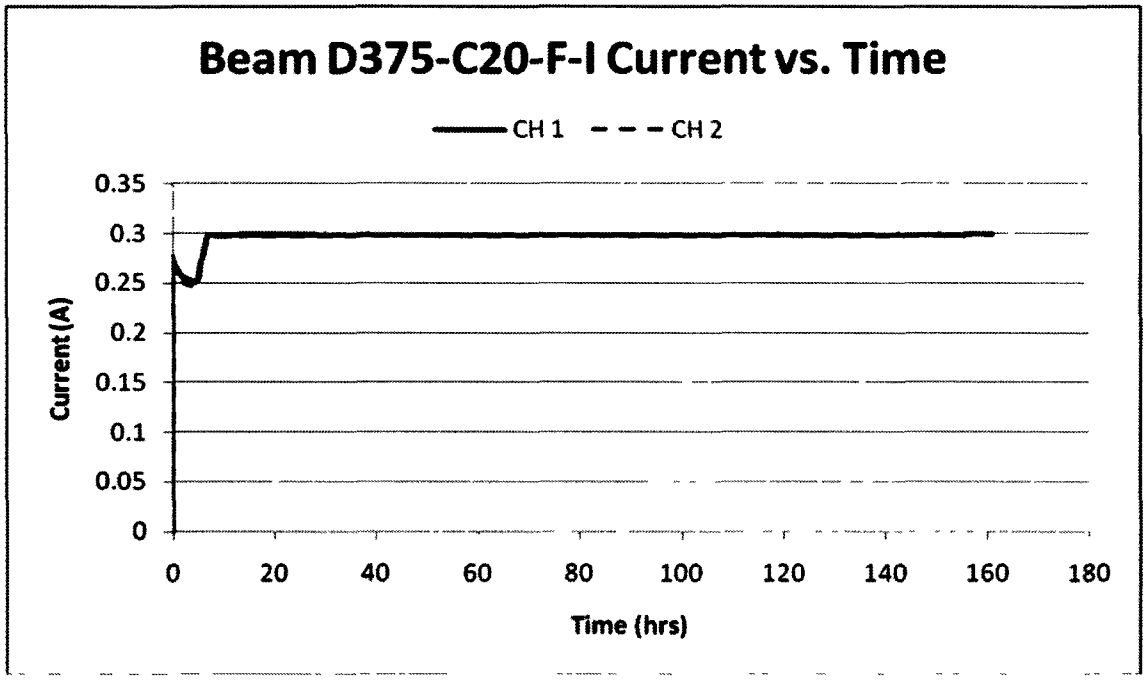
Beam D375-C20-F-I Current vs. Time
CH 1
CH 2
Current (A)
0.35
0.3
0.25
0.2
0.15
0.1
0.05
0
0
20
40
60
80
100
120
140
160
180
Time (hrs)

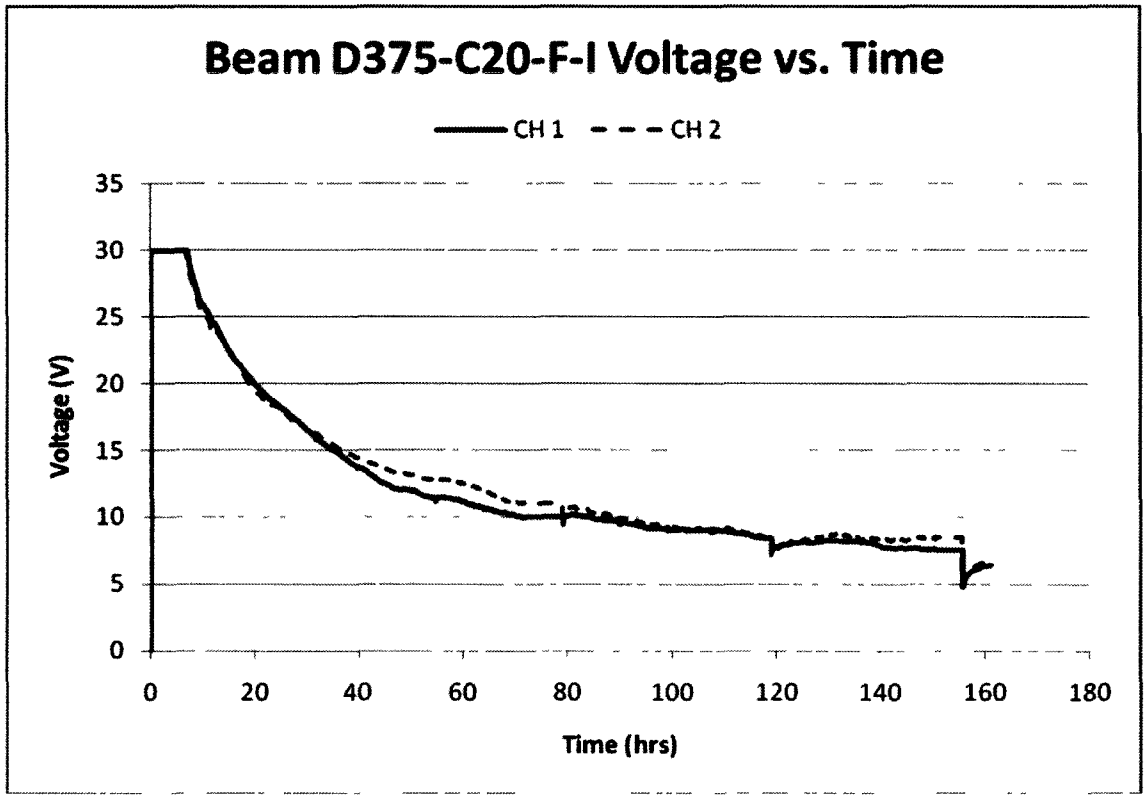
Beam D375-C20-F-I Voltage vs. Time
CH 1
CH 2
Voltage (V)
35
30
25
20
15
10
5
0
0
20
40
60
80
100
120
140
160
180
Time (hrs)

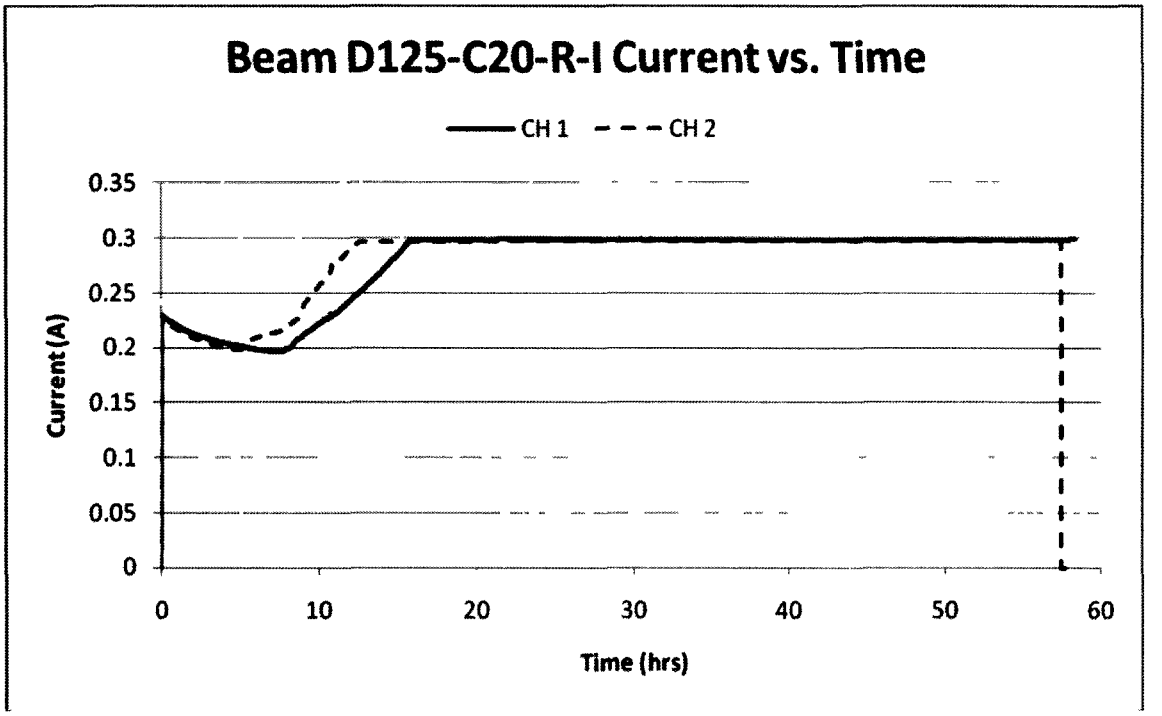
Beam D125-C20-R-I Current vs. Time
CH 1
CH 2
Current (A)
0.35
0.3
0.25
0.2
0.15
0.1
0.05
0
0
10
20
30
40
50
60
Time (hrs)

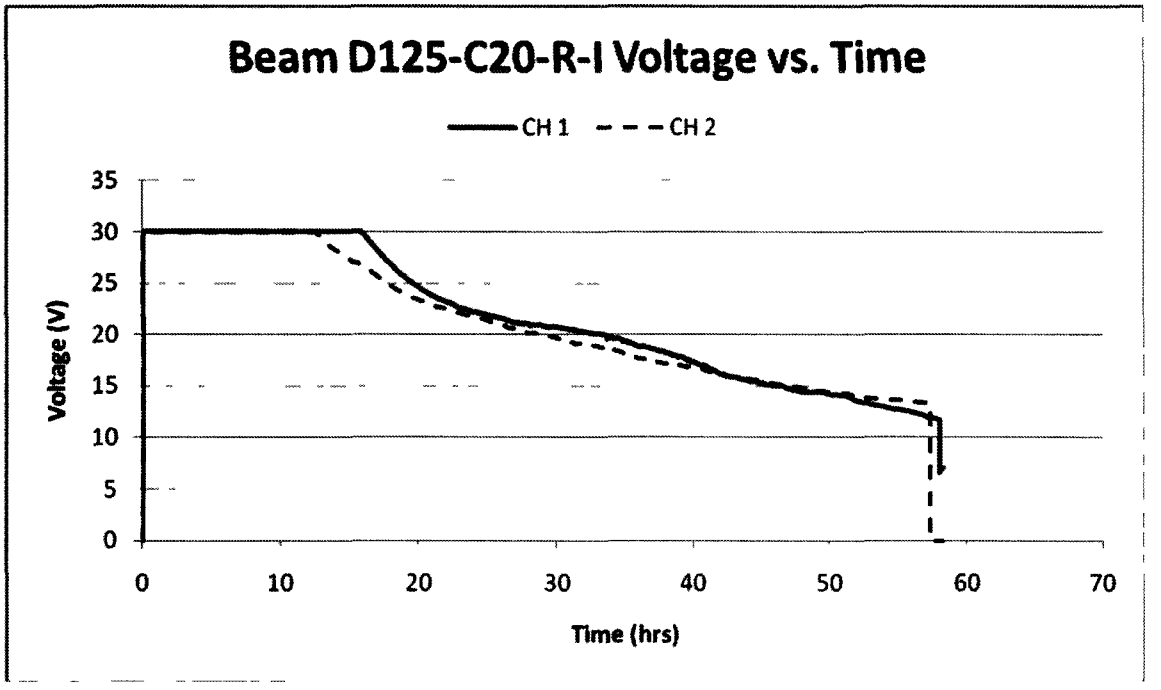
Beam D125-C20-R-I Voltage vs. Time
CH 1
CH 2
Voltage (V)
35
30
25
20
15
10
5
0
0
10
20
30
40
50
60
70
Time (hrs)

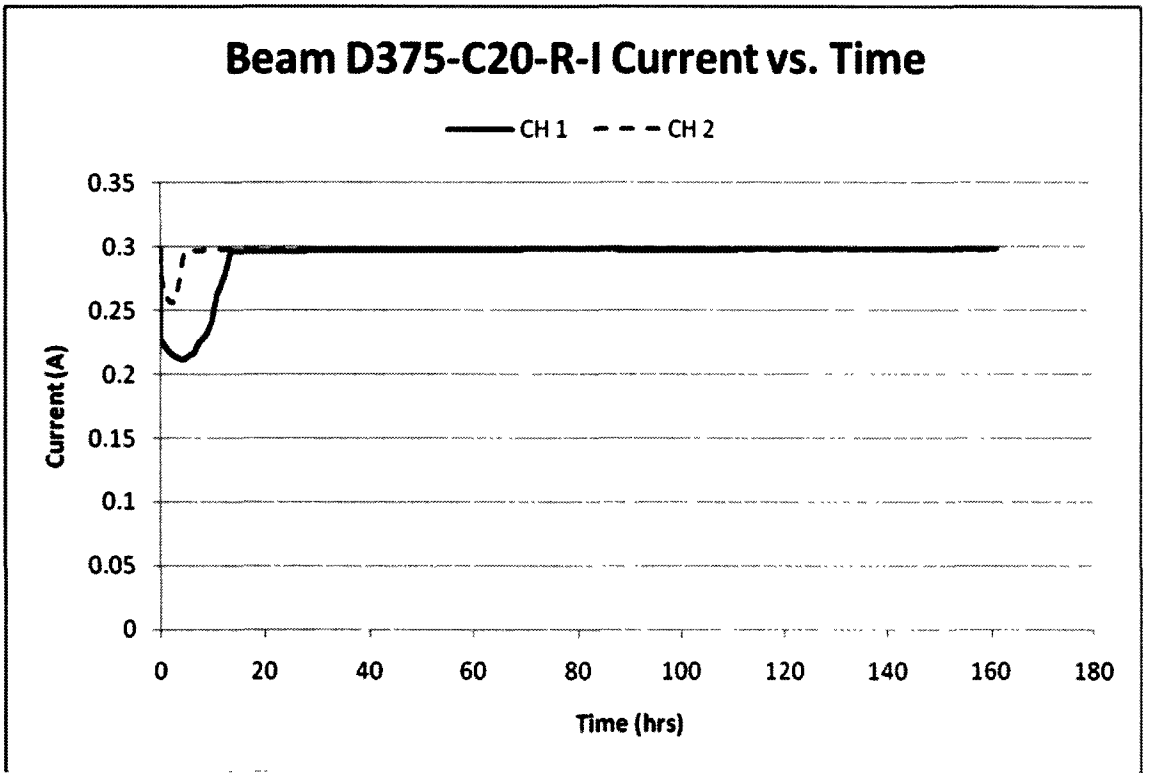
Beam D375-C20-R-I Current vs. Time
CH 1
CH 2
Current (A)
0.35
0.3
0.25
0.2
0.15
0.1
0.05
0
0
20
40
60
80
100
120
140
160
180
Time (hrs)

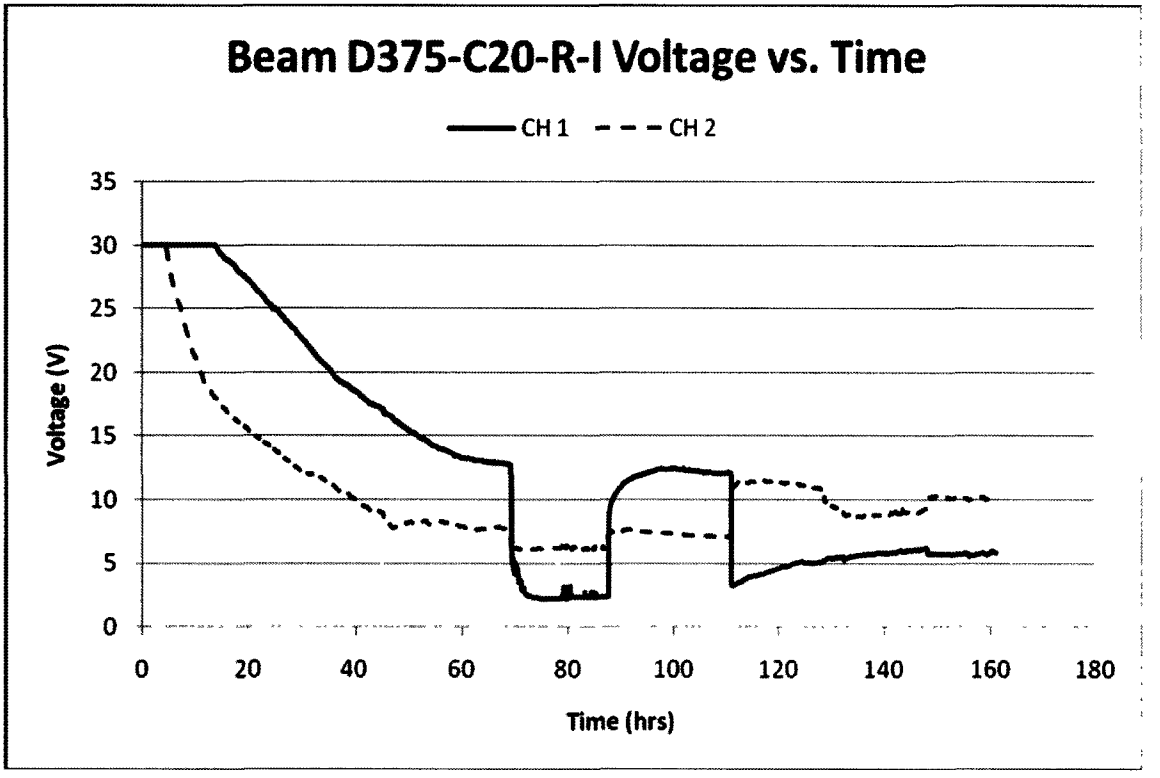
Beam D375-C20-R-I Voltage vs. Time
CH 1
CH 2
Voltage (V)
35
30
25
20
15
10
5
0
0
20
40
60
80
100
120
140
160
180
Time (hrs)

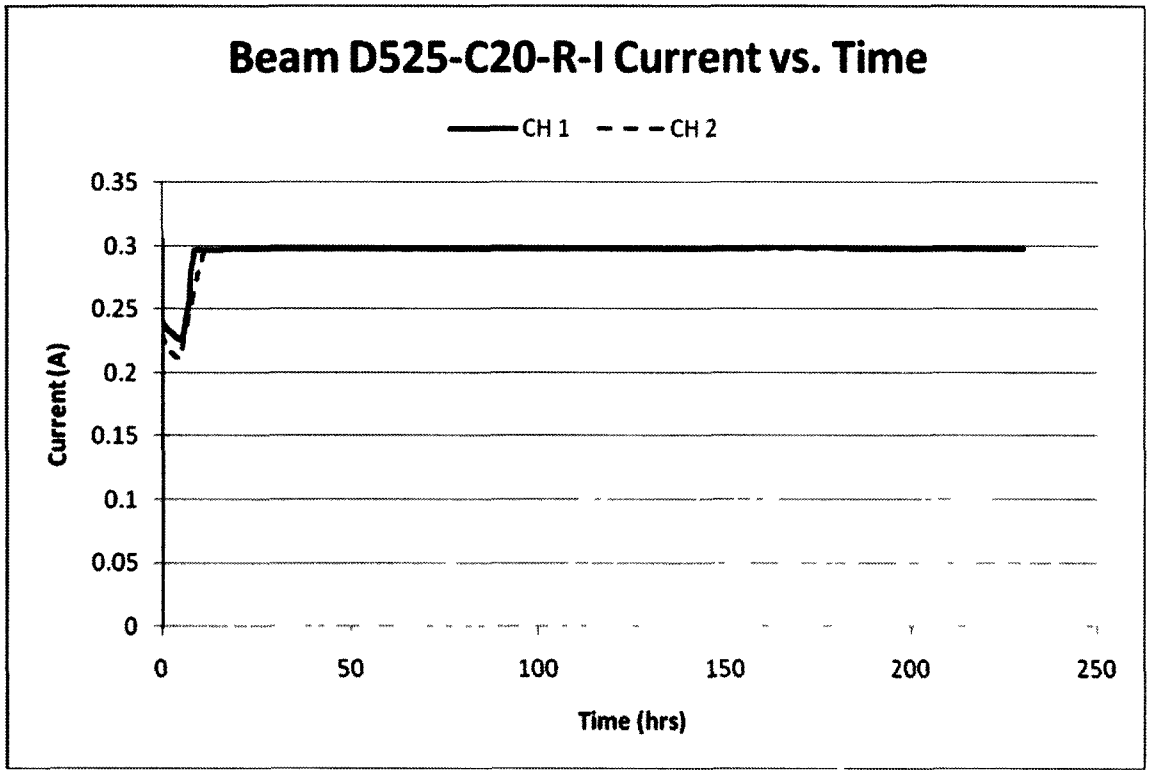
Beam D525-C20-R-I Current vs. Time
CH 1
CH 2
Current (A)
0.35
0.3
0.25
0.2
0.15
0.1
0.05
0
0
50
100
150
200
250
Time (hrs)

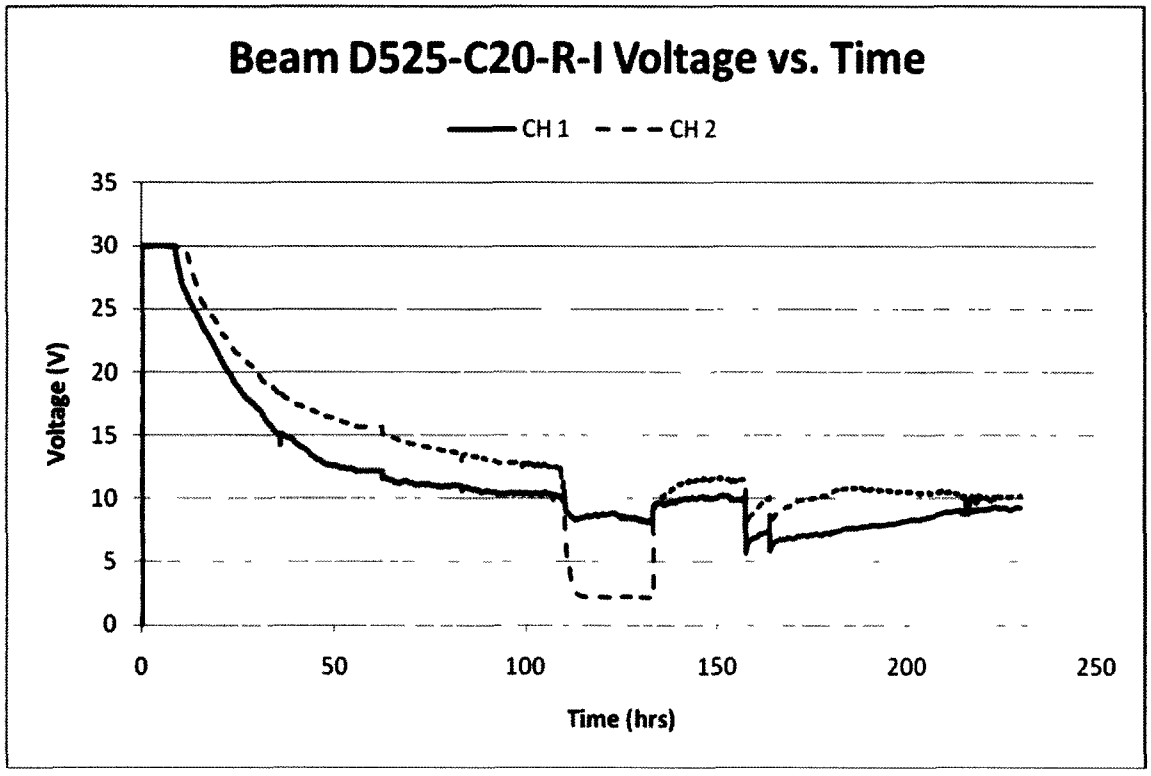
Beam D525-C20-R-I Voltage vs. Time
CH 1
CH 2
Voltage (V)
35
30
25
20
15
10
5
0
0
50
100
150
200
250
Time (hrs)

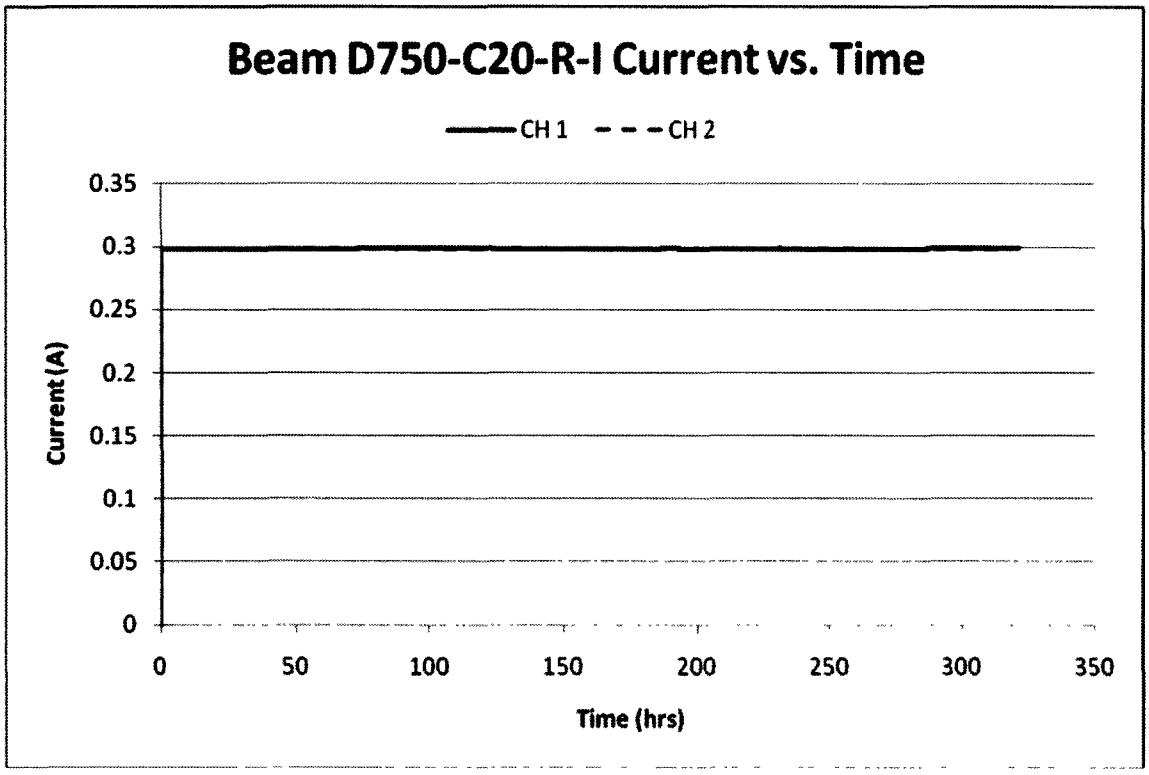
Beam D750-C20-R-I Current vs. Time
CH 1
CH 2
Current (A)
0.35
0.3
0.25
0.2
0.15
0.1
0.05
0
0
50
100
150
200
250
300
350
Time (hrs)

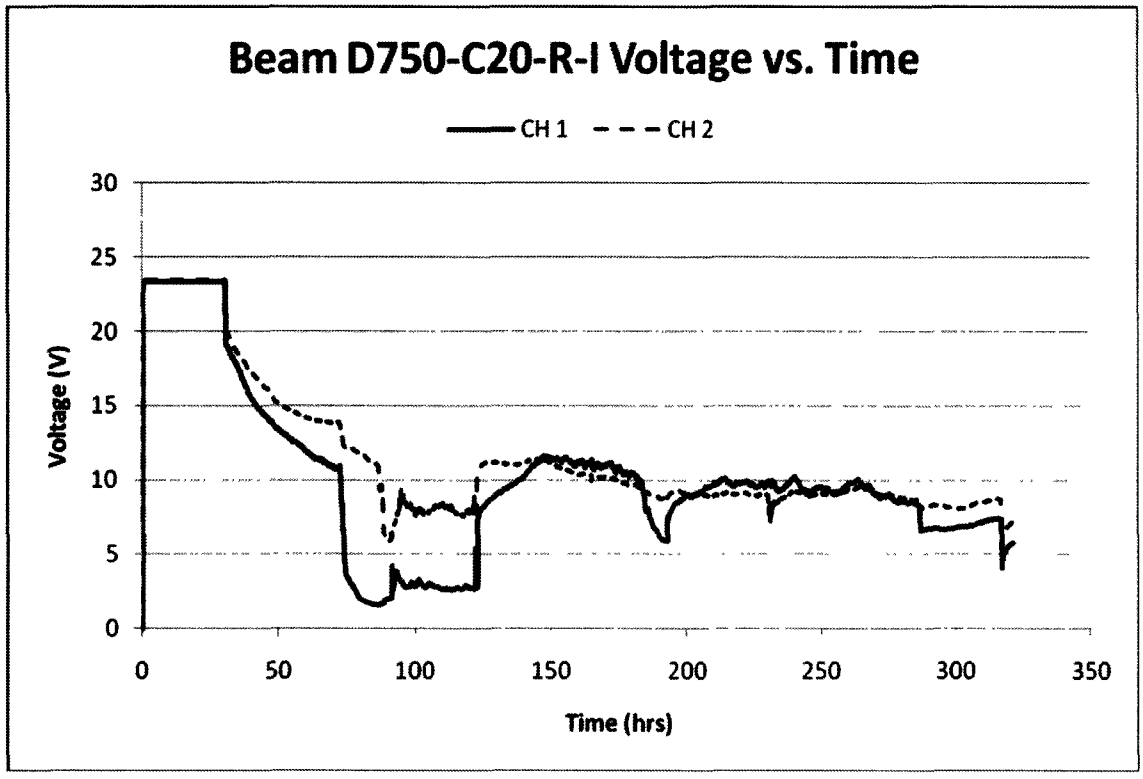
Beam D750-C20-R-I Voltage vs. Time
CH 1
CH 2
Voltage (V)
30
25
20
15
10
5
0
0
50
100
150
200
250
300
350
Time (hrs)

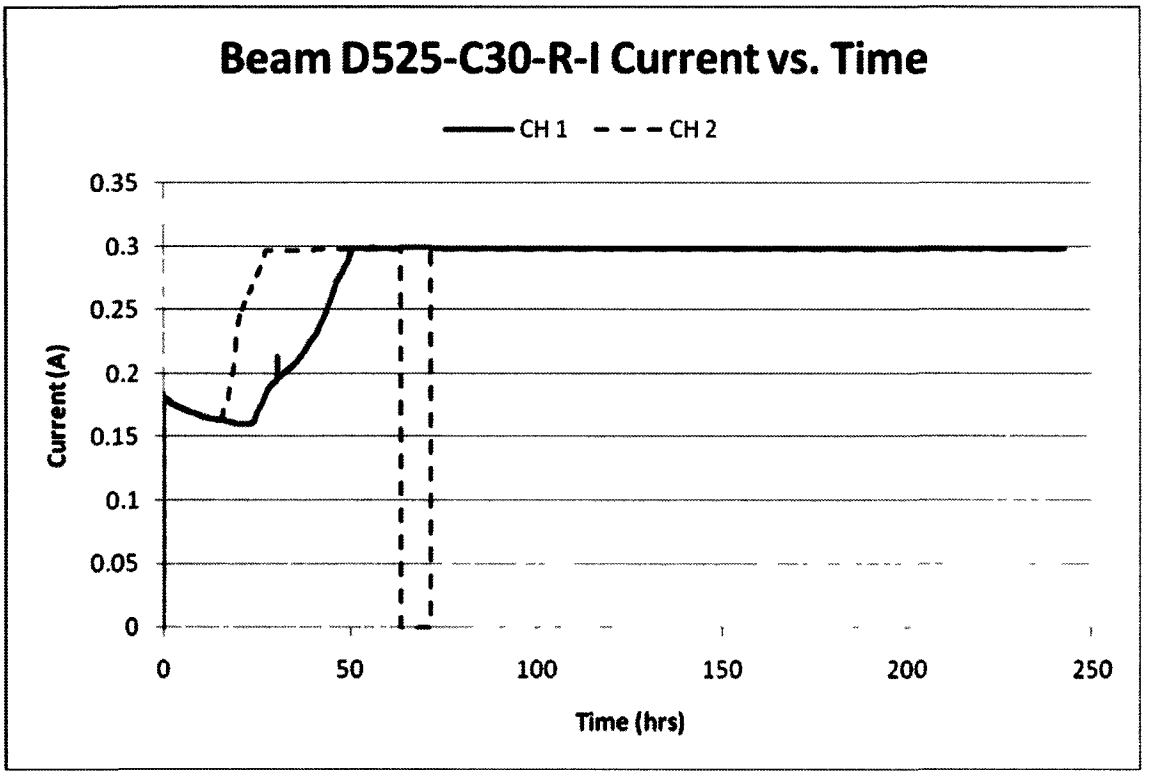
Beam D525-C30-R-I Current vs. Time
CH 1
CH 2
0.35
0.3
0.25
0.2
0.15
0.1
0.05
0
Current (A)
0
50
100
150
200
250
Time (hrs)

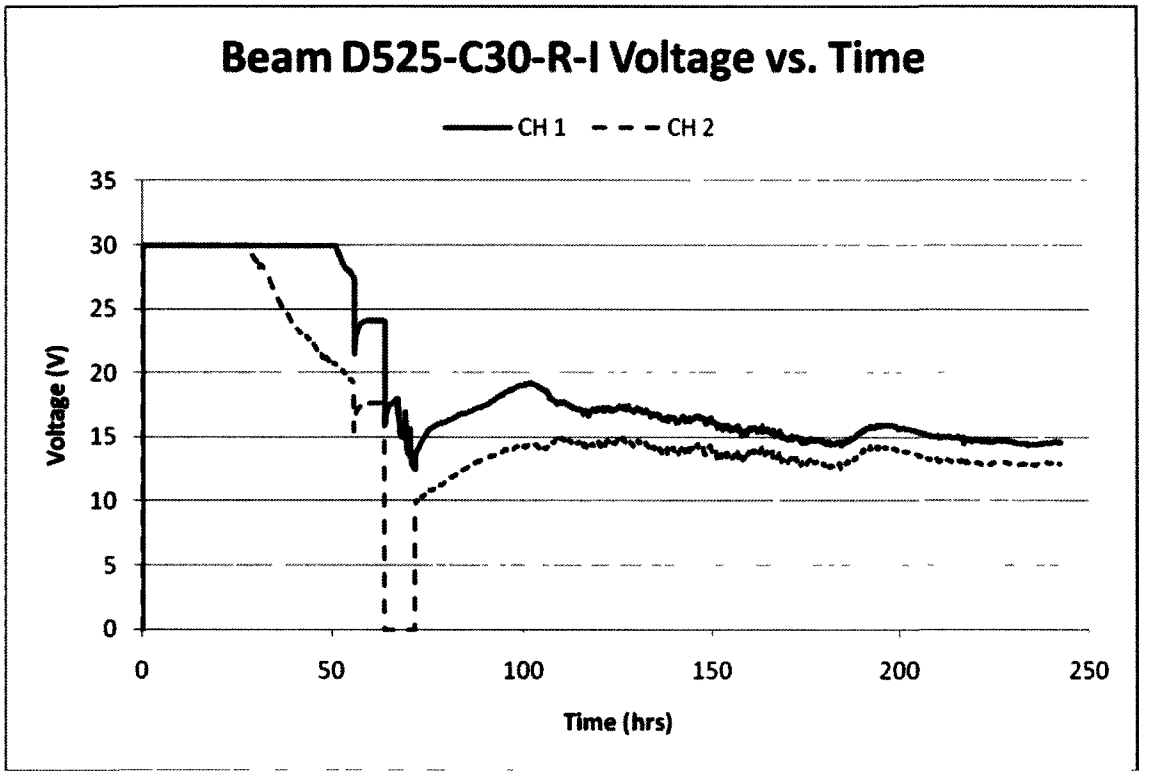
Beam D525-C30-R-I Voltage vs. Time
CH 1
CH 2
35
30
25
20
15
10
5
0
Voltage (V)
0
50
100
150
200
250
Time (hrs)

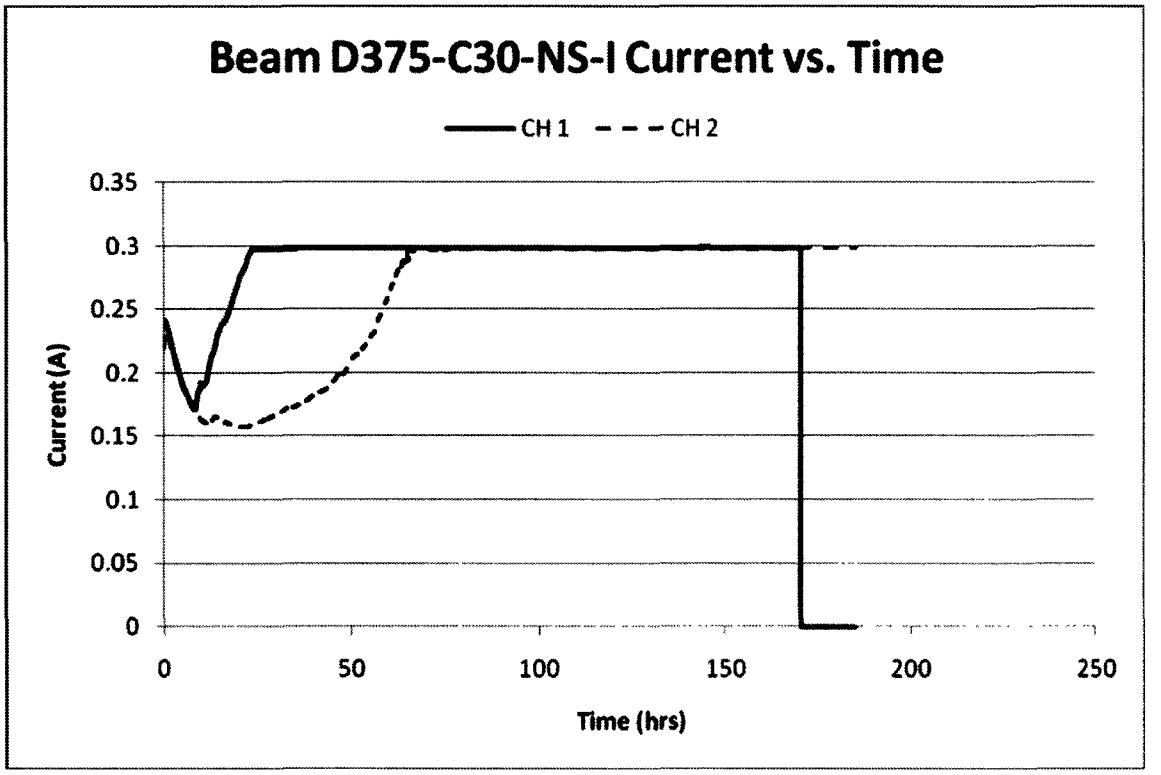
Beam D375-C30-NS-I Current vs. Time
CH 1
CH 2
Current (A)
0.35
0.3
0.25
0.2
0.15
0.1
0.05
0
0
50
100
150
200
250
Time (hrs)

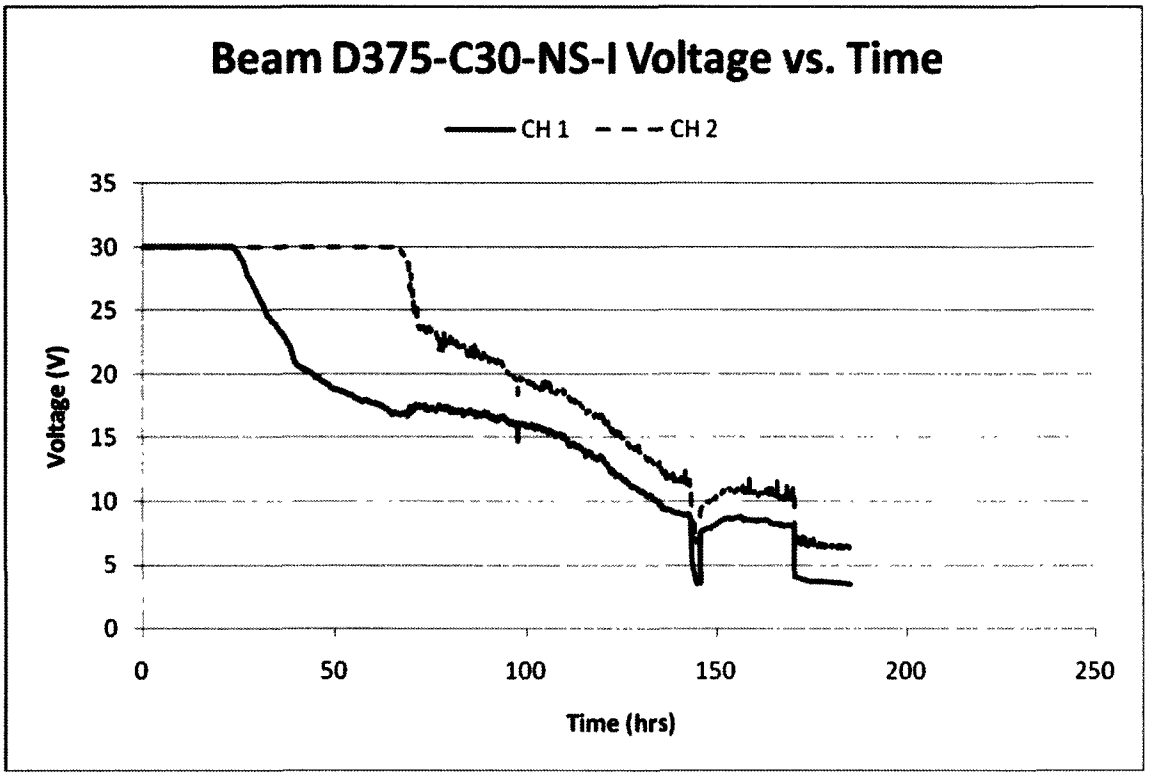
Beam D375-C30-NS-I Voltage vs. Time
CH 1
CH 2
Voltage (V)
35
30
25
20
15
10
5
0
0
50
100
150
200
250
Time (hrs)

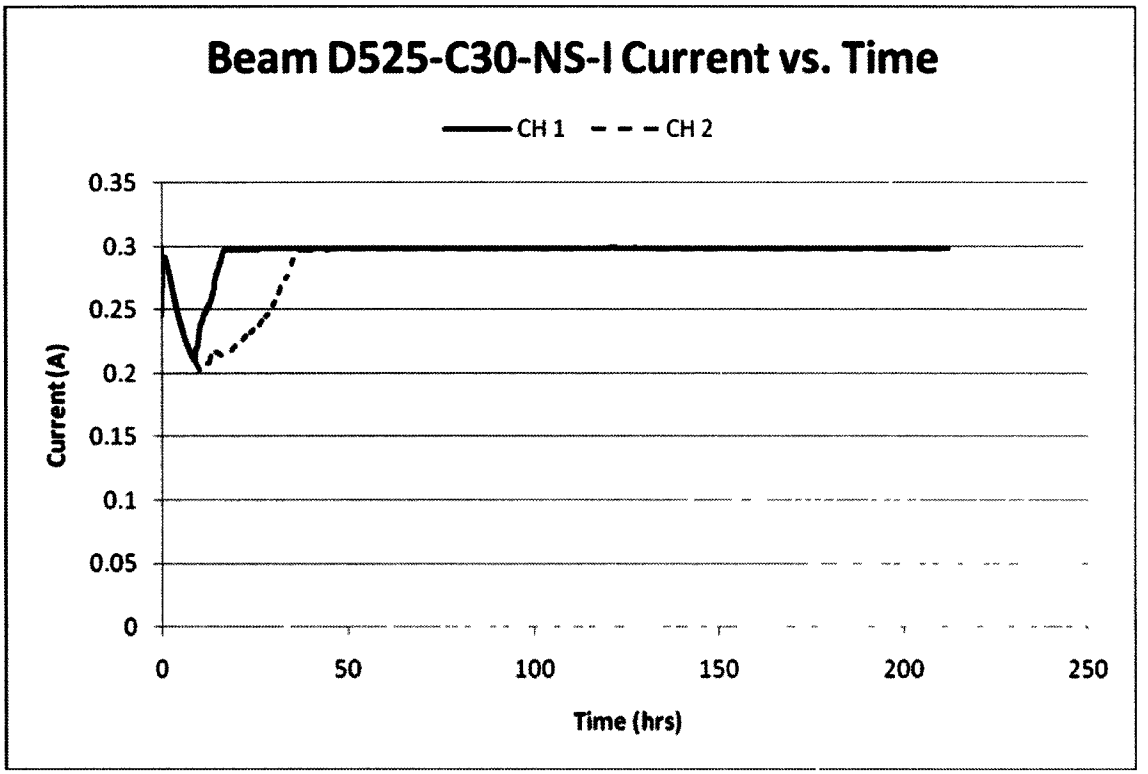
Beam D525-C30-NS-I Current vs. Time
CH 1
CH 2
Current (A)
0.35
0.3
0.25
0.2
0.15
0.1
0.05
0
0
50
100
150
200
250
Time (hrs)

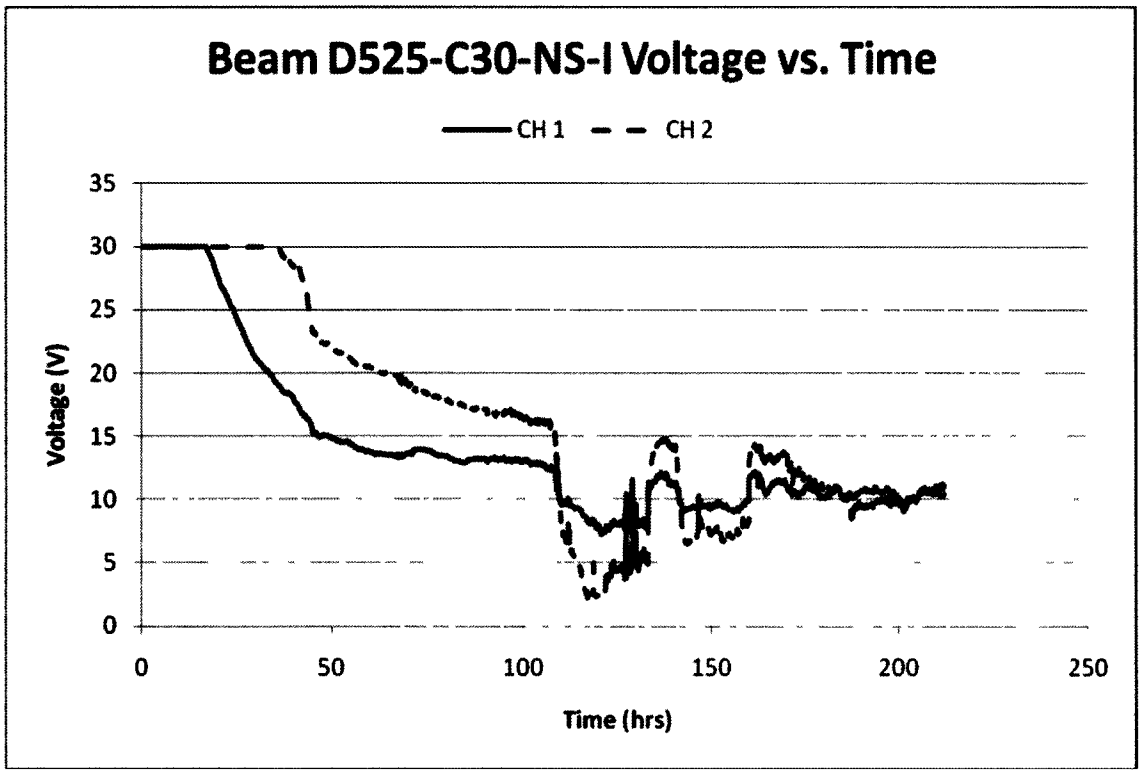
Beam D525-C30-NS-I Voltage vs. Time
CH 1
CH 2
Voltage (V)
35
30
25
20
15
10
5
0
0
50
100
150
200
250
Time (hrs)

Appendix B Crack Mapping

Crack mapping drawings for beam D125-C20-F-I

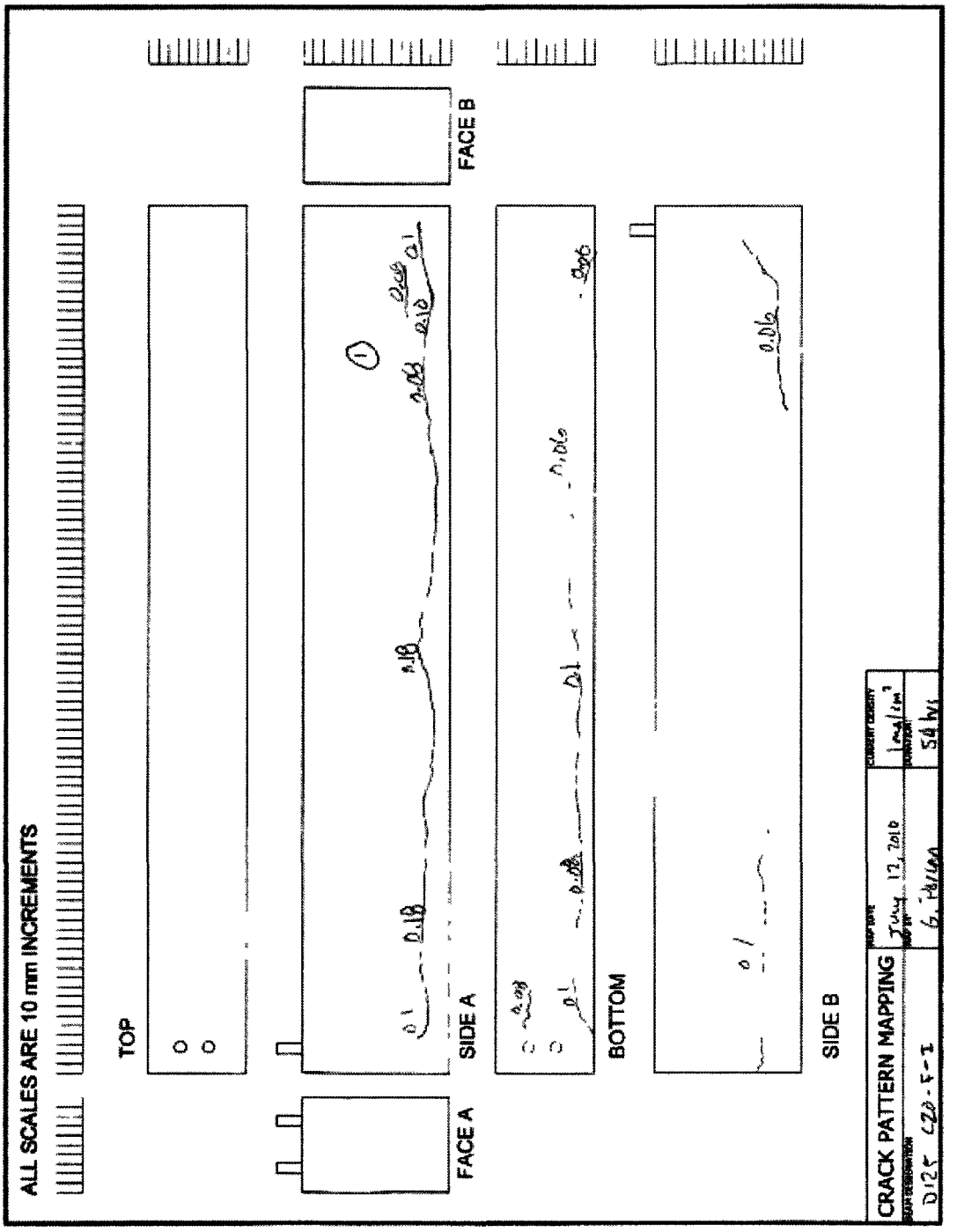

Appendix B Crack mapping drawing for beam D125-C20-F-II

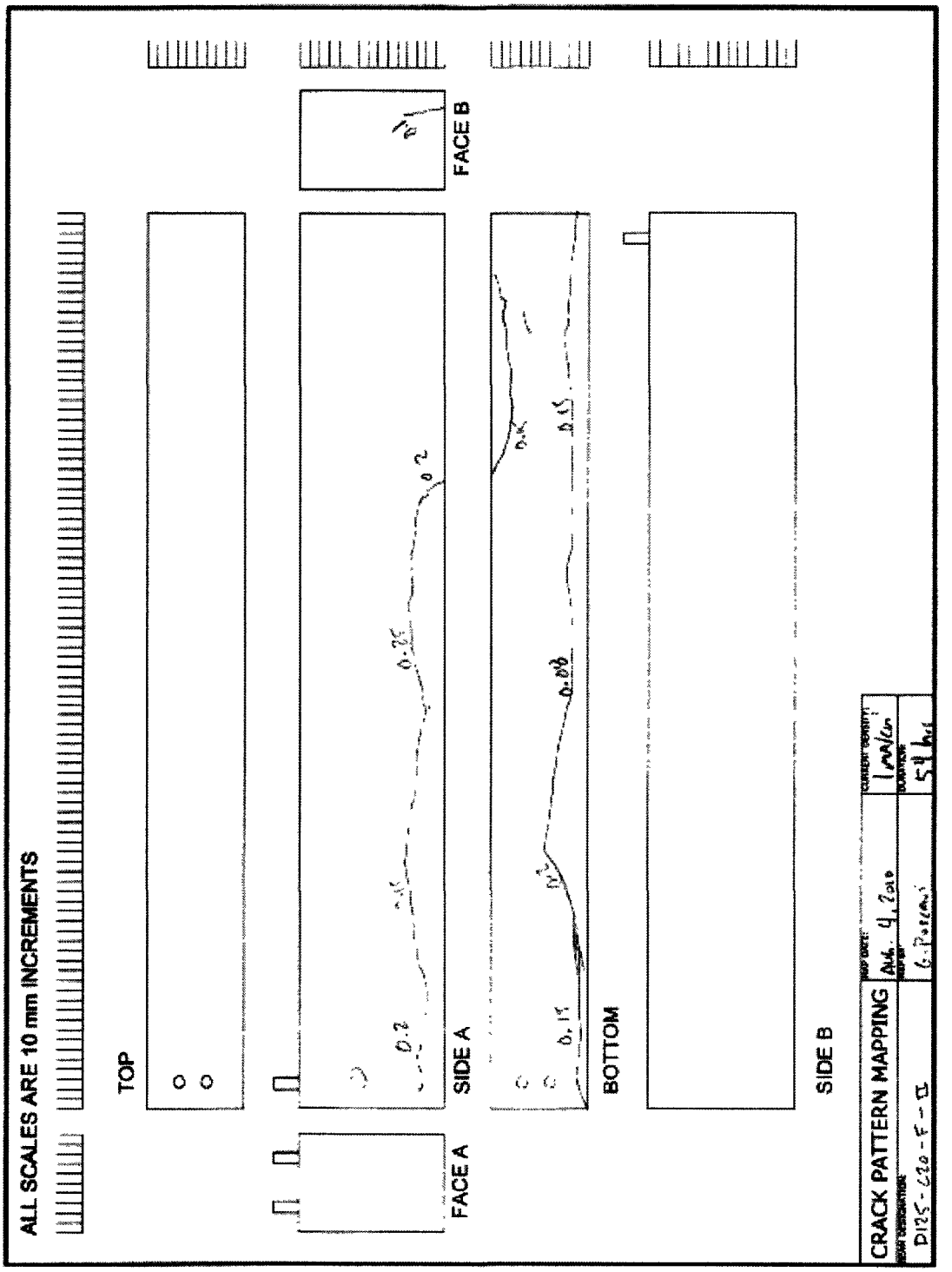

Appendix B Crack mapping drawing for beam D125-C20-R-I

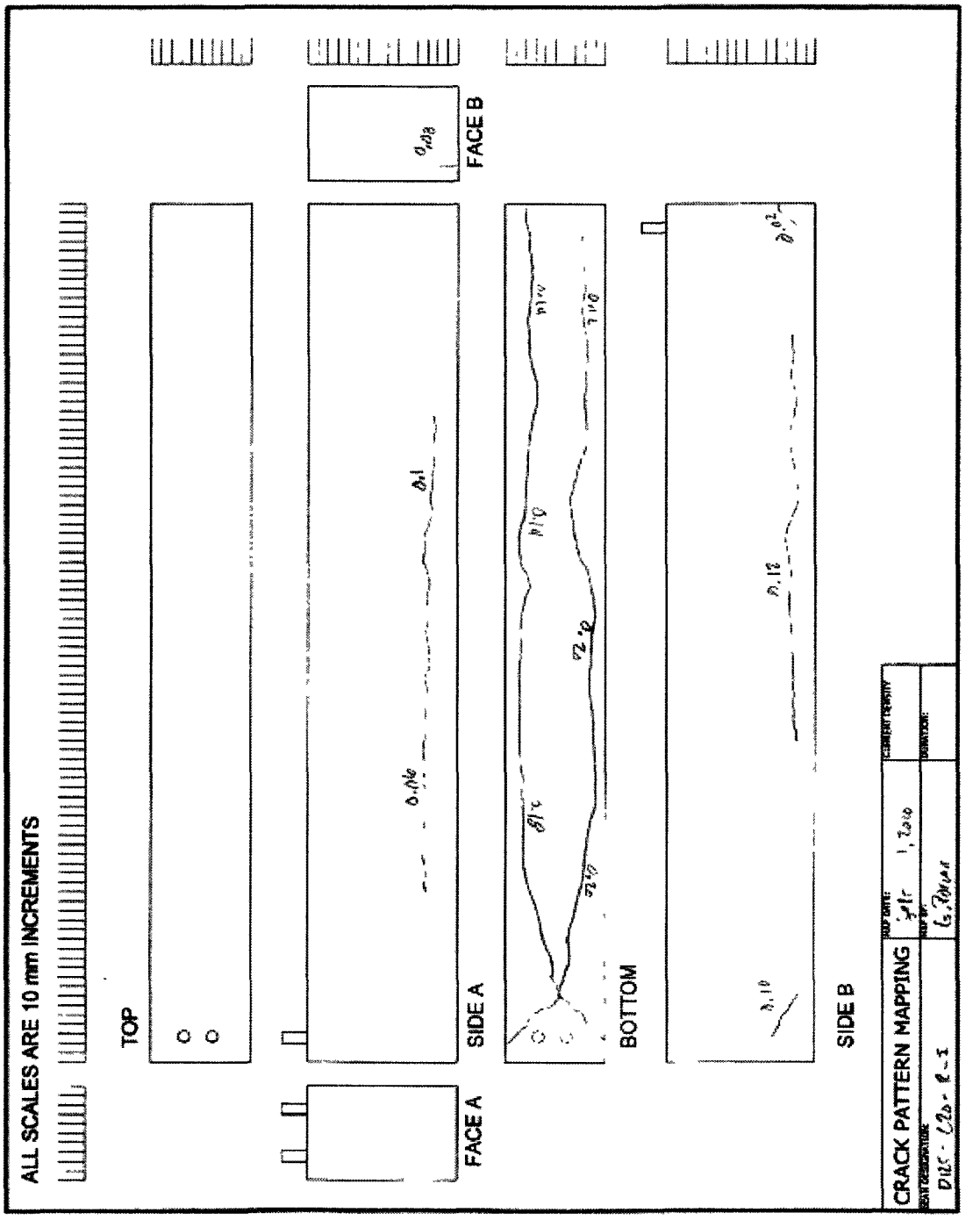

Appendix B Crack mapping drawing for beam D375-C20-F-I

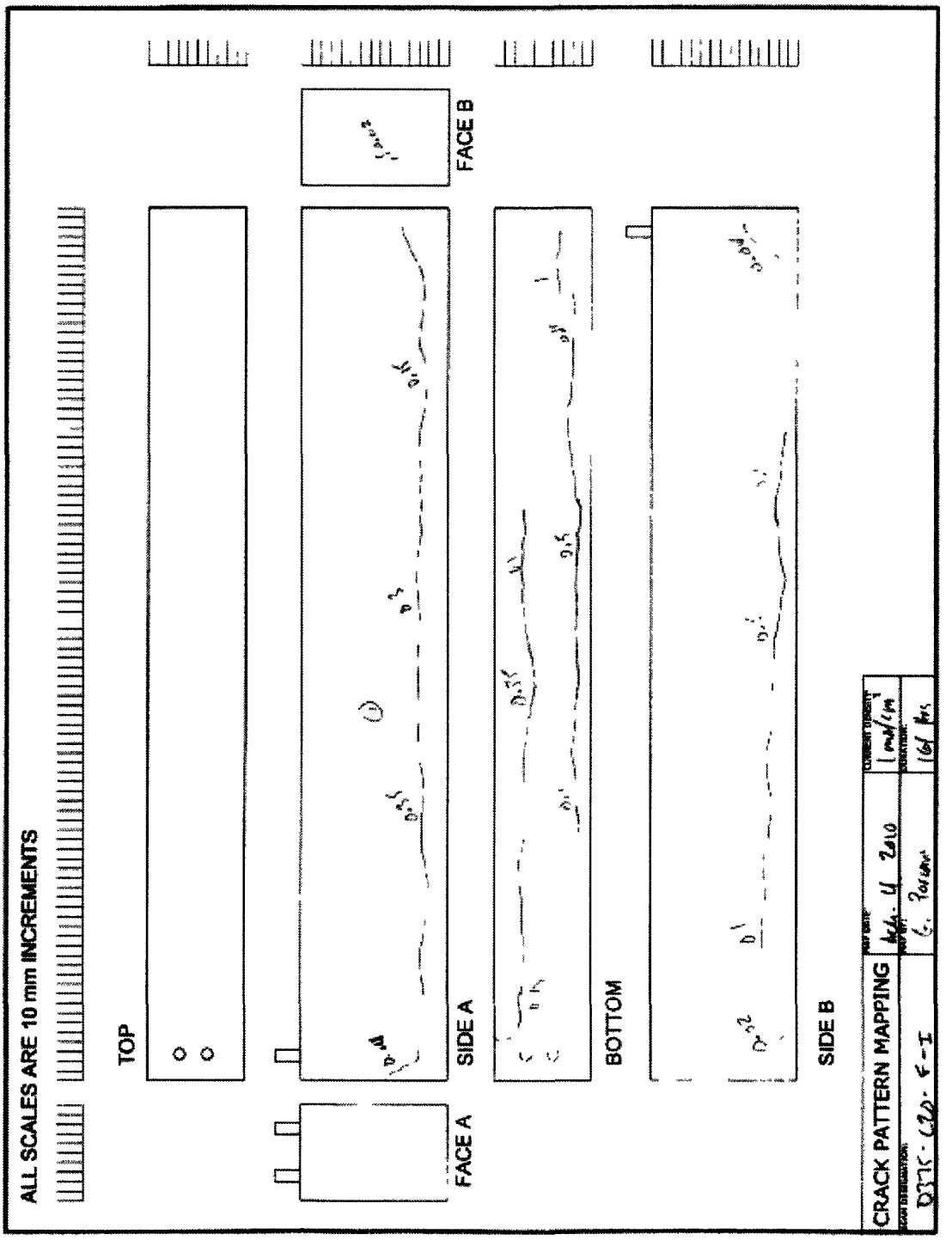

Appendix B Crack mapping drawing for beam D375-C20-R-I

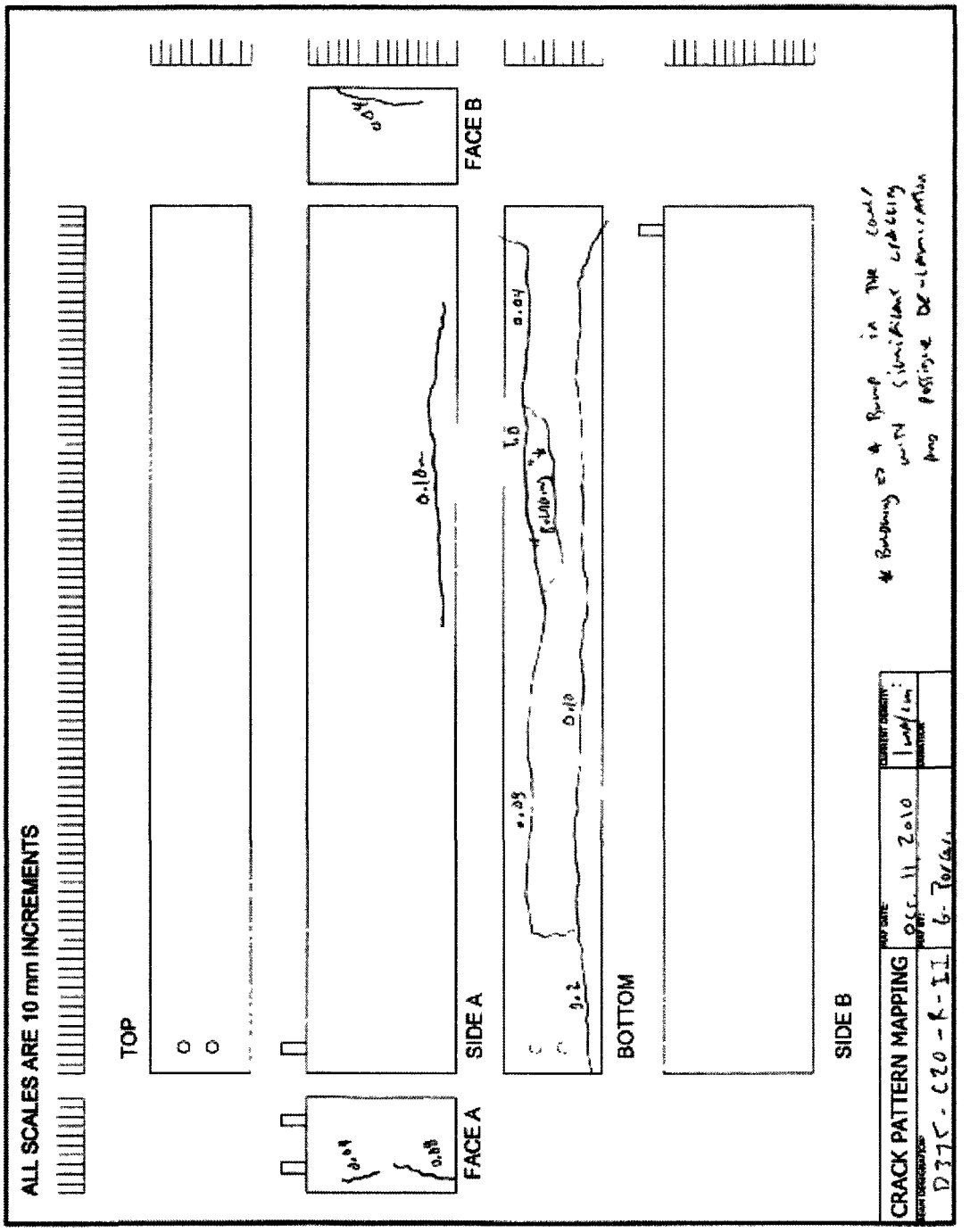

Note: The beam designation hand written on the drawing should read "D375-C20-R-I".

Appendix B Crack mapping drawing for beam D525-C20-R-I

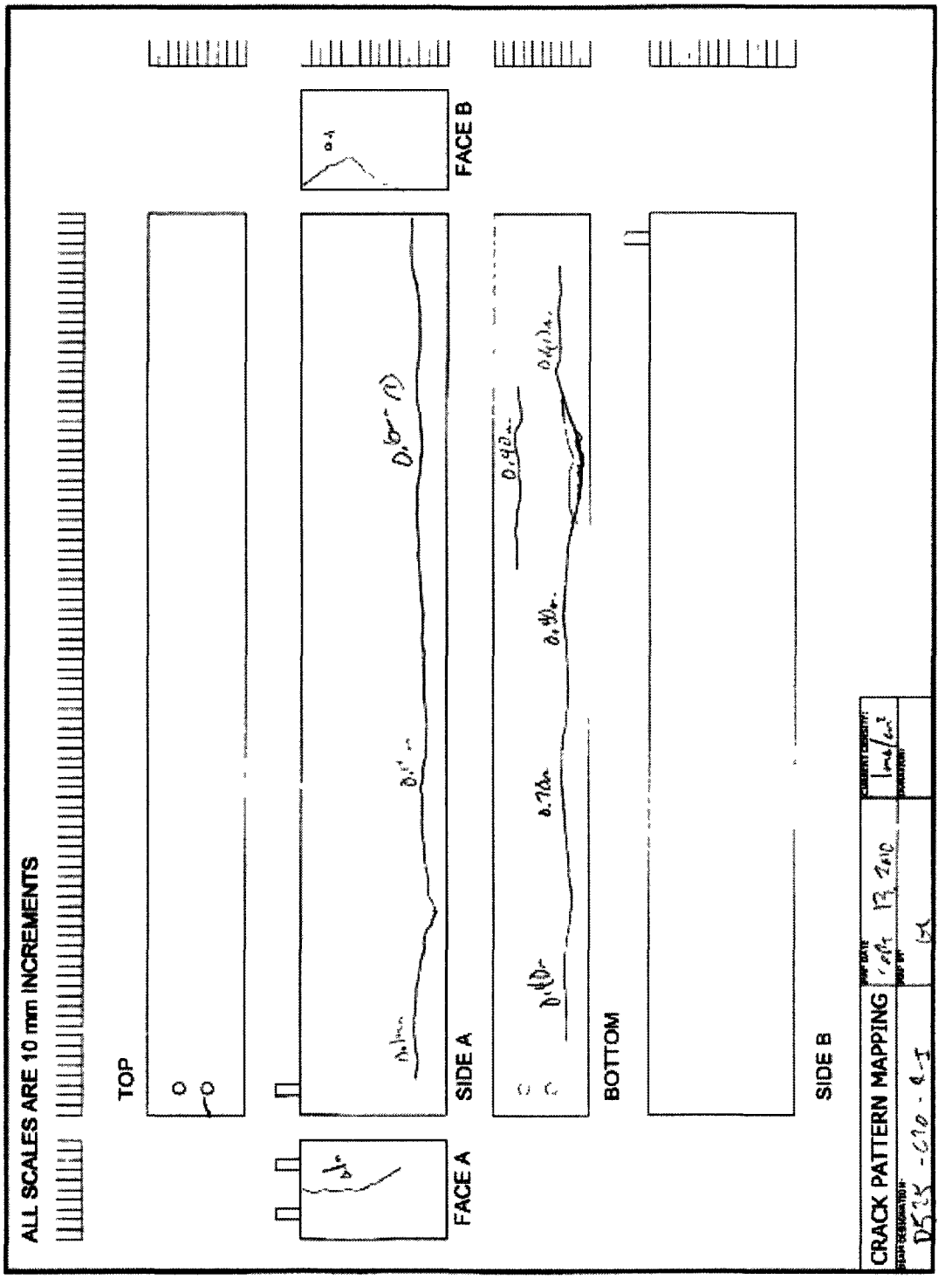

Appendix B Crack mapping drawing for beam D750-C20-R-I

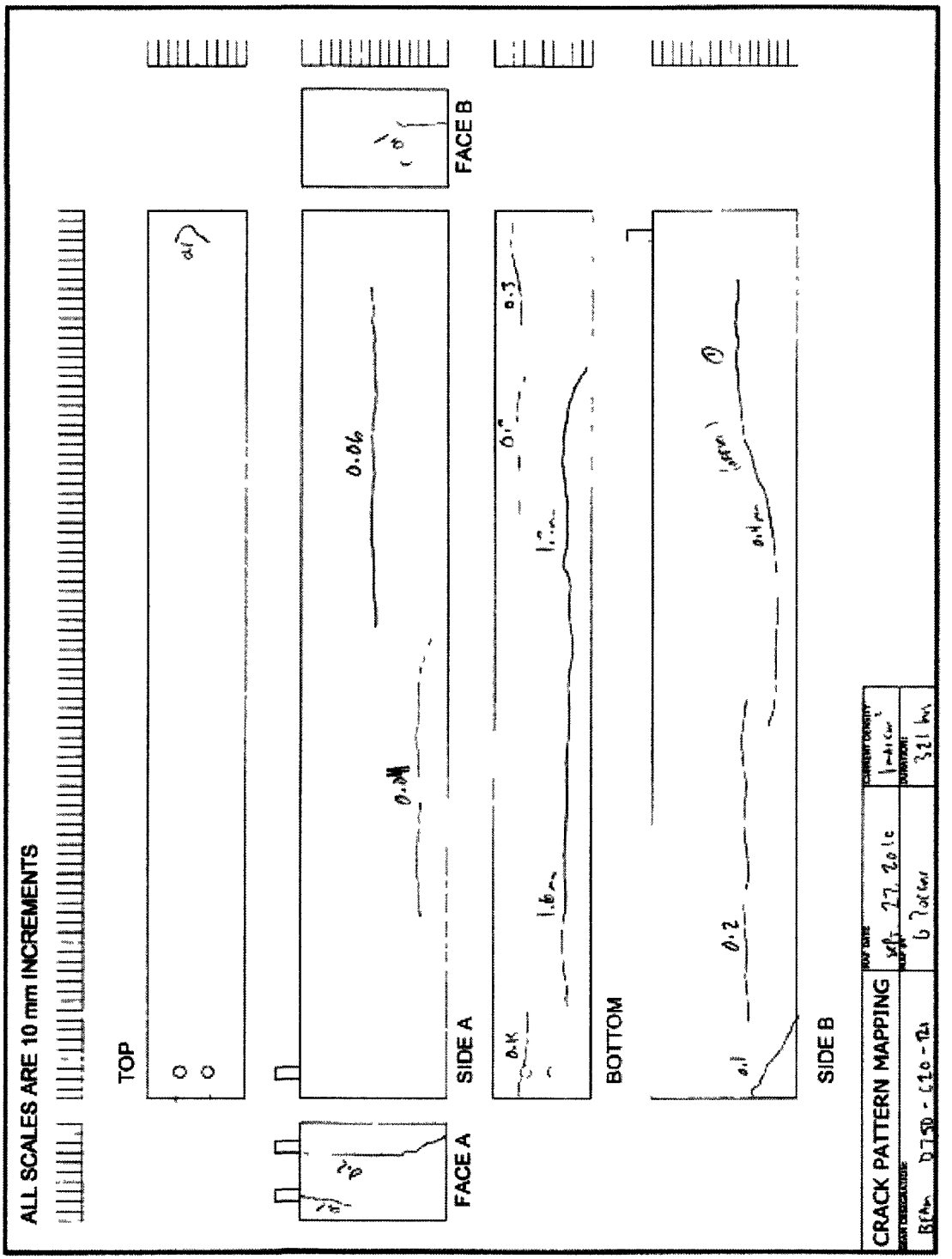

Appendix B Crack mapping drawing for beam D375-C30-NS-I

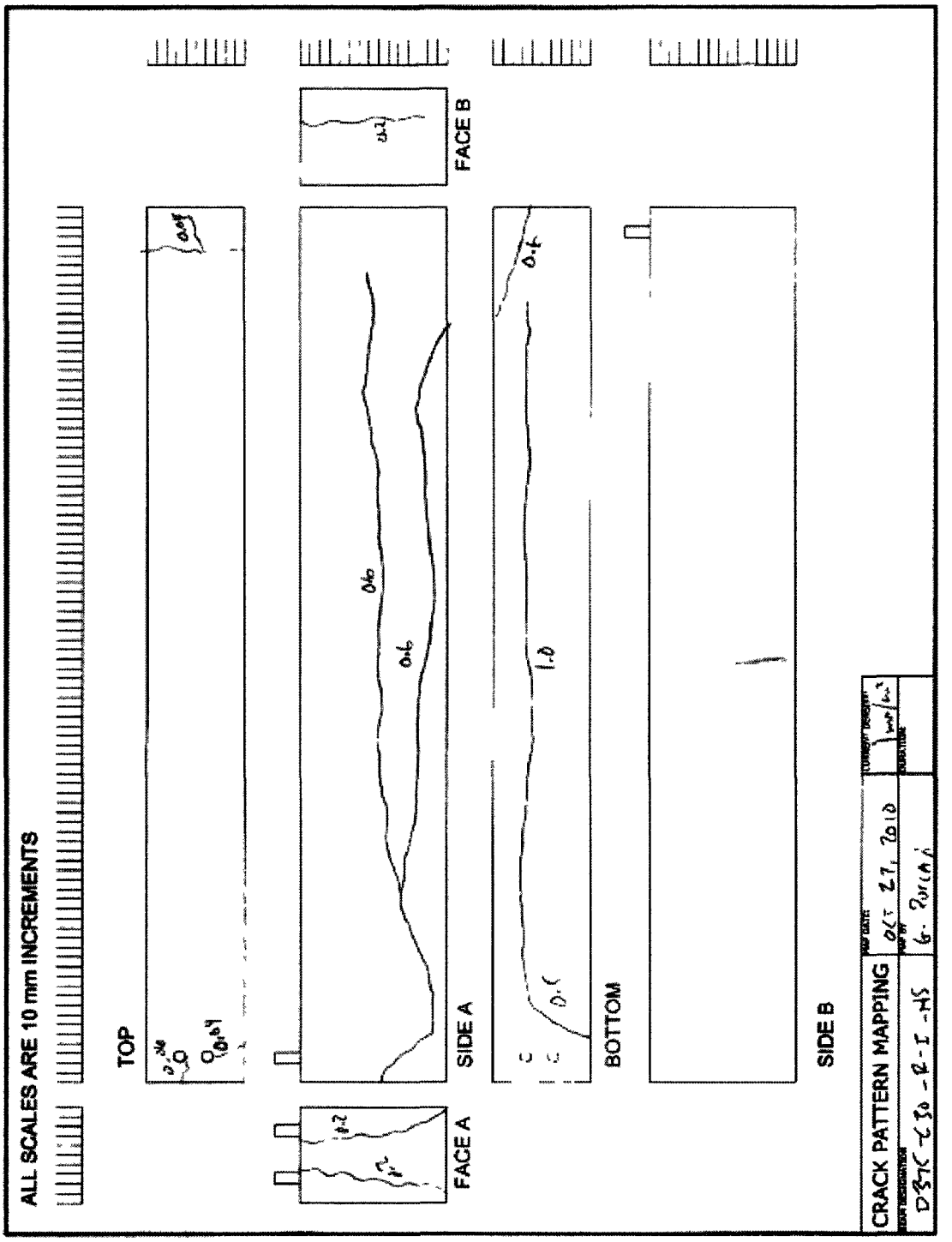

Appendix B Crack mapping drawing for beam D525-C30-R-I

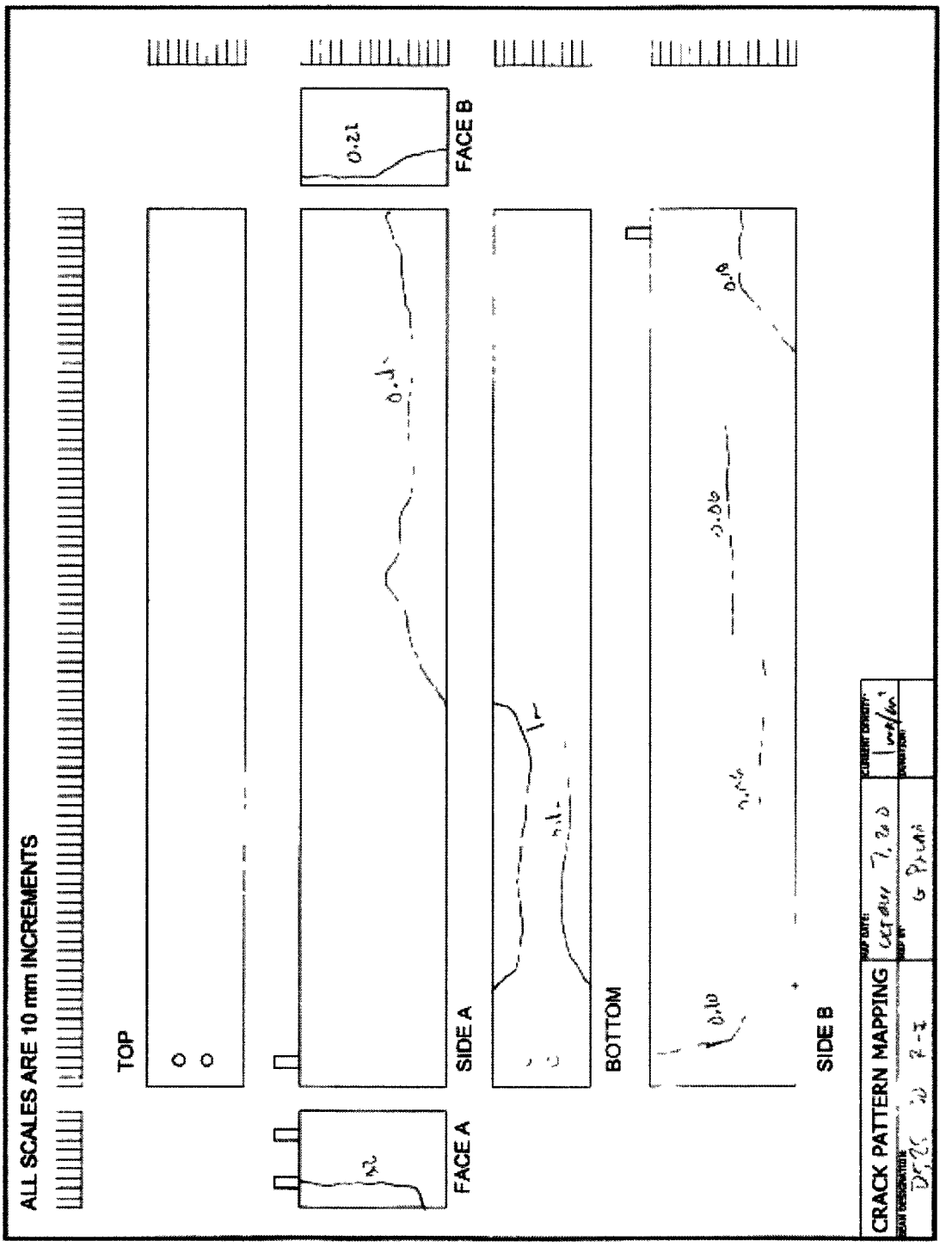

Appendix B Crack mapping drawing for beam D525-C30-NS-I

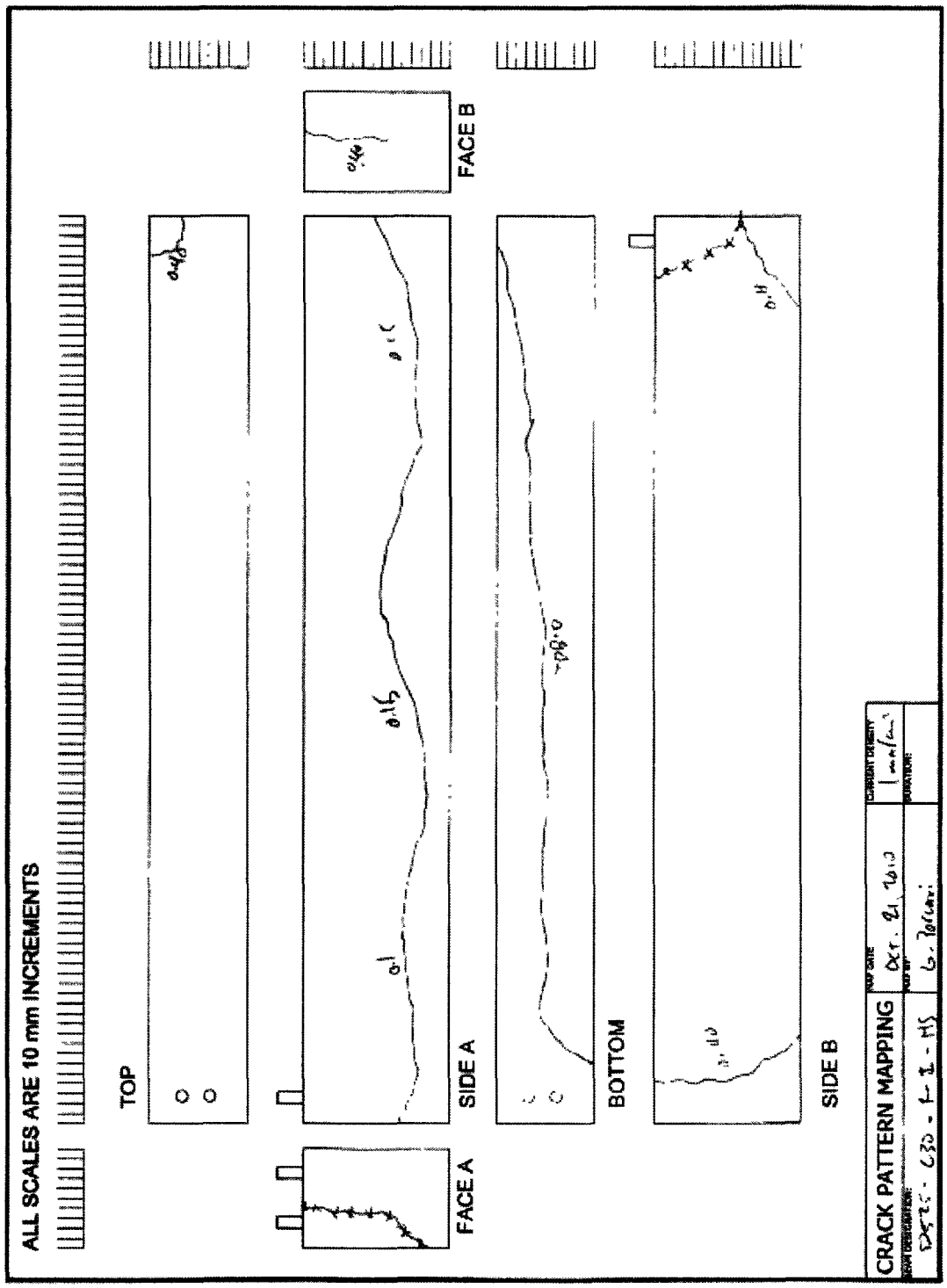

Appendix C Time-Temperature Curves for all Tests